Adaptive Control
of
The Ignition Timing
of
Spark Ignition Engines
Utilising
The Combustion Flame Light Emissions

A thesis
Submitted in Fulfilment of the Requirements
of
Master of Engineering
in the
University of Canterbury
by
R.B. Spencer

University of Canterbury
1985

To my Mother and Father

ABSTRACT

An examination has been made to determine whether the ignition timing in Spark Ignition engines can be accurately controlled from the combustion flame light emissions.

In order to accurately set the ignition advance for optimum engine performance under all conditions of engine operation, an adaptive closed loop spark advance controller is required.

Investigations of visible and infra-red electromagnetic radiation emitted from the combustion flame of four stroke petrol engines have been made. The light emissions were transmitted to light detection equipment through the use of a quartz glass window assembly or through a combination fibre optic cable and spark plug configuration constructed for light emission analysis. The detection equipment was used to produce either photographic records of the light emissions spectrum or flame light intensity curves as a function of time from photodetector output voltages.

The results of these investigations showed that the combustion flame light emissions were strongly influenced by the ignition advance setting and they could be expected to form a suitable input to a spark advance control system.

An electronic knock detection system was constructed using the light emissions intensity as the criteria for determining whether knocking combustion was occurring. The system proved capable of resolving the ignition advance to within 2° crankangle of the limit for knock.

Further testing was completed in order to determine how the combustion product buildup on the inner glass surface would affect the light transmitted to the photodetectors over a long period of engine operation. The photodetectors were able to respond to the light levels transmitted through the glass for medium periods of engine operation (up to 100 hours).

Finally, guidelines are given for further work in this field.

ACKNOWLEDGEMENTS

First, I would like to thank my supervisors, Dr R.K. Green and Dr P.T. Gough, for giving their time and skills during the period of this work.

Dr Gough, thank you for guiding me into the light emissions aspects of the project and for helping me in the photographical work.

Dr Green, thank you for your encouragement and support in every aspect of this work from the obtaining of the initial research grant to making available modern research equipment, and finally for your help in the thesis write-up itself.

I also have appreciated the willing help given by Ron Tinker and Mike Webb on the technical aspects of the apparatus operation and on its initial procurement. I would also like to take this opportunity to thank the people within the Mechanical Engineering and Electrical Engineering, Physics and Chemistry Departments who have given advice, helped in the construction of the apparatus and loaned equipment in aid of the project. I wish to express my gratitude to Paula Dowell for kindly giving her time to the typing of this thesis.

Finally, I would like to thank my Father who has given me "perseverence and encouragement"[1] throughout the period of this work.

CONTENTS

PAGE

LIST OF PLATES

LIST OF FIGURES

LIST OF TABLES

CHAPTER 1

INTRODUCTION & HISTORICAL REVIEW

CONTENTS

1.1 Introduction to Combustion in the Spark Ignition Engine

"The reciprocating four-stroke cycle carburetted Spark Ignition Engine is the dominant internal combustion engine today and will be for many years."

Heywood[41]

The engine thus described has resulted from several centuries of research and development of machines which are capable of converting stored potential energy into the kinetic energy of motion. The earliest internal combustion engines developed by Abbé Jean de Hautefeuille (1678) and Christian Huyghens (1791) were gunpowder engines. These were followed by the gas turbine of John Barber (1791) and the piston engines of Street (1794) and Philippe Lebon (1799). Jean Joseph Lenoir (1860) invented the first gas engine in which the air-gas mixture was spark ignited on the intake stroke without any compression stroke, making it rather inefficient and not competitive with the steam engines of the day. The conception of the four stroke internal combustion engine by Otto in 1876 provided the necessary improvement in efficiency to render the Spark Ignition engine an attractive alternative to the steam engine.

The discovery of oil in Pennsylvania in 1859 brought about the development of the petroleum industry and this, together with the invention of the pneumatic tyre by Dunlop in 1888, induced the birth of the automotive industry.

1.1.1 Principles of Operation

The principles of 4-stroke engine operation, on which Otto based the design of his engine, were proposed by Beau de Rochas in 1862 and are still used today in the design of the common 4-stroke internal combustion engine. The cycle of operations has become known as the Otto Cycle, and they may be summarised as:

1) the intake stroke when the air-fuel mixture is drawn into the cylinder as the piston descends (intake valve open);
2) the compression stroke, which raises the pressure and temperature of the mixture when the piston ascends (both valves closed);
3) the power stroke, whereby a downward force is exerted on the piston from the combustion of the air-fuel mixture (both valves closed);
4) the exhaust stroke, which removes the products of combustion from the cylinder as the piston ascends for the second time (exhaust valve open)[8].

In the Spark Ignition engine the air-fuel mixture is normally prepared before it passes through the intake valve in such a manner that its value is approximately constant over all engine operating conditions. Therefore, part load operation must be achieved by restricting the intake mixture flow using some form of throttling device. Such preparation and control of the intake mixture imposes certain restrictions on other aspects of the engine design such as the compression ratio. Since the mixture is present in the cylinder during the intake, compression and power strokes, it is susceptible to self-igniting if the pressure and temperature of the mixture is raised beyond certain limits characteristic of the fuel at any stage of the 4-stroke process (refer to Section 2.1). These dangerous operating conditions must be controlled through the use of relatively low compression ratios which create low indicated engine efficiencies. The performance of the engine is reduced during part-load engine operation when the throttling of the intake mixture increases the air-pumping work losses resulting in a reduction in efficiency[7].

The advantages inherent in the Spark Ignition engine include its versatility, power to weight ratio, and the cost of manufacture, which enable it to compete favourably with other forms of engines. Hence the Spark Ignition engine has continued to proliferate with modern refinements aimed at improving performance within the constraints of the 4-stroke operating cycle.

1.2 Factors Affecting Combustion Performance

The combustion related parameters which affect the performance of the Spark Ignition engine can be divided into three broad categories depending upon whether they are associated with the fuel, the combustion chamber design, or the ignition timing. The major factors in each of these categories will now be discussed.

The air-fuel mixture is normally prepared in the carburettor in such a way as to provide a homogeneous mixture composition with a mass ratio of approximately 15 parts of air to 1 part of fuel, so that the hydrocarbon fuel is just burned to predominantly stable combustion products. The exact air-fuel ratio required under a particular engine operating condition will depend upon which engine performance criteria are of highest priority; for example, power, fuel economy or low exhaust emissions. The carburettor must be designed to vary the air-fuel ratio in response to these requirements.

For hydrocarbon fuels the charge should be approximately 60% vaporised

when it enters the cylinder under open throttle conditions as this represents a compromise between acceptable fuel distribution to each cylinder and good charge density. Complete vaporisation of the fuel under these operating conditions is undesirable since the vaporised fuel would displace air in the intake manifold.

Once the air-fuel mixture has entered the cylinder it is subjected to compression and the combustion process. The chemical properties of the fuel must be compatible with the engine design in order to ensure that controlled effective combustion takes place. The air fuel mixture must always ignite when the spark is discharged towards the end of the compression stroke. The octane rating of the fuel, that is, its ability to resist self-ignition, must be sufficient to prevent the charge from self-igniting to the degree which would cause damage to the engine structure (refer to Section 2.2.1).

The second category of factors which contribute to effective combustion are those associated with the mechanical properties of the combustion chamber, particularly its shape, compression ratio and the valve timing. The shape of the combustion chamber should ensure that the flame travel from the spark plug to the cylinder walls is minimised since this shortens the overall time for combustion to be completed. The location of the spark plug in a central position in the cylinder head helps to ensure this (Figure 1.1). Turbulence of the gases created during compression and swirl induced by the inlet flow configuration increase the flame speed during combustion which yields a further reduction in the time for combustion to be completed.

The ratio of the cylinder volume with the piston at bottom dead centre to the cylinder volume with the piston at top dead centre is termed the compression ratio, which influences the rate of combustion and the indicated thermal efficiency of the engine. The combustion efficiency increases with increasing compression ratio in a non-linear relationship so that at compression ratios above 20:1, efficiency gains become less significant (Fig. 1.2). However, as has been previously stated, in the Spark Ignition engine the compression ratio is limited by the resistance of the fuel to self-ignition which occurs when the air-fuel mixture is over-compressed. At present hydrocarbon fuels can be manufactured relatively cheaply with octane ratings which enable them to be used in automotive engines with compression ratios between 7:1 and 10:1.

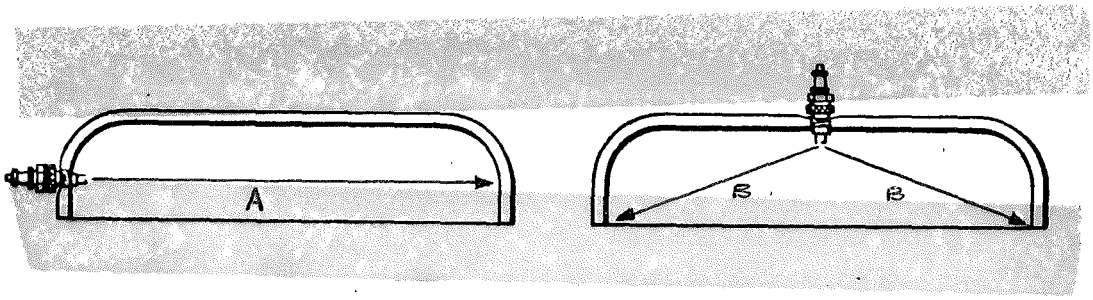

Figure 1.1 The positioning of the spark plug as it relates to the flame travel distance. The positioning of the plug in (b) is preferred as it shortens the idealised flame path length from that depicted in (a)[8].

The third category of factors which affect combustion performance are those associated with the ignition timing. The ignition timing influences the timing of combustion since the combustion process is initiated when the high tension ignition system discharges the spark across the spark plug electrodes. For best combustion performance the combustion process should occur with the piston close to top dead centre through appropriate timing of the ignition advance.

The tendency of the fuel to self-ignite at any stage after the onset of the combustion process is also influenced by the ignition timing. Such self-ignition of part of the air-fuel mixture separately from the spark generated flame front is termed knock or auto-ignition, and is heard as a metallic sound accompanying combustion. This form of combustion can cause undue engine wear or may cause damage to certain engine components so that it must be limited by appropriate control of the ignition advance and by using relatively low compression ratios. Such restrictions invariably limit the efficiency of the Spark Ignition engine. Thus the problem of auto-ignition has been the subject of much attention by engine designers and researchers alike.

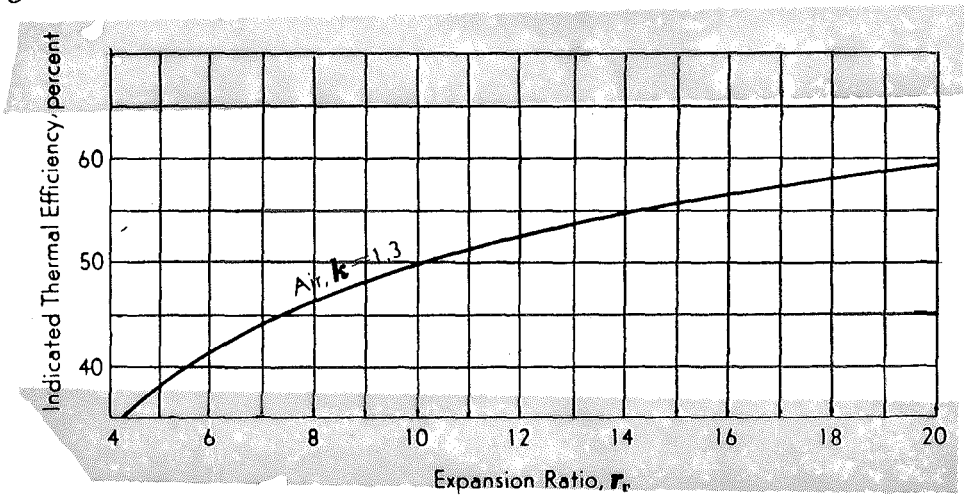

Figure 1.2 Thermal efficiency versus expansion ratio for an engine at wide open throttle, maximum power and λ = .83 (air-fuel equivalence ratio; excess fuel)[8].

1.3 The Problem of Auto-Ignition

The first internal combustion power plant built by Lenoir suffered from knock under load and in the early 1900's, Charles F. Kettering and Thomas Midgely Jr began a research effort to try and eliminate engine knock without reducing fuel economy[12]. Eventually their efforts led them to discover the beneficial properties of tetraethyl lead as an anti-knock agent in 1921[17].

Knock continued to be the most important area of research in the Spark Ignition engine until 1944. During this period high speed photography of the combustion flame was used to examine the differences between knocking combustion and normal combustion[2]. This method of examining the flame proved successful since the behaviour of the flame front differed markedly between the two processes of combustion. The combustion flame light emissions recorded on the photographic film revealed that during auto-ignition a second flame front appeared in the unburned region of the charge before the initial spark generated flame had completely propagated throughout all of the combustion chamber.

In an effort to reduce pollution from exhaust emissions in the 1970s, catalytic converters were fitted to vehicles for use in the United States market. Since catalytic converters could become fouled from the lead anti-knock additive in the petrol, this requirement resulted in the petroleum companies producing a lower octane rating lead free fuel. This development served to re-emphasise the problem of knocking combustion as manufacturers were forced to reduce engine compression ratios and therefore engine power and fuel economy in order to allow knock-free engine operation on the lower octane fuel.

Subsequently, research and development activity has been directed towards making improvements in engine combustion performance by controlling combustion more precisely. Results of this work include improved combustion chamber design which has partially offset the losses mentioned earlier from the reduction in compression ratio. Of the engine variables which can be adjusted while the engine is in operation, Boht and Quayle (1981) make the following comments: *"Leaving aside the more complex and expensive mechanical engine modifications such as variable compression ratio, variable valve timing and stratified charge, the parameters to be controlled are the ignition advance angle and the air-fuel ratio."* [25]

Accurate control of the air-fuel ratio has been made possible by the

development of zirconium based exhaust gas oxygen concentration sensors in the 1970's. When installed in the exhaust system these sensors provide an input to an electronic fuel control system which is able to maintain the air-fuel ratio close to the desired settings for best power or economy, or for lowest exhaust emissions (refer to Appendix 3.1).

Accurate closed loop control of the ignition timing has not yet been provided on automotive engines. One important reason for this lack of progress has been the absence of a reliable sensor which can monitor the combustion process and provide the necessary information input to an ignition advance controller.

1.4 Introduction to Present Work

The high speed photography of the combustion flame light emissions from knocking combustion has already been mentioned. The photographs (which are shown and discussed in Chapter 4) show a clear distinction between the light emissions from knocking and non-knocking combustion, and the object of the author's work has been to examine whether a light emissions detection system could be developed to distinguish between knocking and non-knocking combustion and which would provide the intrinsic input to an ignition advance controller on the Spark Ignition engine.

The flame light emissions would need to provide sufficient information about the combustion process to enable the ignition advance controller to accurately set the ignition advance under any engine operating condition.

The completed system would have to be reliable and its installation should involve minimum modification to the automotive engine structure.

The conventional mechanical components which would be made obsolete by such a system have the advantage that they are relatively cheap and can easily be maintained by existing service personnel. The successful development of a new spark advance system must engender sufficient benefits in order to outweigh the increased cost and maintenance complications associated with a more refined system.

CHAPTER 2

PHYSICAL ASPECTS OF COMBUSTION IN THE SPARK IGNITION ENGINE

CONTENTS

INTRODUCTION

This chapter discusses the important physical aspects of combustion which are influenced by the degree of ignition advance and which directly affect the combustion efficiency. The chemical aspects of combustion will be discussed in Chapter 4. The physical properties of concern include the rate of combustion and the associated tendency of it to knock or auto-ignite.

A description of these combustion processes; normal, auto-ignition and pre-ignition will ensue, followed by a discussion of the advantages and disadvantages of each in relation to effective combustion in the Spark Ignition engine. Finally, the ignition advance system is discussed as it relates to controlling the combustion process in order to achieve effective combustion.

2.1 Process of Combustion

2.1.1 Normal Combustion

A review of the four stroke Otto Cycle upon which combustion in the four stroke Spark Ignition Engine is based is given in Section 1.1.1. For the purposes of this review on the physical combustion process, combustion is defined to be initiated by the spark towards the end of the compression stroke and completed by the time the exhaust valve opens towards the end of the expansion stroke.

As the compression stroke nears completion the combustion chamber will normally contain a more or less homogeneous mixture of fuel vapour and air. Normal combustion commences when the spark is initiated, and an electrical discharge proceeds from one electrode to the other creating a "thin thread of flame"[7] by consuming an extremely small mass of mixture. The flame propagates uniformly from this source throughout the combustion chamber until it consumes the whole charge (Fig.2.1). The flame front, once established, will become wrinkled due to turbulence as combustion proceeds and may break up into turbulent eddies which increase the overall flame velocity. The gas temperature and pressure at the completion of combustion far exceeds that prior to combustion so that useful work can be obtained from the process. The high combustion pressure is timed to create a downward force on the piston after top dead centre (TDC) and the resultant torque is delivered through the crankshaft to the power train.

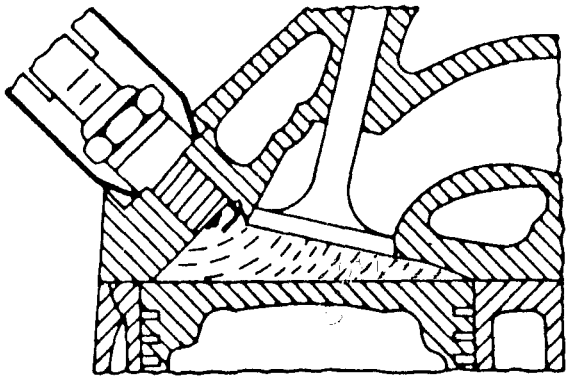

Figure 2.1 Passage of the flame front across the combustion chamber during a normal combustion cycle[8].

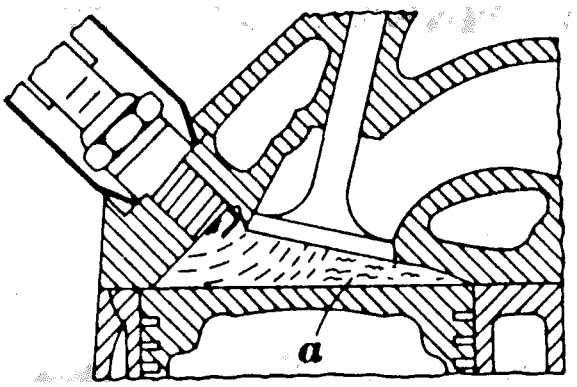

Figure 2.2 Passage of the flame front across the combustion chamber during a knocking combustion cycle. Region 'a' is the self-igniting region[8].

This is the normal process of combustion within the chamber of the Spark Ignition engine. A flame is initiated by the spark and self-propagates across the chamber by bringing the fuel-air mixture just ahead of it into the high temperature explosive combustion region. In this way it proceeds until it is extinguished at the cylinder walls.

2.1.2 Auto-Ignition

2.1.2.1 Self-ignition of a fuel-air mixture

Under certain operating conditions the combustion sequence may follow a different pathway involving self-ignition of part of the mixture. Consider a fuel-air mixture compressed within a vessel and then maintained under constant volume conditions. If the compression is low, then, although the pressure and temperature of the mixture is raised, it will not self-ignite but rather it will eventually cool back down to the temperature of the surroundings (Fig. 2.3; ABC). A chemical analysis of the mixture will generally reveal that some oxidation has taken place. The process can be repeated with successively higher compression ratios until a situation is reached when the mixture will self-ignite if maintained for a sufficiently long period of time under these conditions of high temperature and pressure (Fig. 2.3; AB'C'D). The length of time between compression and self-ignition is called the induction period or ignition delay. It is evident that during this induction period, intermediate reactions are proceeding which prepare the mixture for the

explosive self-ignition reactions. As the compression ratio is raised further the ignition delay is shortened (Fig. 2.3; AB"C"D"). In conclusion, when a fuel-air mixture is brought under sufficiently high temperatures and pressures, it will self-ignite after a certain induction period.

This self ignition property of fuel-air mixtures can alter the combustion process within the Spark Ignition engine leading to two different forms of combustion termed auto-ignition and pre-ignition. Since both of these types of combustion influence the engine performance and they can both be controlled by the ignition advance system, they will now be discussed.

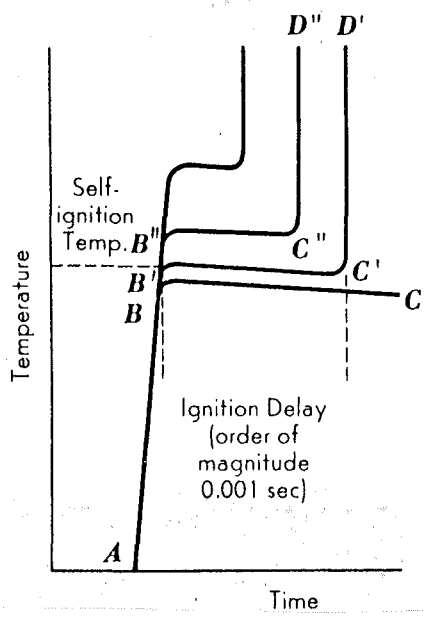

Figure 2.3 The effect of the compression ratio on the ignition delay and self-ignition temperature[8]

2.1.2.2 Auto-ignition during the combustion process

In the Spark Ignition engine when part of the fuel-air mixture self-ignites ahead of the advancing flame front, auto-ignition is said to be taking place. The process may be described by considering the hypothetical combustion chamber of Figure 2.4 which encloses a highly compressed fuel-air mixture and is sub-divided into sections 1, 2, 3, 4. In the beginning the conditions are such that the mixture would not self-ignite, rather the combustion process is initiated by spark and burns though section 1. It will compress the unburned sections 2, 3 and 4 possibly bringing them into a region where they would self-ignite given a long enough induction period. As section 2 burns it will compress and raise the temperature of the unburned sections 3 and 4 still further and

will also compress the gaseous products in section 1. The induction period of sections 3 and 4 has now been shortened due to higher compression temperatures which have been established in these sections. If the ignition delay of the gas in section 4, termed the endgas, is reached before the flame has passed through it[9] then it will spontaneously explode and the process of auto-ignition or knock is said to have taken place.

A closer examination of the auto-igniting region of the charge will reveal more about the combustion mechanism of this process. It appears that some highly stressed points within the endgas become the source of ignition for a second flame front (Fig.2.2) and the gas expansion due to the rapid burning of the secondary flame makes the initial flame appear to remain stationary[10]. As a result of this rapid burning, the temperature and pressure in the endgas section are raised considerably above the other sections. A pressure wave is propagated from this pressure discontinuity which is reflected back and forth through the chamber at acoustic frequencies ranging from approximately 5-10 KHz[11].

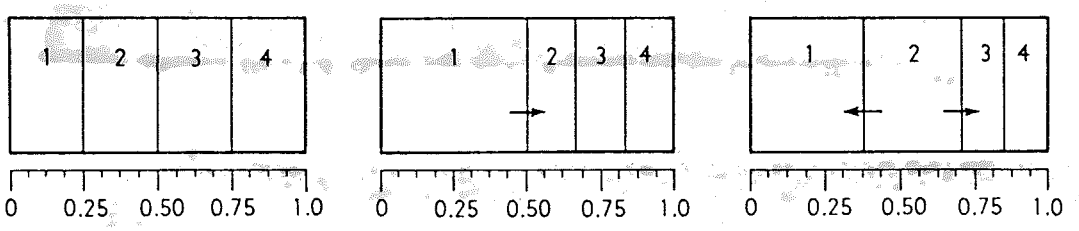

Figure 2.4 Compression of unburned and burned gases as the flame proceeds through the hypothetical combustion chamber.
(a) Flame is initiated in section 1;
(b) propagates through section 1;
(c) propagates through section 2.[8]

This causes the cylinder walls and other engine components to vibrate at this frequency. External to the engine the vibrations propagate pressure waves at the same audible frequency giving auto-ignition the alternative rendering knock or ping.

The pressure differential created by auto-ignition within the combustion chamber increases the gas turbulence, causing the gas to scrub the cylinder walls. This action reduces the laminar air-fuel film thickness in the flame quench zone and increases the heat transfer from the combustion gases to the chamber surfaces. Therefore the temperature of

the cooling medium increases and that of the burnt gases decreases.

If the knocking combustion and resulting turbulence is heavy then the extra energy transferred to the coolant will cause the engine power output to decrease. Sustained operation under these turbulent conditions leads to eventual pitting of the chamber surfaces and high temperature fatigue (Fig. 2.5); both effects shortening the life of the engine[12]. Since heavy knock raises the engine operating temperature through increased heat transfer, it also encourages pre-ignition.

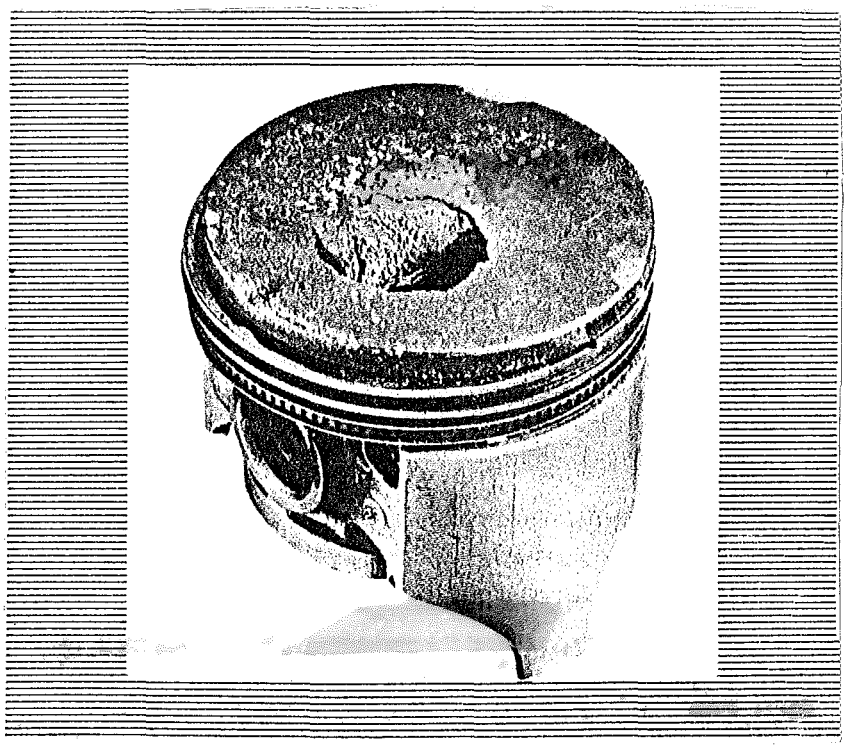

Figure 2.5 The effect of high temperatures and shock waves on a piston, caused by severe high speed knock[13].

2.1.2.3 Pressure crankangle diagrams during auto-ignition

The pressures within the chamber can be detected by a pressure transducer mounted in the cylinder head and a pressure crankangle diagram of knocking combustion is illustrated in Figure 2.6(a). The reflected pressure wave is recorded as a sawtooth waveform superimposed on the last section of the pressure trace with a frequency equivalent to the frequency of the knocking sound emanating from the engine. The pressure oscillation waveform resulting from the auto-ignition of the endgas can be amplified by differentiating the pressure transducer output with respect to time and the result is shown in Figure 2.6(b). This diagram can be alternatively described as a pressure rate diagram and it helps to clarify the point when knock is present during combustion.

Pressure rate diagrams of knocking combustion (Fig. 2.7) taken at several different compression ratios show that the knock intensity may vary depending upon the amount of endgas which auto-ignites. In the low compression ratio case of Figure 2.7(a), knock is not measurable.

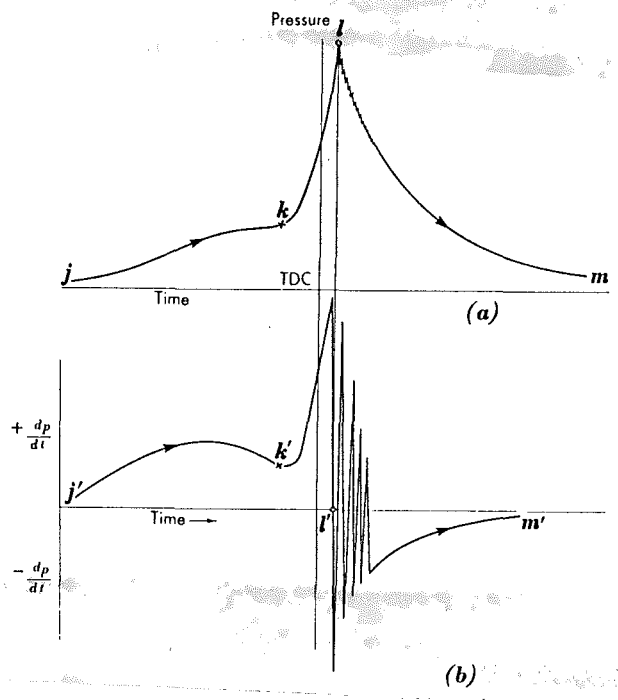

Figure 2.6 Pressure (a) and pressure rate (b) diagrams of knocking combustion[8].

However, as the compression ratio, and therefore combustion temperatures and pressures, are raised a small amount of endgas auto-ignites and causes a break at point A in Figure 2.7(b). The break is followed by high frequency pressure oscillations that provide evidence that knock is present although it is inaudible to the ear. This degree of knock intensity is defined as light knock, a subjective definition but consistently used within this report. At the highest compression ratio the knock is more severe as a larger portion of the endgas auto-ignites and so the engine is defined to be operating in a state of heavy knock. Continued engine operation in this condition is likely to shorten the life of the engine.

In summary knock or auto-ignition develops in the Spark Ignition engine when the endgas temperature is higher than that required for normal combustion so that the shorter induction period of the endgas elapses before it is burned by the primary flame. Consequently, several highly stressed points in the endgas self-ignite forming a second flame which propagates rapidly through the rest of the unburned mixture. It is the endgas region which is self-igniting.

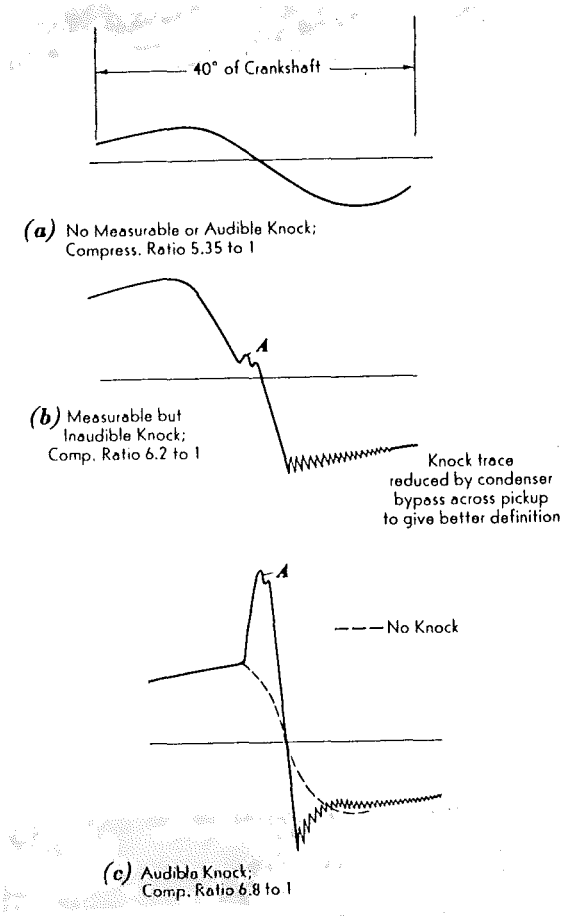

Figure 2.7 Auto-ignition on the pressure rate diagram at three different compression ratios[8].

2.1.3 Pre-ignition

Returning to Figure 2.4, the observation was made that as the flame passed through section 2 of the chamber, the previously burned gases in section 1 would be re-compressed. Similarly, as section 3 burns, it will further compress not only the endgas in section 4, but also further compress the burned gases in sections 1 and 2, implying that the different compression histories of each section will result in a final temperature gradient established within the chamber. A quantitative analysis[8] (p.102), reveals that the temperature will be highest in section 1 and coolest in section 4. During knocking combustion the higher overall combustion temperatures will further accentuate the high gas temperatures in section 1 severely heating the combustion chamber surfaces in this section so that they may cause a subsequent fuel-air mixture to self-ignite before the spark discharge. This is termed pre-ignition and will cause even higher operating temperatures to prevail because combustion is initiated earlier on the compression stroke which raises the pressures and temperatures at TDC and creates higher combustion temperatures.

Therefore the process is often self-perpetuating.

Pre-ignition in a multi-cylinder engine is often destructive since one particularly vulnerable cylinder is likely to pre-ignite while the others run as normal. The reverse piston force in the pre-igniting chamber then opposes the direction of crankshaft rotation, placing severe stress on the connecting rod. Alternatively, the high pre-ignition temperatures may cause failure of a piston crown (Fig. 2.8).

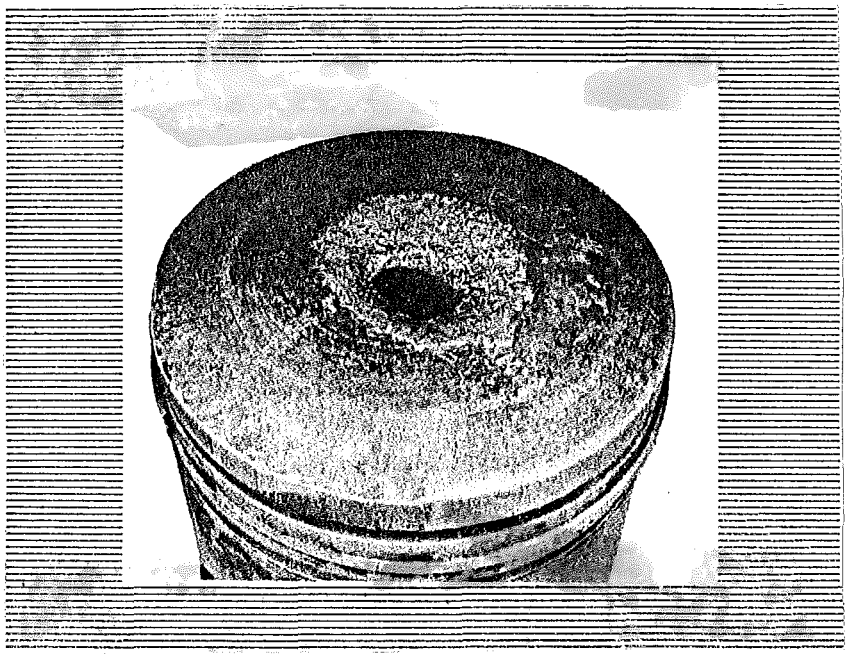

Figure 2.8 The effect of predominantly pre-igniting combustion on the piston, causing high speed fusing[13].

2.2 The Effective Combustion Process

Three processes of possible hydrocarbon combustion have been described: normal combustion, auto-ignition and pre-ignition. The type of combustion best suited to the Spark Ignition will next be considered with regard to meeting the following combustion objectives:

1) Minimum brake specific fuel consumption for any given power output.
2) Minimisation of engine roughness through sudden pressure variations.
3) Freedom from objectional knock.
4) Minimum heat loss to the coolant.

Minimum brake specific fuel consumption for any given power output during the combustion process can be achieved by creating the highest possible expansion ratio from reactants to gaseous products. Therefore the process should remain at constant volume until combustion is

completed in order to enable the highest possible pressure to be developed before expansion. To meet these requirements in the Spark Ignition engine where the combustion chamber volume is continually changing, the combustion process would need to occur instantaneously at TDC.

The minimisation of engine roughness can only be achieved by eliminating sudden pressure variations during the combustion process. In order to create a smooth pressure distribution, instantaneous combustion cannot be considered since it would be too violent. Instead, the combustion pressure should increase to its peak value at a maximum rate of about 250 kPa/deg at medium engine speeds[8]. Such a compromise will undoubtedly lower the thermal efficiency from combustion since maximum pressure must now occur somewhat after TDC, lowering the effective expansion ratio of the gases. It is found for petrol powered Spark Ignition engines that the peak pressure should occur between 5 and 20° after TDC for a satisfactory compromise[14].

Freedom from objectionable knock is necessary since heavy knocking combustion reduces engine life and can lead to pre-ignition. However, some degree of knocking combustion can be desirable in some circumstances, since normal hydrocarbon combustion in an engine does not usually yield a pressure increase rate of 250 kPa/deg. Light knocking combustion can produce a pressure increase rate closer to this value since the auto-igniting flame comsumes the endgas more rapidly.

Heat loss to the coolant must be minimised to increase the engine power available through gas expansion. Heat transfer can be minimised by ensuring that heavy knocking combustion with the associated high gas turbulence does not prevail.

It appears from these considerations that effective combustion in the Spark Ignition engine will be achieved through the normal combustion process where one flame traverses the entire combustion chamber or possibly through light knocking combustion during periods when maximum power is demanded.

2.2.1 Normal Combustion Considerations in the Spark Ignition Engine

The normal process of combustion will be influenced by attention to engine combustion chamber design, the type of fuel used in the engine, and by appropriate control of the ignition advance system. A pressure crankangle curve produced by such an engine is shown in Figure 2.9[7].

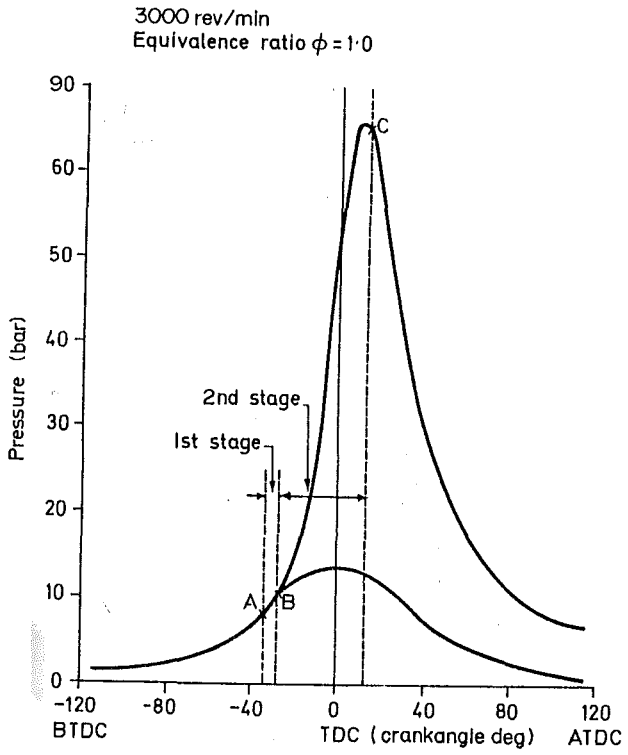

Figure 2.9 A typical indicator diagram showing the two stages of combustion. Stage 1 (A-B) and Stage 2 (B-C)[7].

Auto-ignition has not occurred since there are no high frequency pressure oscillations evident on the trace. During stage 1 from points A to B the combustion is initiated by the spark which occurs for approximately 6°[15] and establishes a flame kernel. As can be seen from Figure 2.9 no significant combustion pressure is developed during this stage. During stage 2 from B to C the flame propagates throughout the rest of the combustion chamber and the pressure increases to its peak value at approximately 10° after TDC. This ensures a peak pressure adequately close to TDC for efficient combustion while minimising negative work through pressure build-up before TDC. The whole of stage 2, the flame development stage, generally takes 35% of the total combustion time[16].

The rate of pressure increase given from the curve is approximately 175 kPa/deg, which is lower than the 250 kPa/deg 'roughness limit' perhaps because of the tendency of the fuel used to auto-ignite if the combustion rate is further increased towards this limit. Such auto-ignition could be used to improve the combustion efficiency during periods of power demand from the engine. The increased efficiency from the hastened endgas consumption would bring the pressure increase rate closer to 250 kPa/deg and bring the peak pressure closer to TDC.

The degree to which the improved combustion properties of light knocking combustion are utilised must be evaluated against any reduction in engine life that this type of combustion may create. Heavy knock is always undesirable since it reduces power, increases the likelihood of pre-ignition and will severely shorten engine life with continuous operation.

Clark et al.[17] made a comparison of the extent to which various vehicle manufacturers utilised the improved efficiency of light knocking combustion. They concluded that several makes of vehicle showed a much higher incidence of light knock than others.

2.3 The Influence of Ignition Timing on Combustion

It has been mentioned that the combustion process will be influenced by the ignition timing. The ignition timing may be used to control the combustion process while an engine is in operation so that the combustion process most nearly approximates the four previously defined objectives for effective combustion.

By adjusting the spark timing the position of the pressure peak after TDC can be controlled. As the spark timing is advanced the combustion process is initiated earlier on the compression stroke and is completed earlier on the expansion stroke, so that the pressure peak is correspondingly advanced. The ignition timing can therefore be used to ensure the peak pressure falls within the 5-20° after TDC region to give effective combustion performance. When the peak pressure falls within this crankangle region, the ignition advance is defined to be set to MBT (minimum advance for best torque).

In order for the ignition timing to maintain the peak pressure at MBT throughout the engine speed range, it must be progressively advanced with increase in engine speed. The formation of the flame kernel (Fig. 2.9; stage 1) from the spark is a relatively constant time process as it is affected primarily by chemical properties of the fuel mixture rather than its physical properties. The explosion at this stage is chain branching rather than thermal in nature (see Chapter 4). With increase in engine speed the kernel formation will therefore take place over a greater number of crankshaft degrees and this is compensated for by advancing the timing with increase in engine speed. The second stage of combustion (Fig. 2.9; stage 2) occurs over a relatively constant crankshaft angle since the flame propagation rate increases approximately

linearly with engine revolutions by way of increased gaseous turbulence. Minimal ignition advance compensation is required to ensure this stage is completed soon after TDC at any speed. Overall compensation for variations in stages 1 and 2 on a function of engine speed, is normally accomplished through the use of a centrifugal advance mechanism or through electronic control.

Alteration of the spark timing also has a second effect which is to alter the overall combustion rate and thus the pressure increase rate. When the spark timing is advanced, more of the mixture burns on the compression stroke increasing the endgas temperature and pressure and causing it to burn more quickly which increases the overall combustion rate. Under certain conditions advancing the ignition timing will create enough temperature stress on the endgas so that it self-ignites and knocking combustion prevails.

Alternatively the ignition timing can be used to ensure the combustion rate is never increased to the extent of objectionable knock. Such knock is likely to occur when the engine is operating with little pressure depression across the throttle plate when high compression pressures and temperatures would shorten the endgas self-ignition delay. The ignition timing should be retarded during these operating conditions to sufficiently lower the stress on the endgas.

In contrast, with high depression across the throttle, the lower compression pressures and temperatures will make the endgas less susceptible to self-ignition. Under these conditions the ignition timing should be advanced until the peak pressure occurs at MBT. Therefore the timing is normally advanced in proportion to the depression across the throttle by means of a mechanical or electronic vacuum related advance system.

In general the ignition timing may also be used to compensate for other variations in engine operating conditions which affect the stress on the endgas and the overall combustion rate. These include the engine coolant temperature, vehicle altitude, ambient temperature, type and octane rating of the fuel used, and whether the engine speed is transient or steady state. These variables are best controlled by electronic systems as described in Chapter 3.

It is evident that since the ignition timing affects both the crank-angle of peak pressure and the combustion rate, it cannot influence them independently of one another. In practice, the timing should be advanced until one of these two variables has reached a boundary limit for efficient controlled combustion. Thus, when a high compression ratio engine is operating at high load with low manifold vacuum, the ignition timing will be used to ensure that knocking combustion does not occur. Alternatively, at low loads, the endgas is unstressed and not susceptible to auto-ignition so that the ignition timing can be advanced until the peak combustion pressure occurs between 5 and 20° after TDC.

2.3.1 Ignition Advance on the Crankangle Diagram

The effect of advancing the ignition timing when the endgas is unstressed is shown in Figure 2.10. The engine which provided these pressure crankangle diagrams was operated at 1800 rpm with a compression ratio of 7:1[18]. A small advance leads to a pressure too far retarded from TDC so that the effective expansion ratio is reduced as is the power. This would be the case with the ignition timing set to 9° BTDC. If the ignition timing is too far advanced, for example 39° BTDC, the average power of combustion also decreases because a large area of pressure build-up and therefore negative work occurs before TDC.

For this engine and these operating conditions, if maximum power occurred 12° after TDC, then the ignition advance should be set to 29° BTDC.

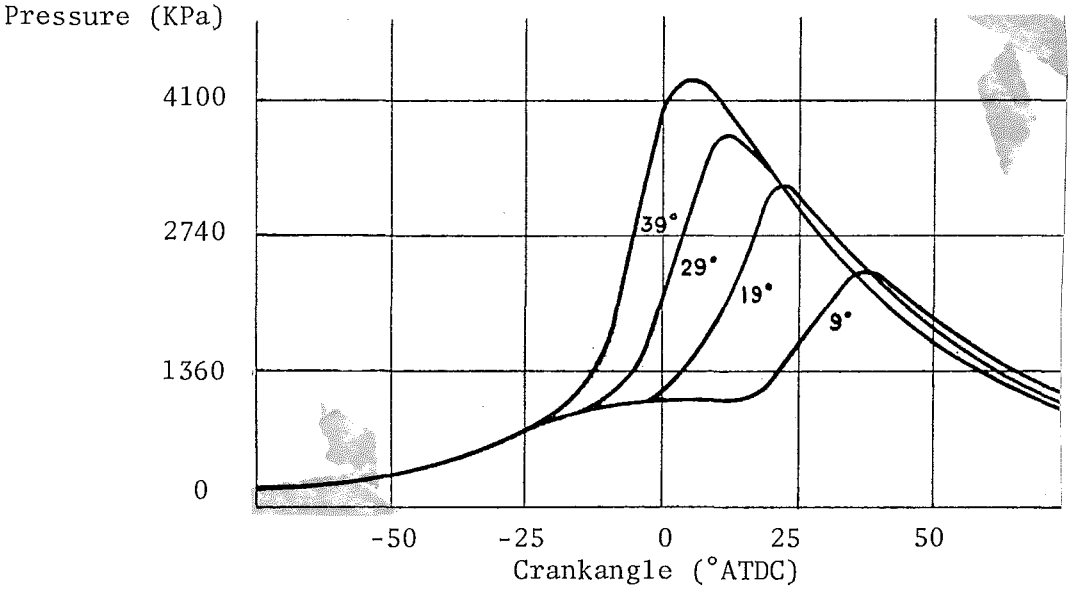

Figure 2.10 The effect on cylinder pressure of advancing the ignition timing[18].

Then the pressure peak would be adequately close to TDC without creating too much pressure build-up and negative work before TDC.

From Figure 2.10 it is also evident that advancing the timing will lead to an increase in the amplitude of the peak pressure. This is because more of the fuel-air mixture has burned before TDC so that the compression pressure on the unburned gas is greater at TDC increasing the effective expansion ratio.

CHAPTER 3

IGNITION TIMING CONTROLLERS FOR THE SPARK IGNITION ENGINE

CONTENTS

INTRODUCTION

The engine control variables which can conveniently be adjusted while a Spark Ignition engine is in operation, are the air-fuel mixture ratio, the ignition advance, the exhaust gas recirculation rate, and the thermactor air rate. The latter two variables are introduced into the combustion chamber and exhaust system respectively in order to reduce exhaust emissions (see Appendix 3.1). Two other parameters which could possibly be controlled in the future are the valve timings and the compression ratio; however, at present these are generally fixed at the time of engine manufacture.

This chapter will summarise the developments in ignition timing control techniques, particularly on vehicles supplied to the United States market over the last decade. Initially the common mechanical advance system will be compared with an ideal spark advance system, and then some of the electronic microprocessor based systems, which approach this ideal, will be reviewed. Finally the fully adaptive microprocessor based spark advance control system will be discussed along with the proposal for an adaptive transducer which is further investigated in succeeding chapters of this report.

3.1 Control Techniques for Meeting Exhaust Emissions and Fuel Economy Regulations

During the 1970's and 1980's more accurate control of the engine operating variables (e.g. air-fuel ratio and ignition timing), was necessitated by the introduction of fuel economy and exhaust emission regulations in the United States of America, Europe and Japan. The United States vehicle market is the largest and has perhaps the most stringent engine performance regulations. In 1977 the U.S. Clean Air Act required certain automobile manufacturers to have developed engine control technology capable of meeting exhaust emission levels of 0.41 g/mi HC, 3.4 g/mi CO and 0.4 g/mi NOx[19]. The Federal Regulations have progressively tightened since then (Table 3.1) requiring continual engine control systems refinement.

In 1985 a 27.5 m.p.g. fuel economy standards programme will be introduced in America requiring the fuel consumption averaged out over all sizes of new cars to be at least 27.5 m.p.g. An examination of the commercial feasibility of this legislation[20] using pessimistic and optimistic scenarios, concludes that over the life of the motor vehicle the savings in petrol to vehicle owners will outweigh any resultant increase in new car prices by $US444 or $US751 respectively. These two scenarios take into account increases in fuel prices, component prices etc. over the life of the vehicle. The study suggests that the introduction of the 1985 regulations in the U.S. will represent a saving to the community as a whole and atmospheric pollution will be reduced.

	49 STATE	CALIFORNIA HC/CO/NOx (g/mile)	CAFE* (m.p.g.)
1978	1.5/15/2.0	.41/0.0/1.5	18
1979	1.5/15/2.0	.41/9.0/1.5	19
1980	.41/7.0/2.0	.41/9.0/1.0	20
1981	.41/3.4/1.0	.39/7.0/0.7	22
1982	.41/3.4/1.0	.39/7.0/0.7	24
1983	.41/3.4/1.0	.39/7.0/0.4	26
1984	.41/3.4/1.0	.39/7.0/0.4	27
1985	.41/3.4/1.0	.39/7.0/0.4	27.5
	*Corporate Average Fuel Economy		

Table 3.1 Emission and fuel economy requirements[21]

The introduction of these stringent regulations has been accompanied by a corresponding improvement in the combustion efficiency of the Spark Ignition engine. In particular, the ignition advance control mechanism has been refined in order to increase available power and reduce the exhaust emissions while maintaining good engine flexibility and vehicle driveability.

3.2 Mechanical versus Idealised Ignition Timing Control

A plot of the spark advance against engine speed and load when the timing is controlled mechanically by centrifugal and vacuum advance yields a multiplanar surface similar to that of Fig. 3.1. Evidently the surface is a compromise dictated to by the simplicity of the control system, since the topography of ignition timing for maximum combustion efficiency for the same engine is shown in Fig. 3.2. This surface follows the knock limit when the engine is prone to knock and otherwise, under lighter loads, follows the minimum ignition advance for best torque (MBT), that is, the minimum advance required to ensure the pressure peaks 5-20° after TDC, (refer to Section 2.3).

Schwarz[23] has made a comparison of mechanically controlled ignition timing versus optimum ignition timing on a 1.6ℓ medium sized vehicle. It was run on the ECE test (dynamometer test schedule) using a 1250 kg inertia flywheel and an air-fuel equivalence ratio set to either $\lambda = 1$ or $\lambda = 1.15$ (excess air). The results in Table 3.2 indicate that the fuel consumption may be considerably reduced through appropriate control of the ignition timing.

An analysis of these results reveals that during idle periods the ignition can be advanced beyond the mechanical setting and this reduces fuel consumption by 15%. This idle advance cannot be reproduced with mechanical advance systems because cranking and idle ignition settings are identical and starting an engine becomes difficult with timing much earlier than 20° BTDC. Because of the high proportion of idle time in the ECE test, this reduced the test consumption by 3-4%.

In the lower engine speed and load range the mechanical advance unit may be 10 - 15°[23] too far retarded. This is because the steepness of the centrifugal advance unit is limited and the vacuum advance mechanism itself can only control the timing by way of one simple advance rate. Optimal setting of the ignition timing in this region yields a 10% reduction in fuel consumption, improved flexibility of engine operation and better acceleration.

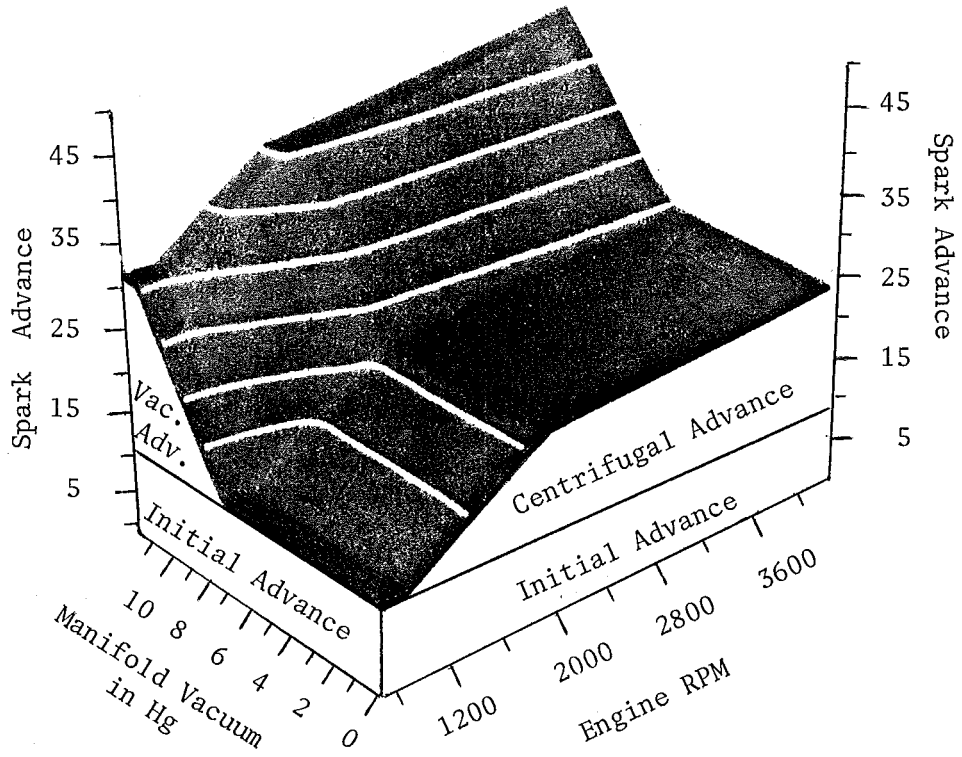

Figure 3.1 Conventional timing advance topography as a function of engine speed and manifold vacuum[22].

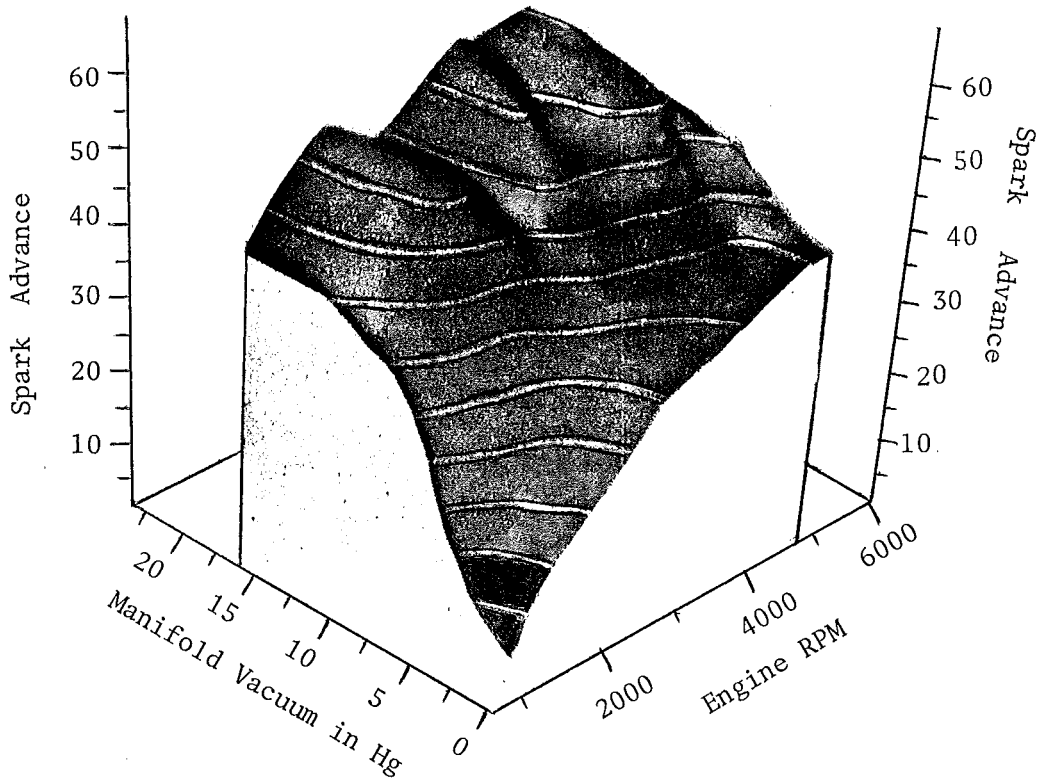

Figure 3.2 Optimal timing advance topography as a function of engine speed and manifold vacuum[22].

	Fuel Consumption 1/100 km	%
Mechanical spark advance Excess-air ratio $\lambda \approx 1.0$	12.6	100
Optimum spark advance adapted to maximum fuel economy Excess-air ratio $\lambda \approx 1.0$	11.2	89
Mechanical spark advance Excess-air ratio $\lambda \approx 1.15$	11.7	100
Optimum spark advance adapted to maximum fuel economy Excess-air ratio $\lambda \approx 1.15$	10.8	93

Table 3.2 Fuel consumption of a medium sized car with a 1.6ℓ cylinder engine run on the ECE test (hot)[23].

At high engine loads the ability of an optimal controller to follow the knock limit further reduces fuel consumption and improves engine torque. Mechanical systems require a retarded safety margin of up to 20° when operating in this region to allow for variations in fuel octane rating, engine condition and manufacturing tolerances in the distributor drive and timing drive mechanisms[24,25].

Further improvement in engine efficiency could be obtained by raising the compression ratio; however, this increases the likelihood of knocking combustion. If the compression ratio is increased the timing must be retarded for the new knock limit further than the new advance curve for maximum torque. Then the advantage of increasing the compression ratio is lost with a mechanical advance unit because whenever power is demanded from the engine, knock becomes prevalent and an added safety margin must be imposed between the ignition point and the knock limit. On the contrary, it has been suggested that optimal control systems could utilise the greater efficiency of a higher compression ratio by almost complete removal of this mechanically imposed safety limit[26].

Along with these benefits over conventional control, more complex control has become necessary because of other recent engine developments. Turbo-charged vehicles are becoming increasingly popular, requiring knock sensitive controllers, and as fuel prices continue to increase, vehicles which burn

lean fuel-air mixtures are being developed which place new demands on the ignition advance system.

Turbocharged engines become susceptible to knocking combustion when operating at boost pressures because the higher compression pressures and temperatures during boost make the endgas region more vulnerable to auto-ignition. The mechanical advance system knock safety margin, which must be imposed under these conditions to account for mechanical tolerances, reduces some of the benefits of turbocharging in a similar way as an increase in the compression ratio. Therefore turbocharged vehicles require more refined ignition timing control and are normally equipped when the turbochargers are factory fitted[11].

The air-fuel mixture ratio may be made more lean to improve the vehicle fuel economy during cruising conditions[27]. However, combustion considerations show that the flame development time increases as the mixture strength is weakened, so that the ignition timing system must compensate by increasing the spark advance angle before TDC (top dead centre)[28]. If the fuel mixture is made lean only during vehicle cruise periods, the ignition timing controller must be sensitive to this and respond with appropriate advance.

When a vehicle is cruising and maximum power is not demanded from the engine, exhaust emission levels become an important criteria for engine control. In order to reduce the level of NOx emissions, the timing must be retarded since this ensures lower combustion temperatures and consequently reduces the level of nitrous oxide emissions. Also during engine warm-up the timing can be retarded to reduce the exhaust emissions. The ignition timing controller should be sensitive to these conditions in countries where exhaust emissions are of concern.

3.3 Pre-programmed Electronic Ignition Timing Controllers

Optimal ignition timing which can respond correctly to the above requirements, represents an ideal which can only be approximated in any practical control system. Microprocessor control of the ignition timing can offer better approximation to the ideal than can a mechanical system because it can be made as sensitive as the control system designer desires[29,30]. Any number of engine operating parameters can be sensed and fed into the microprocessor and it can control any number of engine variables[31,32,33].

3.3.1 The GM(MISAR) and Ford Control Systems

A good example of a microprocessor based ignition timing controller is the MISAR. This was the first microprocessor control unit to be used on a production vehicle and it was introduced on the 1977 standard model Oldsmobile Toronado manufactured by General Motors[22].

The input signals to the MISAR (Microprocessed Sensing and Automatic Regulation) controller are primarily crankshaft angle, TDC reference signal, intake manifold vacuum and coolant temperature. The microprocessor processes these inputs and then retrieves the appropriate dwell angle and ignition advance from a pre-programmed memory map. The output is fed to a simplified high energy ignition distributor which completes the system.

The crankshaft angle and TDC reference signal are sensed by a toothed disc mounted to the front of the crankshaft. The magnetic reluctance of the metal teeth is sensed by a hall effect transducer and the signal is shaped and amplified by circuitry at the sensor site giving approximately 0.6 crankshaft degree resolution. The amplification occurs at the transducer so that the weak transducer signal will not deteriorate due to high frequency interference from the high tension system by the time it reaches the microprocessor.

The intake manifold vacuum is sensed by an integral strain gauge and silicon diaphragm which deflects in response to the differential between atmospheric and manifold pressure. The resistive change forms part of a resistance bridge and is amplified by an integral electronics network to give an output voltage proportional to sensed pressure differential. The circuitry is designed so that the output signal is ratiometric with the supply voltage to eliminate any errors caused by fluctuations in the supply voltage. This is an important consideration in the application of electronics to the automotive environment.

The coolant temperature sensor is based on a thermistor. This requires the non-linear analogue output from the thermistor to be passed through an A to D convertor and then to be linearised by microprocessor software.

The microprocessor is mounted in the passenger compartment as a tradeoff between long input lead length and minimisation of high frequency interference from the high tension ignition system. The microprocessor itself consists of two metal-oxide-silicon/large-scale-integration (MOS/LSI) chips,

each approximately the size of a postage stamp. These two, along with the quartz crystal oscillator and comparitor, are mounted on a ceramic substrate on the printed circuit board assembly of Fig. 3.3 The largest device at the centre of the substrate is the CPU. The other MOS/LSI device is the read only memory (ROM) chip with 1024 ten-bit words of memory. This memory must be programmed upon manufacture and it contains the dwell angle and ignition advance data.

The pre-programmed ignition advance data is variously termed an ignition surface, memory map or look up table, since it contains more than 200 ordered triples of engine speed, manifold vacuum and required advance covering the complete range of engine operation. The microprocessor determines the ignition advance by selecting the correct triple from memory, dependent upon the engine speed and manifold vacuum inputs. The triples each approximate a small region of the ignition advance surface being dispersed at every 200 r.p.m. and 1.5 inches of vacuum. There is a separate region of ROM memory which contains a look up table to modify the ignition advance timing according to the coolant temperature.

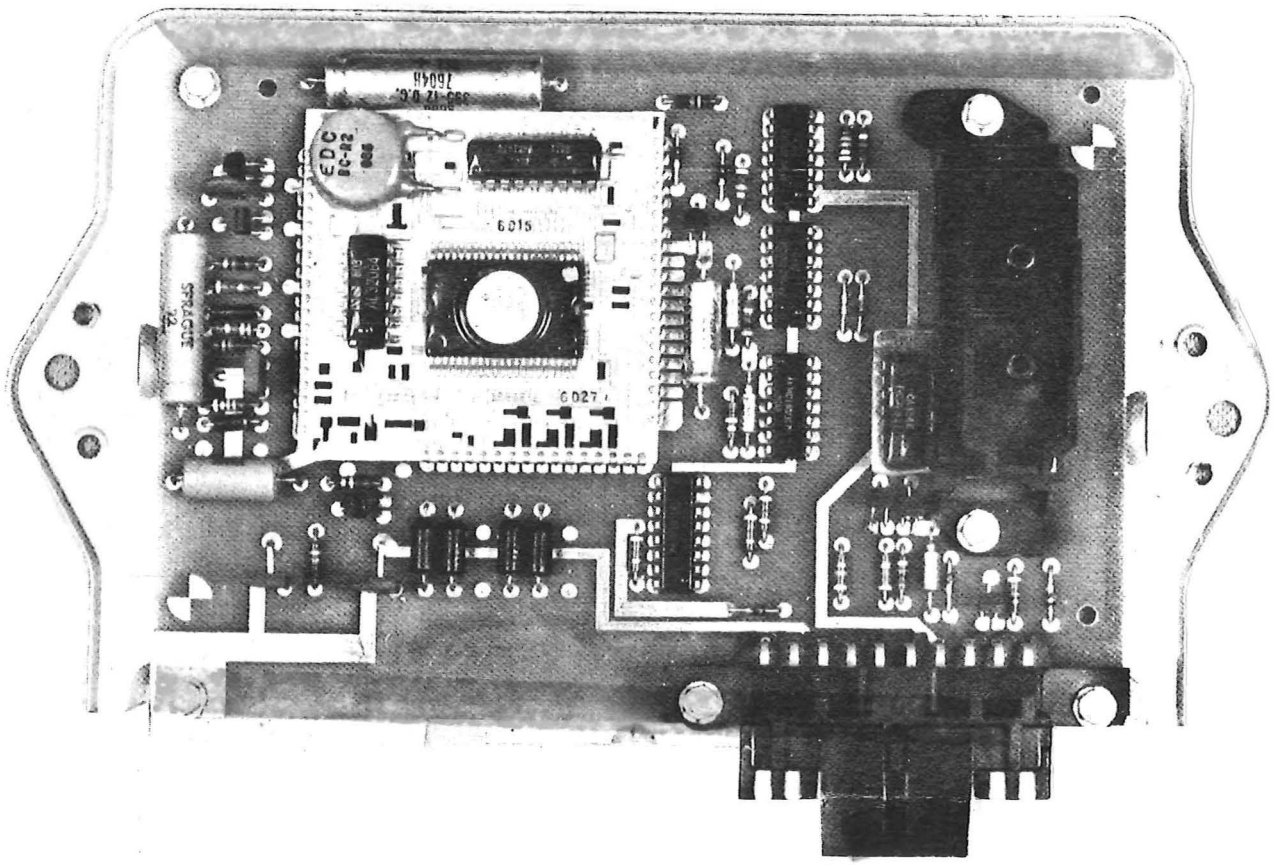

Figure 3.3 Microprocessor substrate assembly. Quartz crystal at upper left; ROM to its right; CPU in centre; and linear quad comparitor[22].

The microprocessor operates asynchronously from the engine by means of its own quartz timing clock having a serial word time of 36 microsecs. With a typical program cycle of about 335 instructions, the system is able to up-date the spark timing every 12 milliseconds.

During engine start-ups the microprocessor control is disabled and the timing is fixed at 20 BTDC. This provides efficient operation during cranking when the supply voltage may have dropped to 4 volts during which time correct operation of the microprocessor is not assured. This fixed timing is also selected if one of several malfunctions occur within the microprocessor control system so that the vehicle is not completely disabled.

In determining the best ignition advance surface (Fig. 3.2), G.M. made economy and driveability high priorities. The ignition timing was advanced either to MBT values where possible or to the knock limit when this occurred earlier than MBT. Then in the operating conditions where emissions control was important, the timing was sufficiently retarded to an acceptable value in order to reduce emissions.

The resulting surface topography of Fig. 3.2 includes valleys corresponing to the automatic shift sequence, peaks for conditions requiring full advance and a butte for moderate speed/light load economy. A Toronada equipped with the MISAR system averages 1.2 m.p.g. better economy, lower exhaust emissions, excellent driveability, and is likely to produce more power when it is demanded.

General Motors have continued to improve their microprocessor based control system since the introduction of the MISAR system in 1977[34]. In 1981 they developed the C-4 system which added control of the exhaust gas recirculation (EGR) system, the catalytic convertor and the fuel mixture ratio. The C-4 ignition timing control system was an extension of the MISAR system with the advance angle becoming the algebraic sum of five tables stored in memory:

1. The previously described MISAR system load and r.p.m. table gives the main advance.
2. Steady state advance. If the engine is operated under steady state conditions for long enough, it is found that the ignition timing may be advanced slightly further. The degree of extra advance is based on r.p.m. load and temperature conditions.

3. Coolant advance. Modifies the main advance (point 1) according to coolant temperature.
4. Altitude advance. Modifies the main advance (point 1) according to altitude.
5. Start up advance, unlike MISAR, is not fixed but is based upon current coolant temperature minus initial coolant temperature.

Ford Company engineers introduced their first electronic control system on the 1978 model, Lincoln Versailles. This system was developed as a low volume pilot program and utilised seven input and feedback sensors in order to control spark timing, EGR rates and thermactor air interactively. Thermactor air is fed into the exhaust manifold to improve the effectiveness of the catalytic converter in oxidising CO and reducing NOx.

During 1978 and 1979, Ford introduced two other microprocessor based systems, the second of which was capable of controlling the four key engine operating parameters: ignition timing, air-fuel ratio, EGR flow rate, and thermactor air. (See Appendix 3.1.)

The ignition advance was controlled through the use of look-up tables in the microprocessor memory similar to G.M's C-4 system ignition tables. Further development of Ford's system is necessitated in order to meet the 1985 CAFE (Corporate Average Fuel Economy) requirements of 27.5 m.p.g. In order to improve ignition control Ford are developing an effective engine knock sensor enabling knock to be directly sensed and controlled by the microprocessor.

3.3.2 Inherent Disadvantages of the Pre-programmed Controller

The Ford and G.M. developed microprocessor control systems have proved successful in controlling the main engine variables, however more sophistication is required in order to meet future economy and exhaust emissions regulations. The systems which have been described rely on pre-programmed ignition timing maps which do not allow for changes in octane rating of the fuel used, alternative fuels, engine wear or engine to engine variations. In order to allow for these unpredictable variations, the rigid pre-programmed ignition surface must be replaced with an adaptive control strategy.

3.4 Adaptive Electronic Ignition Timing Control Systems

In an adaptive control system the combustion process is continuously monitored by the use of appropriate combustion transducers which feed the

state of combustion back to the controller. The controller is then able to suitably alter the ignition timing until the combustion process is rendered most efficient, that is, until the ignition timing is set to MBT or the knock limit.

3.4.1 The Adaptive Controller

The spark advance adaptive control system can be divided into two sub-systems: the input transducer which supplies the vital combustion information, and the controller which adjusts the spark advance in response to the information it receives from the transducer.

The operation of the microprocessor based adaptive controller can be explained with reference to the flow diagram of Fig. 3.4. This diagram describes a logic sequence which could be implemented to bring the combustion to MBT or to the knock limit. The first step is to determine whether the engine is knocking. If it is knocking, the controller will retard the ignition timing until the knock disappears (or the knock intensity drops to an acceptable level).

If the engine is not knocking, the controller will determine whether the ignition timing is set to MBT. This is a two step process:

1. If the pressure is peaking earlier than it should be, for example, at 2° ATDC, the controller will respond by retarding the timing until MBT is reached.
2. Alternatively, if the peak pressure is delayed beyond this optimum region, for example at 25° ATDC, the controller will respond by advancing the timing until the limit for knocking combustion is reached or until MBT, whichever occurs first. It will then maintain the timing at that setting until the engine status changes.

3.4.2 The Adaptive Transducer

The input transducer must supply the necessary information on engine knock and the peak pressure position to the adaptive controller. Over the past five years several semi-adaptive spark advance controllers have been installed in production vehicles. These incorporate adaptive transducers which can input the information to the controller which then responds by retarding the ignition timing accordingly.

Several of these semi-adaptive control systems will now be discussed and then the chapter will conclude with an examination of some alternative

transducers which could be used for inputs to a fully adaptive control system. As yet the author does not know of any such control system which is installed on a production vehicle; however, several experimental systems have been tested and one of these will be reviewed.

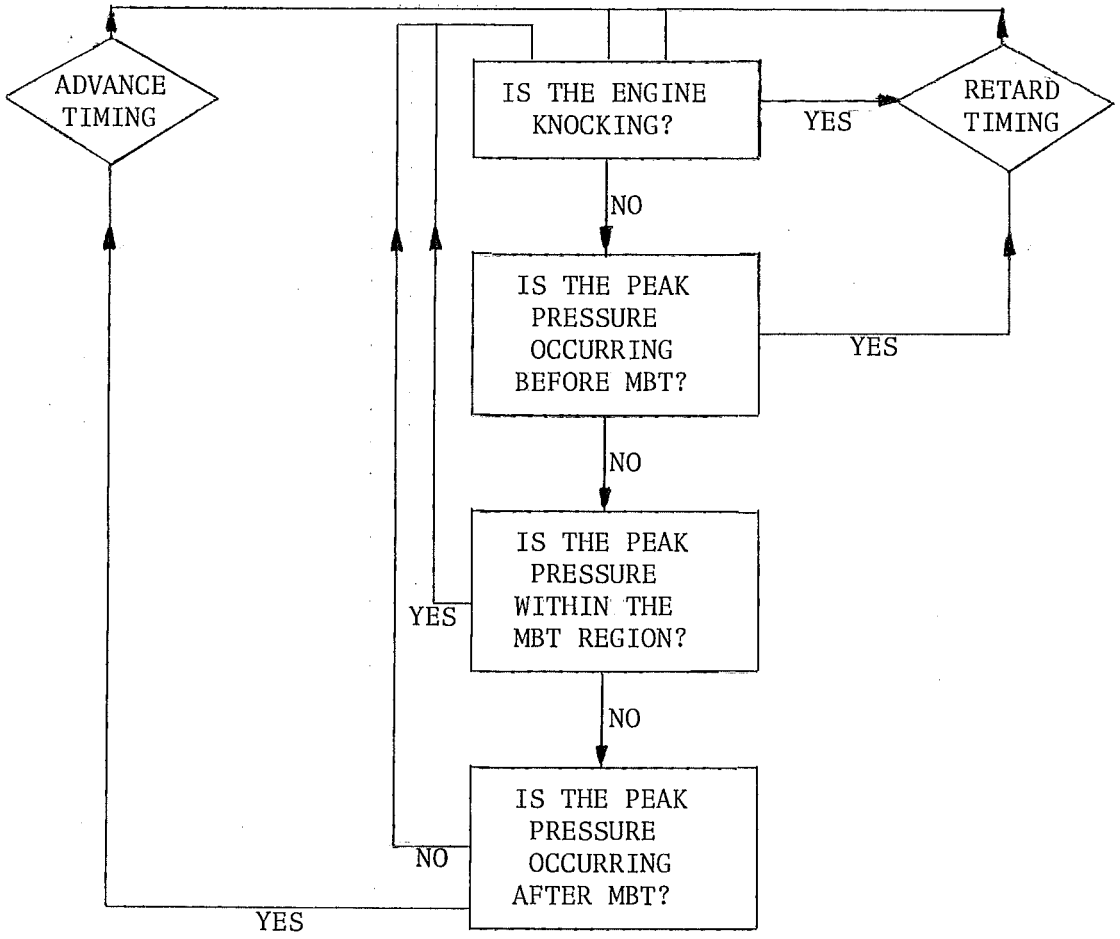

Figure 3.4 Flow diagram showing advaptive controller logic sequence.

3.4.2.1 Semi-adaptive transducers

The detection of knocking combustion itself has, in the past, been achieved by sound recognition, the engine vibration characteristic of knock, combustion chamber pressure and combustion chamber flame intensity. The audible sound of knock (a 'ping') may be heard by ear and this can be helpful in research and testing situations. Knocking combustion also causes the combustion chamber walls to vibrate as a result of the pressure oscillations within the chamber induced by knock. The characteristic frequency of this vibration ranges from 5-10 K Hz and is often sensed by vibration detectors attached to the outside of the combustion chamber, such as the outside of the engine block or cylinder head, or within the

intake manifold.

Automotive manufacturers are beginning to install these vibration sensors or accelerometers as part of a semi-adaptive control system so that the engine can be operated closer to the knock limit. Chrysler have been fitting a piezoelectric accelerometer to V8 powered vehicles destined for California from the 1980 model year. The vibration sensor is mounted in the intake manifold and, when it detects knock, a microprocessor controller immediately retards the ignition timing up to 11°. The timing is then returned to normal at the rate of 2°/second. Saab/Scania mount the piezoelectric accelerometer on the block between cylinders 2 and 3 and use it to control the wastegate opening on turbocharged engines[11].

General Motors have been fitting a magneto-restrictive accelerometer to their turbocharged vehicles since the beginning of the 1980's (Fig. 3.5)[35].

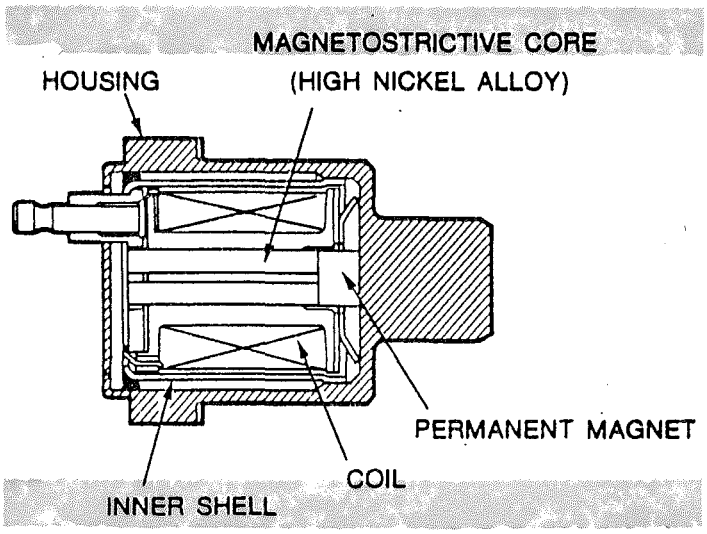

Figure 3.5 Magnetostrictive knock sensor[35].

The output voltage of this sensor is proportional to the vibration level at the knock frequency. The unit is mounted in the intake manifold and reacts to all vibrations within the knock frequency bandwidth including those caused by the valves, pushrods and normal engine cylinder firings. This appears as electrical background noise and when knock occurs, it is selected for by a comparator which subtracts the signal from the noise (Fig. 3.6) and outputs the processed signal to the ignition retard controller. The controller will quickly retard the timing when knock occurs, and then re-advances the spark at a much slower rate. However, it only retards the timing below the standard timing curve and does not advance it to seek

out knock.

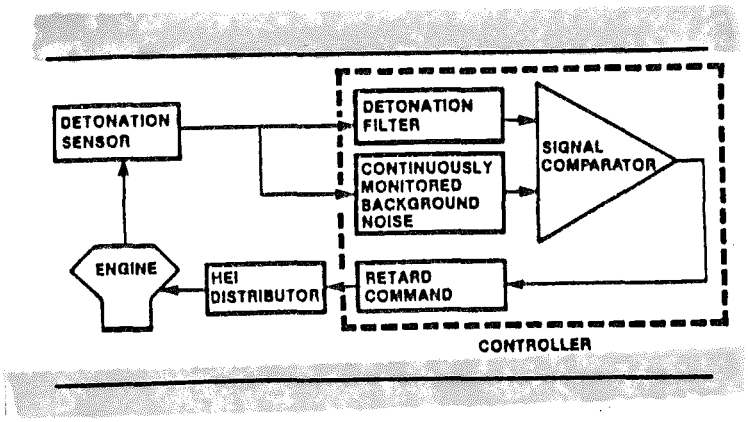

Figure 3.6 Electronic logic for the knock sensor[35].

The disadvantage with all these systems is that they do not monitor the angle of peak pressure so that they cannot select for MBT. They merely retard the ignition timing if the engine begins to knock incipiently.

3.4.2.2 Fully adaptive transducers

In attempting to develop a transducer which is capable of providing sufficient information about combustion to a fully adaptive controller, researchers at Stanford University have developed a piezoelectric washer, (Fig. 3.7)[36]. This washer is positioned under the spark plug when it is installed in the cylinder head. Fluctuating cylinder pressures on the base of the plug cause stress variations on the piezo-washer and these result in a voltage charge produced across the transducer output terminals. The transducer is claimed to be capable of detecting the pressure oscillations associated with knocking combustion and also the position of peak pressure during normal combustion. This would make it capable of supplying sufficient information for fully adaptive spark timing control. This piezo-washer is still not marketed commercially on automotive engines to the knowledge of the author, and this may possibly be due to electrical signal to noise ratio problems, or long term reliability problems since the washer is quite brittle.

Another method which could be suitable for operating an adaptive controller is to directly monitor the cylinder pressure with an appropriate pressure sensor. This transducer will give both the angle of peak pressure and the occurrence of knock through high frequency pressure oscillations. Ceramic-based piezoelectric pressure transducers are the most likely form of

pressure sensor for use in production vehicles.

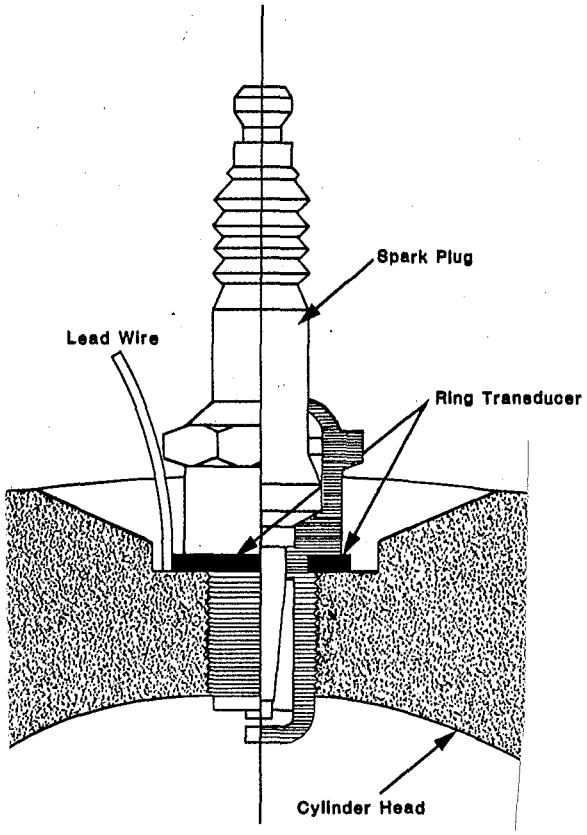

Figure 3.7 Piezoelectric washer mounted under spark plug to detect fluctuating cylinder pressures[36].

3.4.3 An Experimental Adaptive Control System

The use of a piezoelectric pressure transducer as the input to a completely adaptive control system has been studied by Bhot and Quayle[37]. Tests were carried out on a Ford Excort 1100 cc engine with the transducer mounted into one of the cylinders. The output of the transducer was used either to set the timing to MBT or if this induced knock, to set it just below the knock limit.

The test results in Table 3.3 give the peak pressure angle for maximum engine torque for a range of speeds and loads. The table indicates that the peak pressure angle during steady state engine operation tends to fluctuate about a mean value because of cycle to cycle differences in air-fuel ratio, gas turbulence and cylinder charge distribution, all of which alter the flame speed. The pressure angle deviations given in Table 3.3 represent a 95% confidence limit within which the peak combustion pessure should fall.

The adaptive ignition advance system should remain stable in the presence of the peak pressure signal fluctuations so that the controller must perform some form of cycle to cycle averaging on which to base the ignition timing angle. However, under transient conditions of changing engine speed or load, the spark timing controller should respond by advancing or retarding the timing, otherwise during engine acceleration, the ignition will be retarded and, during deceleration, over-advanced[38]. Thus, any timing averaging process designed to overcome cyclic variation problems must be kept to a minimum to enable rapid adaption during engine transients[39].

Speed r.p.m.	Throttle Position	Peak Pressure Angle	Peak Pressure Variation
1540	Low	19°	±3.6°
1506	Half	21°	±4.5°
1516	Full	18°	±45.°
2080	Low	20°	±4.8°
2030	Half	20°	±4.8°
2115	Full	19°	±3.6°
2470	Low	19°	±3.7°
2960	Low	23°	±4.5°
2950	Half	21°	±4.5°
2925	Full	22°	±3.6°
4240	Low	24°	±3.6°
3980	Half	22°	±5.0°

Table 3.3 Peak pressure angle for an Escort 1100 over a range of speeds and loads[37].

Bhot and Quayle suggest an averaging schedule to ensure that:

1. The ignition timing does not vary with peak pressure angle fluctuations during steady state running conditions.
2. Under the most demanding transient conditions, the timing is retarded less than 4° from the ideal. An example of such a transient is when the engine accelerates from 2000 to 2500 r.p.m. in 0.05 seconds.

Such an averaging algorithm is particularly necessary for successful control of small engines where the operating range of the engine is wider, the

load changes are very rapid and the engine is more sensitive to changing operating conditions.

Results showed that the engine fuel economy was improved by up to 5% as compared with a mechanical advance system. Also, the fully adaptive system can compensate for changes in fuel type (see ref. 40), octane rating, engine wear, manufacturing tolerances and discrepancies in component calibration.

They concluded that an adaptive control system could be based upon a piezoelectric pressure transducer and this would maintain the ignition timing to within 2-3° of optimum under steady state conditions. One advantage of such an in-cylinder piezo pressure transducer is its relative simplicity; however, reliability in the harsh combustion chamber environment, especially without water cooling of the transducer, would be a major problem during long term operation.

Adaptive control systems may be required not only to control the ignition timing for best torque, but also to control it as a function of the engine exhaust emissions, particularly NOx[41,42]. In order to achieve this the necessary ignition retard values must either be pre-programmed or an NOx sensor would need to be installed in the exhaust system to provide an NOx level input to the controller. The controller would then adaptively regulate the NOx levels through ignition advance and EGR rates. These extra demands placed on the microprocessor based adaptive controller should not cause any major problems.

In summary, it has been shown that the control of ignition timing has become more refined over the last decade. The advances in the spark timing control systems are summarised in Table 3.4, and range from mechanical control to fully adaptive control systems currently being developed. The main design problem with this latter type of control system is the development of an effective adaptive transducer.

3.5 Combustion Generated Light as the Basis for an Adaptive Transducer

It is possible that the light emitted from the combustion flame could be used as the basis for a fully adaptive transducer. Photographic analysis of the combustion flame has revealed that the properties of the flame light are affected by knocking combustion and cylinder pressure, the basic criteria for sensing knock and the MBT timing.

The remainder of this report examines how the properties of the combustion

flame light are affected by knock and combustion pressure. Firstly the current literature on combustion flame light is reviewed, and then an examination of the suitability of an appropriate transducer is undertaken.

Designation	Type of servo-control	Functions
Simple all electronic	Open loop	Similar to mechanical systems with better precision and time invariability
Sophisticated all electronic	Open loop	Complex map with several intercorrelated input parameters
All electronic with engine knock detection	Partially closed loop controlled (engine knock)	The advance is looped to the engine knock when this appears so as to maintain it to an acceptable level
Self-adapting	Full closed controlled	The advance is looped both to the engine knock and a motor output parameter in order to maintain the latter at an optimum level

Table 3.4 Progress of spark advance control systems[33].

CHAPTER 4

LIGHT EMISSIONS FROM ENGINE COMBUSTION

PROCESSES

CONTENTS

INTRODUCTION

The development of a fully adaptive spark advance control system which responds to changes in the combustion flame light emissions requires a knowledge of how the light is produced and how it is affected by changes in engine operating conditions. The light (or more correctly electromagnetic radiation), is emitted mainly as a result of the chemical reactions which are involved in the air and hydrocarbon fuel combustion process. The wavelength region in which the electromagnetic radiation is emitted is conducive to the application of relatively cheap visible and infra-red radiation detectors.

The chapter will begin with a discussion of the chemical reaction pathway involved in the combustion of hydrocarbon fuel based air-fuel mixtures. This will provide a basis on which to study the electromagnetic radiation which is emitted from various species formed during the chemical reaction pathway as it proceeds from reactants to products.

4.1 Combustion of Hydrocarbon Fuels in the Spark Ignition Engine

The motive power for the Spark Ignition Engine is most commonly supplied through the combustion of hydrocarbon fuels. The molecular structure of the hydrocarbon fuel consists of a chain of single or double bonded carbon atoms surrounded by hydrogen atoms of the correct proportion to electronically stabilise the molecule. When the hydrocarbon fuel is mixed in the correct ratio with oxygen (or air) under the right temperature and pressure conditions, a series of explosive reactions will take place leading, in the main, to stable products of carbon dioxide and water vapour. As the reaction proceeds the high temperatures and large numbers of radicals in the reaction zone cause a steep thermal and radical concentration gradient to the surrounding unburned gas. This concentration gradient causes radical diffusion into, and preheating of, the unburned gas just ahead of the flame until it begins to react explosively. In this fashion the flame self-propagates through the unburned mixture as a travelling wave of combustion. This explosive process forms the basis for the emission of light and other electromagnetic radiation.

The explosion itself is caused by two interacting factors; firstly by the nature of the combustion chemisty which is of the branching-chain type and secondly, by the high temperatures which are produced during the reaction and which rapidly accelerate the reaction rate. These two factors will be treated independently in Section 4.1.1, and then an interactive model will be postulated to explain the overall explosion mechanism which is observed in practice.

4.1.1 Thermal and Chain Branching Explosions

Explosions can result from pure thermal considerations since the self-heating produced by an exothermic reaction dramatically increases the chemical reaction rate. If the heat loss due to conduction, convection and radiation remains equal to the rate of heat production, then the system will remain thermally stable, whereas if the heat loss remains below that of heat production, then auto-catalysis and a thermal explosion will result. Heat losses, which will limit the explosion rate, will be influenced by the shape of the combustion chamber and any changes in the vessel wall temperature.

An examination of the complex series of reactions such as those which exist in combustion processes will reveal that explosions can also result

as a consequence of the chemical reaction pathway. This reaction pathway consists of a network of simultaneous, interdependent reactions called branching-chain reactions.

In these reactions highly reactive chemical entities are formed which then react further to produce more such species. The species involved will normally be free atoms or radicals. The initial production of these species is highly endothermic and once produced they react rapidly with stable molecules to form similar species so that the "chain" process is initiated. Overall, four distinct processes can be identified in a chain reaction:

1) Initiation Reactions

In these reactions, atoms or radicals will be formed by the dissociation of a reactant molecule due to thermal conditions called thermal degradation, radical attack or an external energy source such as an electric spark. Hydrogen radicals could be the first formed in this highly endothermic and hence slow process. The reaction may be catalysed on the combustion chamber walls. The general equation would be expressed

$$I \rightarrow X^{\circ} + R^{\circ}$$

where I is the initial reactant and X and R resulting radical species.

2) Propagation Reactions

Propagation results from a radical attacking a parent molecule to form another active centre

$$X^{\circ} + I \rightarrow Y^{\circ} + P$$

where Y is the new propagated radical and P the product. Y is quite probably different from X. These reactions predominate especially at higher temperatures and in hydrocarbon combustion the OH and H radicals are the major participants.

3) Chain Branching Reactions

Branching is the chain step which is necessary to achieve a non-thermal explosion. It itself is explosive because two or more radicals are formed for each radical consumed.

$$X^{\circ} + I \rightarrow 2Y^{\circ} + \ldots\ldots\ldots$$

This reaction may have a higher activation energy than the propagation reaction with which it competes so that it may not occur very rapidly.

Branching in hydrocarbon reactions often results when a monoradical (H), formed by breaking a single bond,reacts with a species containing a double bond (O). Or else a biradical (O) may react with a saturated molecule.

4) Termination Reactions

Termination results when two radicals combine to form a single stable molecule or to form a molecule and radical which is unable to propagate the chain. Termination is one means by which the branching reaction is prevented from accelerating without limit as it competes for active centres:

$$X^{\circ} + Y^{\circ} + M \rightarrow XY + M.$$

The third body M is required to dissipate excess energy from the highly exothermic reaction. These reactions predominate in the post flame region and liberate perhaps 75% of the total charge in enthalpy rendering them essential to the engine combustion process.

An explanation of the interaction between the thermal and radical explosion mechanisms will now be given as suggested by Gaydon and Wolfhard[46].

Thermal conduction plays an important role in the overall combustion process, this being apparent from the increase in burning velocity the more a mixture is pre-heated. However, a purely thermal explosion would only occur with short induction times at very high tempratures so that at normal engine temperatures it must be initiated from an ignition source. In a spark-ignition engine the spark initiates the chain reaction process by producing the necessary population of free radicals. Flame initiation and propagation at the leading edge of the flame front is then caused by radical diffusion from propagation and branching reactions just behind the flame front. Then the flame propagation can occur at appreciably lower temperatures than a 'pure' thermal explosion.

Flame propagation, however, cannot be explained entirely by radical diffusion without also considering heat transfer. If this were not so then the addition of free radicals to an unheated mixture would be sufficient to initiate an hydrocarbon explosion. Instead it is found that the radical furnishing propagation and branching steps are sufficiently endothermic to require an activation energy which can be supplied thermally. The flame propagation, therefore, depends both on heat transfer and radical diffusion and the less efficient process will tend to be rate determining.

4.1.2 Zones of Hydrocarbon Oxidation

The oxidation of hydrocarbons through these branching-chain reactions can be divided into two distinct processes termed low temperature oxidation below approximately 400°C, and high temperature oxidation above this temperature. Low temperature oxidation consists of a series of reactions which proceed relatively slowly and end in products such as aldehydes, ketones, alcohols and alkenes which do not represent the equilibrium products. However, small amounts of the final combustion products such as water vapour and carbon oxides are formed also, and so a study of low temperature oxidation helps give some understanding of how the high temperature oxidation system proceeds. In the high temperature case the reactions continue almost to equilibrium, the final chemical composition being mainly carbon dioxide and water vapour with very low concentrations of partially oxidised hydrocarbons and nitrous oxides.

Both the low temperature and high temperature reaction zones are in evidence in the spark ignition engine combustion process so that each zone will now be investigated in greater detail.

4.1.2.1 The Low Temperature Zone

Within the low temperature zone several separate regions may be distinguished. With the reactant mixture temperature below 200°C the reaction will proceed very slowly. As the mixture temperature is increased compounds including carbon monoxide and water begin to appear along with others such as hydrogen peroxide, formaldehyde and carbon dioxide[47]. Further increase in temperature to 300-400°C brings the system into the cool-flame region. In this region the system may fluctuate alternately between an explosive region, in which a pale blue flame called a cool flame propagates through the mixture, and the former slow reaction region.

If two cool flames traverse the vessel before the system moves into the high temperature explosive region, the process is termed delayed ignition. If there is one cool flame before high temperature combustion, the process is called two stage ignition. In cases where there is no external source of ignition, it appears that the cool flames themselves may eventually transfer the system from the low to the high temperature explosion zone.

The branching-chain reactions in the low temperature zone are consecutive, often competitive, and of the type:

$$\text{hydrocarbon} + \text{radical} \xrightarrow{\text{H abstraction}} \text{alkyl radical} + \text{product} \qquad \text{(a)}$$

followed by:

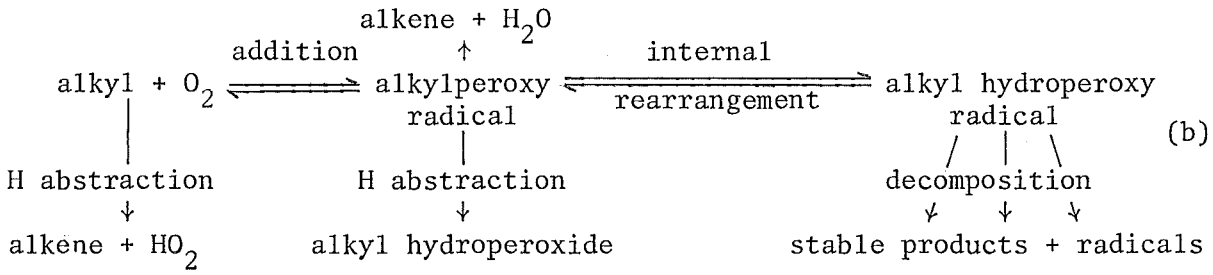

(b)

Therefore, as mentioned previously, the low temperature reaction products consist of many partially oxidised and unsaturated compounds (aldehydes, alkenes etc.). Reaction (a) describes the chain initiation process while reaction (b) represents chain propagation since the products of each step include new radicals.

These radicals may also partake in some chain branching reactions, however at such relatively low temperatures the less endothermic propagation reactions will dominate thereby limiting the cool flame explosion rate. The system must then shift into the high temperature zone to complete the conversion of the reactants into low energy equilibrium products.

4.1.2.2 The High Temperature Zone

As the system moves into the high temperature zone the cool flames are replaced by an intense blue flame (or orange if the mixture is fuel rich), the reactants are almost wholly converted into equilibrium products and most of the enthalpy of reaction is released. This overall high temperature process can be divided into three distinct phases; a preheat phase; a 'true' reaction phase; and a recombination phase[48,49].

(1) The preheat phase

In most hydrocarbon systems the preheat phase (see Appendix 4.1) initiates the fuel degradation to lower hydrocarbons, olefins and hydrogen. Thus the composition of reactants in the reaction zone becomes independent of the fuel involved which explains why flame temperature and burning velocities vary so little between them.

e.g. $C_4H_{10} + X^\circ \rightarrow C_4H_9^\circ + HX$

$C_4H_9^\circ \rightarrow CH_3^\circ + C_3H_6$

$C_4H_9^\circ \rightarrow C_2H_5 + C_2H_4$

(2) The reaction phase

In the reaction phase, radical-radical reactions become more significant than in the low temperature zone and degenerate branching species such as peroxides and aldehydes are replaced by simple radicals and atoms. The higher temperatures will now enable the chain branching reactions to compete favourably with the less endothermic chain propagation reactions making this phase relatively highly explosive.

In the reaction phase the olefinic compound produced during the ignition phase would be susceptible to radical attack with smaller carbon fragments being produced:

$$C_2H_4 + OH^\circ \rightarrow C_2H_3^\circ + H_2O$$

$$\vdots\ O_2 \text{ (mode unspecified)}$$

$$\downarrow$$

$$CH_2O \rightarrow HCO \rightarrow CO$$

During the reaction phase several hundred chain reactions are known to take place and probably many more that are not known. However the principal types of reactions are probably typified by lean methane oxygen flame reactions at low pressures:

$$CH_4 + O \rightarrow CH_3 + OH$$

$$CH_4 + OH \rightarrow CH_3 + H_2O$$

$$CH_4 + H \rightarrow CH_3 + H_2 \text{ (in fuel rich flames only)}$$

then the methyl radicals react mainly to produce:

$$CH_3 + O \rightarrow CH_2O + OH$$

followed by

$$CH_2O + M \rightarrow CO + H_2 + M$$

$$CH_2O + OH \rightarrow CHO + H_2O$$

and $CHO + O_2 \rightarrow CO + HO_2$.

Most of the CO_2 is formed from the reaction:

$$CO + OH \rightleftharpoons CO_2 + H.$$

Important chain branching reactions are:

$$H + O_2 \rightleftharpoons OH + O$$

$$O + H_2 \rightleftharpoons OH + H$$

$$OH + H_2 \rightleftharpoons H_2O + H.$$

Termination reactions compete for radicals and control the explosion rate:

$$OH + OH \rightleftharpoons H_2O + O$$

$$OH + OH + M \rightarrow H_2O_2 + M .$$

(3) The recombination phase

After the reaction phase process is finished, there are still many radicals left and CO has yet to be oxidised to CO_2. The post flame or re-combination phase (often termed afterburning) is an extended region which accounts for further recombination and CO oxidation when the air-fuel mixture ratio permits. Perhaps 75% of the energy stored in the primary fuel is released as heat in this recombination phase.

The main products of the reaction are H_2O, CO, and CO_2 although the concentration of the latter only significantly increases in the last stages of the phase reactions. The typical recombination reactions include:

$$H + OH + M \rightarrow H_2O + M$$

$$H + H + M \rightarrow H_2 + M$$

$$H_2 + CO_2 \rightleftharpoons H_2O + CO$$

$$OH + CO \rightarrow CO_2 + H$$

or $$O + CO \rightarrow CO_2^*$$

where M is an energy absorbing surface and CO_2^* is an electronically excited state of CO_2 which emits a blue glow (see Section 4.3.2) in returning to its ground state.

The overall high temperature reaction process produces quasi-stable products such as formaldehyde which are subsequently consumed. In fact, many free radicals could be included in this category such as HO_2, CH_3, CH_3O_2, H_2 and especially O and OH which persist in very high concentrations throughout most of the reaction.

4.1.2.3 The Temperature Zones in the Spark Ignition Engine

Both the low and high temperature zone reactions are observed during the combustion process in the spark ignition engine. During the compression stroke, low temperature reactions proceed forming intermediate combustion products such as ketones and aldehydes. The light emissions during these reactions are of the cool flame type. Then towards the end of the compression stroke the mixture is brought into the high temperature zone by the powerful radical producing ignition source (the spark). The use of a spark to initiate the high temprature sequence means that these explosive reactions can be timed to occur at the correct piston position and it also overcomes the inherently long ignition delay of hydrocarbon fuels. However not all the intermediate products of the low temperature zone reactions will be involved in the high temperature zone reaction process. In particular, those species which are in the flame quench regions of the combustion chamber, for example, close to the cylinder walls, will escape the reaction of the high temperature zone and will be emitted along with the other exhaust gases. These intermediate species are considered to be undesirable pollutants when released into the atmosphere in such a manner.

Towards the conclusion of the high temperature zone reactions large amounts of carbon monoxide will be oxidised to carbon dioxide (refer to Section 4.3.3 on afterburning) and most of the heat release from the primary fuel will be obtained.

4.2 Electromagnetic Radiation from Engine Combustion

Combustion reactions react sufficiently fast for a flame to propagate through the mixture. During the combustion process electromagnetic radiation from the flame will be emitted mainly in the ultra-violet, visible, near infra-red and far infra-red regions. Figure 4.1 serves to locate this region within the total electromagnetic spectrum.

Relatively inexpensive visible and near infra-red photodetectors are currently available and it is in this region of the electromagnetic spectrum that useful information can be obtained on engine performance (Fig. 4.2). The remainder of this chapter will concentrate on radiation emission from within the visible and infra-red regions and will conclude with some experimental studies by Withrow and Rassweiler on visible light emissions from spark ignition engines.

The terms light and radiation or electromagnetic radiation are often used interchangeably in published literature although light should really only refer to that portion of the electromagnetic spectrum which is visible to the eye. [The terms are used interchangeably in this report in situations when it is considered that this does not cause confusion.]

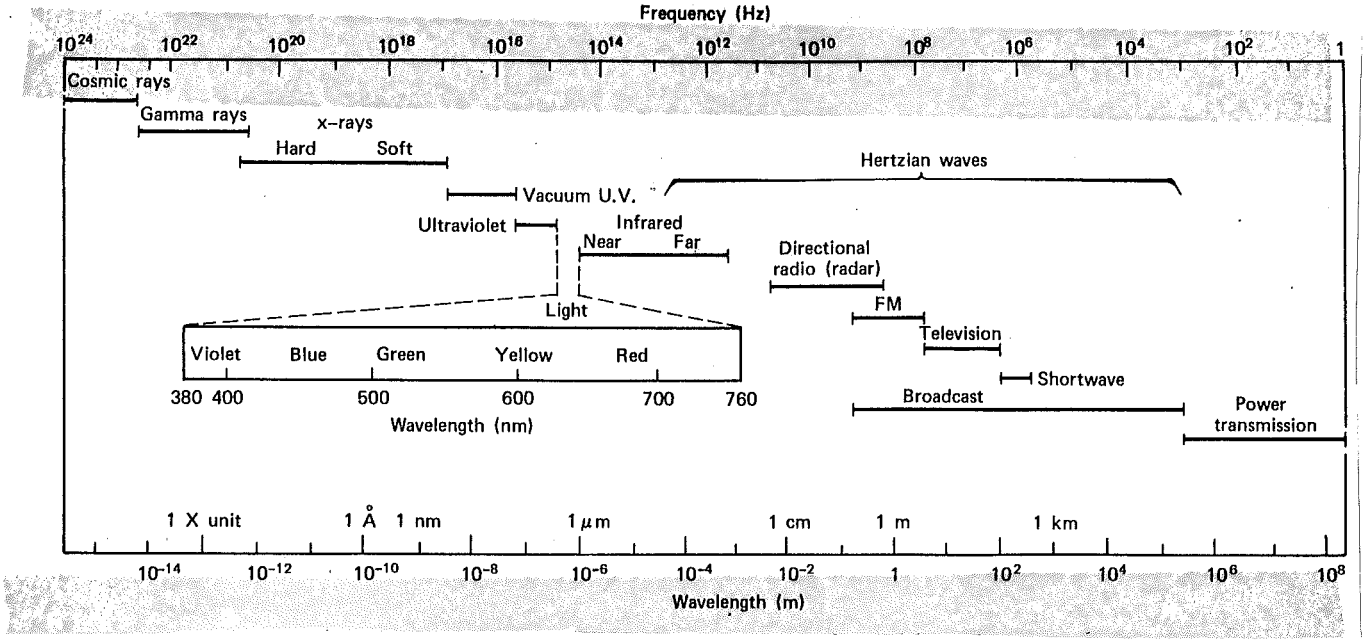

Figure 4.1 The electromagnetic spectrum[50].

Historically, the greatest advances in molecular spectroscopy (the study of flame spectra) were made in the 1920's. During this time, light emitting bands were assigned to the free radicals OH, CH, C_2 and HCO, which were previously unknown to exist in combustion reactions. The discovery of these free radicals allowed further development of chemical combustion theory, particularly the chain reaction process. Some of the chemically reacting species such as OH and H_2O do not emit or absorb light in the visible region while HO_2 and CH_3 are not normally observable at all, so that optical spectroscopy cannot give a complete account of the hydrocarbon reaction mechanism[51].

Until recently, detailed examinations of the chemical structure of flames have been limited to low pressure stationary flames which are easier to analyse. However, high pressure closed vessel explosions such as those in the Spark Ignition Engine will differ only in detail, where the specific heat of the gases is less (C_v instead of C_p) and the final temperatures and pressures will be higher. Most of the following notes on hydrocarbon light emissions can be applied to either case, but emphasis has been placed on closed vessel explosions wherever possible.

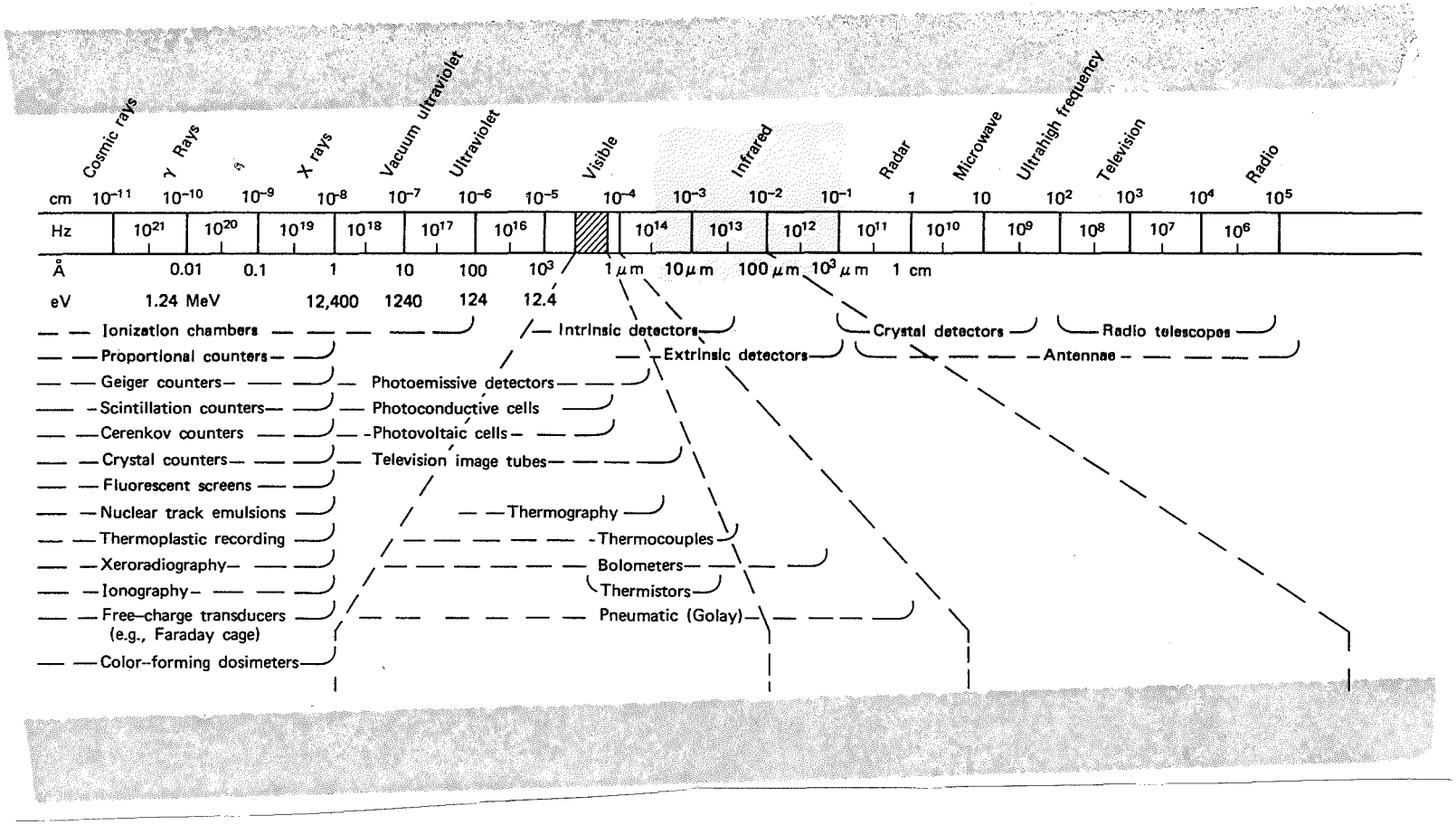

Figure 4.2 Radiation detectors in the visible and infra-red electromagnetic spectrum[50].

4.2.1 The Cause of Electromagnetic Radiation

Any excited chemical species (atom, radical or molecule) may emit electromagnetic radiation by decreasing its rotational, vibrational or electronic energy. These three forms of energy storage within the species are quantised in value so that they can only change by discrete amounts.

The electronic energy of the species will change when an electron is sufficiently excited so that it makes a transition into a higher energy orbit. A certain quantum of energy will be absorbed by the electron during the transition, so that the phenomenon may be described as absorption. The excited species may then re-emit a quantum of energy when a valency electron moves from a high energy orbital into a lower energy orbital.

The vibrational energy of the species results from the sinusoidally changing bond lengths between the atoms which form it. For example, for a diatomic species AB (Fig. 4.3), the vibration frequency about the mean interatomic length ℓ may assume different quantised levels. In changing from one vibration frequency to another, a discrete quantity of energy will be absorbed or emitted. The species may also rotate at one of several quantised frequencies and changes in the energy of rotation will result in similar energy absorption or emission. In practice, the discrete rotational energy levels are usually close enough to be considered continuous.

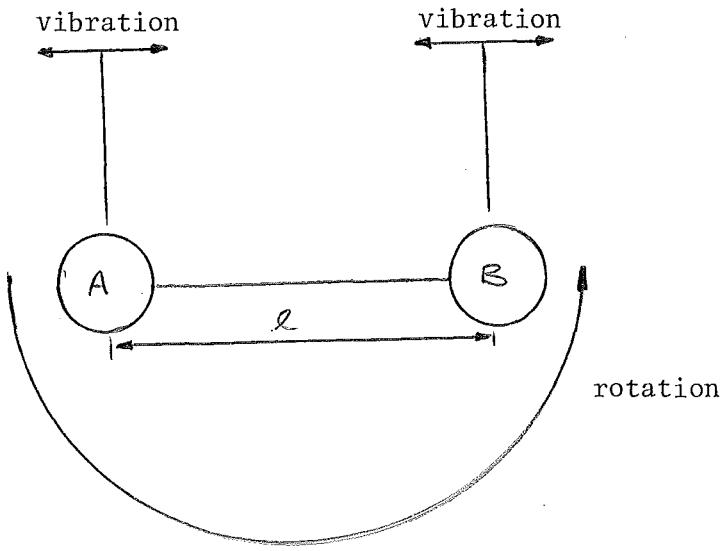

Figure 4.3 Vibration and rotation energies of a diatomic molecule.

The energy absorbed or emitted can result from collisions, chemical reactions or by absorption or emission of electromagnetic radiation. Collisions and chemical reactions may produce excited species as described by the equations:

$$A + M \rightarrow A^* + M$$
$$A + B \rightarrow C^* + D.$$

In the first reaction the collision of species A with M results in an energy transfer to A so that it is excited to A*. This normally involves a loss of internal energy from molecule M, vibrational energy transfer being most effective. The chemical reaction in the second equation results in the production of an excited species C*, and this process is termed chemiluminescence. If the energy is absorbed from electromagnetic radiation which is incident upon the species, the representation would be:

$$A + h\nu \rightarrow A^*.$$

The energy absorbed (or emitted by the reverse of this reaction) must be of a fixed discrete value dependent upon the particular energy transition which is taking place within the species. Therefore, the energy quantity $h\nu$ has a fixed value for any one transition where h is Planck's constant and ν the frequency of the electromagnetic radiation. Since the radiation wavelength is inversely proportional to frequency, a high energy transition implies a high $h\nu$ term, and thus a high frequency or short wavelength radiation. An example of this type of radiation is ultra-violet light. Smaller energy transitions produce long wavelength radiation which corresponds to the infra-red region of the electromagnetic spectrum.

Vibrational and rotational energy transitions are closely spaced and are therefore normally low energy transitions, so that emissions from them changing their energy state tend to be in the infra-red region. Electronic orbital transitions are comparatively high energy transitions and they emit in the ultra violet, visible and near infra-red regions of the spectrum.

4.2.2 Electromagnetic Radiation in Hydrocarbon Flames

In order to excite the electrons into high energy orbitals so they can emit light by returning to lower orbitals, they must receive sufficient energy input. The species' electrons may receive the required energy by impact with an extraneous discharge of high energy electrons and this is how the chemical species in the path of the spark plug discharge emit light. However generally in a hydrocrarbon flame there is a low

concentration of electrons and these will not have enough energy to cause excitation upon impact with atoms or molecules. The conversion of the translational energy of molecules into electronic excitation is also unlikely to account for much emission[46]. The chemiluminescence process is considered to be the major source of electronic excitation because in combustion systems, high tempratures in the reaction zone lead to high concentrations of radicals.

Although the formal behaviour of chemiluminescent reactions is understood, it is difficult to ascribe one particular reaction mechanism to each emitting species because of the unknown nature of the potential energy curves of the excited electronic orbitals for each radical[48].

Since each chemical species has a number of possible electronic excitation, vibration or rotation states, it will have a characteristic series of absorption or emission wavelengths which form what is called the species radiation spectrum. An absorption spectrum is identical to an emission spectrum except that radiation is being absorbed rather than emitted. Although the species radiation spectrum will be made up of an array of bands, one for each energy transition, often the band structure becomes so fine that it appears continuous forming a continuum region on the electromagnetic spectrum. For example, the dissociation of molecules, ionisation of atoms or recombination processes will sometimes create a continuum region. When a particle becomes incandescent it will also emit a continuum of radiation and if it is in equilibrium with the surroundings, the radiation intensity as a function of wavelength will approach black body radiation (Fig. 4.4). Normally the incandescence emitted from the particle will only approximate this and the radiation is then termed grey body radiation. Such radiation will have certain discrete bands combined with the continuum because the emitter is not in complete thermodynamic equilibrium with its surroundings. This is the case with hydrocarbon flames in the Spark Ignition engine. They emit a continuum mainly because of hot carbonaceous particles present and also discrete bands, since the flame is optically thin and not in thermodynamic equilibrium with its surroundings.

From the black body radiation shown in Fig. 4.4, it is reasonable to assume that most of the radiation from the grey body hydrocarbon flame will be emitted in the near infra red region of the spectrum, that is, between 1μm and 2μm.

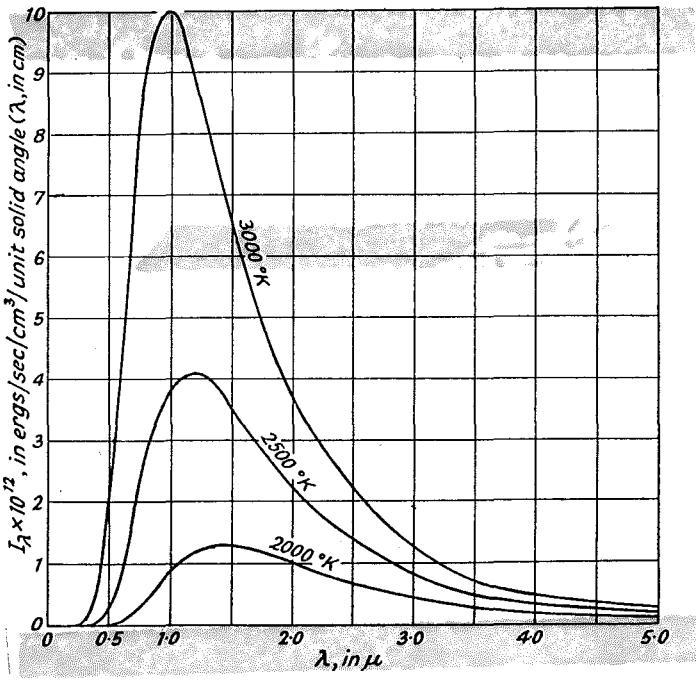

Figure 4.4 Black body radiation at various temperatures as a function of wavelength[46].

4.3 The Infra-Red and Visible Radiation from Hydrocarbon Flames

The chemical species present in the hydrocarbon flame which emit in the infra-red region will now be discussed and then those emitting radiation within the visible region (along with the OH radical which emits ultra-violet light).

4.3.1 The Infra-Red Region

As has been mentioned, the majority of flame radiation lies in the infra-red. It releases between 2-20% of the heat of combustion whereas the visible region seldom emits more than 0.4% of the energy.

Hartley[51] studied the effect of air-fuel ratio on infra-red emissions using coal-gas as the fuel. For very lean mixtures the energy emitted in the infra-red was about 10% of the total combustion energy, rising to 18% for stoichiometric concentrations and then falling slightly for richer mixtures. As the mixture was further enriched the infra-red rose to a second maximum as soot started to form and the flame became luminous to the eye. Infra-red emissions are also affected by the gaseous pressure in the combustion zone, higher pressures reducing emissions, probably because of increased self-absorption. For lean flames the infra-red emission will be mainly due to CO, CO_2 and H_2O vibration-rotation band

spectra but there is normally some infra-red black-body radiation due to the presence of soot particles, particularly in rich flames.

Quantitative measurements of the infra-red emission from flames show that it is a strong function of the afterburning phenomenon (Section 4.3.3). Steele[51] used a stroboscopic method to study infra-red emissions from engines and filtered out the main 4.4μm band from carbon monoxide and 2.8μm band from H_2O and CO_2 band superposition (Fig.4.5).

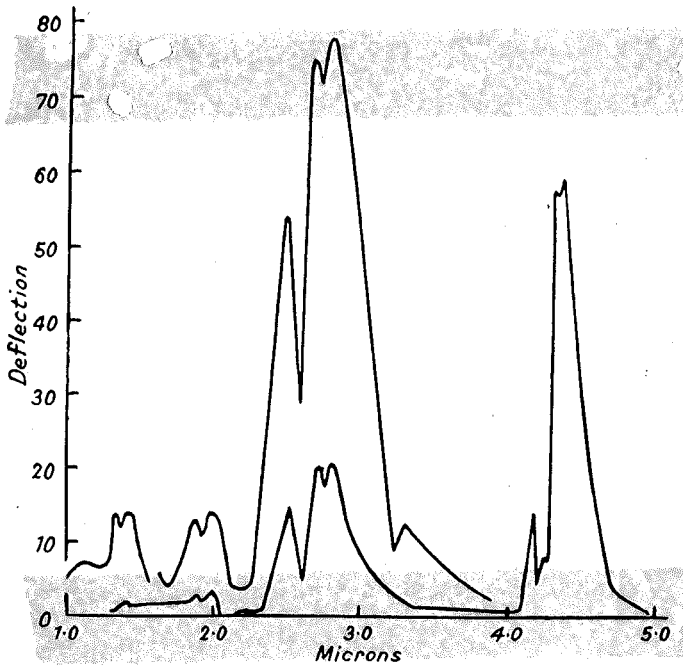

Fig. 4.5 Near infra-red hydrocarbon flame emissions from H_2O and CO_2[51].

He showed that the infra-red emissions continued to increase for some 20° crankangle after the passage of the flame front. These observations are best explained by relating them to the afterburning phenomenon and the pressure and temperature changes associated with the burning of the last part of the mixture. Further out in the infra-red region (14-22μm) Ludwig, Ferriso, Malkmus and Boymton[51] have observed high thermal emission from CO_2 and H_2O (Fig. 4.6).

4.3.2 The Visible Region

In the visible region the hydrocarbon flame spectrum is also made up of bands superimposed on a continuum. The strongest band systems will be represented by the free radicals C_2, CH, OH and HCO (Plate 4.1)

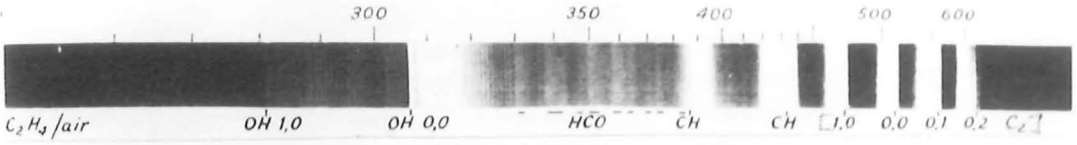

Plate 4.1 Hydrocarbon flame spectrum showing radical bands[51]

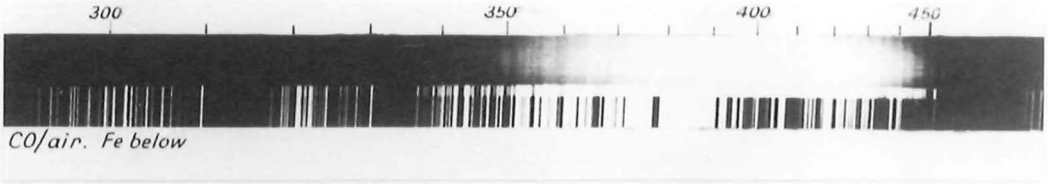

Plate 4.2 Burning CO spectrum showing bands and continuum[51]

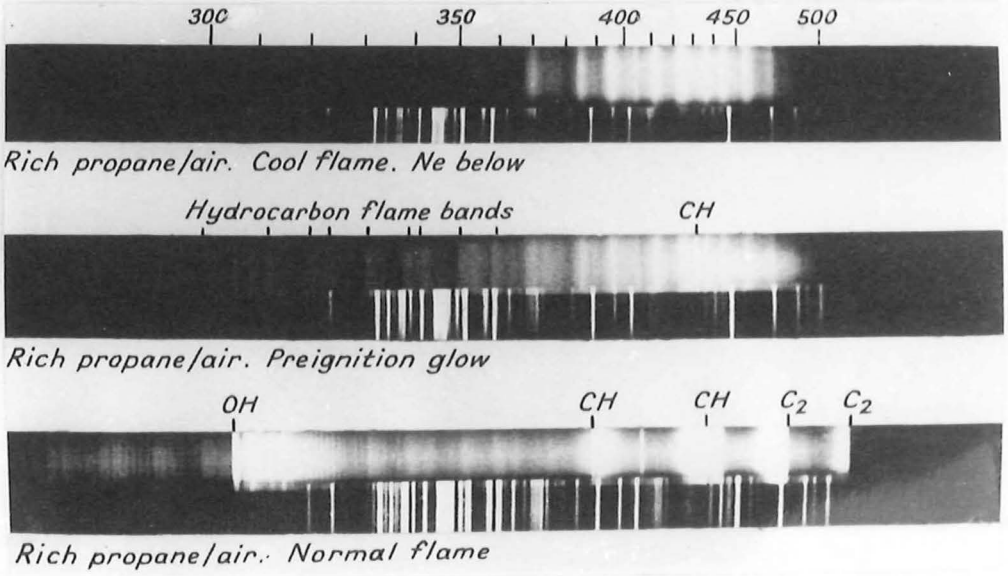

Plate 4.3 Cool flame, pre-ignition and normal combustion flame emissions from a rich propane-air mixture[51]

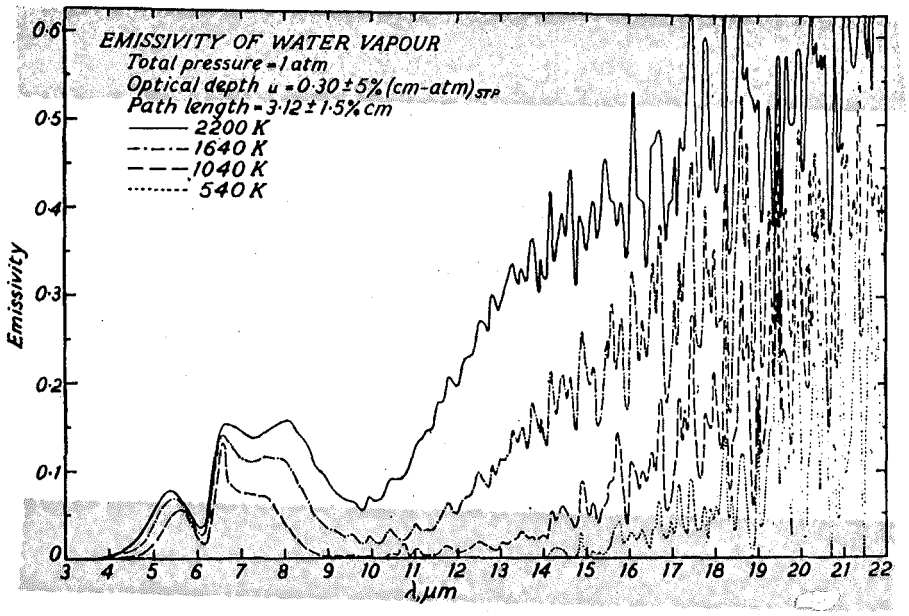

Figure 4.6 The far infra-red thermal emissivity of water vapour[51].

and a weaker series of bands due to burning carbon monoxide (Plate 4.2). In them the electronic transition from the ground state to the lowest of the excited states requires relatively little energy so that they are excitable by comparatively low temperature flames and are radiators of mainly visible light. Conversely, the more permanent constituents of flame gases (O_2, N_2, H_2O) are devoid of low lying electronic levels and so are not electronically excited by flame temperatures.

The strongest visible continuum systems are emitted from three sources. Firstly, solid carbon particles (note that these are different from the C_2 radicals mentioned above) emit black or grey body radiation and therefore add mainly to the red in the visible region. Secondly, burning carbon monoxide adds to the continuum in the blue-violet. A third less strong continuum comes from the recombination reactions of nitric oxide and atomic oxygen in the yellow region of the spectrum. One prominent line spectra, due to sodium and situated in the yellow (580 nm) may be excited in violent explosions.

The large numbers of radical producing branching chain reactions have already been discussed with examples of the types of reactions expected in hydrocarbon flames. Since the radicals themselves are often the product of chemiluminescent reactions, they will each emit spectra characteristic of the species. The chemical species which emit electromagnetic radiation will now be examined separately and the likely chemiluminescent excitation

reactions, when known, will be included. Then the burning carbon monoxide and solid carbon continua will be reviewed giving an overall account of the visible hydrocarbon flame spectrum.

- The CH radical bands

The CH radical is a prominent emitter which is almost certainly formed in its excited state by the strong exothermic reaction:

$$C_2 + OH \rightleftharpoons CO + CH^*$$

CH radicals give two intense blue-violet bands, one at 431 nm and the second at 390 nm (Plate 4.1).

- The C_2 radical bands (The Swan Bands)

The Swan Bands dominate the C_2 spectrum and are situated at 474, 517 and 564 nm (Plate 4.1), giving a characteristic green colour (Plate 4.1). Experimental work by Pretty[52] finally established the Swan Bands as being emitted from the C_2 radical; however, the cause of this excited radical from hydrocarbon flames is still not quite certain. For the higher hydrocarbons, it could be accounted for by thermal decomposition (cracking) of the hydrocarbon, however the bands also appear in methyl derivatives so that polymerisation must be occurring at some stage. It is noted that substances which increase flame speed also strengthen the C_2 bands. The bands tend to fade away as the mixture strength is weakened below stoichiometric.

- The HCO radical bands (Vaidya's Bands)

These bands are strongest in weak mixtures of all hydrocarbons and lie between 250 and 400 nm. The strongest bands are sandwiched between OH at 310 nm and the 390 nm CH band (Plate 4.1).

- The OH radical bands

A strongly exothermic reaction produces OH throughout the reaction zone as these radicals form intermediates in hydrocarbon oxidation.

$$CH + O_2 \rightarrow CO + OH^*.$$

The spectral studies of Minkoff, Everett and Broida[51] suggest that more OH emission comes from the burnt gases than the flame front. The bands are not visible as they occur in the ultra-violet region at 310 nm (Plate 4.1).

- The burning CO bands and continuum

In hot hydrocarbon flames the CO spectrum is dominated by a continuum in the blue (Plate 4.2) with a superimposed weak series of bands in the same region caused by excited CO_2. The CO is burning in air according to the reaction

$$CO + O \rightleftharpoons CO_2^*.$$

The photographic infra-red (up to 950 nm) shows some extension of the continuum and CO_2 bands but towards longer wavelengths both systems become weaker until the infra-red vibration rotation bands are observed (Section 4.3.1).

- The carbon particle continuum

Solid carbon (this is not the C_2 radical) can be detected even in lean fuel mixtures adding a yellow background continuum to the hydrocarbon light emission spectrum. This observation can be explained from the equilibrium reaction:

$$2CO \rightleftharpoons CO_2 + C \text{ solid}.$$

Temperature as well as fuel mixture determine whether carbon will form as the equilibrium will proceed to the right at low temperatures and to the left at higher temperatures (above 1000° K).

In fuel-rich flames the carbon will combine to form solid soot particles causing the carbon continuum to intensify and dominate the system spectrum. The radiation from these flames approaches black body intensity. Several theories have been proposed to explain the carbon formation (Appendix 4.2), but as yet there is a lack of conclusive evidence for any of them.

4.3.3 The Afterburning Phenomenon

Photographs of flame travel in an internal combustion engine (Section 4.4) reveal a strong re-illumination of the hot gases after the flame has passed through the chamber. This phenomenon is often termed after-burning, and the light emission is dominated by that of the CO flame spectrum, the OH, CH and C_2 bands being undetectable. The light emitted after the flame has travelled through the chamber is not, therefore, due to hydrocarbon oxidation but results from the delay in completion of the slow carbon monoxide combustion reactions. The increase in light intensity is also a manifestation of the pressure and temperature rise which occurs

as a result of the burning of the last part of the charge. Also, when the flame travels across the chamber, temperature gradients will be established rising from the gases burning last to the gases burned first in the vicinity of the spark plug so that the re-illumination will be strongest around the spark plug region.

Withrow and Rassweiler[51] suggest that the equilibrium

$$H_2 + CO_2 \rightleftharpoons CO^* + H_2O$$

$$2CO_2 \rightleftharpoons 2CO^* + O_2$$

may represent the afterburning reactions since they are influenced by pressure and temperature changes as the charge reaches chemical equilibrium, although this afterburning, if observable, is generally of short duration in engine explosions. David[51] recorded afterburning persisting for 14 seconds in large vessels of exploding dry CO/O_2 mixtures.

4.3.4 Emissions from Knocking Hydrocarbon Explosions

Withrow and Rassweiler[52] have examined the light emission spectrum of an internal combustion engine under both normal running and knocking conditions. The strongest spectral bands during normal combustion have been described as arising from C_2, CH, HCO and OH. During a knocking cycle the bands of C_2 and CH became very much weaker in the region of the cylinder where the charge was auto-igniting. However radical emissions were observable with normal intensity up until the point in time when the charge began to auto-ignite. This suggests that the knocking and non-knocking explosions differ only in the burning of the last auto-igniting part of the charge. The reduction in strength of the C_2 and CH bands in the auto-igniting section, Withrow and Rassweiler reasoned, could not be due to changes in density, physical movement of the gases or temperature influencing radical excitation. The chemical reactions which produce or consume C_2 and CH must have changed. During normal combustion the excited C_2 and CH radicals are produced in the flame front where the hydrocarbons are being cracked; yet in knocking combustion self-ignition does not give rise to such cracking reactions, perhaps because the basic propagation mechanism changes from being dominated by radical diffusion to thermal diffusion[51]. This theory is strengthened by the observation that pre-ignition glow spectra, which also represent self-ignition reactions, also have weak C_2 and CH emission bands (Appendix 4.3).

During their studies of the electromagnetic radiation spectrum in the Spark Ignition engine, Withrow and Rassweiler also examined the electromagnetic absorption spectrum. During knocking combustion they found strong absorption of formaldehyde bands in the auto-igniting region of the charge immediately prior to it auto-igniting. However during normal combustion there was no absorption in this region of the charge. This observation has been interpreted to mean that the auto-igniting endgas undergoes at least two-stage combustion[53]. The first stage involves reactions of the cool flame type which produce formaldehyde and the second stage involves the high temperature zone reactions. This theory is supported by the observation of methane and benzene which do not produce normal cool flame regions and are also less prone to knock.

In examining the spectrum of knocking hydrocarbon combustion, a heavy continuum in the red may sometimes be observed which will affect the analysis in this region. It is considered most probably to be caused by the cracking of lubricating oil, due to the higher temperatures reached in knocking explosions.

4.3.5 Various Effects on Emissions Intensity

4.3.5.1 Effect of tetra ethyl lead

The effect of ethyl lead on emissions is to introduce new emission lines from PbO and Pb (at 364, 368 and 406 nm) in the flame front. It also causes the C_2 and OH emission strength to be restored in the auto-igniting zone. Emission from high temperature incandescent carbonaceous particles may be reduced. However, the formaldehyde absorption bands still appear even when knock is suppressed by the tetra-ethyl lead. This observation raises further questions concerning the exact nature of the auto-igniting zone reactions.

4.3.5.2 The effect of mixture strength on light emissions

The band systems of C_2, CH, OH, and HCO are generally superimposed on a continuum spectrum composed from carbonaceous particles and combustion of carbon monoxide. These systems vary considerably in relative intensity as a function of air-fuel mixture strength.

A comparison of the band systems as a function of mixture strength identifies the C_2 radical bands as strongest in rich mixtures, CH at slightly less rich mixtures, while OH has a flat maximum slightly on the rich side of the stoichiometric air -fuel ratio. When the continuum emissions

are analysed in rich mixtures of burning hydrocarbons the red end of the spectrum is found to dominate due to carbonaceous particle emission. This is not only a result of a higher concentration of carbon particles but because of higher temperatures causing stronger thermal emission. It has been pointed out earlier that carbon formation may occur throughout the mixture range so that this continuum will also be present to some degree in all mixtures whether rich or lean. However, at stoichiometric and weaker mixtures, the blue burning carbon monoxide continuum becomes very strong and will tend to dominate the spectrum.

4.3.5.3 Effect of flame velocity on light intensity

The intensity and spectrum of the light emissions from the Spark Ignition engine are also influenced by the flame velocity. For example, a rapidly burning flame will burn with a greater light intensity for the same mixture of hydrocarbon fuel, since the chemiluminescent reaction rate is increased. However such a flame would also consume the mixture more rapidly so that it would emit light for a shorter period of time or crankshaft angle. If the overall light intensity were to be plotted as a function of crankshaft angle, the curve of Fig. 4.7a could be expected. The flame intensity increases as the flame kernel is established from the spark plug and continues to increase as the flame develops throughout the cylinder. During this period the total light intensity will be influenced by such factors as temperature, afterburning and knock. Eventually, as combustion nears completion, the flame will be extinguished and the light intensity will decrease to zero. In comparison a more rapidly burning flame would be expected to produce a light intensity plot similar to Fig. 4.7b. The light intensity has a higher peak value and is of shorter duration.

The flame velocity will be influenced by the conditions within the combustion chamber:

1. Mixture strength. The speed at which the flame passes through the chamber is maximised when the fuel mixture is slightly on the rich side of stoichiometric.

2. Pressure. Pressure has little direct effect on flame velocity although it has been suggested that flame fronts become wrinkled at high pressures which effectively increases the propagation rate (see point (3)).

3. Turbulence. In low pressure laminar flame conditions (low pressure

flames) the burning velocity is well defined. Under turbulent conditions the flame speed increases considerably and this is probably for two reasons. Firstly the turbulence tends to break up the flame front (wrinkled flame concept) so that it has greater surface area and consumes more reactants as it travels. Secondly the swirling effect of turbulence may improve thermal and radical diffusion; however it is not known how important this latter effect is. The main emission bands (CH, OH, C_2, HCO) do not appear to change in relative intensity although they are diminished in overall intensity under more turbulent conditions.

4. Temperature. The burning velocity will generally increase with the square or the cube of the preheated mixture temperature.

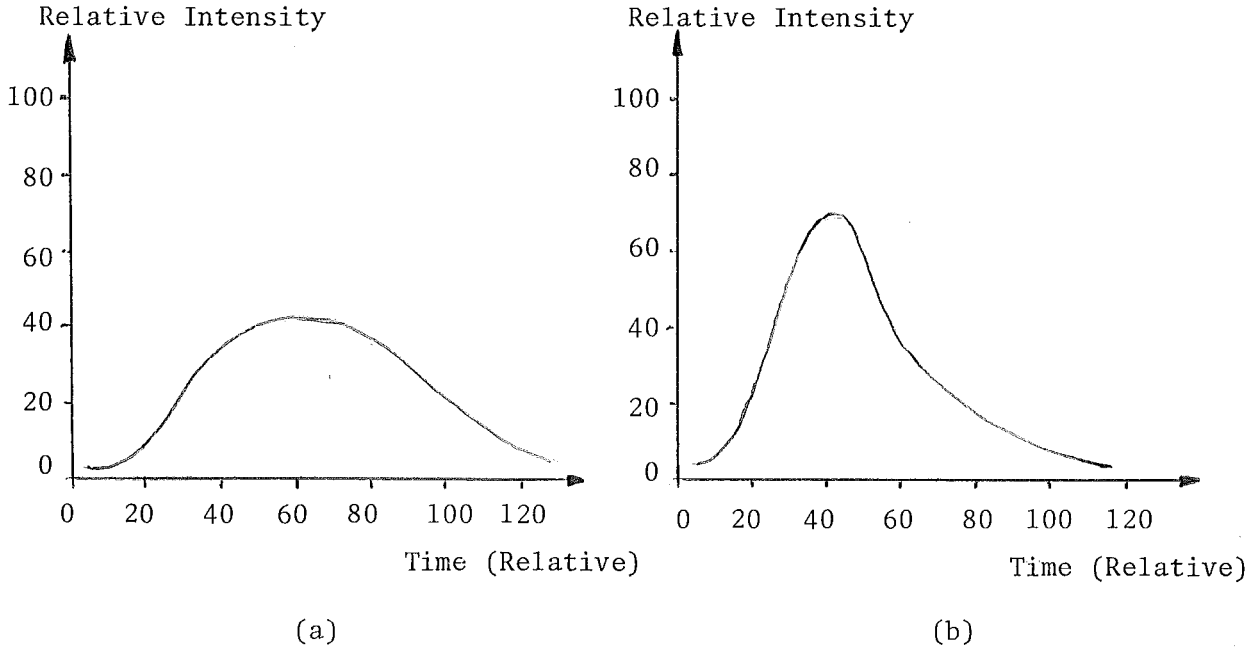

Figure 4.7 Expected light intensity as a function of crankshaft angle; (a) normal propagation rate; (b) rapid propagation.

4.3.5.4 Correspondence of light emissions to cyclic variation

There is little information available on the cyclic variations of light intensity in the Spark Ignition Engine. An examination has been made by Smith and Starkman[54] concerning the cyclic variation of the OH radical light emissions. In their study they found the OH emissions to vary by as much as 50% from cycle to cycle whereas the simultaneous pressure recordings indicated cyclic pressure variation of between 10% and 15%.

4.4 Combustion Photography in the Spark Ignition Engine

In the period between 1930 and 1940, Withrow et al. made some comprehensive investigations into the light emissions from hydrocarbon flames in the Spark Ignition engine. A summary of some of the important aspects of this work is given in Reference (55) by Lewis and reviewed here.

4.4.1 Normal Combustion

Withrow and Boyd investigated combustion light emissions in the Spark Ignition engine by photographing the combustion flame through a long narrow window mounted in the cylinder head. A film recording system mounted over the window was devised so that the film moved past the window at a fixed rate, recording the progress of the combustion flame. The resulting exposure shows the flame intensity as a function of time, Plate 4.4. In this plate the slit window extended vertically from the x axis up to the 5" mark. The film was passed over the window in the horizontal direction from right to left. The 45° boundary represents the flame front as it travels across the cylinder. The high luminosity from the charge which burned first closest to the spark plug can be observed in the plate. This region continues to glow brightly even after the flame front has travelled throughout the chamber and died away at the chamber walls. It is considered to be due to the higher temperatures and pressures developed closer to the plug.

The delayed appearance of the bright zone on the right of the plates is considered due to the burned gas behind the flame front and probably reflects the afterburning phenomenon.

Withrow and Rassweiler continued the investigation through the use of a high speed camera which photographed the whole chamber of a quartz L-head engine, Plate 4.5. Photographs were taken at the rate of 5000/second this being limited by the combustion flame light intensity and the film sensitivity.

Plate 4.6 shows a single non-knocking explosion at an engine speed of 2000 r.p.m. The unsymmetrical propagation evident in the initial shots suggests that there is mass movement of the charge which was induced during the intake stroke. The bright spot beginning in picture 11 and continuing throughout the rest of the frames is caused by incandescent carbon, probably arising from decomposed lubricating oil. By picture 13 increased temperature luminosity around the spark plug is again apparent and confirmed by the rapid pressure rise at that point on the simultaneous

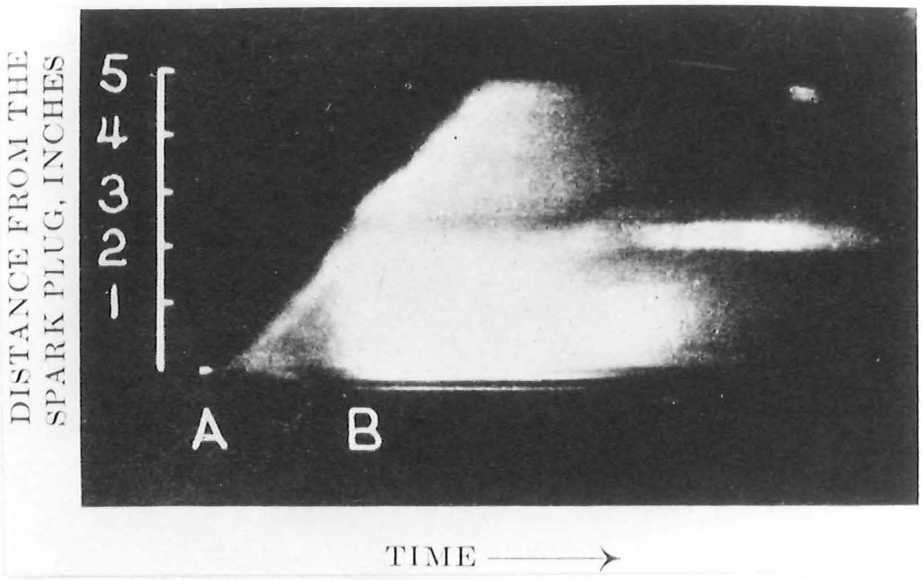

Plate 4.4 Flame propagation through combustion chamber (continuous record)[55].

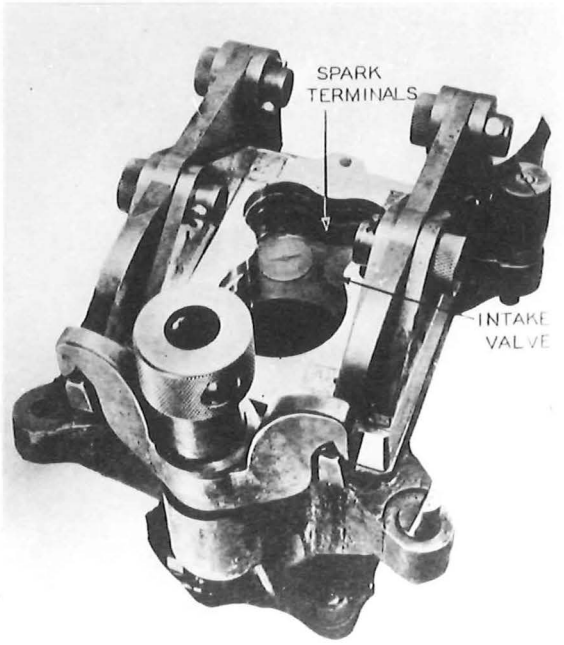

Plate 4.5 Modified quartz glass cylinder head. (Withrow and Rassweiler)[55].

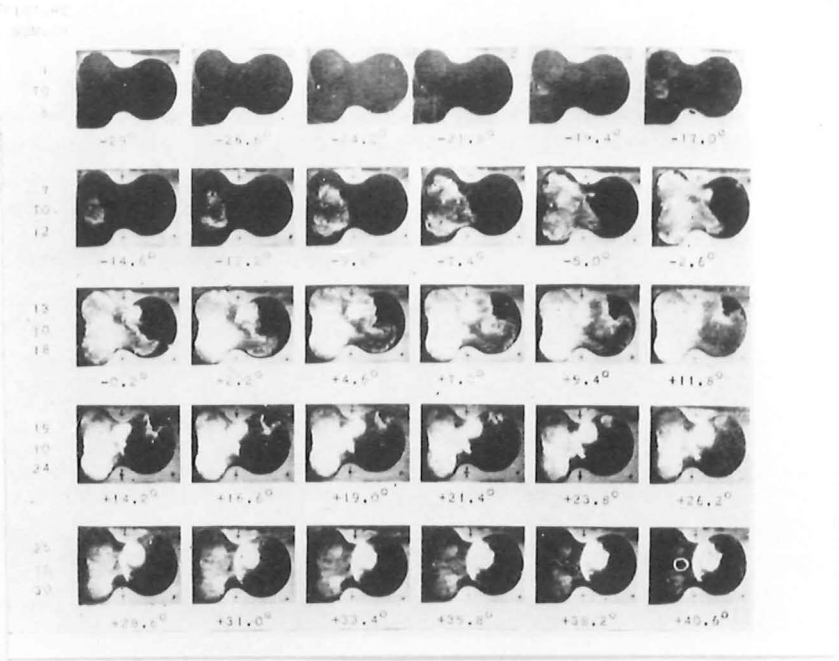

Plate 4.6 High speed photography (5000 frames/second) of normal combustion. Engine speed 2000 r.p.m. [55].

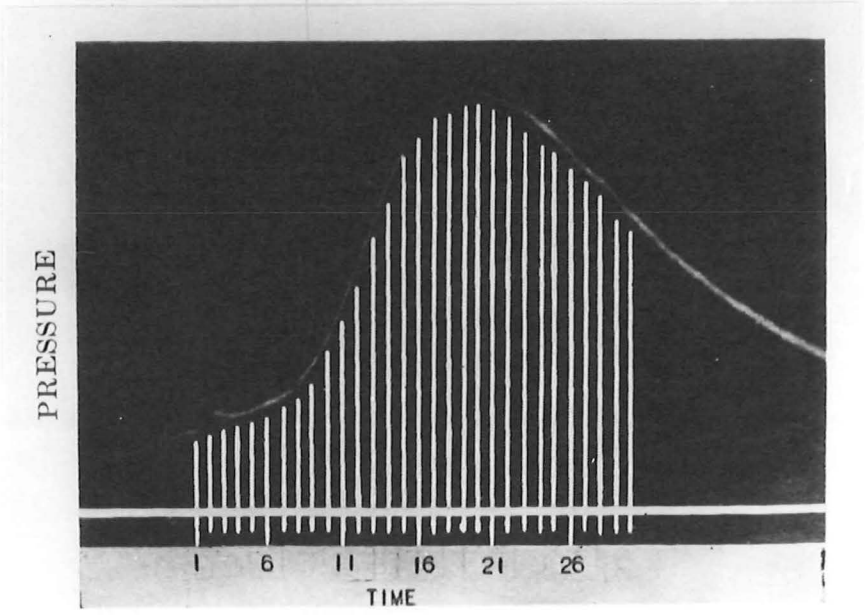

Plate 4.7 Simultaneous pressure trace of the normal combustion sequence shown in Plage 4.6[55].

pressure trace (Plate 4.7). The pressure trace identifies exposure 20 as that of maximum pressure and the luminosity is also the most intense at approximately picture 20.

Mass movements of the charge are evident throughout since the luminous carbon spot drifts leftwards as the burning gases ahead of it expand in pictures 18 to 29 and rightwards as the piston descends from shots 19 to 30.

4.4.2 Knocking Combustion

The processs of knocking combustion was photographed by Withrow and Rassweiler using the same high speed photography technique and a knocking combustion cycle is shown in Plate 4.8. The pictures reveal normal combustion up to frame 12, but in frame 13 auto-ignition begins to occur at the extreme right, well beyond the flame front. Very rapid inflammation of the rest of the charge is evidenced by the flame having passed through the whole chamber by frame 14. These photographs reveal that knock is occurring through an auto-ignition process in the end section of the charge rather than originating in the flame front.

When the knocking combustion is exposed to a moving film through a long narrow window the result is typified in Plate 4.9. The periodic re-illumination observed in the photograph is caused by a pressure wave being reflected within the chamber. The hot gases are compressed at the same rate as the pressure wave resulting in luminosity fluctuations of the same frequency as the pressure wave. These luminosity fluctuations indicate that the light intensity is a strong function of pressure. This conclusion is confirmed by the coincidence of maximum pressure and maximum light intensity during the normal combustion events (Plates 4.6 and 4.7).

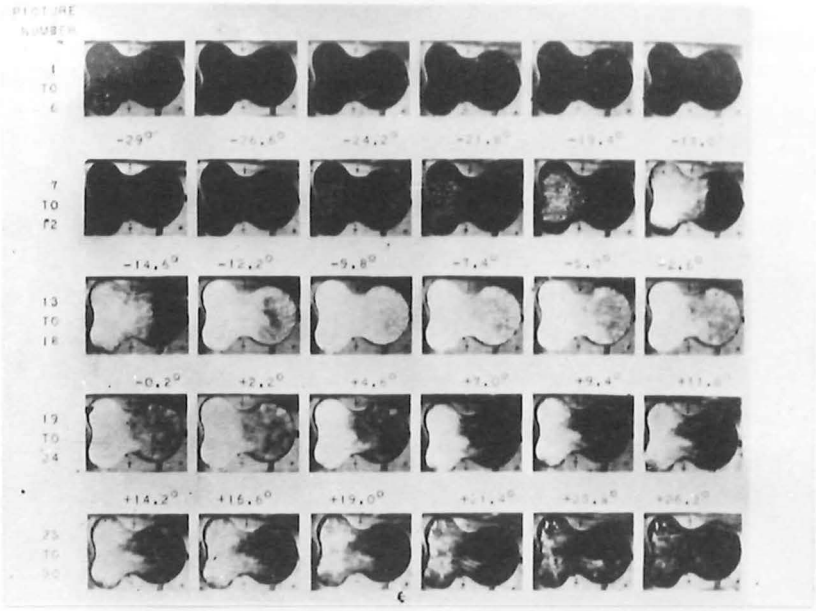

Plate 4.8 High speed photography (5000 frames/second) of knocking combustion. Engine speed 900 r.p.m.(55)

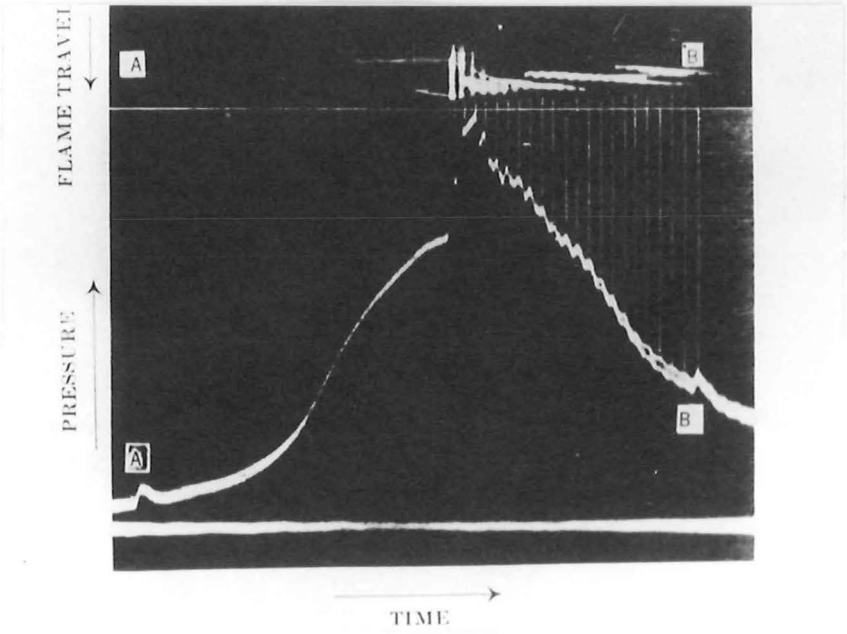

Plate 4.9 The correspondence of light frequency oscillations and pressure oscillations during knocking combustion(55).

CHAPTER 5

EXPERIMENTAL APPARATUS AND TEST PROCEDURE

CONTENTS

INTRODUCTION

The apparatus and test procedures used to examine the combustion flame light in certain Spark Ignition engines are detailed in this chapter. The chapter is divided into three sections. The first section explains the method used for obtaining an electromagnetic spectrum of the combustion flame and the second section explains how the broadband light intensity of the flame was measured. Both of these investigations utilised Ricardo E6 engines with a quartz window mounted within the auxiliary spark plug hole. The third section describes how the broadband light intensity equipment was further developed so that observations of the flame light intensity could be made in standard automotive Spark Ignition engines.

5.1 Measurement of the Spectrum of the Combustion Flame

5.1.1 Apparatus

5.1.1.1 Quartz Glass Window Assembly

In order to record the spectrum of the combustion flame light, a quartz glass window assembly was constructed which could be screwed into the 14 mm diameter auxiliary port in the Ricardo E6 cylinder head (Plates 5.1 and 5.2). The window assembly was composed of a 3 mm thick by 15 mm diameter quartz glass disc which was cemented into an aero-engine spark plug housing. An exploded view of the assembly is shown in Plate 5.4. The quartz glass itself is able to withstand temperatures of up to 1500° C and at 3 mm thick it is acceptably transparent to wavelengths from 250 nm to 4 μm, Fig. 5.1.

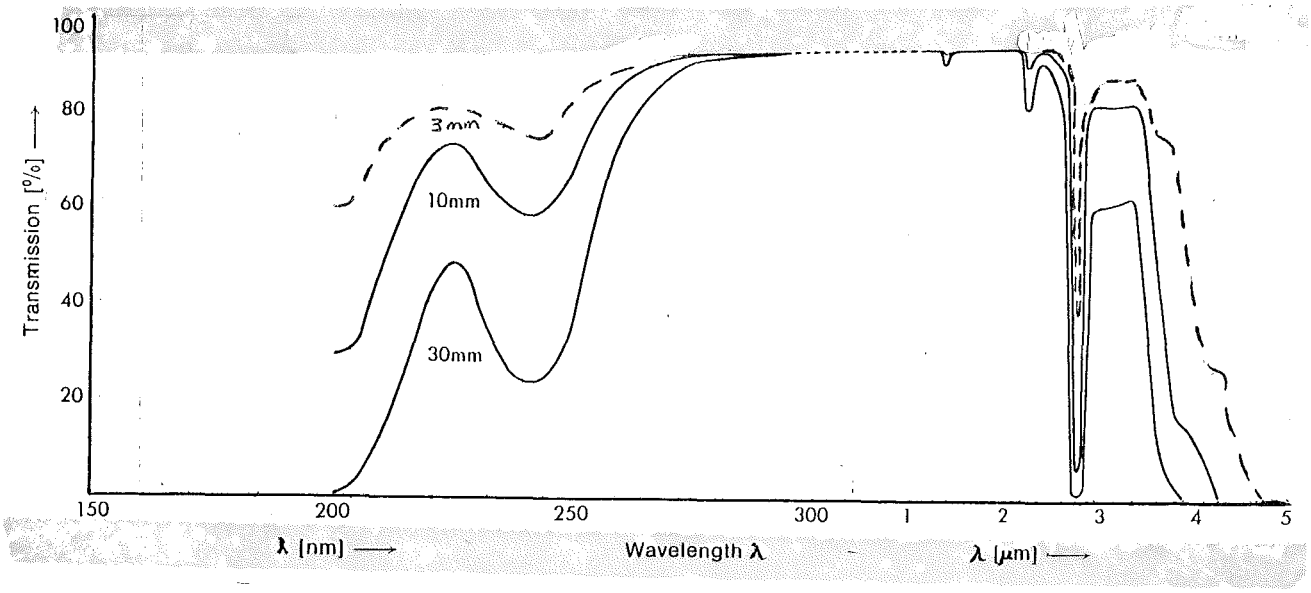

Figure 5.1 Transmittance of quartz glass as a function of wavelength. The window used was 3 mm thick(57).

The complete window assembly could then easily be inserted directly into the auxiliary port in the Ricardo cylinder head enabling the combustion flame to be analysed during normal engine operation (Plate 5.3).

5.1.1.2 Spectrometer and Photographic Apparatus

The glass window was mounted in the Ricardo engine in order to enable the spectrum of the combustion flame to be measured by spectrum analysis equipment. This equipment was set up in close proximity to the window assembly (Plate 5.5). The spectrum was produced by a 5" Spectrometer (manufactured by The Precision Tool & Instrument Company, Serial No. 5182-HB) which refracts light by passing it through a triangular prism, (Plate 5.6). The spectrum was photographically recorded through

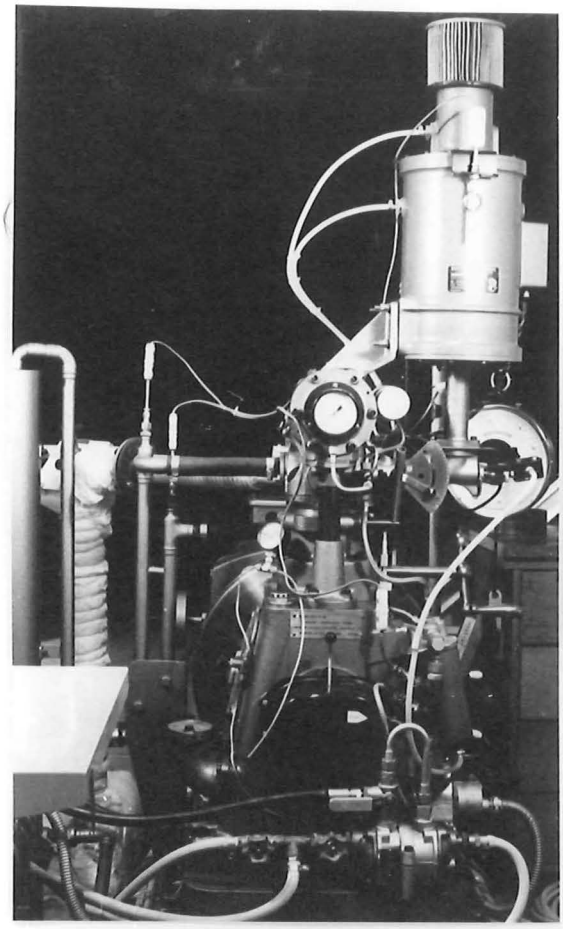

Plate 5.1 Ricardo E6 variable compression ratio engine.

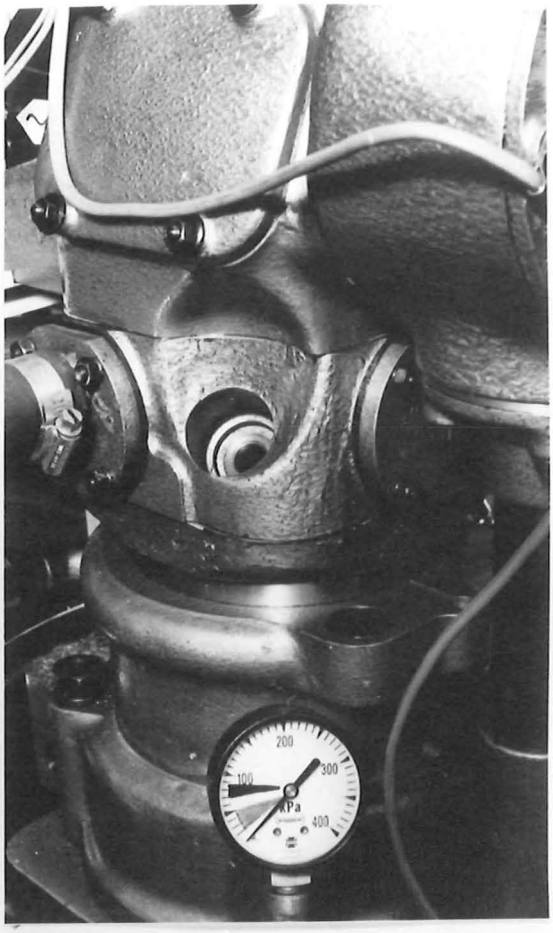

Plate 5.2 Auxiliary port in the cylinder head.

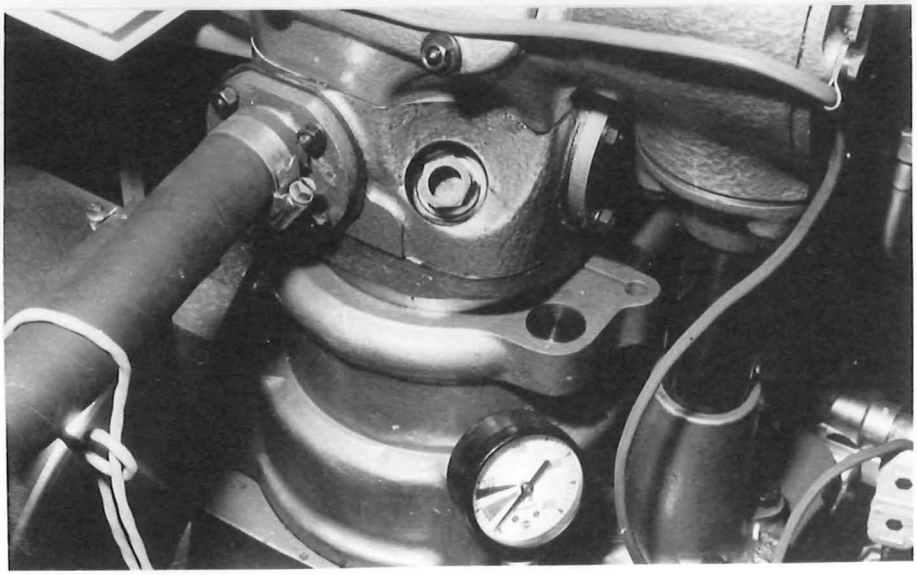

Plate 5.3 Glass window assembly installed in the cylinder head.

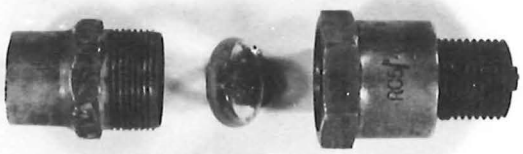

Plate 5.4 Quartz glass window assembly.

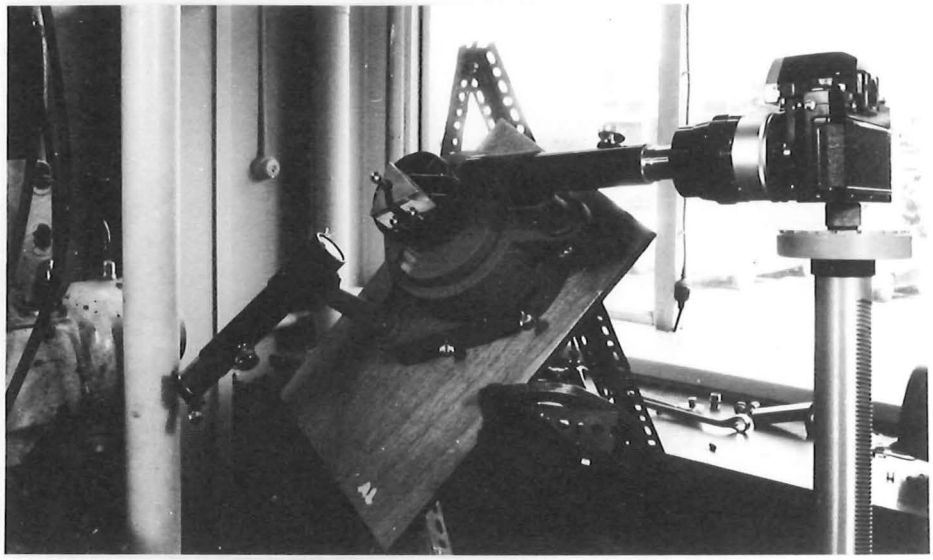

Plate 5.5 Apparatus to record the flame light spectrum.

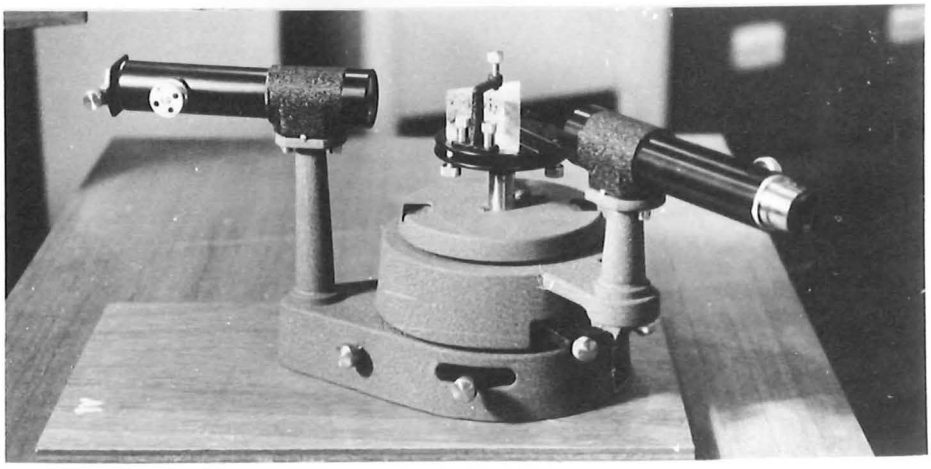

Plate 5.6 The spectrometer used to produce the flame spectrum.

the use of a Nikon Nikomat camera fitted with a 1:1 macro lens. Three types of film were used for recording purposes: visible monochromatic film, infra-red film (Ectachrome 2236) and panchromatic colour film. The visible and infra-red monochromatic films gave a combined light wavelength coverage from approximately 250 to 900 nm. The negatives of these films were subsequently analysed by means of a densitometer so that the flame spectrum light intensity could be represented in graphical form as a function of the light wavelength. The axes of these graphs were calibrated by comparing them with similar graphs of the spectral lines given by helium and mercury light sources and produced on the same recording apparatus. The spectral lines from these two sources have known wavelengths so the densitometer graph axes could be calibrated from them[50].

5.1.2 Test Procedure

A Ricardo E6 engine (specifications: Appendix 5.1) was operated in combination with the flame spectrum recording apparatus under the following conditions:

Engine:	Ricardo E6 (No. 27/49)
C.R.:	8:1
Speed:	2000 r.p.m.
Throttle:	3/10
Ignition Timing:	10° or 50° BTDC
Water Temperature:	≈60°C
Carburettor main jet:	Lean, 8; Stoichiometric, N; Rich, 2.
Fuel:	96 octane.

Testing was initiated after the engine had reached the above water temperature and then two series of tests were completed on each of the three types of film:

Series 1: The ignition advance was varied while all other operating conditions remained approximately constant and with the air-fuel mixture ratio set to approximately 15:1 (N).

Series 2: The air-fuel mixture ratio was varied to the rich (≈11:1) or lean (≈17:1) side of stoichiometric while all other operating variables were maintained constant and the ignition advance was set to give maximum engine power at the stoichiometric air-fuel mixture ratio.

During these series of tests the flame spectra were photographed

with exposure times of 4 seconds (except Plate 6.2) and with the maximum camera aperture setting. Such relatively long exposure times were necessary because of the low intensity of the spectrum light and this resulted in one frame integrating the spectrum light from approximately 67 combustion events. All testing was undertaken at night in order to minimise the interference from other extraneous sources of light.

5.2 Combustion Flame Light Intensity Measurements

5.2.1 Apparatus

Further testing was undertaken in order to examine the broadband light intensity of the combustion flame. In order to view the combustion flame the quartz glass window assembly was fitted into the Ricardo engine cylinder head as previously described.

5.2.1.1 Light Intensity Recording Apparatus

Light intensity detection equipment was then located outside the window assembly in the cylinder head (Plate 5.7). The equipment was used to measure the relative intensity of the combustion flame as a function of crankangle by means of a photodetector, amplifier, oscilloscope, xy recorder and crankangle pulse generator, and these will now be described.

5.2.1.2 Photodetectors

The photodetector was mounted in close proximity to the glass window through the use of an air-cooled photodetector to window adaptor which ensured that the photodetector operating temperature did not exceed 45° C (Plate 5.8). When these photodetectors are combined into appropriate electronic circuits, they convert incident radiation within a certain range of wavelengths into a proportional voltage output across their terminals (Plate 5.9)[61,62]. Three detectors, each responsive to light in a different region of the electromagnetic spectrum, were sequentially mounted over the window in order to measure the intensity of the flame radiation in different assembly regions of the spectrum. The response of each detector as a function of wavelength is given in Fig. 5.2. The silicon detector (specifications: Appendix 5.2) responds to light from blue (400 nm) wavelengths through to the near infra-red (1.1 μm). The lead-sulphide detector (specifications: Appendix 5.3) responds to radiation within the 1-3 μm near infra-red region and the lead-selenide detector (specifications: Appendix 5.4) responds to radiation within the 2-4.5 μm infra-red region.

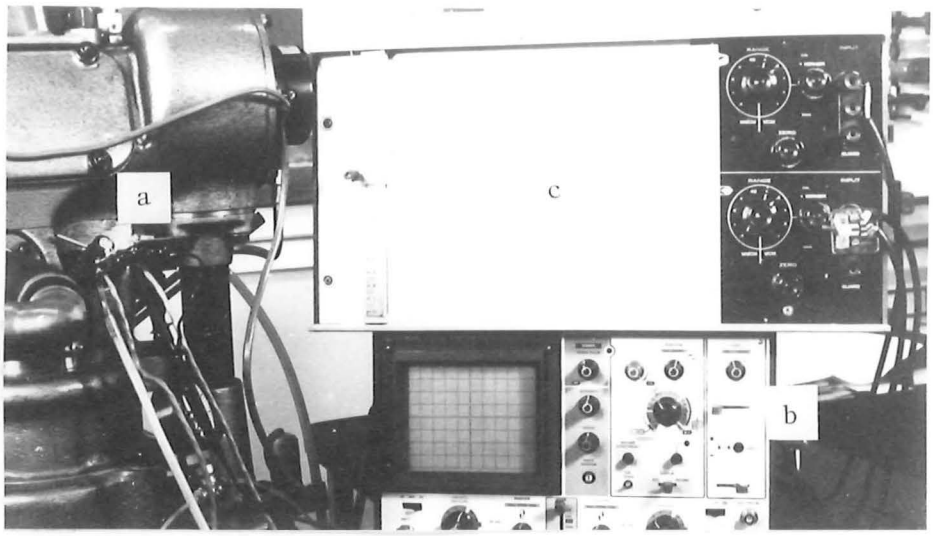

Plate 5.7 Complete apparatus to record the flame light intensity.
(a) Photodetector and amplifier circuitry;
(b) digital oscilloscope; (c) x-y recorder.

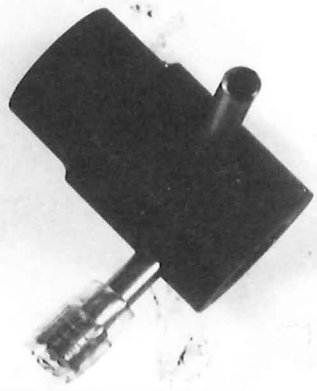

Plate 5.8 Photodetector to window adaptor.

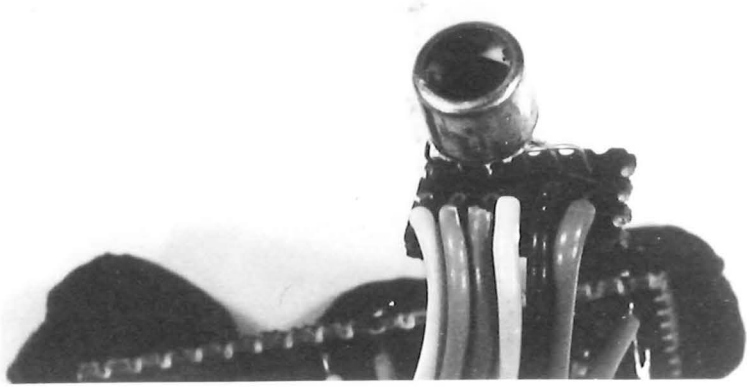

Plate 5.9 Photodetector (with integral op. amp.)

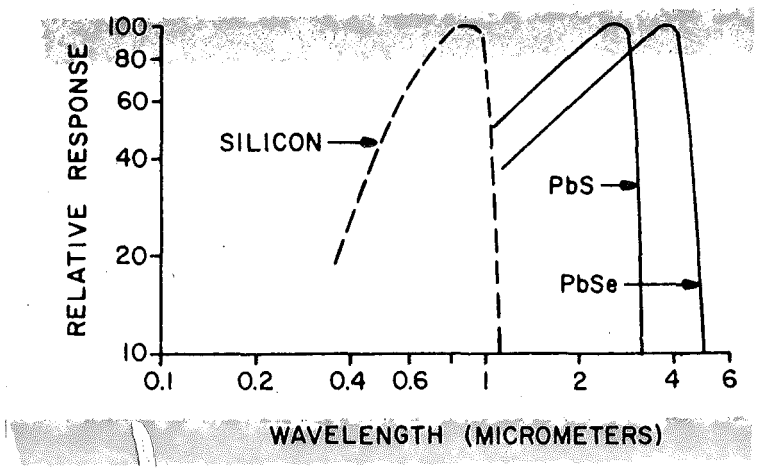

Figure 5.2 Relative response of silicon, lead sulphide (PbS) and lead selenide (PbSe) detectors as a function of wavelength[58].

5.2.1.3 Amplifiers

In order to amplify the photodetector outputs so they would provide a satisfactory input signal to the oscilloscope, the amplifier circuits of Figs 5.3 and 5.4 were constructed.

The lead-salt (lead-sulphide and lead-selenide) detectors behave as light dependent resistors and so these were connected into the voltage divider network in the circuit of Fig. 5.4. The RC (resistor-capacitor) section of this circuit provides DC (direct current) isolation between the voltage divider and op-amp (operational amplifier) since the op-amp represents a comparatively low impedance input which could otherwise affect the output of the voltage divider network. The RC network has a low cut-off frequency of 6.7 Hz so that the combustion event should occur at least 6.7 times per second to be satisfactorily amplified. Therefore the minimum (4 stroke) engine speed should be twice this or about 15 revs per second. The operational amplifier amplifies the signal by a factor of R1/R2 or a factor of 10 in the figure[59].

In contrast the silicon detector behaves as a light dependent voltage generator when it is connected to a high input impedance op-amp. Thus it was connected to a J-FET input transistor op-amp (Fig. 5.3) where the resistor R_f determines the signal amplification and the voltage output is proportional to the light intensity at the input.

5.2.1.4 Oscilloscope

Depending on the photodetector being used, the output of one of these amplification circuits was fed directly into one channel of a digital storage oscilloscope (Hitachi model VC-6015). The other channel of the

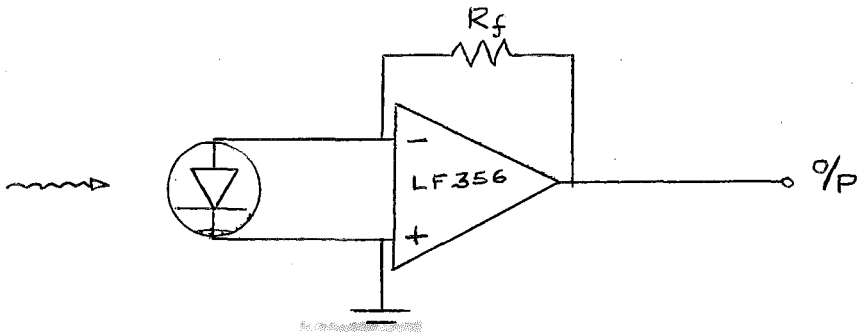

Figure 5.3 Silicon detector amplification circuit.

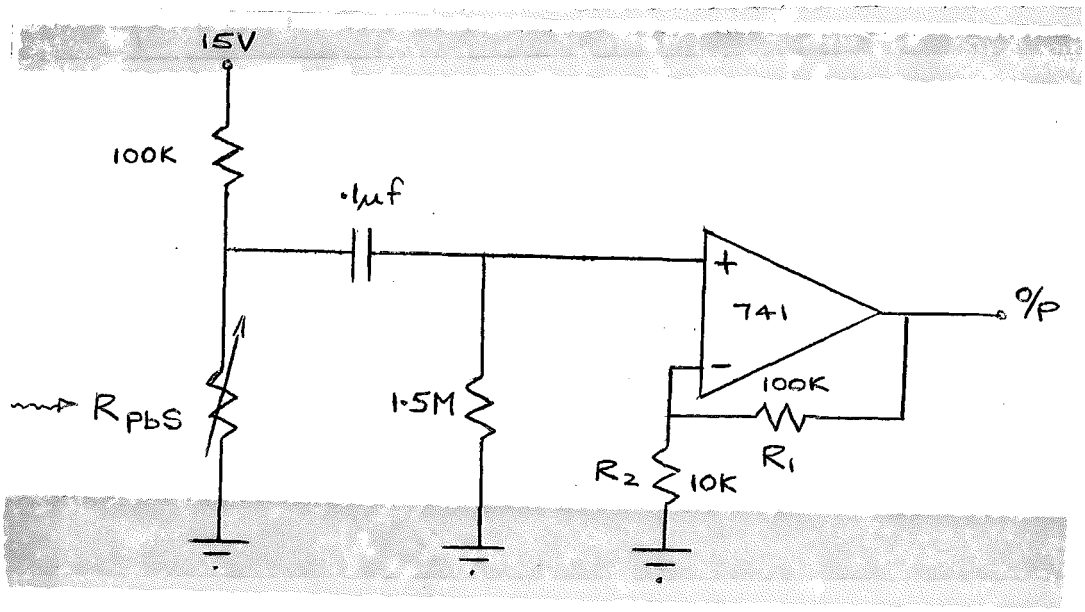

Figure 5.4 Lead-salt detector amplification circuits.

scope was connected to a crankangle pulse generator (made by Cussons and supplied with the Ricardo engine) which gives 10° crankangle voltage pulses and 5° pulses around TDC.

5.2.1.5 Recorder

An XY recorder (Hewlett Packard, model 7035B) was linked to the oscilloscope XY recorder output so that the light intensity and crank-angle traces could be transferred from the oscilloscope screen directly on to A4 paper.

5.2.2 Test Procedure for Light Intensity Measurements

The Ricardo engine (specifications: Appendix 5.1) operating conditions during the light intensity measurements were:

Engine:	Ricardo E6 (No. 138/82)
C.R.:	9:1
Speed:	15-45 r.p.s.
Throttle:	Set for approximately 1/3 or 2/3 or full engine torque
Water Temperature:	≈ 60° C
Ignition Timing:	10° - 50° BTDC
Fuel Injection rate set to:	Lean
	Stoichiometric
	Rich
Fuel:	96 octane.

The procedure during testing was to run the engine until the water temperature reached approximately 60°C and then to install the cleaned window for testing purposes. Two series of tests were performed. The first series was undertaken with each of the three photodetectors and the second series using the silicon photodetector only.

Series 1: The ignition timing was varied while other operating conditions remained approximately constant and the fuel mixture ratio was set to stoichiometric.

Series 2: The fuel mixture ratio was altered to rich or lean while all other conditions remained approximately the same and the ignition timing set to give maximum engine power.

5.3 Development of Optic Spark Plugs

Spark Ignition engines currently manufactured for use in automobiles have only one access port into the combustion chamber, the spark plug port. Therefore in order to continue investigations of the combustion flame in these engines, it was decided that a combination spark plug and glass window should be developed. The resulting 'optic plug' should have the same heat range as the conventional spark plug it replaces and other critical performance criteria should remain unchanged. This section describes progress towards the development of such a plug and a test procedure to establish its effectiveness.

A spark plug manufacturing company must produce a range of spark plugs in order to meet the requirements of a wide variety of engine designs, for example the differing spark plug requirements for low compression or high compression ratio engines must be taken into account.

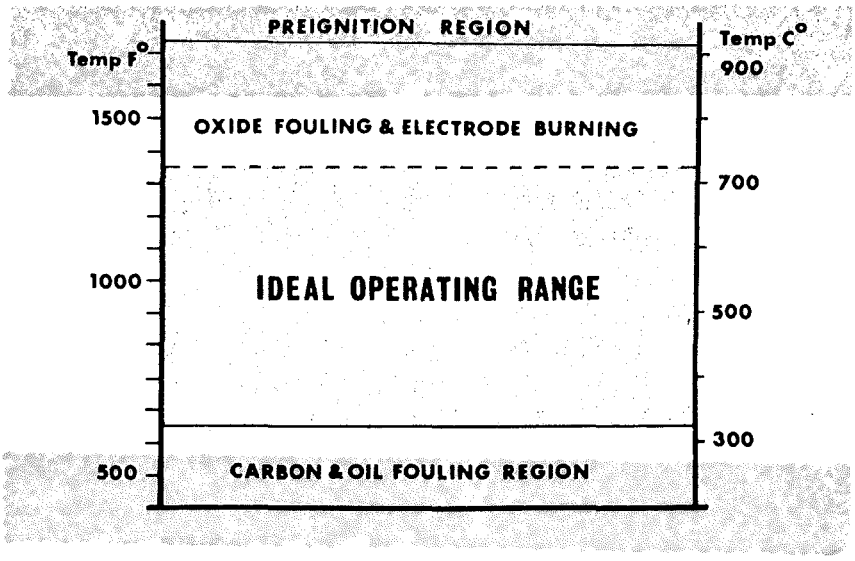

Figure 5.5 Operating characteristics of the spark plug insulator tip as a function of its temperature[13].

The spark plug insulator tip temperature should be maintained within the temperature range of Figure 5.5. (The insulator tip is the section of the porcelain insulator which surrounds the inner end of the centre electrode.) When the insulator tip temperature is in this region the combustion product fouling due to low tip temperatures will be minimal, and the probability of the insulator tip causing pre-ignition due to high tip temperatures will be small. The temperature of the insulator tip is maintained in this region by:

1. Varying the length of the thermal conduction path between the insulator tip and the base of the plug.
2. Varying the diameter of the heat conducting centre electrode, Fig.5.6.

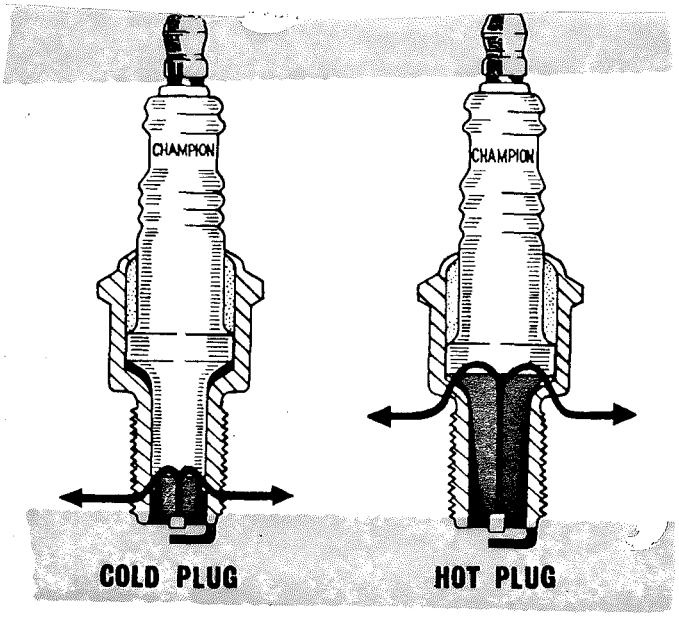

Figure 5.6 Temperature control of spark plug insulator tip[13].

Since a low compression ratio engine will operate with consistently cooler combustion temperatures than a high compression ratio engine, a range of spark plugs are manufactured to meet the different tip to base heat conductivitiy requirements[56]. These heat range requirements must also be considered when developing optic spark plugs for use in a variety of automotive engines. A similar series of optic plugs would need to be developed with equivalent heat ranges. In order to minimise the time spent in developing optic plugs with the correct heat range characteristics, it was decided to adapt normal spark plugs to form an optic plug (refer to Appendix 5.5 for initial prototype optic plugs). Such adaption was achieved through the creation of hollow centre electrode spark plugs which enabled the combustion flame to be viewed through the hole in the centre electrode.

5.3.1 Development of Hollow Centre Electrode Spark Plugs

The standard Champion spark plug centre electrode is constructed from two butt welded rods, Plate 5.10 and Fig. 5.7(a). In the figure the right-hand rod section is manufactured from nickel alloy metal so that it can withstand high temperatures and chemical corrosion within the combustion chamber into which it protrudes. The left-hand rod section in the figure is extruded from a cheaper metal stock since it is housed entirely within the spark plug insulator and merely acts as an electrical conductor between the high tension endstud and the nickel alloy section.

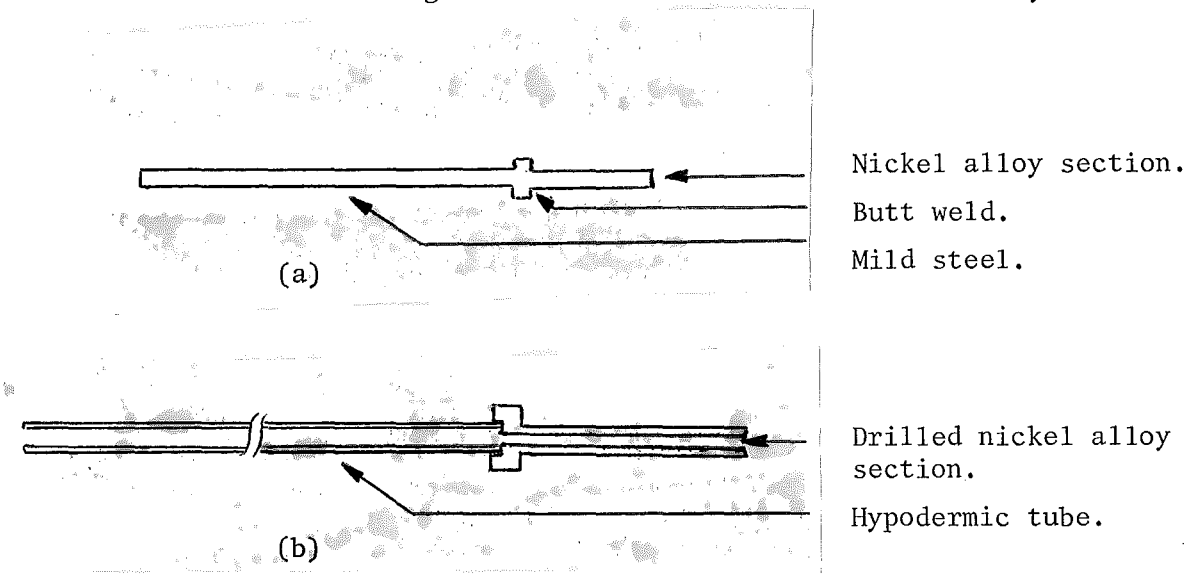

Figure 5.7 (a) Standard N7Y centre electrode (scale: approx.1:1).
(b) Hollow centre electrode (not drawn to scale).

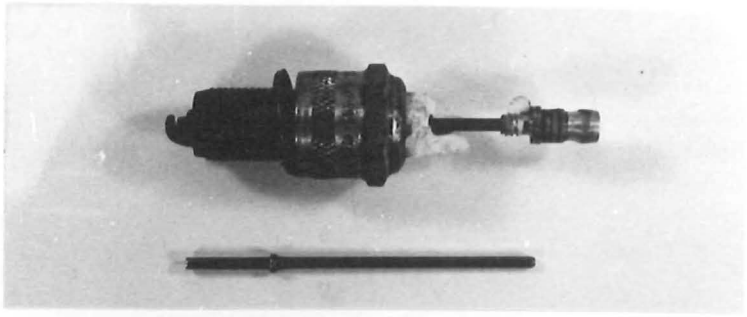

Plate 5.10 Spark plug with the upper insulator removed exposing the centre electrode and a standard centre electrode above it.

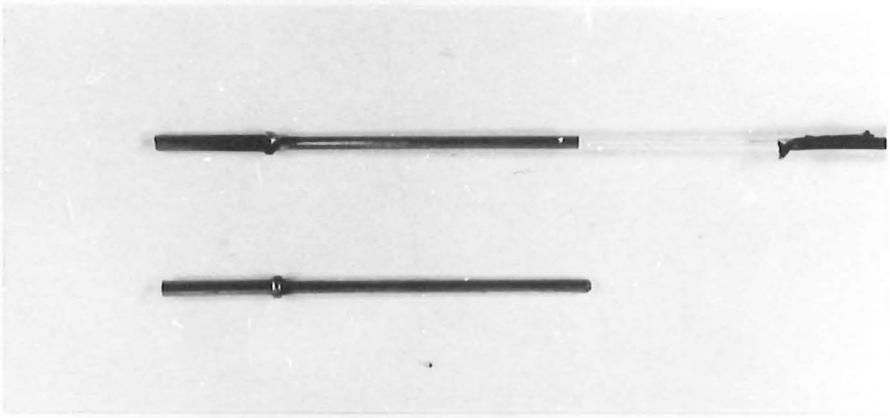

Plate 5.11 Comparison of standard centre electrode (uppermost in plate) versus hollow centre electrode (with glass rod inserted; refer to Section 5.3.2).

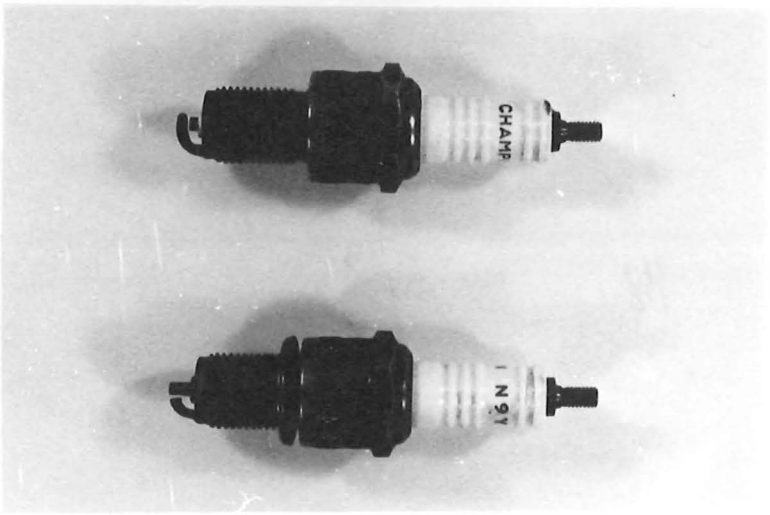

Plate 5.12 Comparison of standard spark plug (lowest in plate) versus hollow centre electrode spark plug.

In order to make a hollow centre electrode the original centre electrode was parted at the butt weld and the nickel alloy section was drilled to between 1 - 1.25 mm, (Fig. 5.7(b)). The second section was replaced with an 2.05 mm O.D. (outside diameter) hypodermic tube which was braised to the drilled nickel alloy section. A completed hollow centre electrode is compared with the original in Plate 5.11, and since its external dimensions were approximately the same, it could be returned to Champion Spark Plugs Ltd for casting on their spark plug assembly line.

The completed hollow centre electrode plug is shown in Plate 5.12. There are two main differences between this plug and the standard plug:

1. The spark plug gap is formed on the side of the centre electrode in order to increase the light transmitted into the centre electrode hole.
2. The centre electrode is reduced by drilling it hollow and therefore its thermal conductivity is also altered. An estimate of the effect of this drilling on the heat range of the plug can be made by comparing a hollow centre electrode Champion N7Y spark plug with a Champion N9Y plug in standard form.

The N7Y is two heat ranges cooler than the N9Y, being separated from it by the N8Y, and this change in heat range is achieved by changing the diameter of the centre electrode in order to alter its thermal conductivity. The insulator length between the two plugs remains unaltered. However, if the N7Y centre electrode is drilled hollow to 1.10 mm its cross sectional area becomes almost identical to the N9Y centre electrode cross sectional area:

Plug model:	N9Y	N7Y	N7Y (drilled)
Centre electrode diameter:	2.29 mm	2.54 mm	2.54 mm
Diameter of hole (d):	0.0 mm	0.0 mm	1.1 mm
Centre electrode cross-sectional area $(\frac{\Pi\phi^2 - \Pi d^2}{4})$:	4.12 mm^2	5.07 mm^2	4.12 mm^2

Therefore the properties of a spark plug which determine its heat range, the length of the insulator from tip to base and the cross sectional area of the centre electrode (refer to section 5.3), are approximately the same when comparing the N9Y and hollow centre electrode N7Y spark plugs. Thus it is postulated that drilling the centre electrode makes the N7Y plug heat

range similar to that of an N9Y although this should be confirmed through testing.

5.3.2 Development of Fibre Optic Spark Plugs

The hollow centre electrode spark plug was made into an optic plug by inserting fibre optic cable down the length of the hollow centre electrode. Fibre optic cable is most effective in transmitting light efficiently from one region to another, so it was used to transmit the combustion chamber flame light along the fine centre electrode hole and from there to the photodetector some distance from the plug (see Appendix 5.6). The location of the photodetector some distance from the engine, through the use of fibre optic cable, also helps to reduce high frequency electrical interference from the ignition system.

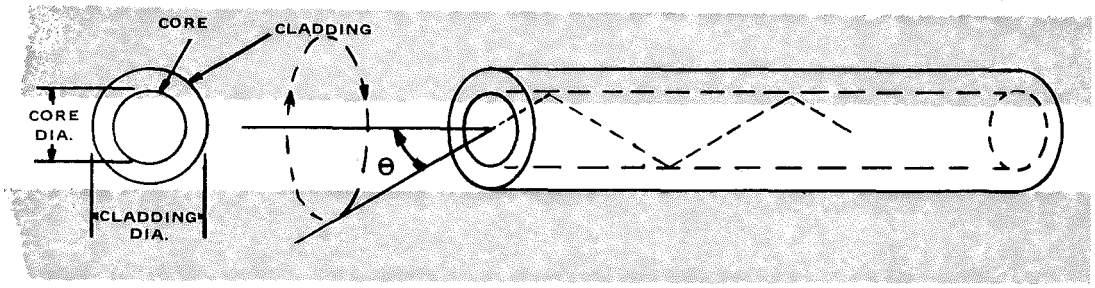

Figure 5.8 Fibre optic strand showing the cone of light of solid angle θ which can be transmitted[63].

The fibre optic cable is able to transmit light from a region of the combustion chamber determined by the acceptance angle (θ) of the fibre (Fig. 5.8). In this way the cable can be used to advantage since it extends the viewing region within the combustion chamber as compared to viewing the combustion light directly through the hollow centre electrode hole.

The type of optic fibre used for this purpose was determined mainly by the temperature conditions within the combustion chamber. A single quartz core, quartz clad 1.2 mm fibre strand was selected as it could withstand temperatures up to 1500° C and it also had a large enough diameter to transmit a sufficient quantity of light to the photodetector.

The strand (Code Number HIP-S1000 from Optics for Research, Britain) was supplied coated with a fine layer of silicon polymer and sheathed with a plastic jacket. These coatings were removed from the strand to various exents (Fig. 5.9) before it was cemented into the spark plug

with a sodium silicate based cement. The optic strand was then polished flush at the inner end of the spark plug centre electrode to a 0.25 micron finish. The outer end of the fibre optic cable was terminated with an AMP connector and polished to the same finish. The completed optic plug configuration is shown in Plate 5.13.

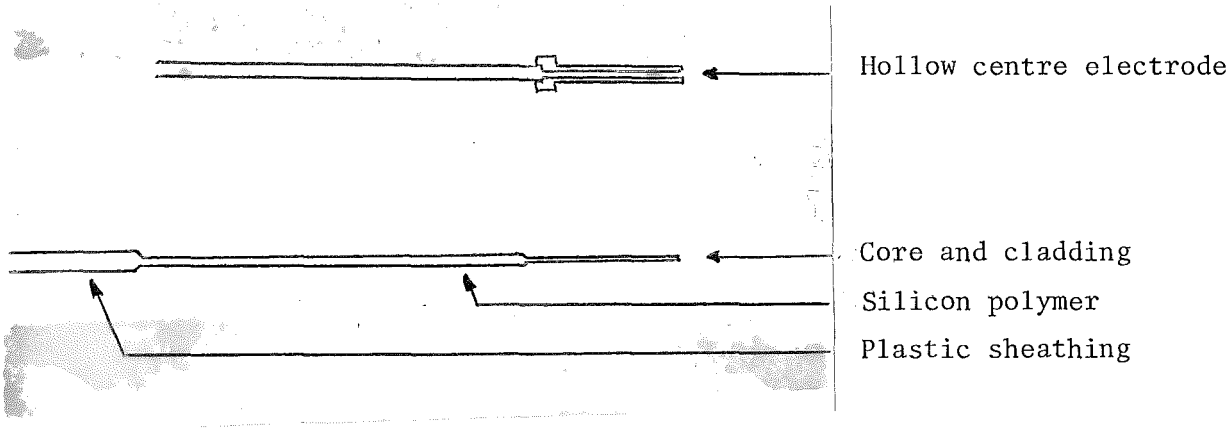

Figure 5.9 Removal of fibre optic sheathing prior to insertion and cementing into the hollow centre electrode spark plug.

5.3.3 Test Procedure for the Optic Spark Plugs

The optic plugs enabled light intensity measurements to be made in standard automotive engines. For testing purposes the optic plug was connected up to the light intensity recording apparatus as reviewed in Section 5.2, via the AMP connector system. Combustion flame light intensities were measured from the Ricardo E6 engine, a Mitsubishi Lancer 1300 cc engine (Plate 5.14) and a Ford Cortina 1600 cc engine in order to determine whether:

1) the optic plug system would respond to the light oscillations peculiar to knocking combustion;
2) the system would continue to operate satisfactorily over an extended period of time.

The operating conditions of the Ricardo engine were the same as outlined in Section 5.2.2 except that the fuel mixture ratio was not altered from stoichiometric. Testing on this engine was undertaken in order to verify point 1) above.

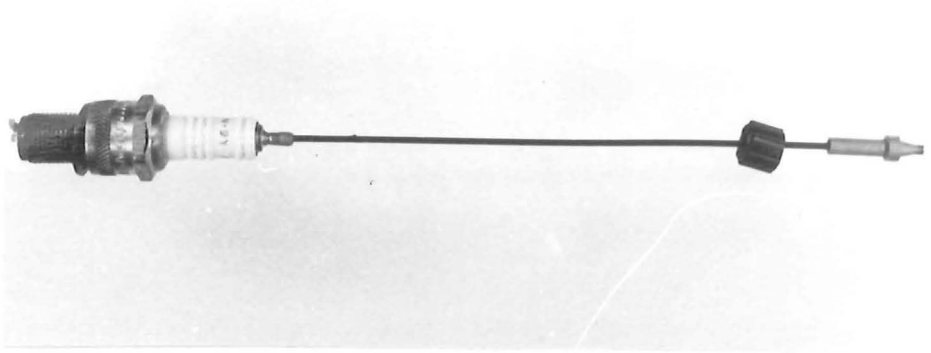

Plate 5.13 Completed optic spark plug.

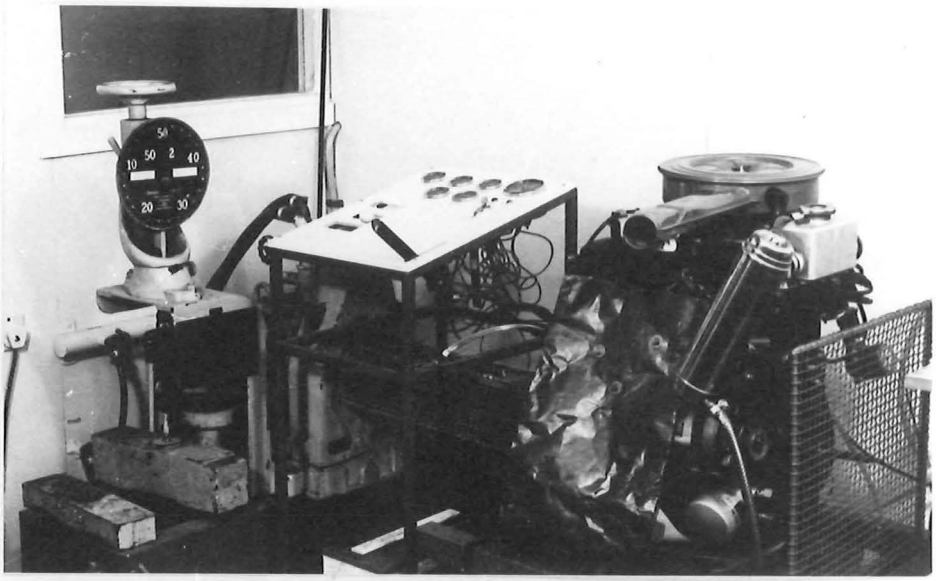

Plate 5.14 Mutsubishi Lancer engine and dynamometer test bed.

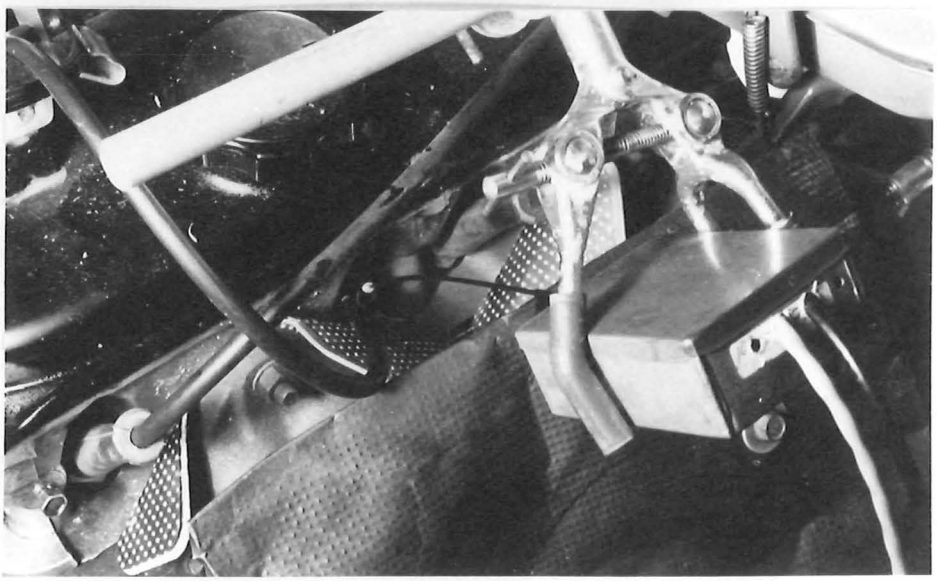

Plate 5.15 Optic plug, photodetector and amplifier installed on the Lancer engine.

The operating procedure for the two automotive engines depended upon which of the two objectives above was being verified. The ability of the optic plug system to monitor knock (point 1) was examined by operating either engine at high load and low engine speed and then advancing the distributor until knocking combustion was audible. The other engine operating conditions and specifications were:

Engine: Ford Cortina Mk III 1600 cc (Serial No. 711M6015BA)
Specifications: Set to standard except the ignition advance.
Water Temperature: Normal operating range (80° to 90° C)
Fuel: 96 octane.

The long term reliability of the optic plug (point 2) was considered to be constrained by combustion product fouling on the inner end of the optic cable; so the long term operation was simulated by operating a Lancer engine and optic plug assembly (Plate 5.15) for long periods of time with engine speeds and loadings designed to correspond to city driving conditions. These conditions create high combustion product contamination of the combustion chamber surfaces. The engine and engine dynamometer were set to one of three alternative conditions for time periods from one half hour to 8 hours operation.

1. Idle.
2. '50 km/hr'
3. Short periods at '80 km/hr'.

The 50 km/hr and 80 km/hr operating conditions were simulated by the following engine speeds and loads:

Speed to be simulated (km/hr)	Engine Speed (r.p.m.)	Engine Torque (Nm)
50	1900	22.6
80	3000	30.2

The conditions during engine testing were:

Engine: Mitsubishi Lancer 1300 cc (Serial No. 4G11/11BB0809)
Specifications: Set to standard.
Water Temperature: Normal operating range (80° to 90° C)
Fuel: 96 octane.

The apparatus described in this chapter was used to examine the electromagnetic radiation emitted by the combustion flame and to produce the results given and discussed in Chapter 6.

CHAPTER 6

RESULTS, OBSERVATIONS AND CALCULATIONS

CONTENTS

INTRODUCTION

The results obtained through the use of the experimental apparatus and test procedures outlined in Chapter 5, are summarised in this chapter. It is sub-divided into three major sections. The first section (6.1) gives the results of the combustion flame spectrum analysis under rich, lean, stoichiometric and knocking engine operating conditions. The associated equipment has been described in Section 5.1. The second section (6.2) provides the results gained from tests utilising the silicon and lead-salt based detector apparatus, outlined in Section 6.3, the third section, gives the results of tests which utilised the optic plug assembly detailed in Section 5.3.

6.1 The Effect on the Flame Spectrum of Altering the Spark Timing and Air-Fuel Ratio

The results obtained using the combustion flame spectrum analysis equipment consist of:

(1) A series of plates depicting the combustion flame spectrum for various different air-fuel mixture ratios and ignition advances (Plates 6.1 to 6.4).

(2) A series of densometer curves for the flame spectrum taken under the same operating conditions as in point (1) above. (Figures 6.3 to 6.6.)

The densitometer curves were produced from monochromatic negatives of the visible and infra-red flame spectrum. Those visible and infra-red densitometer curves recorded for the same operating conditions were then combined to give a spectrum range from 900 nm to 400 nm.

The calibration of the optical density axis of these curves was achieved by comparing the flame spectrum negatives with a photographic step tablet (Kodak No.2) in order to match one of its graded densities with the least dense region of the spectrum negative. Then successively higher densities on the tablet were recorded by the densitometer on to the spectrum densitometer curve y axis. The scale is given as the logarithmic optical density of the spectrum negatives.

The calibration of the densitometer curve wavelength axis was accomplished by photographing the spectral lines of fluorescent (35 white) and mercury light sources through the same spectrometer and recording apparatus and producing similar densitometer curves from the negatives (Figures 6.1 and 6.2). The spectral lines from these light sources have known wavelengths[50] and so a calibrated wavelength axis suitable for all the densitometer traces could be derived from them.

Interpreting from these two light sources gives spectral lines with a maximum calibration error of 5 nm on the wavelength axis. However beyond the spectral line at 580 nm and up to 900 nm the wavelength axis was extrapolated so that the calibration error is expected to increase from 5 nm error at 580 nm up to 50 nm error at 900 nm.

Results:

Air-Fuel Ratio	Ignition Advance (°BTDC)	Plate	Figure
≈15:1 (≈stoich)	10	6.1	6.3
≈15:1 (≈stoich)	50	6.2	6.4
≈17:1 (lean)	10	6.3	6.5
≈11:1 (rich)	10	6.4	6.6

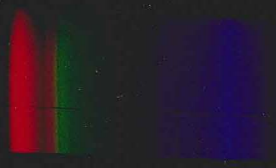

Plate 6.1 Combustion flame spectrum of normal combustion

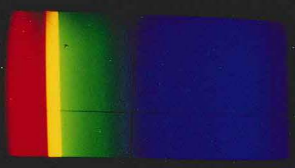

Plate 6.2 Combustion flame spectrum of knocking combustion

Plate 6.3 Combustion flame spectrum of lean combustion

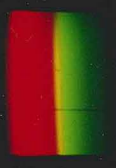

Plate 6.4 Combustion flame spectrum of rich combustion

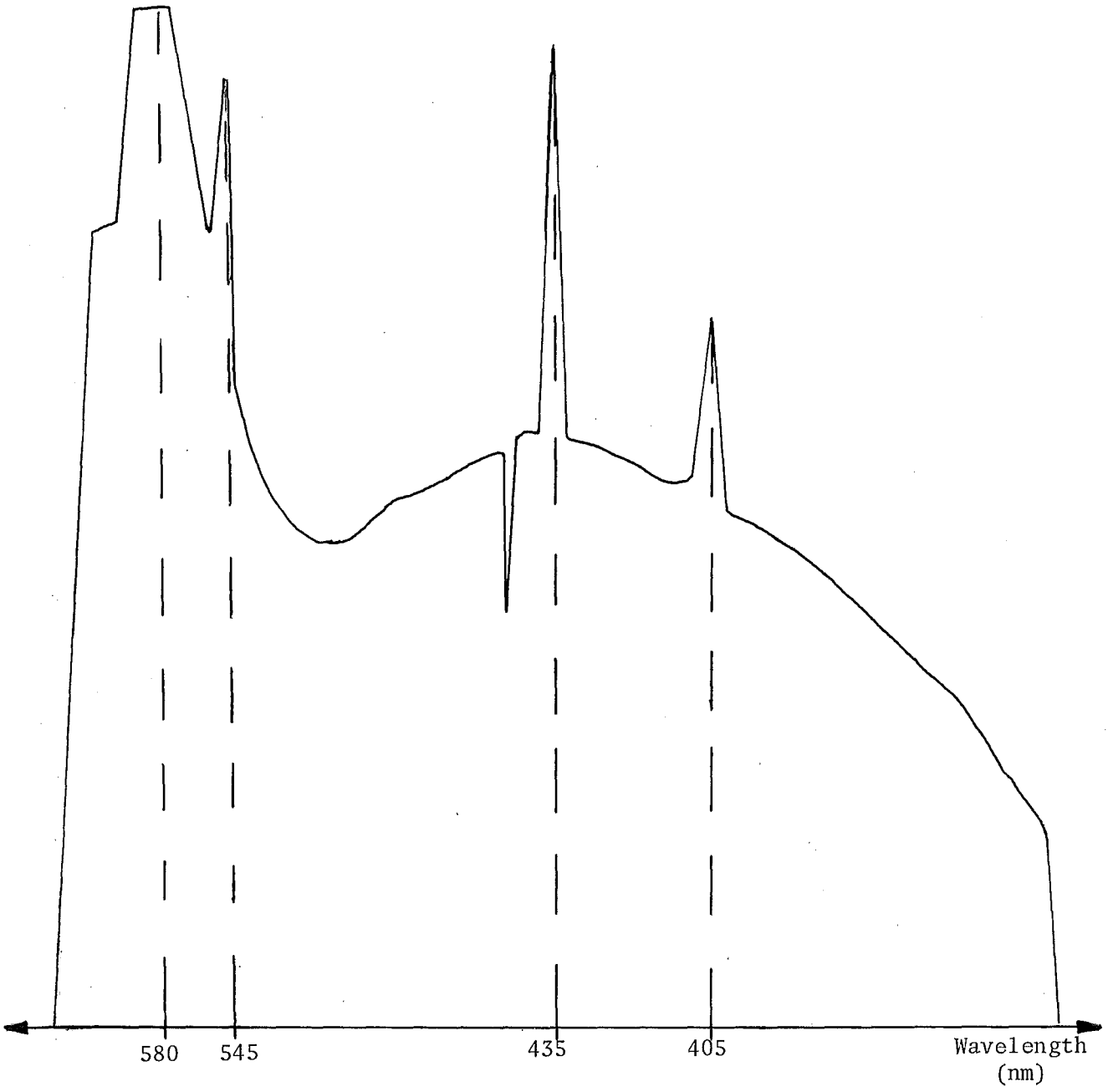

Figure 6.1 Line spectrum produced by a fluorescent light source through the flame spectrum recording apparatus.

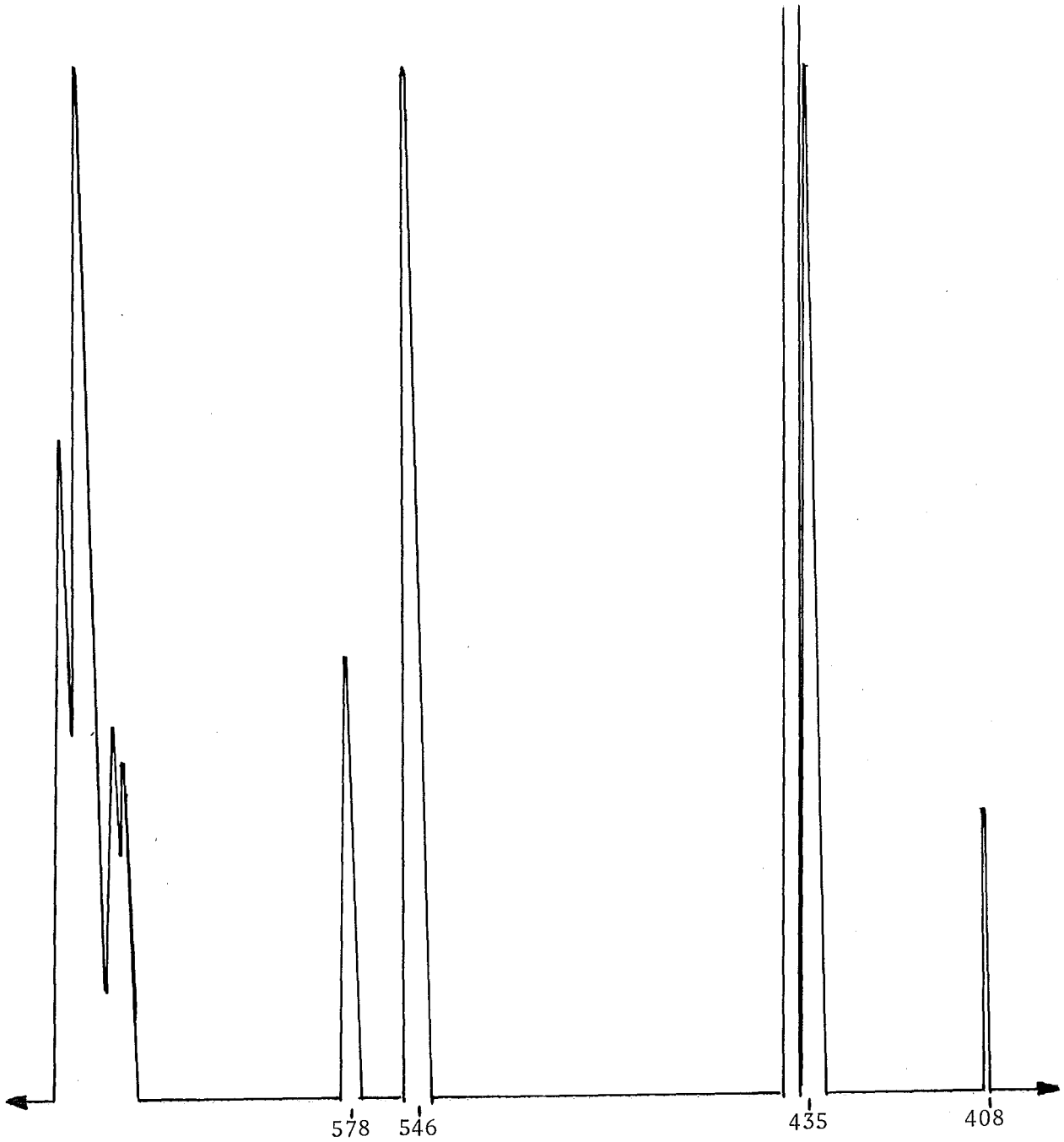

Figure 6.2 Line spectrum produced by a mercury light source through the flame spectrum recording apparatus.

Observations

A direct comparison of Plates 6.1 and 6.2 gives a direct visual comparison between the combustion flames in a non-knocking (left-hand plate) and knocking operating condition. The flame is generally brighter in the knocking condition and the yellow region is especially strengthened. This is verified by a comparison of the corresponding densitometer traces (Figures 6.3 and 6.4) where the yellow band is depicted at approximately 580 nm. This is the region in which the C_2 radical has an emission band (Plate 4.1; 0, 2 band) and it is concluded that the more rapid and higher temperature auto-ignition combustion process has caused the intensity of this band to increase. The intensity of this band might also be affected by trace amounts of sodium present as an impurity in the intake mixture which would emit light in this region if sufficiently excited (refer to Section 4.3.2).

The overall increase in the spectrum light intensity during knocking combustion is probably due to the higher combustion temperatures under these conditions causing the light emissions to increase (refer to Section 4.3.3). The higher combustion temperatures are also likely to be the reason for the increased near infra-red emissions during knocking combustion (refer to Figure 4.4).

The other local maxima shown in Figure 6.3 can be accounted for by radical light emissions. The peaks situated at approximately 503 nm and 465 nm are almost certainly due to two other C_2 bands. The peak at approximately 455 nm is not considered to be due to the hydrocarbon flame since the minimum immediately to the left of it is believed to be caused by the spectrometer sighting grid which causes a discontinuity in the spectrum (this grid can be observed in Plate 6.2). It is assumed that the flame spectrum should follow the dotted line drawn above this minimum.

The peak at approximately 430 nm is most likely due to the corresponding CH band at this wavelength and the peak at approximately 406 nm is considered to be a Pb or PbO line (Section 4.3.5.1) from the tetra-ethyl lead anti-knock additive in the fuel. The intensity of this band increases with knocking combustion.

The CH and C_2 bands are all of lower relative intensity in the knocking combustion trace as compared to the normal combustion trace

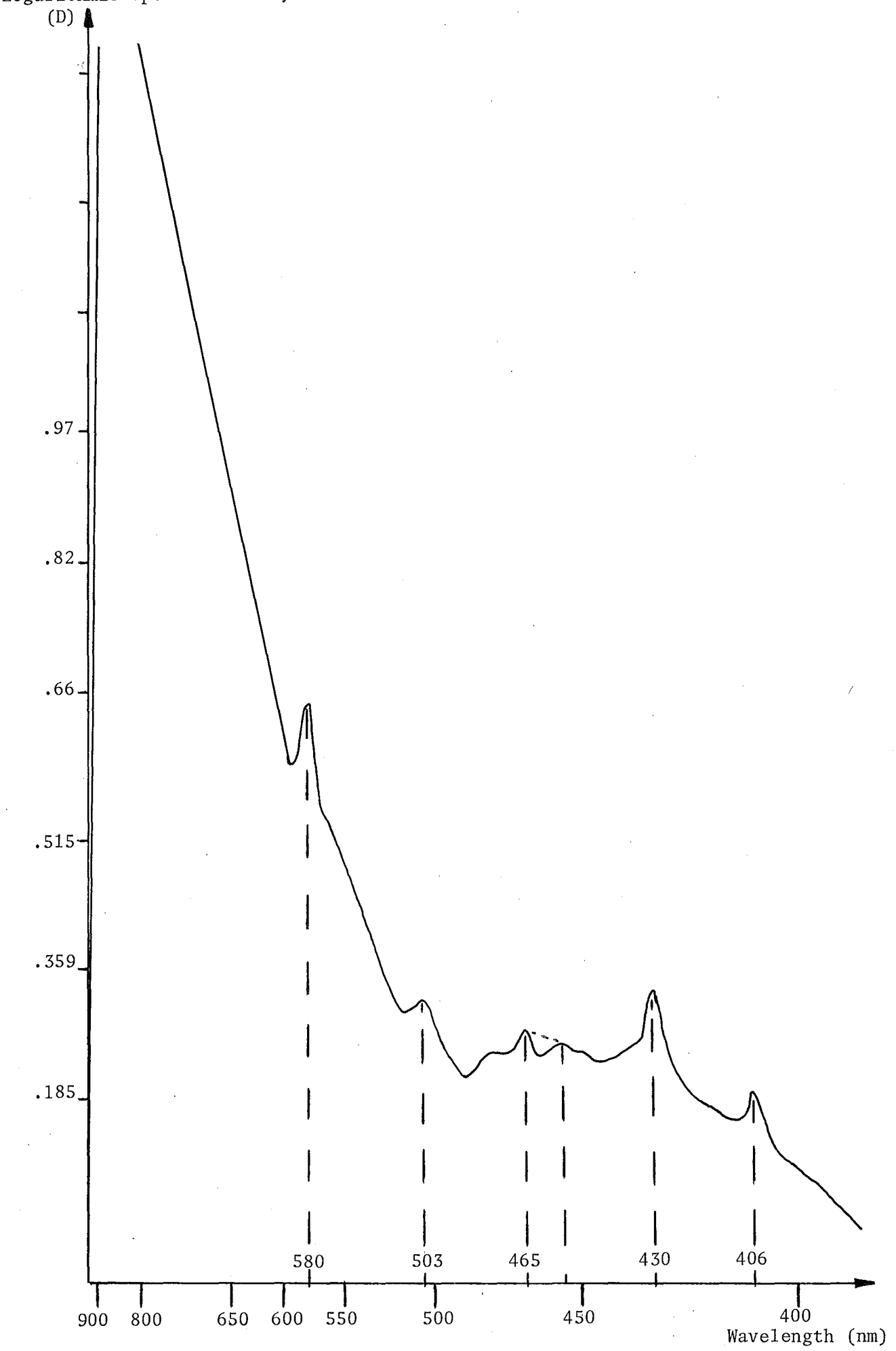

Figure 6.3 Spectrum of optical density as a function of wavelength for approximately stoichiometric air-fuel mixture ratio.

Figure 6.4 Spectrum of optical density as a function of wavelength during knocking combustion.

and this could be a result of the reduced CH and C_2 emissions in the auto-igniting section of the charge (refer to Section 4.3.4) which would also reduce their overall intensity in the spectrum.

The general continuum background light intensity below the radical peaks does not steadily decrease from near infra-red wavelengths to blue wavelengths as it would do if it were wholly composed of black body radiation in the form of carbon particle luminescence (Figure 4.4). Instead the trend of the graph is to decline steadily until about 470 nm and then form a second broad maximum until it starts decreasing again about 420 nm. It is expected that this addition to the generally decreasing curve is caused by the burning carbon monoxide continuum (Plate 4.2) which extends from 450 to 370 nm (refer to Section 4.3.2).

When Plates 6.1 and 6.3,(approximately) stoichiometric and lean mixtures respectively, are compared the main contrast is in the overall intensity of the two spectra, the lean spectrum being slightly less intense. The corresponding densitometer traces (Figures 6.3 and 6.5) differ mainly in the intensity of the local maxima which are relatively more intense in the trace of stoichoimetric combustion. The increase in the intensity of the C_2 and CH bands as the air-fuel mixture is strengthened is in accordance with trends described in Section 4.3.5.2. It is also noted that the PbO band is more intense on the stoichiometric trace and there is a slight increase in the intensity of the 580 nm band, the latter probably being due to the increased combustion temperatures at stoichiometric air-fuel mixture ratios.

The peak which is encircled in Figure 6.5 is not considered to be part of the combustion flame spectrum since it is unusually narrow and is not repeated in any of the other spectra. It could have resulted from a water or developing stain on the negative or a scratch mark. If the spectrum of a rich combustion flame (Plate 6.4) is compared to the stoichiometric case (Plate 6.1) the most significant difference is the lack of light intensity towards the blue end of the spectrum in the latter plate; however, the green, yellow and red spectrum region is more intense. The respective densitometer traces confirm this difference (Figures 6.3 and 6.6). The trace of rich combustion is more intense from 900 nm to approximately 450 nm, but then decreases below the stoichiometric spectrum light intensity.

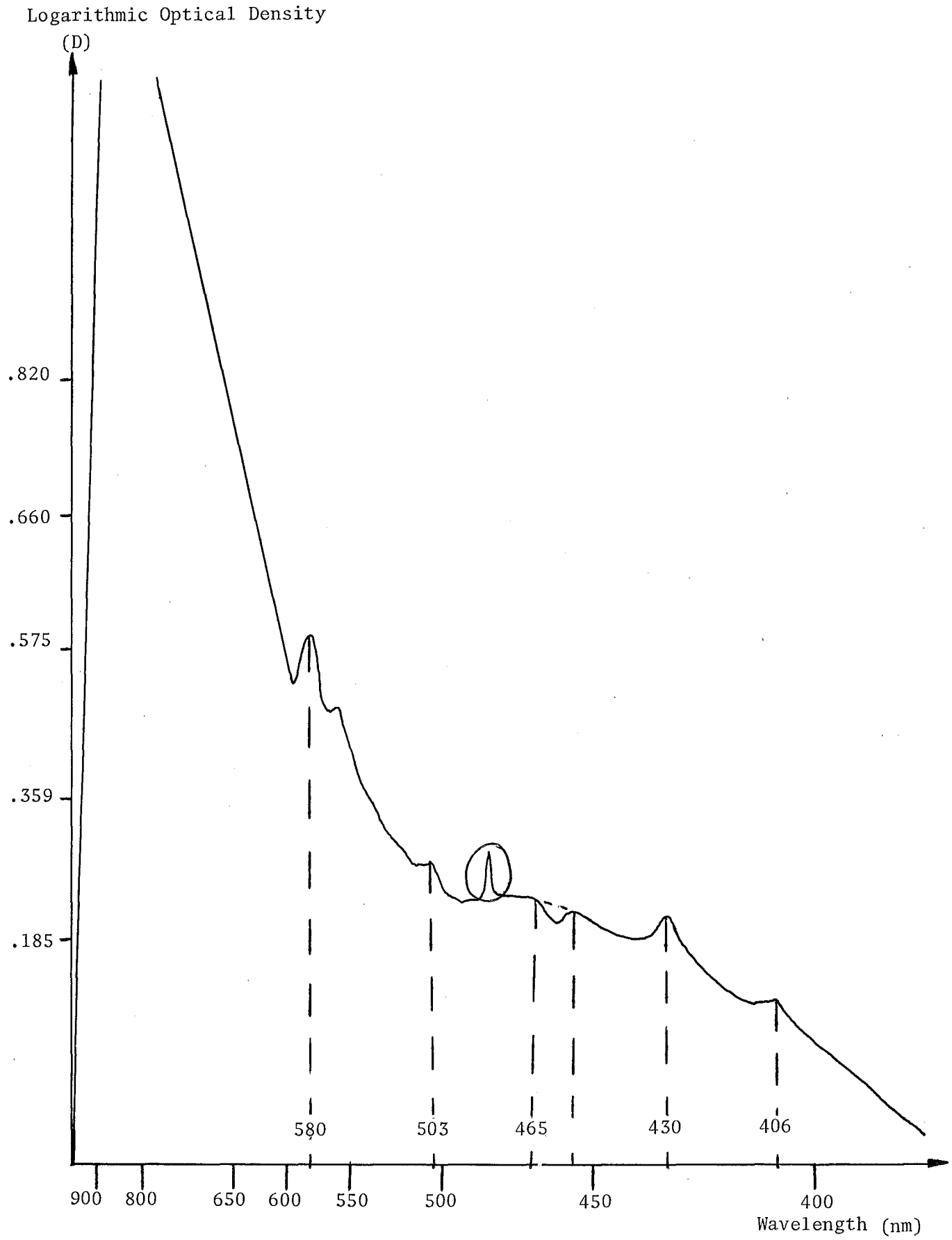

Figure 6.5: Lean air-fuel ratio flame spectrum giving the optical density as a function of wavelength.

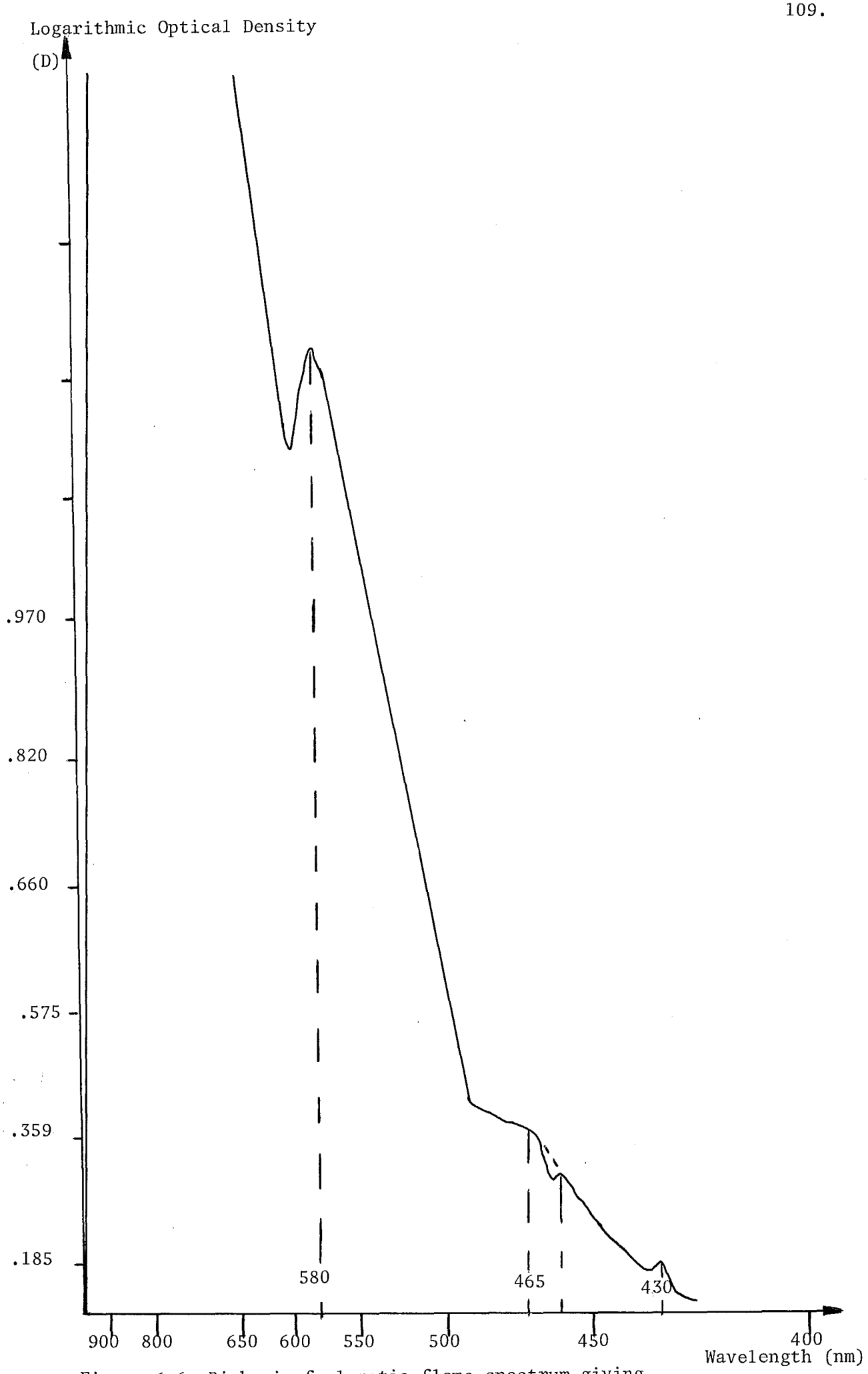

Figure 6.6 Rich air fuel-ratio flame spectrum giving optical density as a function of wavelength.

The increase in light intensity in the red region is due to the higher concentration of solid carbon particles in the rich flame. The increase in the infra-red radiation given on the densitometer trace of fuel rich combustion is due to the higher combustion temperatures associated with this operating condition, causing stronger thermal emission (refer to Section 4.3.1). The decrease in light intensity at the blue end of the spectrum is possibly caused by a decrease in the emissions from the burning carbon monoxide continuum (refer to Section 4.3.3).

The local maxima caused by radical emissions are not as prominent in the trace of fuel rich combustion although the radical emissions are expected, from other literature (Section 4.3.5.2), to be strongest in this operating condition. The lack of prominence of the radical emissions in the rich combustion curve may be caused by the relative increase in the background continuum intensity during rich operation which results in a reduction in the relative intensity of the radical maxima .

6.2 The Combustion Flame Light Intensity as a Function of Crankshaft Angle

The combustion flame light intensity curves recorded as a function of crankshaft angle are described in Section 6.2.1, which refers to results produced by the silicon photodetector apparatus, and in Section 6.2.2, which gives results produced by the lead-salt detectors and associated apparatus. The silicon photodetector is responsive to electromagnetic radiation from 400 nm to 1.1 μm (refer to Section 5.2.1.2) so that the light intensity curves produced from this detector reveal the combustion flame emissions in this region of the spectrum only. The first series of curves (Section 6.2.1.1) depict the response of the silicon based photodetector to changes in the air-fuel mixture ratio. Since the photodetector response did not alter significantly over a comparatively large change in air-fuel mixture ratio (refer to Appendix 3.1), this testing was discontinued.

The second series of curves (Section 6.2.1.2) from the silicon photodetector were recorded in order to provide an understanding of the influence of the ignition timing on the light emissions from the combustion flame. The number of curves represents a permutation of three different speeds, three different loadings and three different ignition advance settings in order to cover a broad range of engine operating conditions. These initial results showed that the light intensity was largely independent of engine speed enabling further testing to be confined to fixed values of engine speed.

The third series of graphs (Section 6.2.1.3) give a more detailed account of the way the light emissions, as detected by the silicon photodetector, are affected by advancing the ignition timing, by knocking combustion, and by cyclic variation.

The lead sulphide detector is responsive to radiation from 1 μm to 3 μm and can therefore detect the H_2O and CO_2 vibration and rotation bands that are centred at 2.8 μm (refer to Section 4.3.1). The lead selenide detector is responsive to radiation from 2 μm to 4.5 μm and is capable of detecting emissions from the above band and also from the CO band at 4.4 μm. The series of curves produced from these photodetectors are given in Section 6.2.2.

The photodetectors have a linear output response to increasing light intensity inputs so that the corresponding light intensity scale given with the curves is linear. The scale enables a comparison to be made of the relative light intensities between sets of curves recorded under the same operating conditions. These curves are normally presented in sets of 3 in this chapter. During engine operation combustion product built-up on the inner surface of the window caused light intensity variations at the detector which were not attributable to the combustion flame itself; however, these sets of results were taken over a relatively short time interval (approximately 30 minutes).

With reference to the engine operating conditions, the torque loadings created by the dynamometer on the engine and referred to throughout the rest of this chapter are defined as follows:

a) Low Torque at a fixed engine speed is defined to be approximately 1/3 of maximum torque at the same engine speed.

b) Medium Torque is defined to be approximately 2/3 of maximum torque at this engine speed.

c) High Torque is defined to be approximately full torque at this engine speed (with air-fuel mixture ratio at approximately stoichiometric setting).

6.2.1 The Response Curves from the Silicon Photodetector

6.2.1.1 The Effect on the Flame Light Intensity of Altering the Fuel Mixture Ratio

Engine Speed: 15 r.p.s. Engine Torque: Low

Throttle Position: 0.8/20. Ignition Advance: 30° BTDC

Results

A/F Ratio	Figure
15.0	6.7
14.6	6.8
14.1	6.9

Observations

The three graphs are very similar except that the lean air-fuel mixture ratio gave a slightly lower peak light intensity.

The shape of the graphs (refer to Section 4.3.5.3) shows how the light intensity increases after the flame kernel is formed somewhat before TDC until it reaches a maximum by which time the flame has propagated throughout the mixture. The decreasing section of the curve takes account of the afterburning, recombination reactions and burning carbon monoxide reactions.

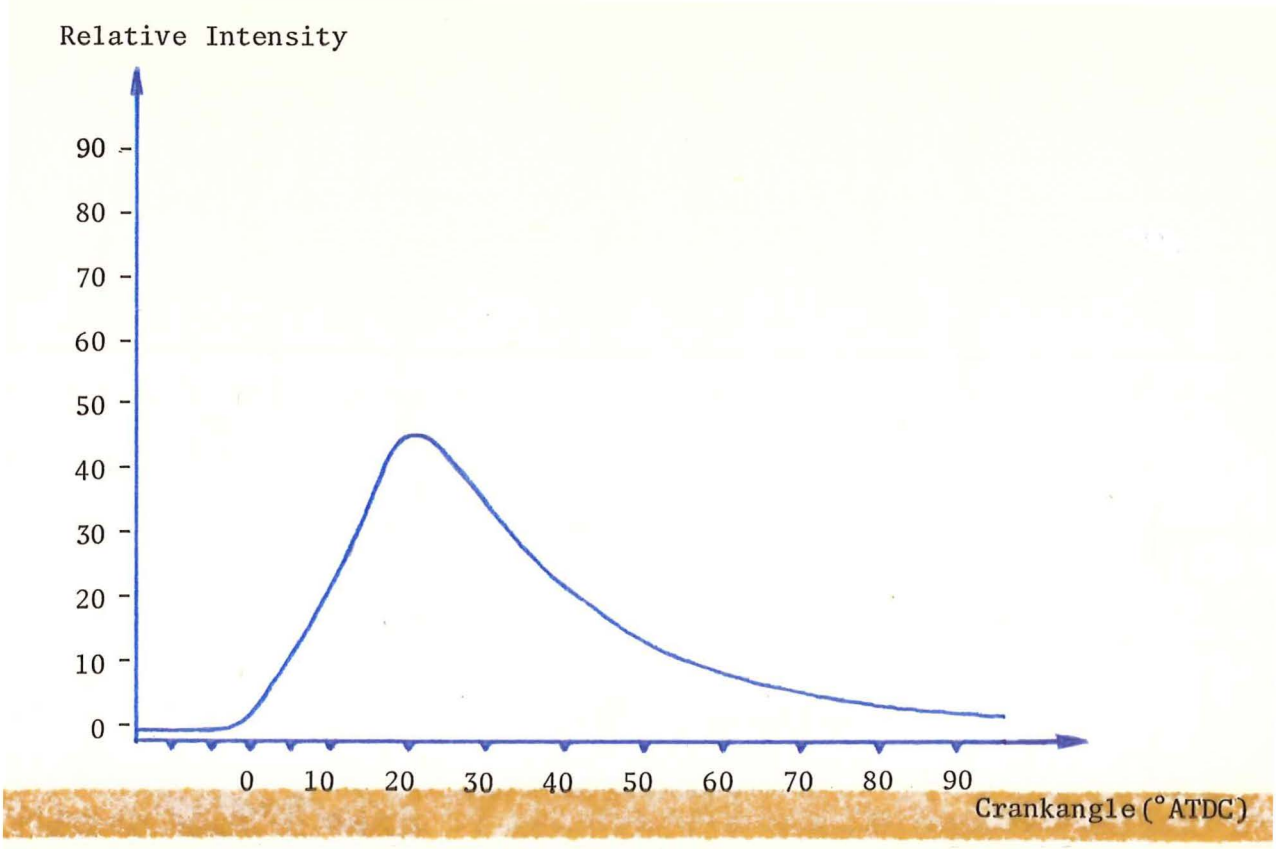

Figure 6.7 Combustion flame light intensity as a function of crankshaft angle (air-fuel ratio 15:1)

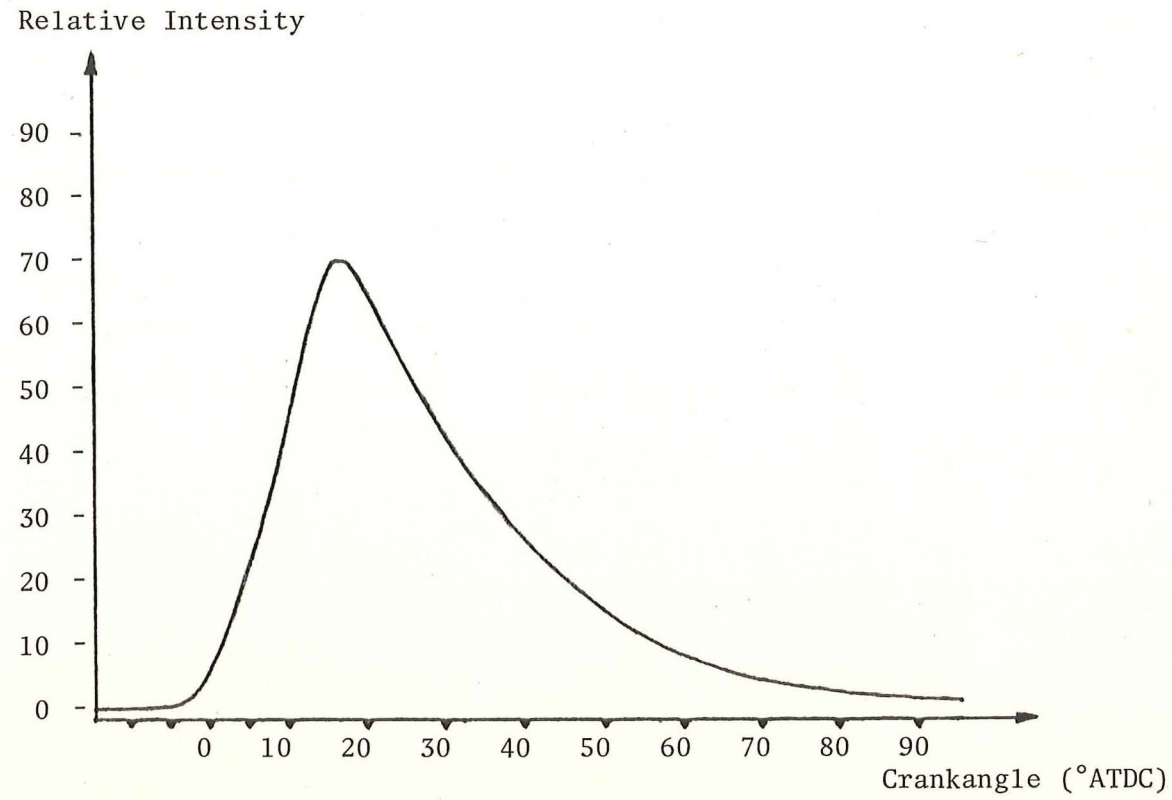

Figure 6.8 Combustion flame light intensity as a function of crankshaft angle (air-fuel ratio 14.6:1)

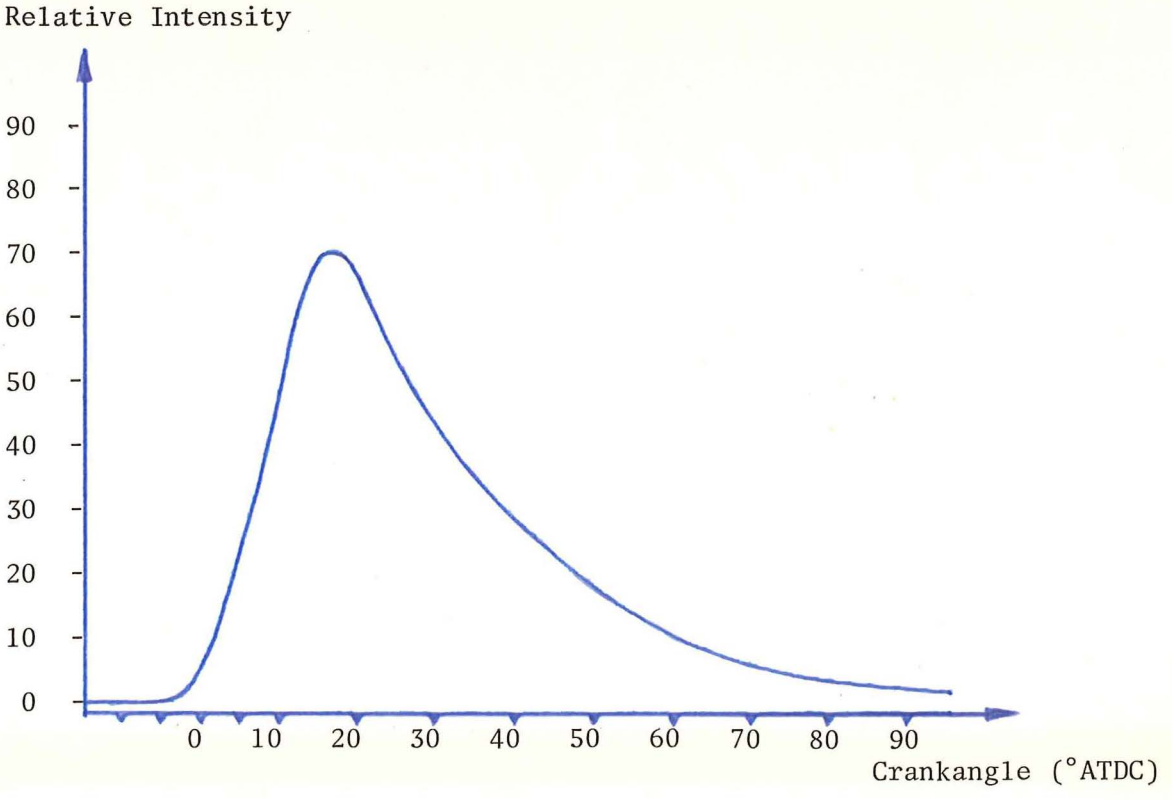

Figure 6.9 Combustion flame light intensity as a function of crankshaft angle (air-fuel ratio 14.1:1)

Engine Torque: Medium

Throttle Position: 2.1/20

Ignition Advance: 23° BTDC

Results

Air-Fuel Ratio	Figure
15.3	6.10
14.8	6.11
14.4	6.12

Observations

The graphs are within the bounds of cyclic variation (refer to Section 6.2.1.3) which makes the minor differences in these curves insignificant over this range of air-fuel ratios.

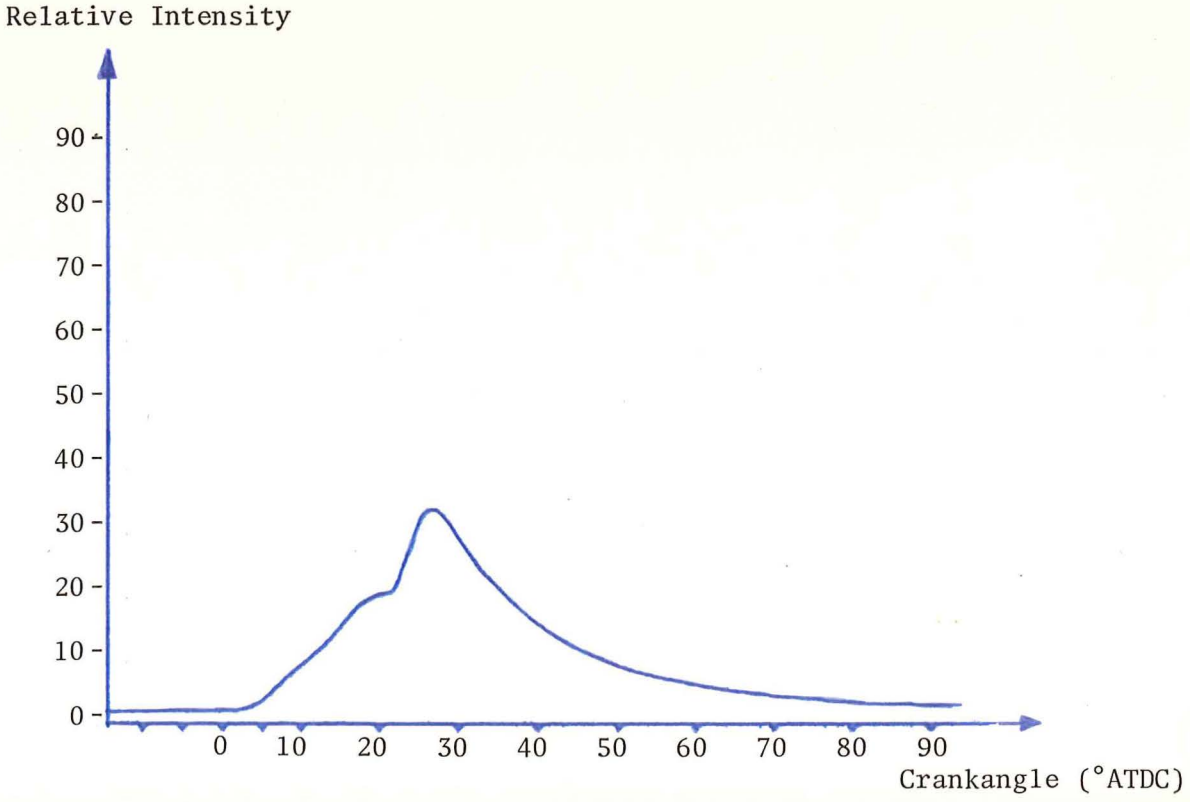

Figure 6.10 Combustion flame light intensity as a function of crankshaft angle (air-fuel ratio 15.3:1)

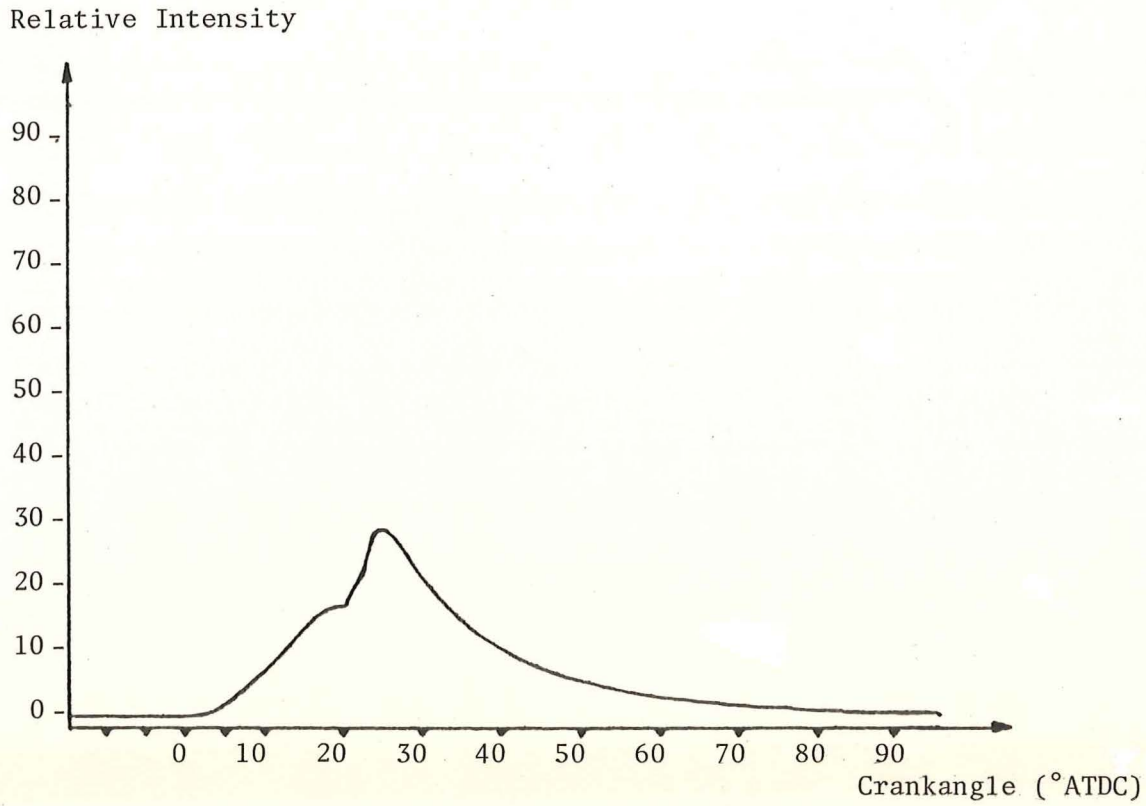

Figure 6.11 Combustion flame light intensity as a function of crankshaft angle (air-fuel ratio 14.8:1)

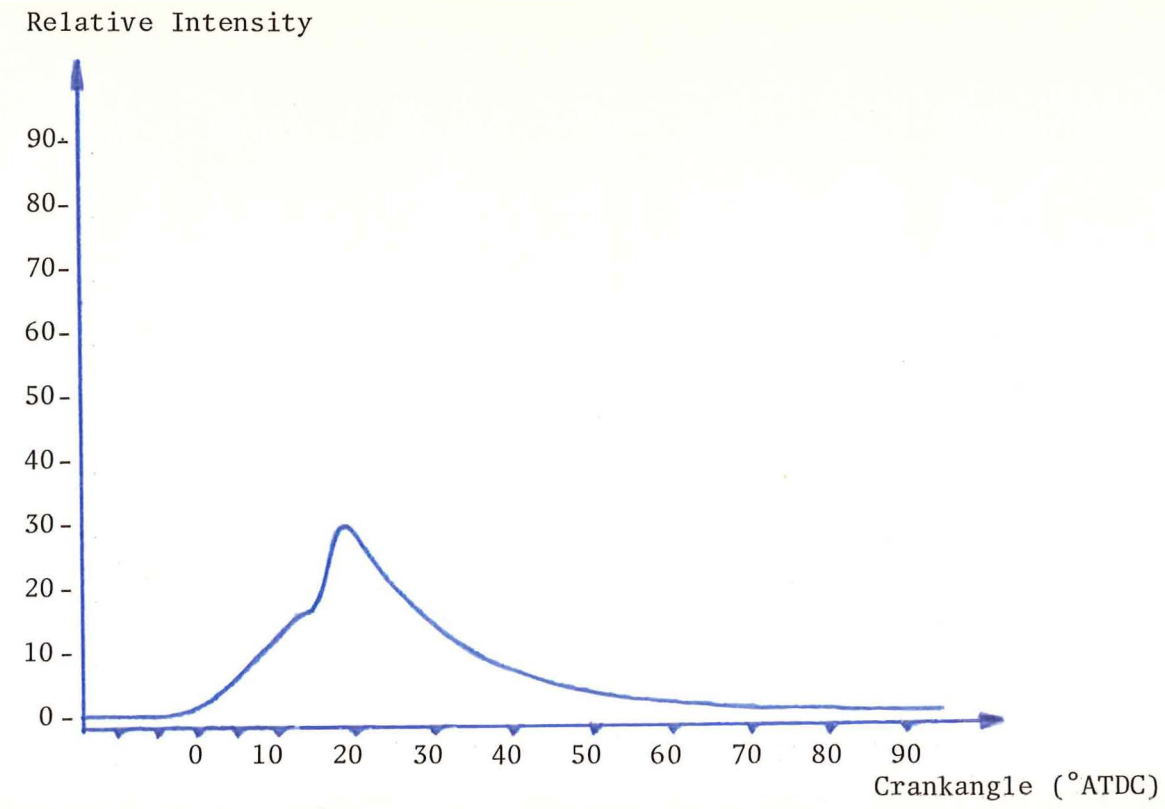

Figure 6.12 Combustion flame light intensity as a function of crankshaft angle (air-fuel ratio 14.4:1)

Engine Torque: High.
Throttle Position: 20/20
Ignition Advance: 11° BTDC.

Results

A/F Ratio	Figure
15.0	6.13
14.1	6.14
10.9	6.15

Observations

The light intensity scale in Figure 6.14 is half that of the others accounting for the majority of the difference in amplitude between this graph and the lean mixture light intensity graph.

At the rich setting (Figure 6.15) the light intensity is definitely reduced. This result is at variance with the previous two sets of results and it could possibly be due to the sooting up of the glass window under these conditions when the air-fuel mixture ratio was more rich than in the previous two sets of results.

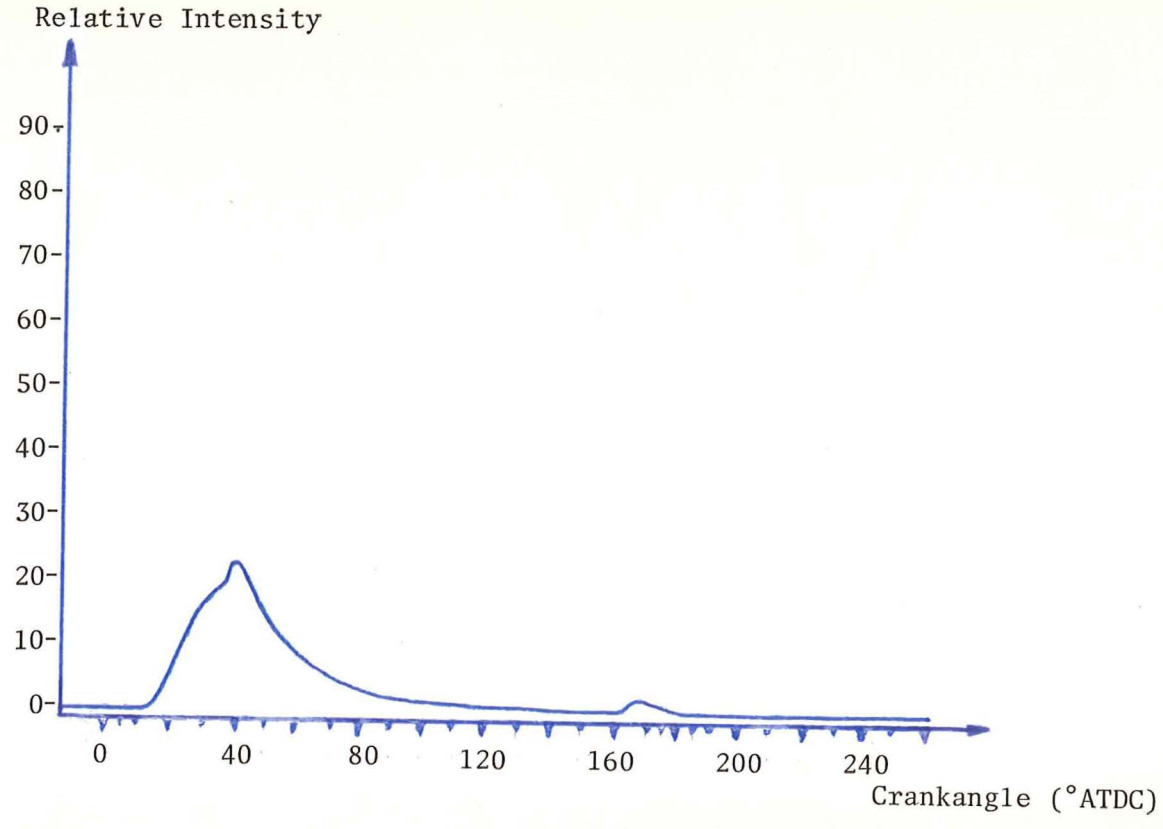

Figure 6.13 Combustion flame light intensity as a function of crankshaft angle (air-fuel ratio 15:1)

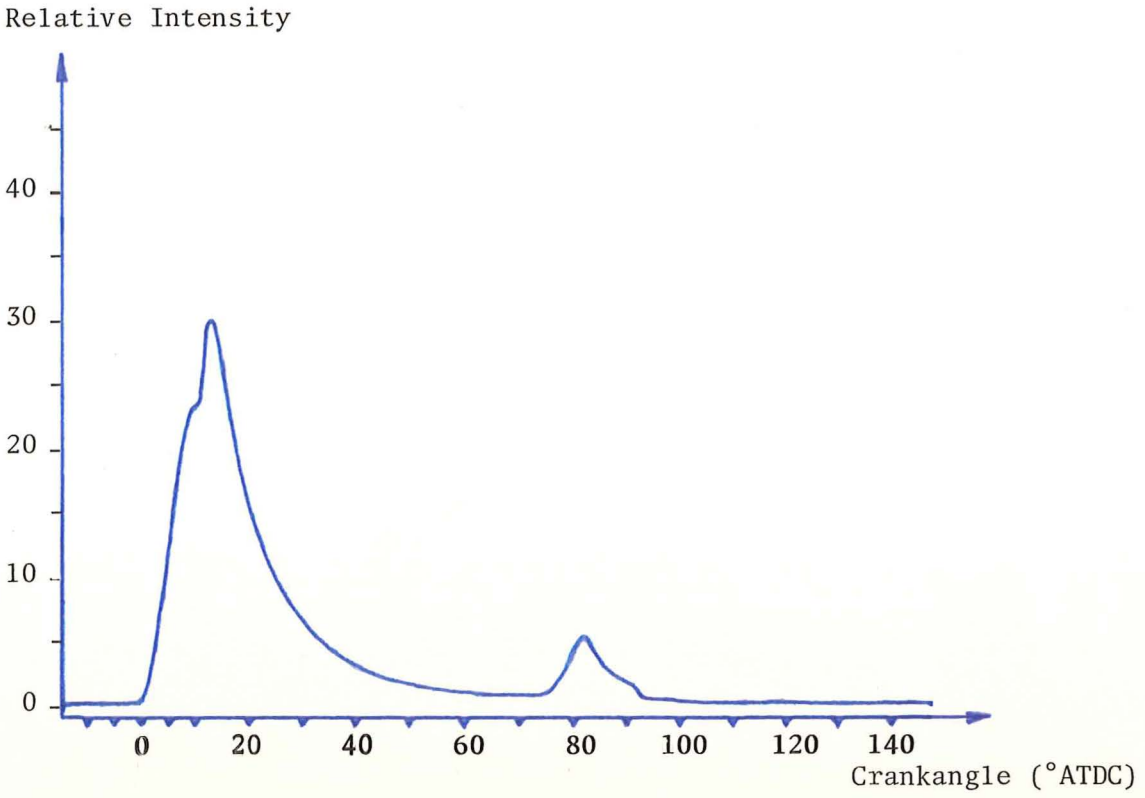

Figure 6.14 Combustion flame light intensity as a function of crankshaft angle (air-fuel ratio 14.1:1)

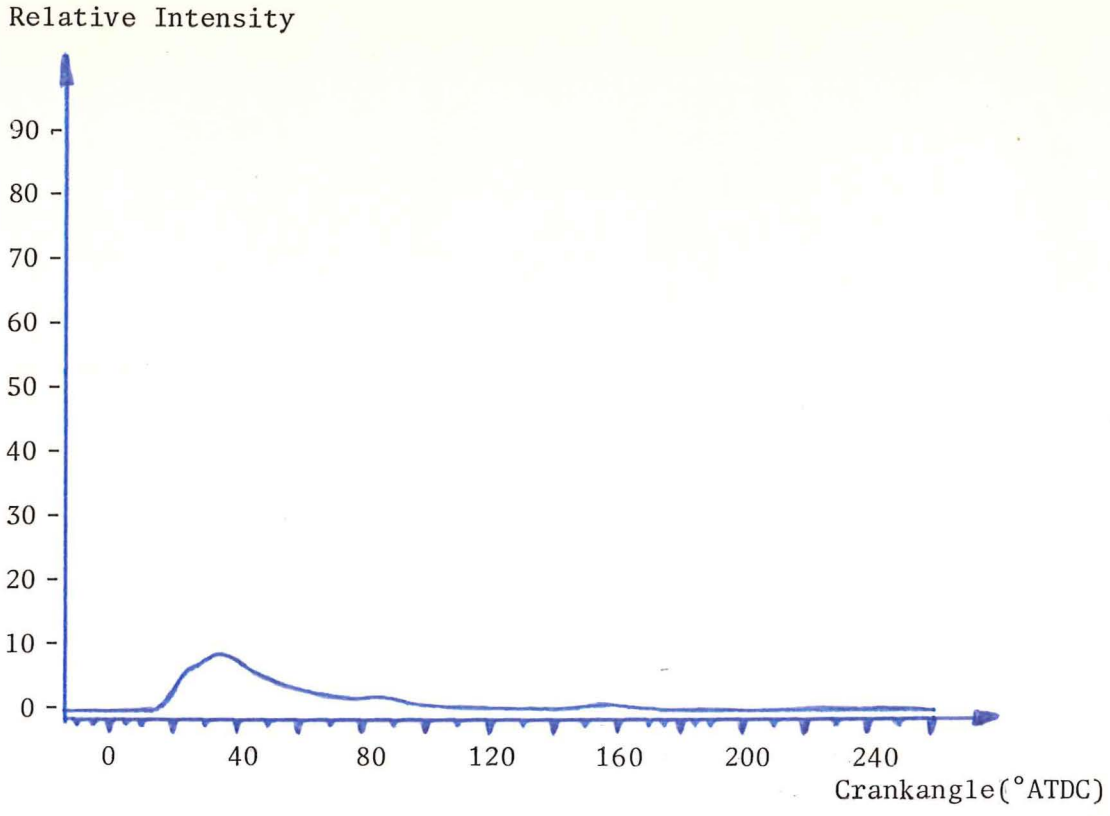

Figure 6.15 Combustion flame light intensity as a function of crankshaft angle (air-fuel ratio 10.9:1)

6.2.1.2 The Effect on the Flame Light Intensity of Advancing the Ignition Timing

Engine Speed: 15 r.p.s.

Engine Torque: Low

Throttle Position: 0.8/20

Results

Ignition Advance (°BTDC)	Torque (Nm)	Figure
21	11.3	6.16
30	11.7	6.17
43	11.3	6.18

Observations

Knocking combustion was inaudible and neither was it apparent from the light trace even as the ignition was advanced past MBT (30° BTDC). Note how the light intensity curves begin at a more advanced crankshaft angle as the ignition timing is advanced.

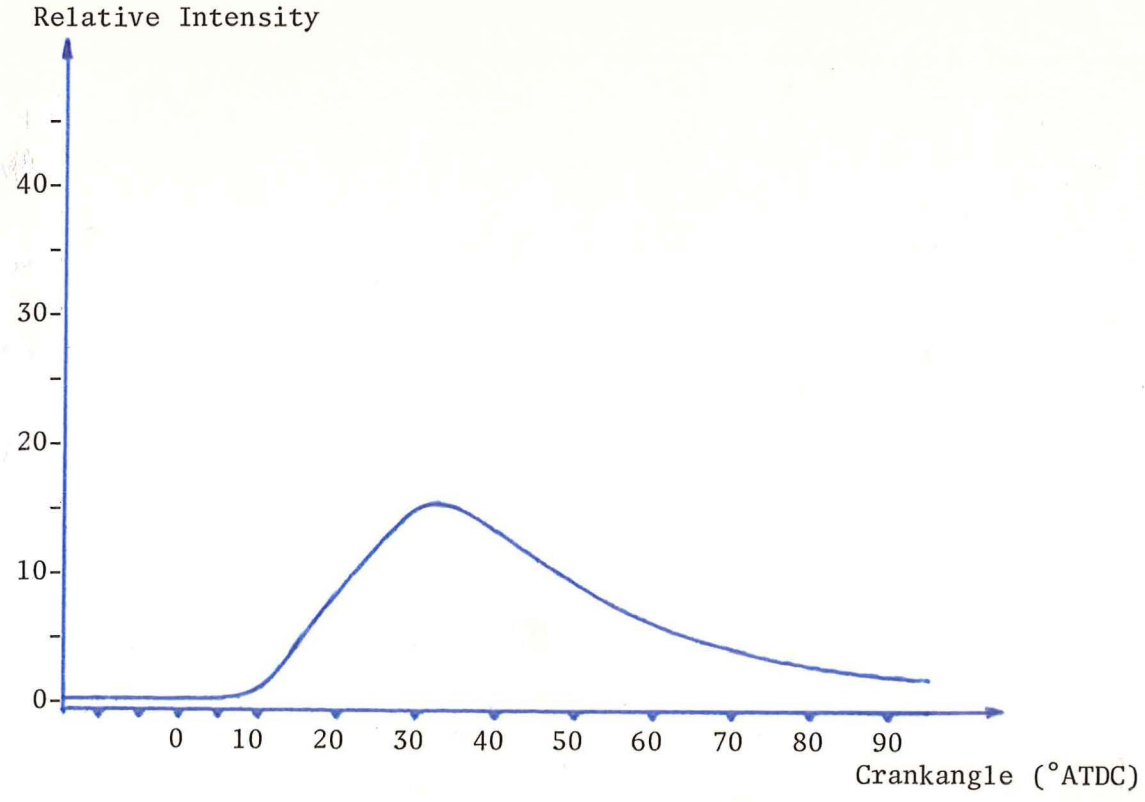

Figure 6.16 Combustion flame light intensity as a function of crankshaft angle (ignition advance 21° BTDC).

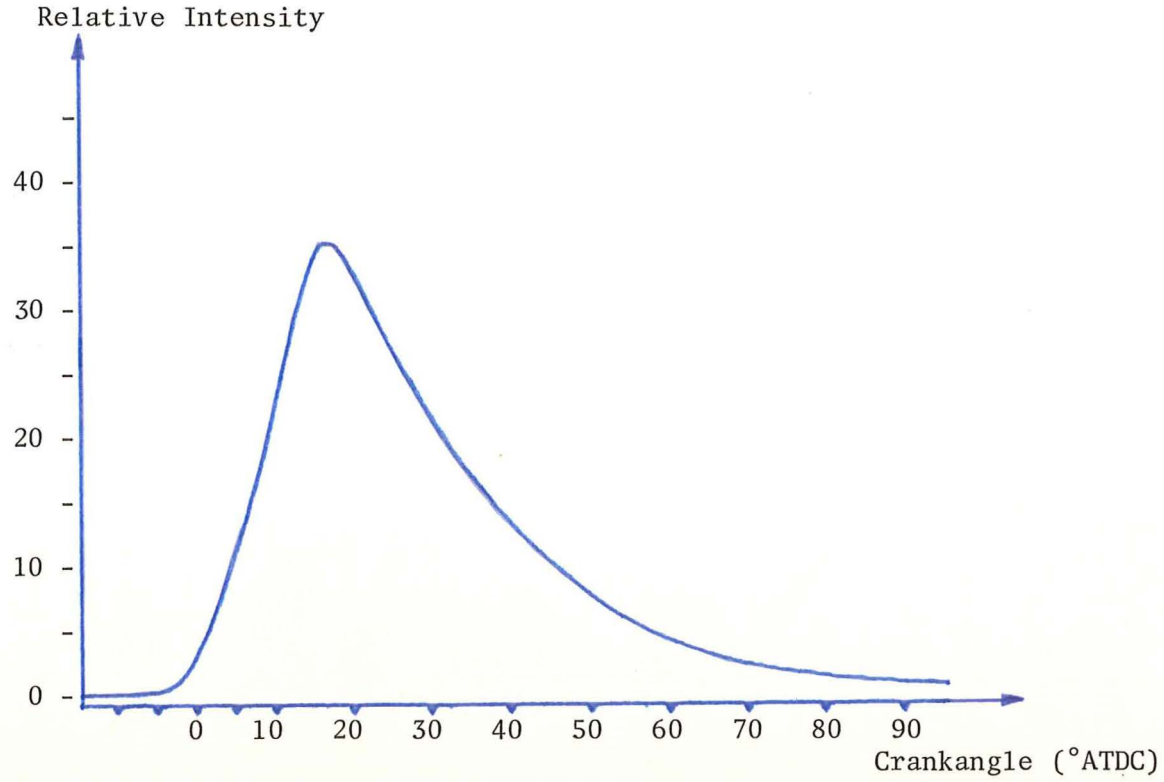

Figure 6.17 Combustion flame light intensity as a function of crankshaft angle (ignition advance 30° BTDC)

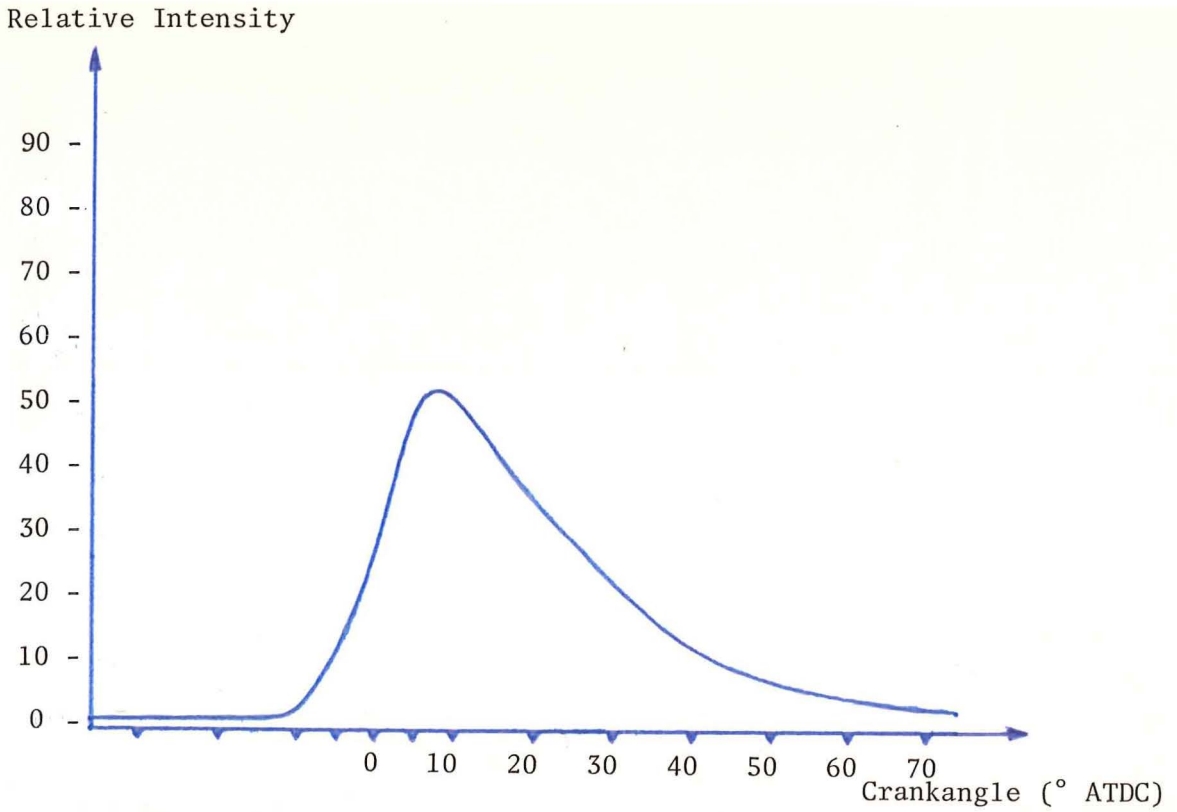

Figure 6.18 Combustion flame light intensity as a function of crankshaft angle (ignition advance 43° BTDC)

Engine Torque : Medium.

Throttle Position: 2.1/20

Results

Ignition Advance (°BTDC)	Torque (Nm)	Figure
23	23.0	6.19
26	23.2	6.20
28	23.0	6.21

Observations

Knocking combustion could not be heard by ear at 23° advance. Occasional pinging could just be heard at 26° advance (MBT), and continuous quiet pinging was audible when the ignition was advanced to 28° BTDC and beyond. The curve in Figure 6.21 is chopped slightly at the top due to over-amplification but it shows slight light intensity fluctuations on the negative slope section due to knocking combustion. These light intensity oscillations are expected to correspond to similar light intensity oscillations described in Section 4.4.2.

The cause of the inflexion on the leading edge of the curve is considered to be due to the afterburning phenomenon (refer to Section 4.3.3) and it is discussed in detail in Section 7.3.1.5.

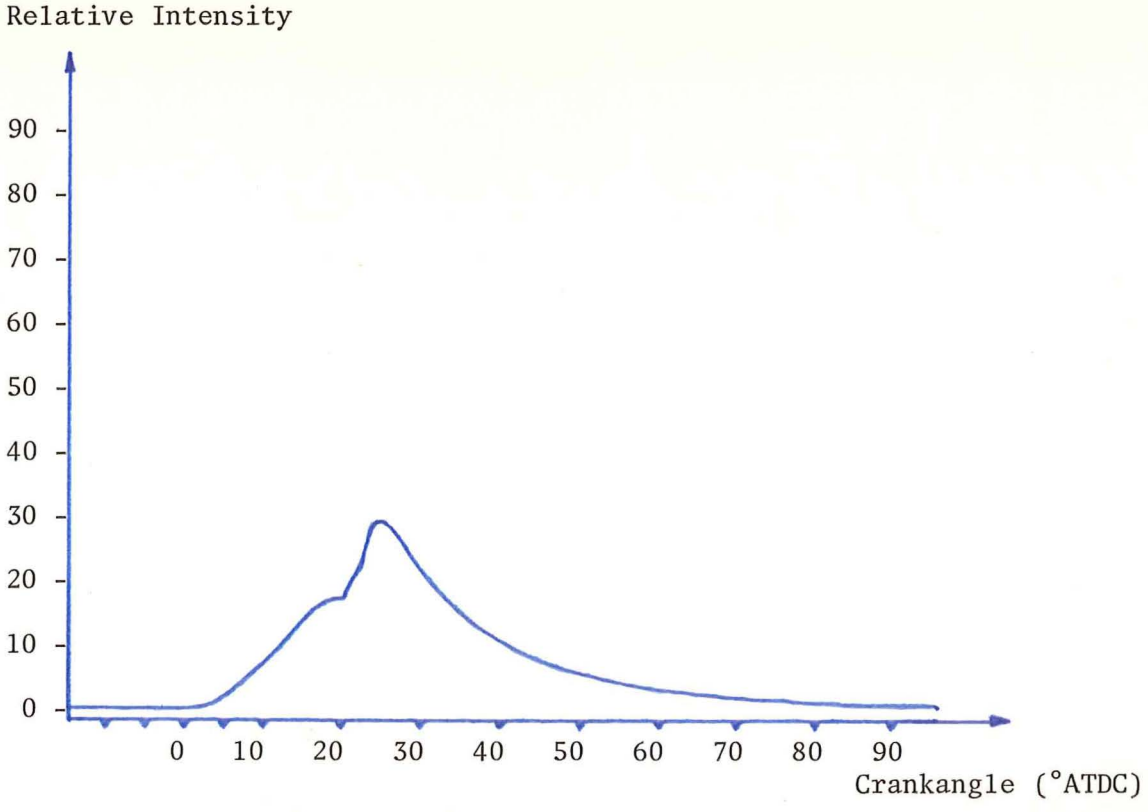

Figure 6.19 Combustion flame light intensity as a function of crankshaft angle (ignition advance 23° BTDC)

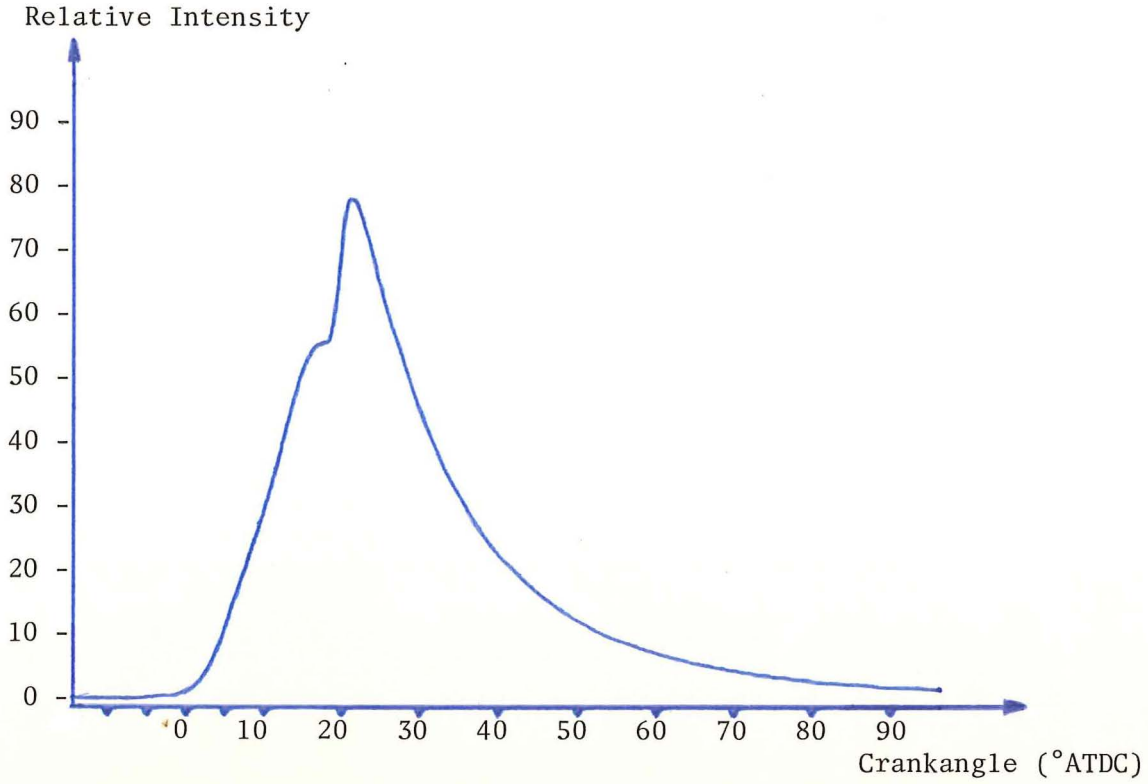

Figure 6.20 Combustion flame light intensity as a function of crankshaft angle (ignition advance 26° BTDC)

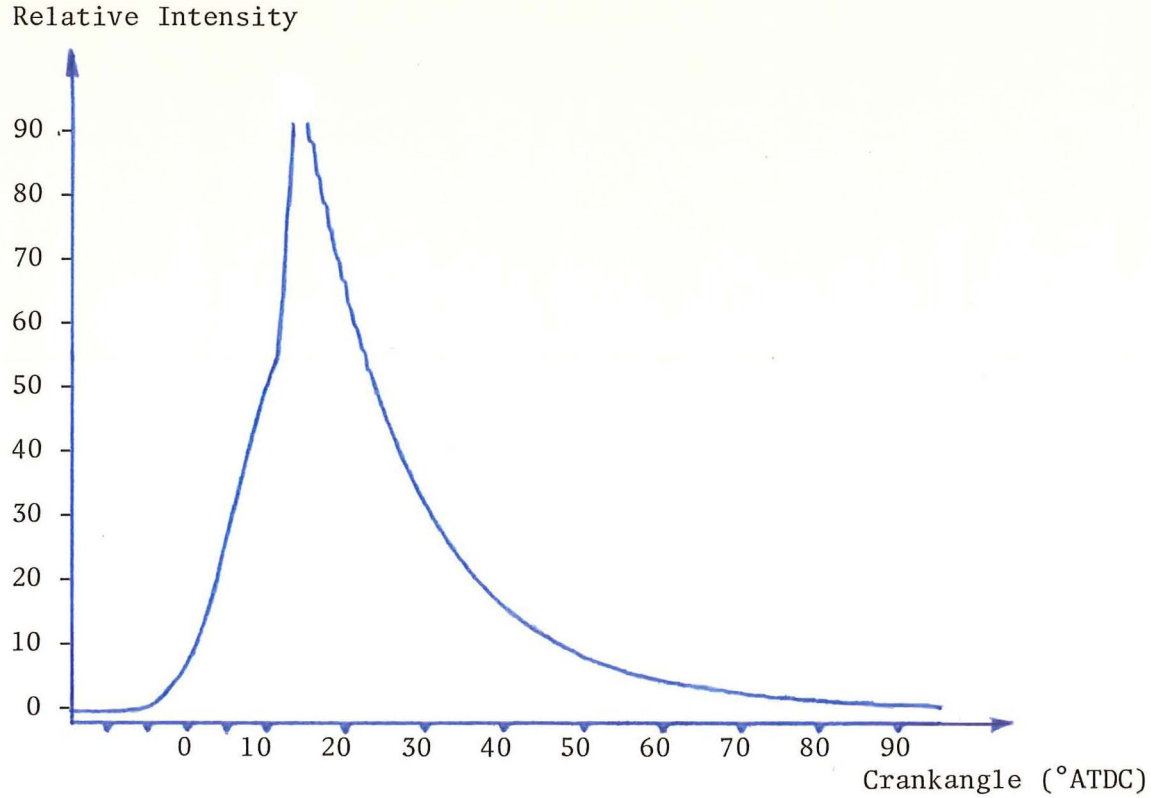

Figure 6.21 Combustion flame light intensity as a function of crankshaft angle (ignition advance 28° BTDC)

Engine Torque: High

Throttle Position: 20/20.

Results

Ignition Advance (° BTDC)	Torque (Nm)	Figure
8	33.1	6.22
13	35.1	6.23
14	34.7	6.24

Observations

When the ignition timing was set to 8° BTDC knock was not audible; however at 13° advance pinging was audible during some combustion cycles. At 14° BTDC knocking combustion was occurring in most combustion cycles, being detected audibly and by the consistently re-occurring oscillating line on the trailing edge of the light intensity traces.

The increase in knock intensity as the ignition timing is advanced is due to the higher endgas temperatures in the latter case (refer to Section 2.1.2.2) which cause a larger proportion of it to self-ignite.

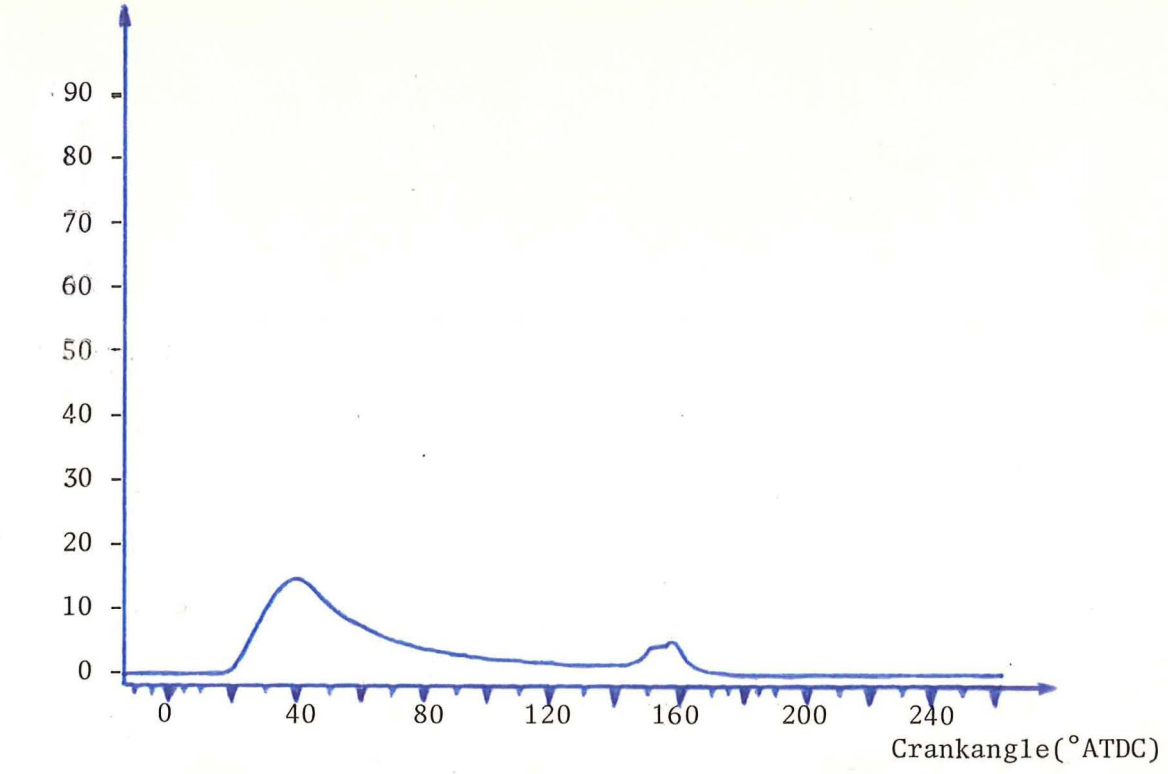

Figure 6.22 Combustion flame light intensity as a function of crankshaft angle (ignition advance 8° BTDC)

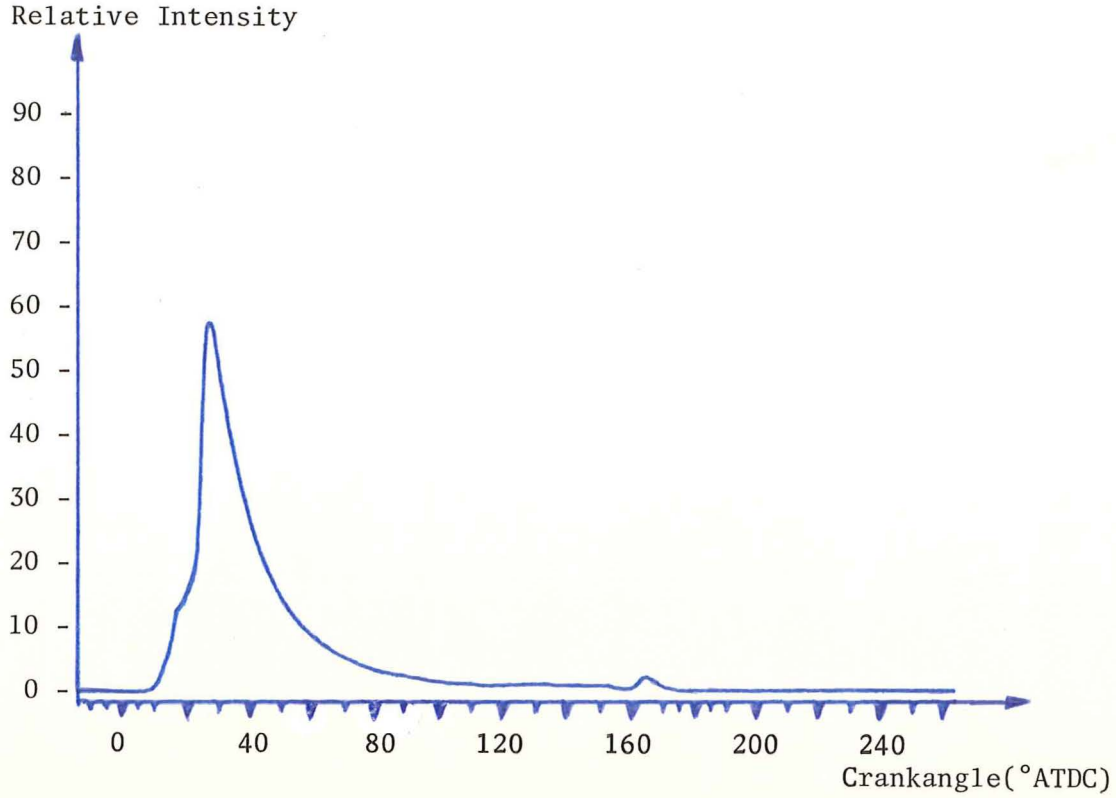

Figure 6.23 Combustion flame light intensity as a function of crankshaft angle (ignition advance 13° BTDC)

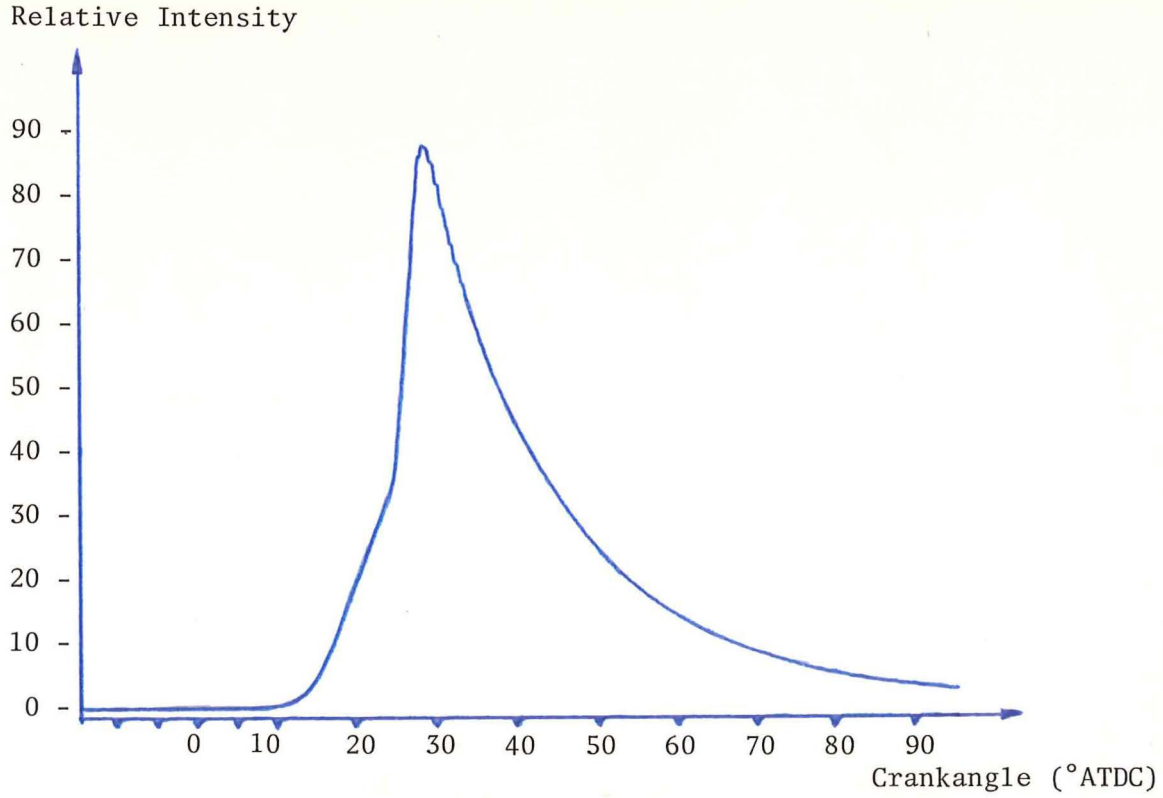

Figure 6.24 Combustion flame light intensity as a function of crankshaft angle (ignition advance 14° BTDC)

Engine Speed : 30 r.p.s.

Engine Torque: Low.

Throttle Position: 1.7/20.

Results

Ignition Advance (°BTDC)	Torque (Nm)	Figure
28	11.5	6.25
34	12.0	6.26
48	11.7	6.27

Observations

Knocking was neither audible nor apparent on the traces at any ignition advance angle. The flame light intensity increases from zero intensity at at more advanced crankshaft angle as the ignition timing is advanced. This is because of the earlier flame initiation as the ignition advance is increased. The appearance of the inflexion in Figure 6.27 is expected to be from the same cause as previously observed inflexions and in some graphs yet to be described the inflexion takes the form of a minimum in-between two maxima. For a discussion of this phenomenon, refer to Chapter 7.

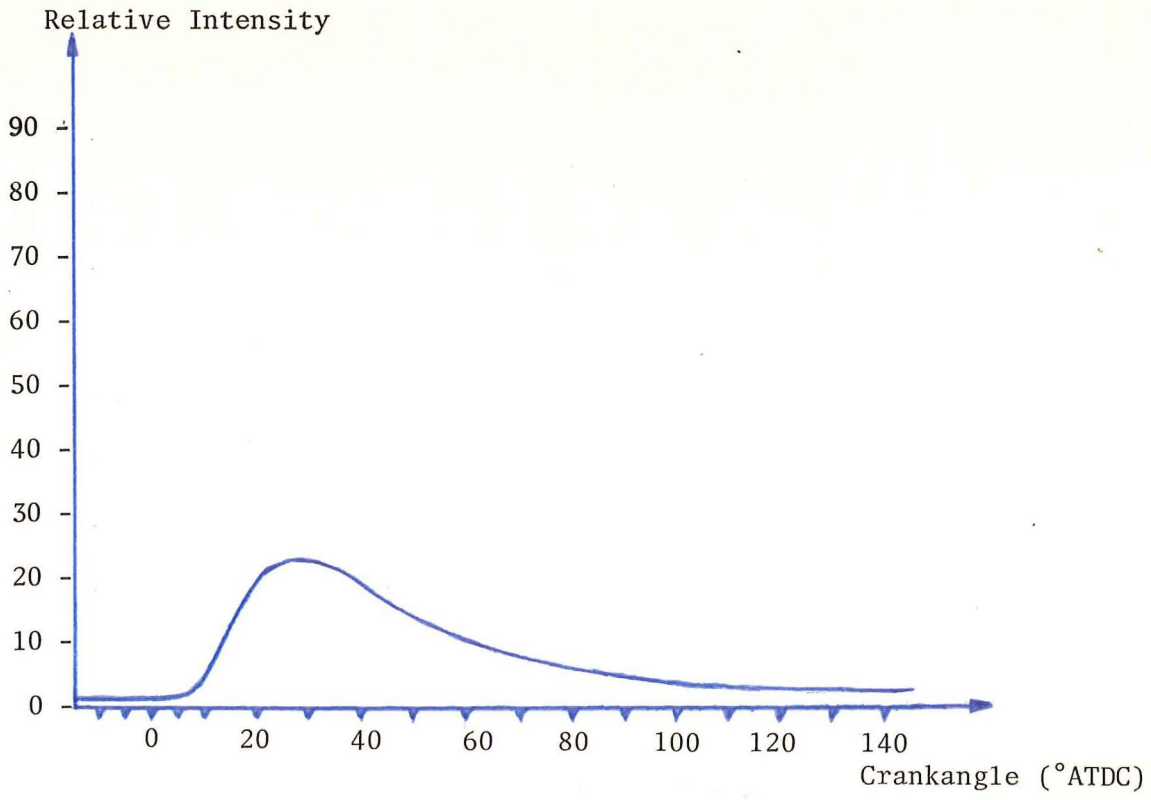

Figure 6.25 Combustion flame light intensity as a function of crankshaft angle (ignition advance 28° BTDC)

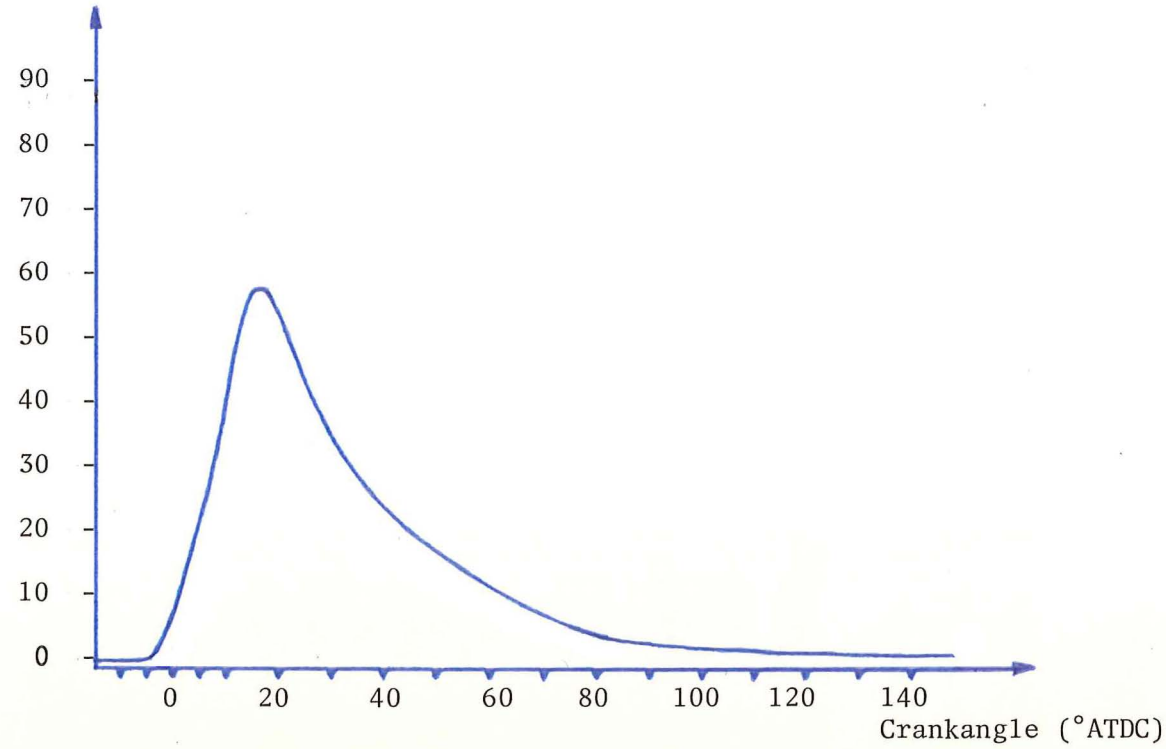

Figure 6.26 Combustion flame light intensity as a function of crankshaft angle (ignition advance 34° BTDC)

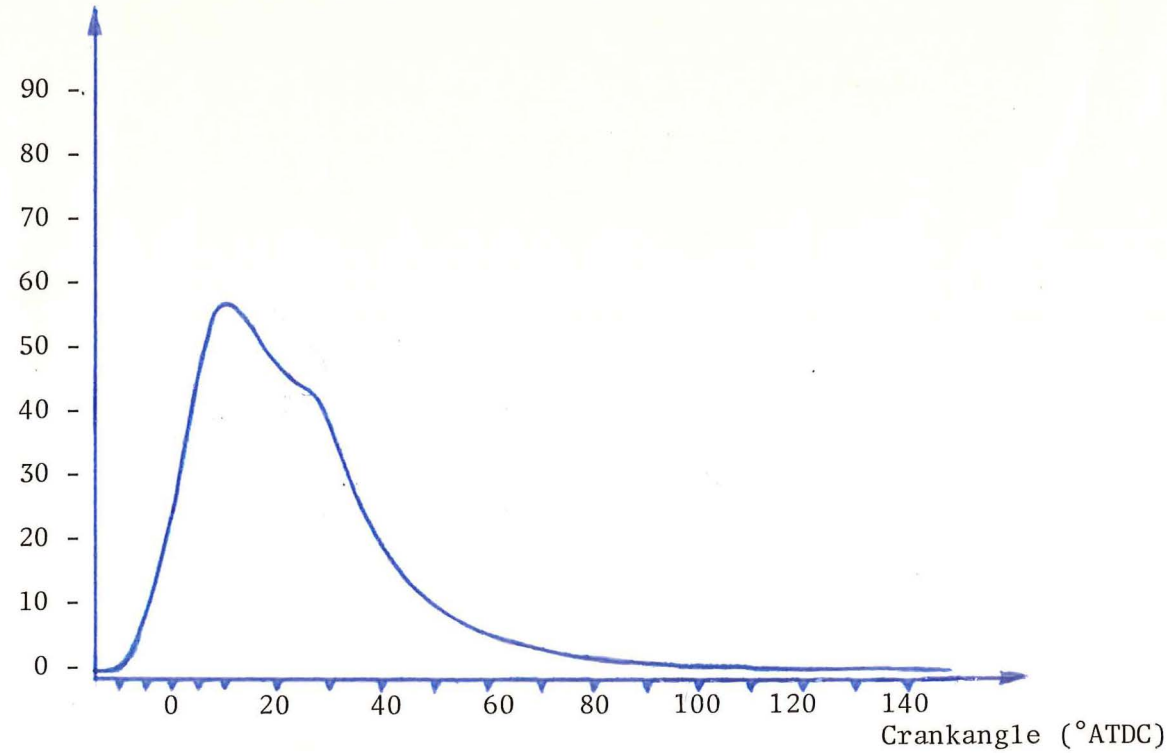

Figure 6.27 Combustion flame light intensity as a function of crankshaft angle (ignition advance 48° BTDC)

Engine Torque : Medium

Throttle Position 3.1/20.

Results

Ignition Advance (°BTDC)	Torque (Nm)	Figure
27	21.8	6.28
34	21.8	6.29
38	22.1	6.30

Observations

As the ignition timing is advanced the intensity curve shape changes from bell-shaped (Figure 6.28) to the shape of Figure 6.29 with two local maxima . This advance angle of 34° BTDC also caused quiet and infrequent pinging to occur when traces similar to Figure 6.30 would sometimes appear. When the ignition timing was advanced to 38° BTDC, the quiet pinging was audible continually and it consistently produced traces with the oscillating trailing edge of Figure 6.30.

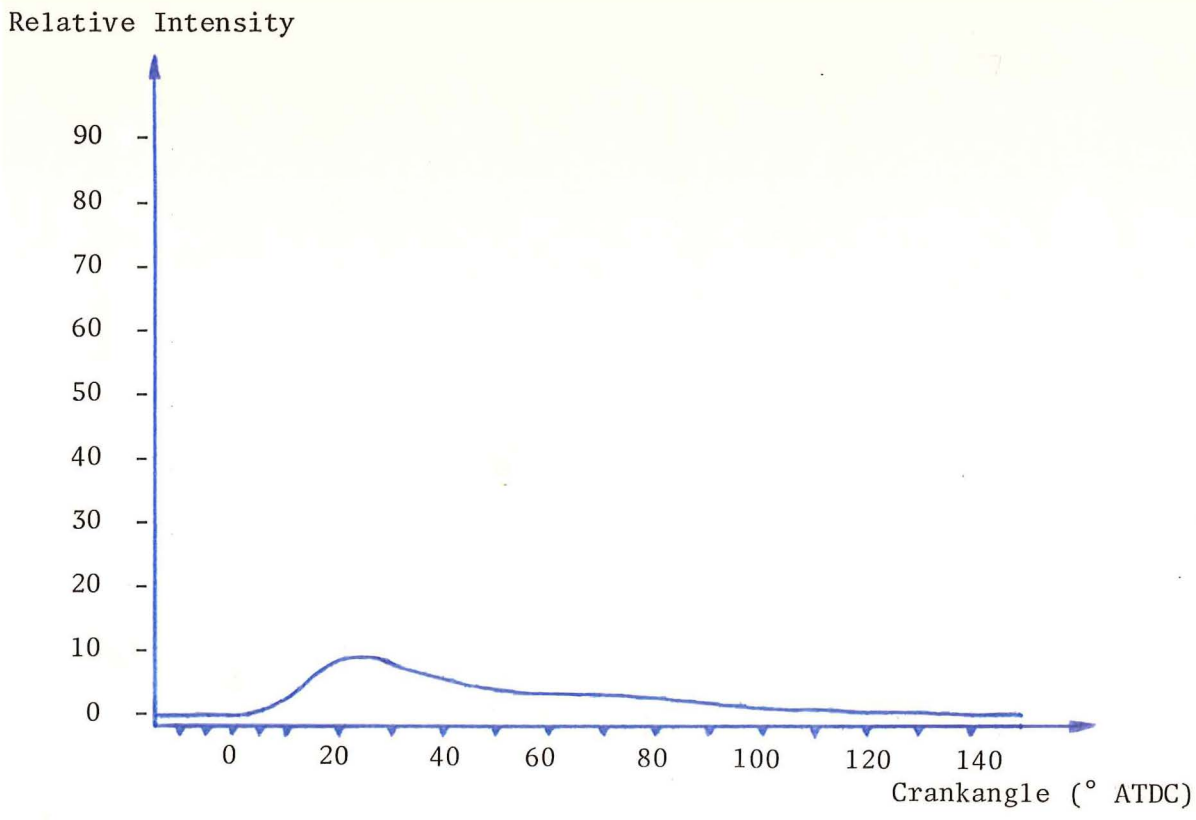

Figure 6.28 Combustion flame light intensity as a function of crankshaft angle (ignition advance 27° BTDC)

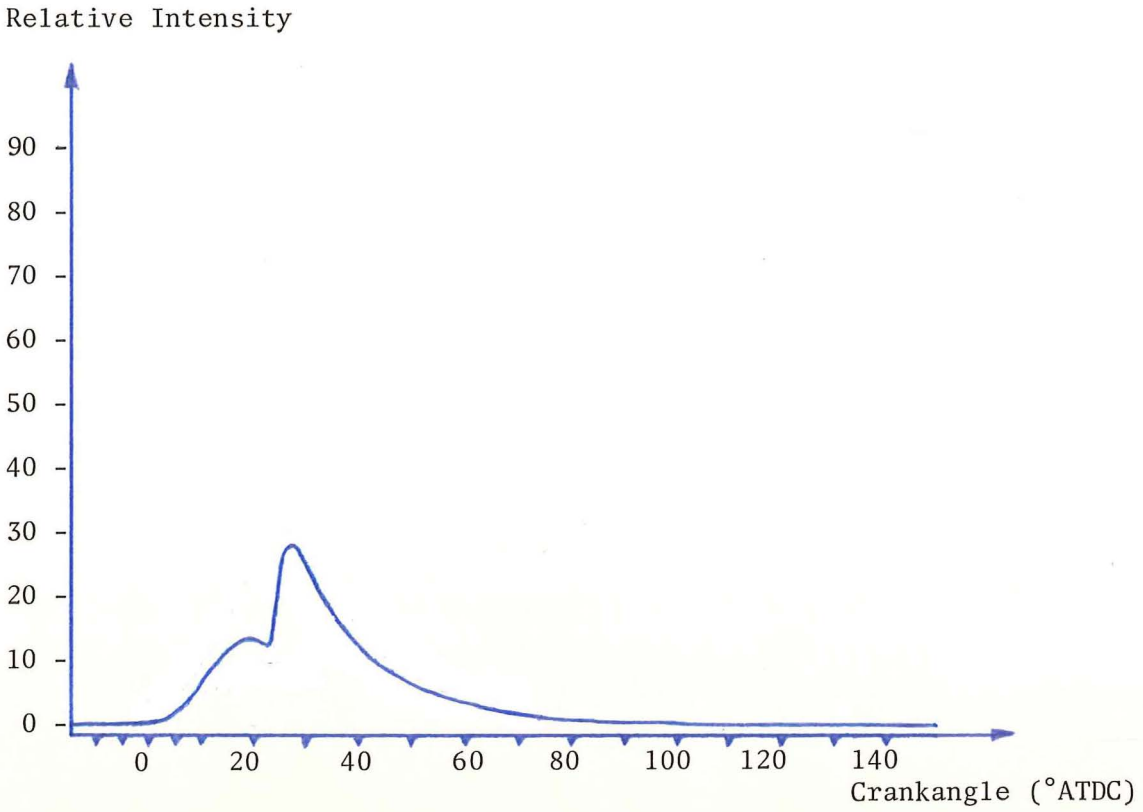

Figure 6.29 Combustion flame light intensity as a function of crankshaft angle (ignition advance 34° BTDC)

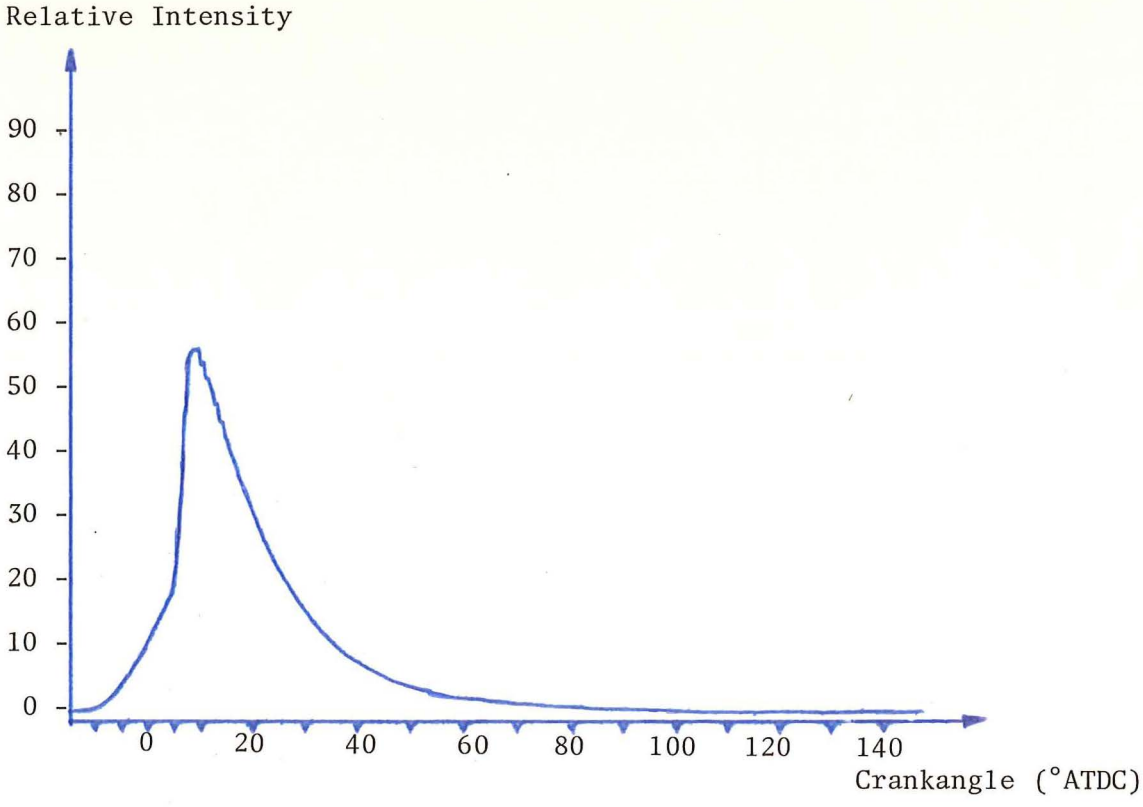

Figure 6.30 Combustion flame light intensity as a function of crankshaft angle (ignition advance 38° BTDC)

Engine Torque: High.

Throttle Position: 20/20.

Results

Ignition Advance (° BTDC)	Torque (Nm)	Figure
14	31.3	6.31
19	33.1	6.32
21	33.5	6.33

Observations

As at medium loads, the curve develops a second maximum on the trailing edge (Figure 6.32) before knocking combustion is induced through further advancing the ignition timing. Note the inflexion two-thirds of the way up the leading edge of Figure 6.33. Medium-heavy audible knock was occurring in an estimated 50% of the combustion cycles at this advance of 21° BTDC.

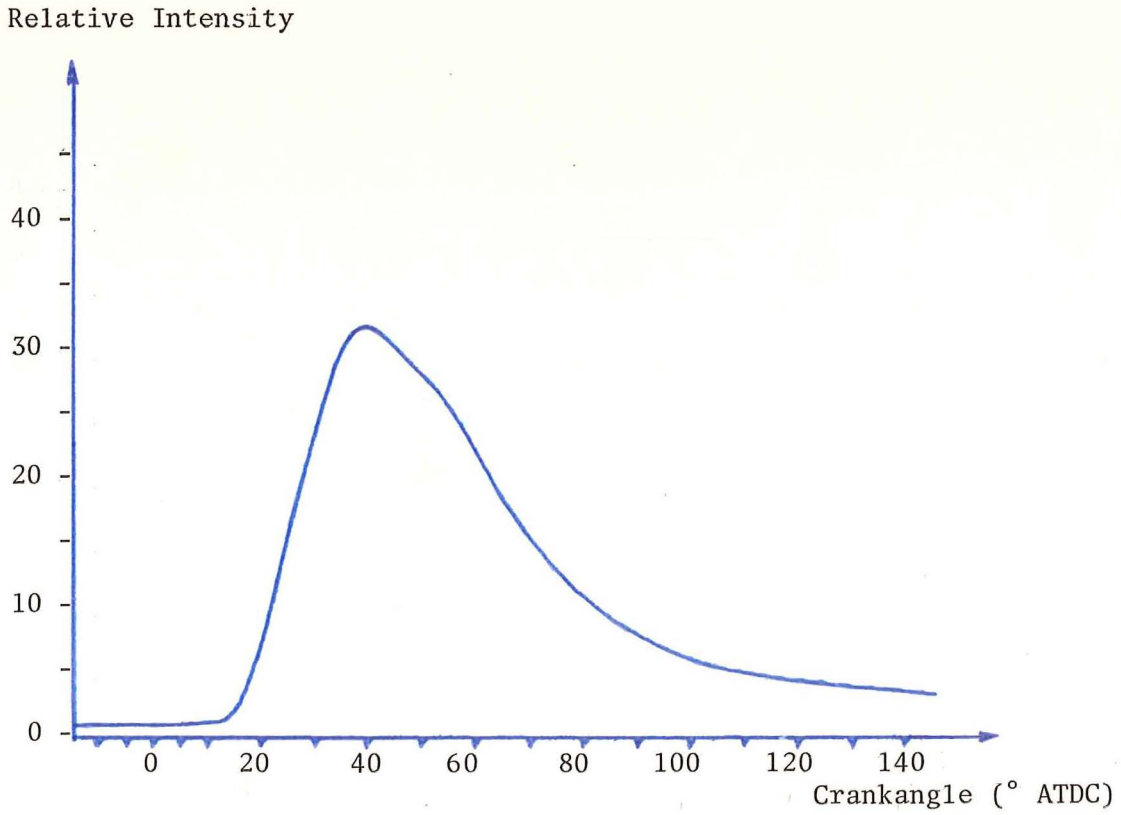

Figure 6.31 Combustion flame light intensity as a function of crankshaft angle (ignition advance 14° BTDC)

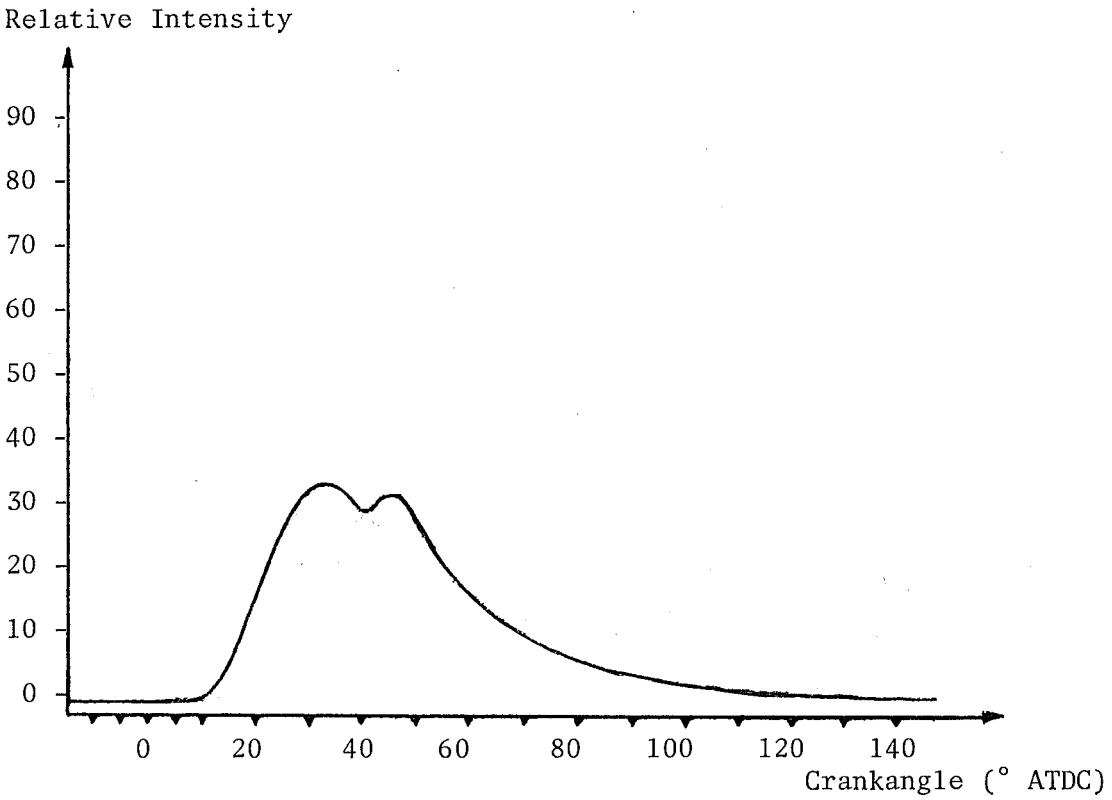

Figure 6.32 Combustion flame light intensity as a function of crankshaft angle (ignition advance 19° BTDC)

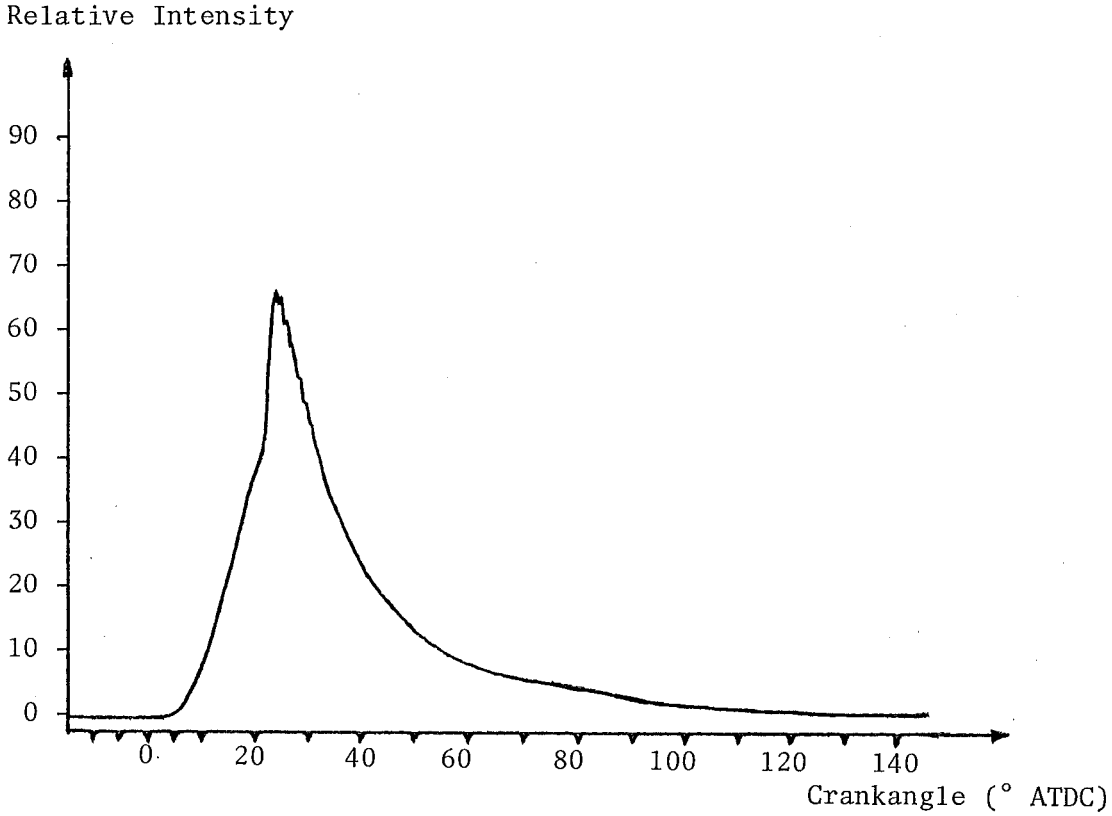

Figure 6.33 Combustion flame light intensity as a function of crankshaft angle (ignition advance 21° BTDC)

Engine Speed: 45 r.p.s.

Engine Torque: Low.

Observations

The light intensity traces follow a trend similar to the low torque light intensity traces at 30 r.p.s.

Engine Torque: Medium.

Throttle Position: 3.9/20.

Results

Ignition Advance (° BTDC)	Torque (Nm)	Figure
26	21.8	6.34
35	22.3	6.35
45	21.8	6.36

Observations

The trends are similar to those at medium loads at either 15 r.p.s. or 30 r.p.s. Thus, when the ignition timing was advanced past MBT, light knock would be induced as shown in Figure 6.36.

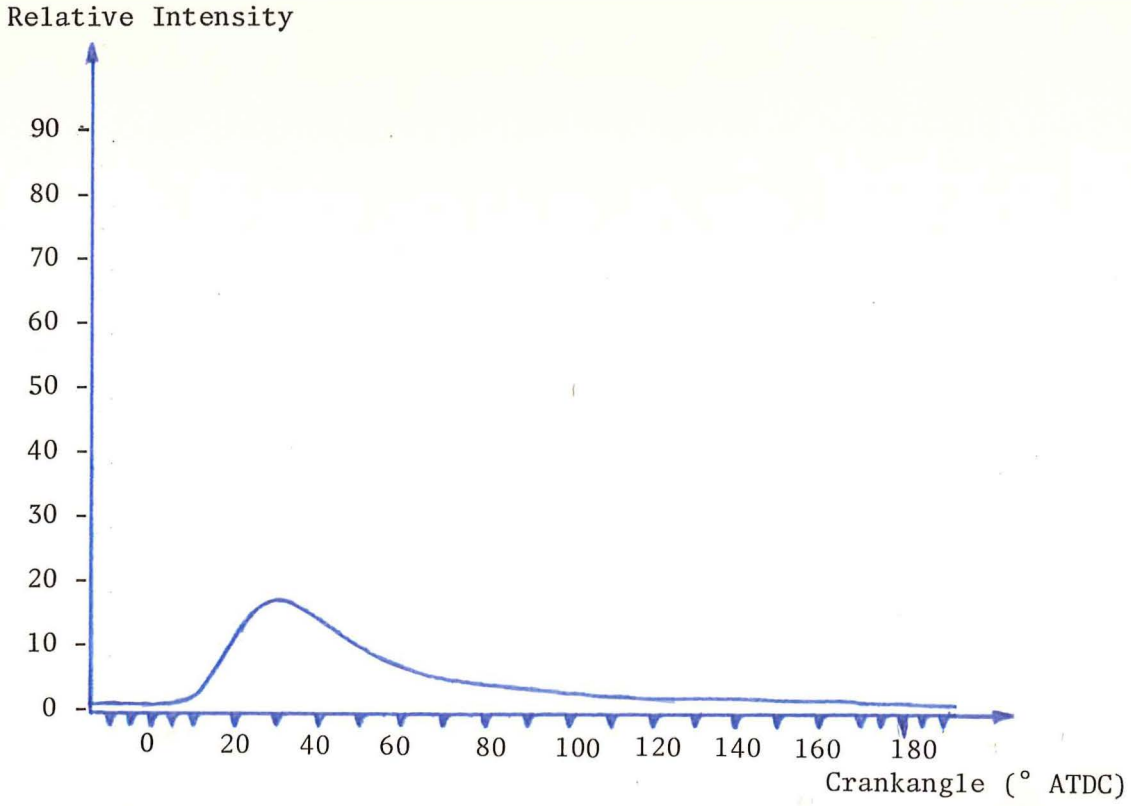

Figure 6.34 Combustion flame light intensity as a function of crankshaft angle (ignition advance 26° BTDC)

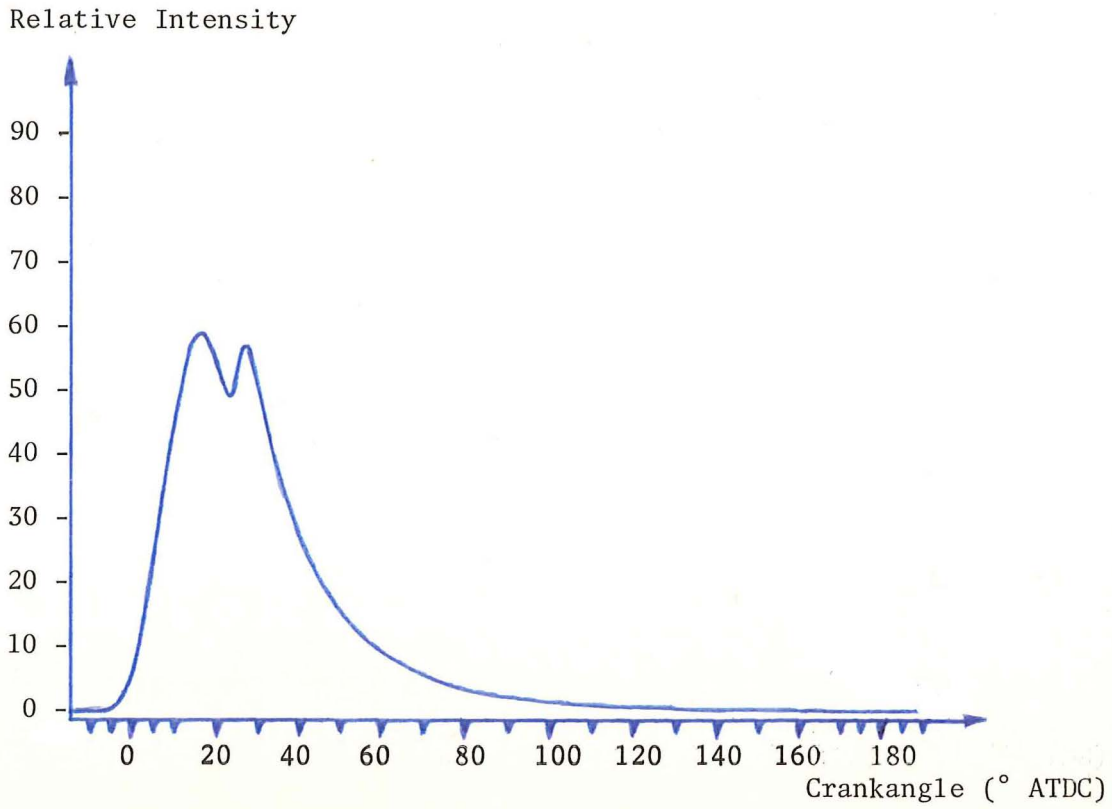

Figure 6.35 Combustion flame light intensity as a function of crankshaft angle (ignition advance 35° BTDC)

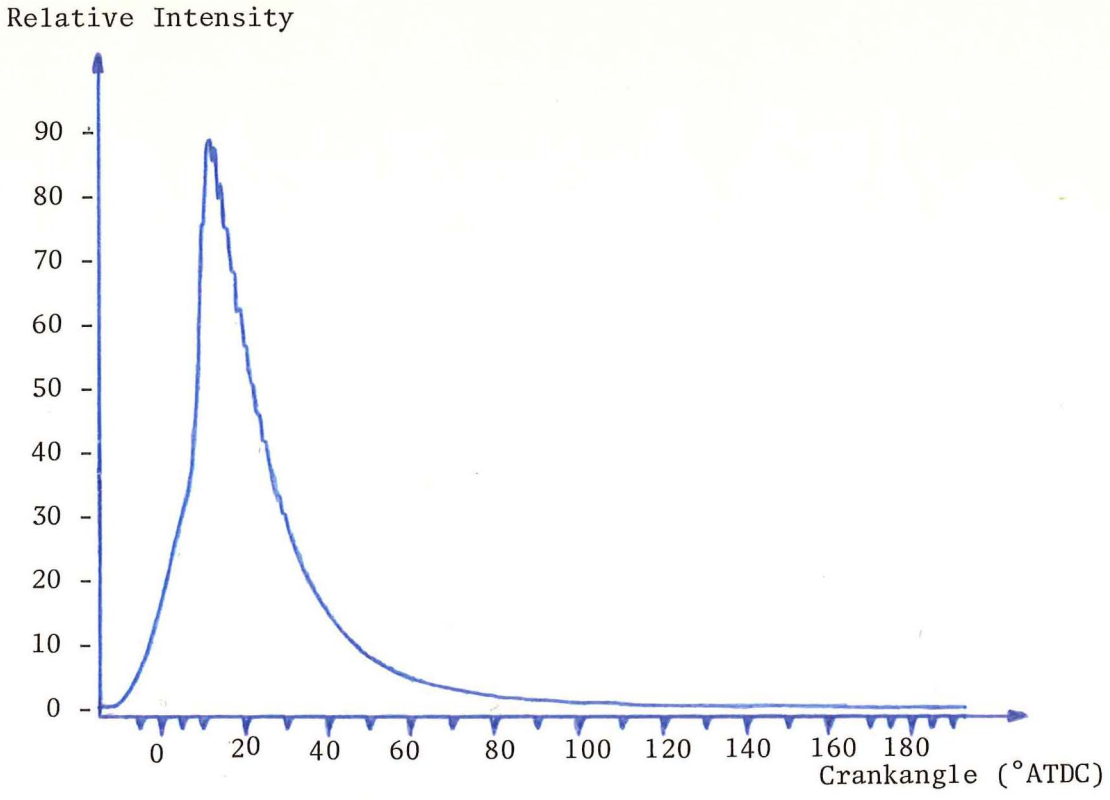

Figure 6.36 Combustion flame light intensity as a function of crankshaft angle (ignition advance 45° BTDC)

Engine Torque: High
Throttle Position: 20/20.

Results

Ignition Advance (° BTDC)	Torque (Nm)	Figure
19	31.8	6.37
28	35.4	6.38

Observations

The second maximum is apparent on the light intensity traces even when the ignition timing is well retarded from the knock limit (Figure 6.37). The graph of knocking combustion (Figure 6.38) indicates that the first pressure and light oscillation discontinuity occurs on the leading edge of the curve. The secondary light intensity disturbance apparent in both graphs from a crankangle of 150° ATDC to 190° ATDC is occurring when the exhaust valve opens (130° ATDC).

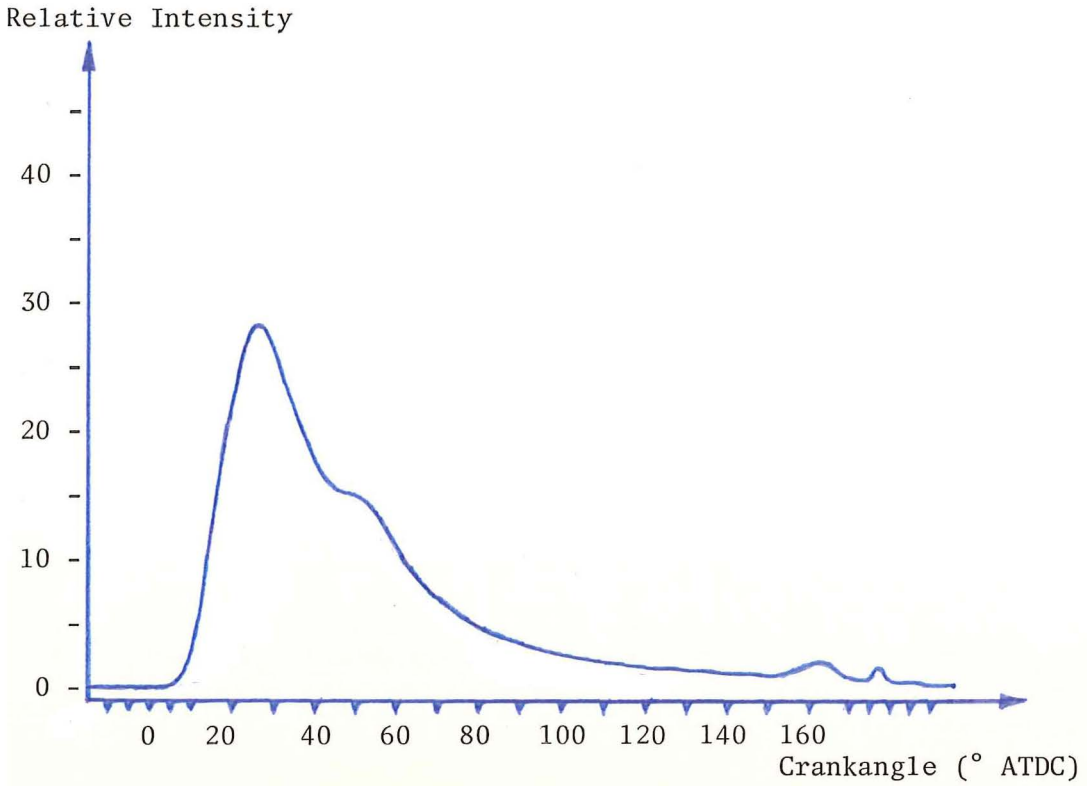

Figure 6.37 Combustion flame light intensity as a function of crankshaft angle (ignition advance 19° BTDC)

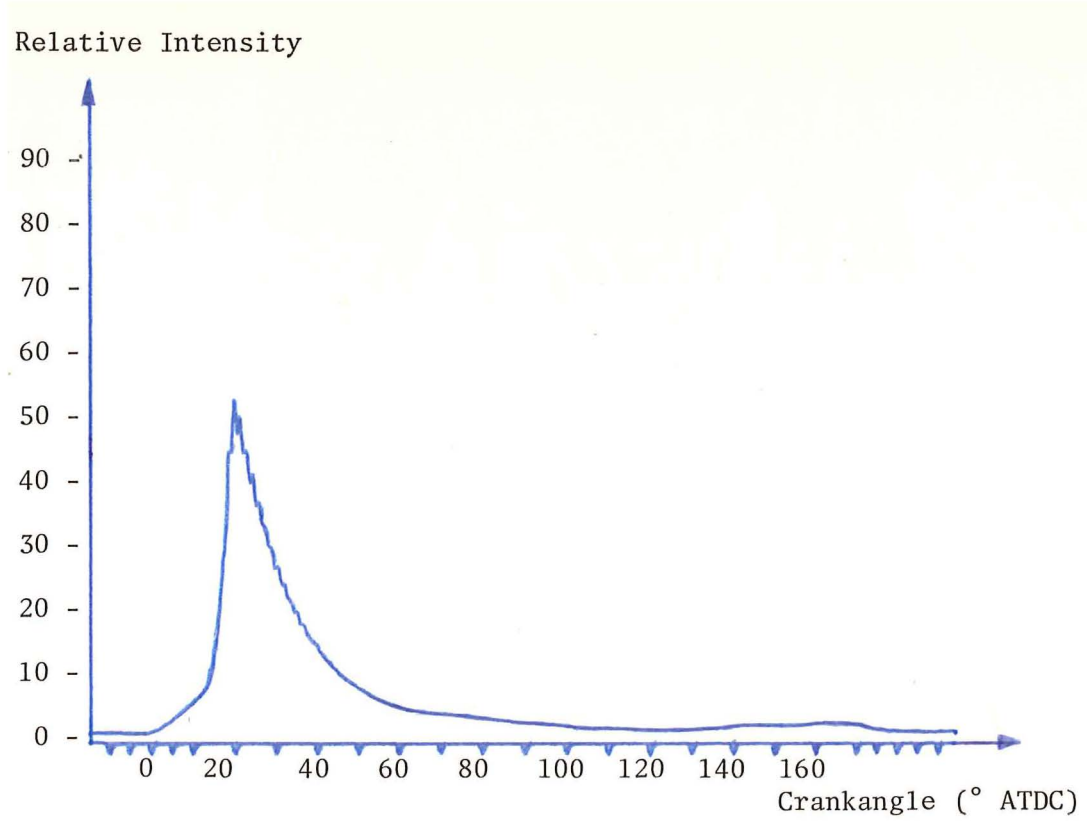

Figure 6.38 Combustion flame light intensity as a function of crankshaft angle (ignition advance 28° BTDC)

6.2.1.3 The Flame Light Intensity as a Function of Ignition Advance Knocking Combustion and Cyclic Variation

Results

IGNITION ADVANCE

Ignition Timing (° BTDC)	Engine Torque	Throttle Position	Engine Speed (r.p.s.)	Figure
28-53 in increments of 5°	Low	1.7/20	30	6.39
25-45 in increments of 5°	Medium	3.9/20	45	6.40
18°, 22°, 26°, 28°	High	20/20	45	6.41

Observations

The crankangle advance at the initiation of each light intensity curve appears to correspond closely with the ignition advance. Thus in Figure 6.39 the total ignition advance between the extreme curves is 25° and the advance of the initiation points of these curves is approximately 23°. There is a similar correspondence between the ignition advance and the initiation of each light intensity curve in Figures 6.40 and 6.41.

Some general observations can also be made concerning the change in shape of the light intensity curves as the ignition timing is advanced. With retarded timing the curves are a simple bell shape and as the timing is advanced, a second maximum becomes apparent during the latter stages of combustion. As the ignition timing is further advanced, the second maximum becomes dominant over the first and eventually all trace of the first maximum may disappear. (Figures 6.40 and 6.41). Further advance of the ignition timing may cause auto-ignition to occur and produce a corresponding oscillating trailing edge on the light intensity curve.

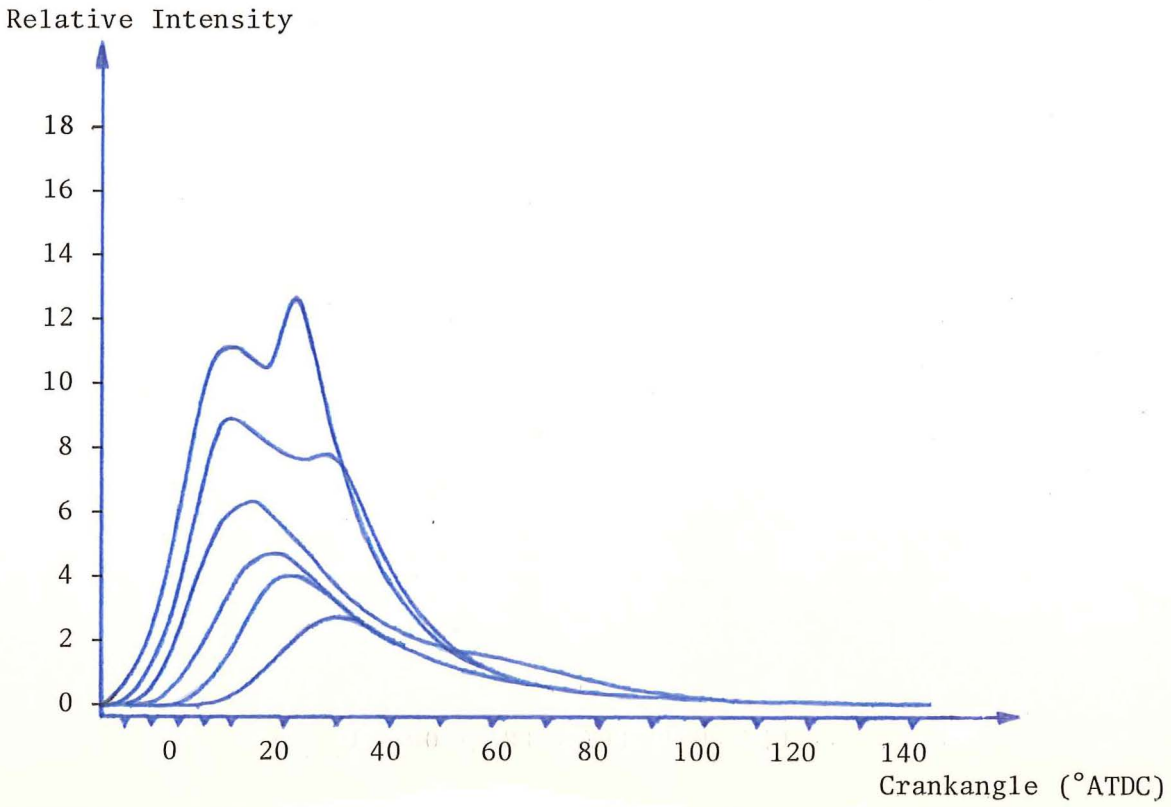

Figure 6.39 Combustion flame light intensity as a function of crankshaft angle (ignition advance settings from lowest to highest curve in order: 28°, 33°, 38°, 43°, 48°, 53° BTDC)

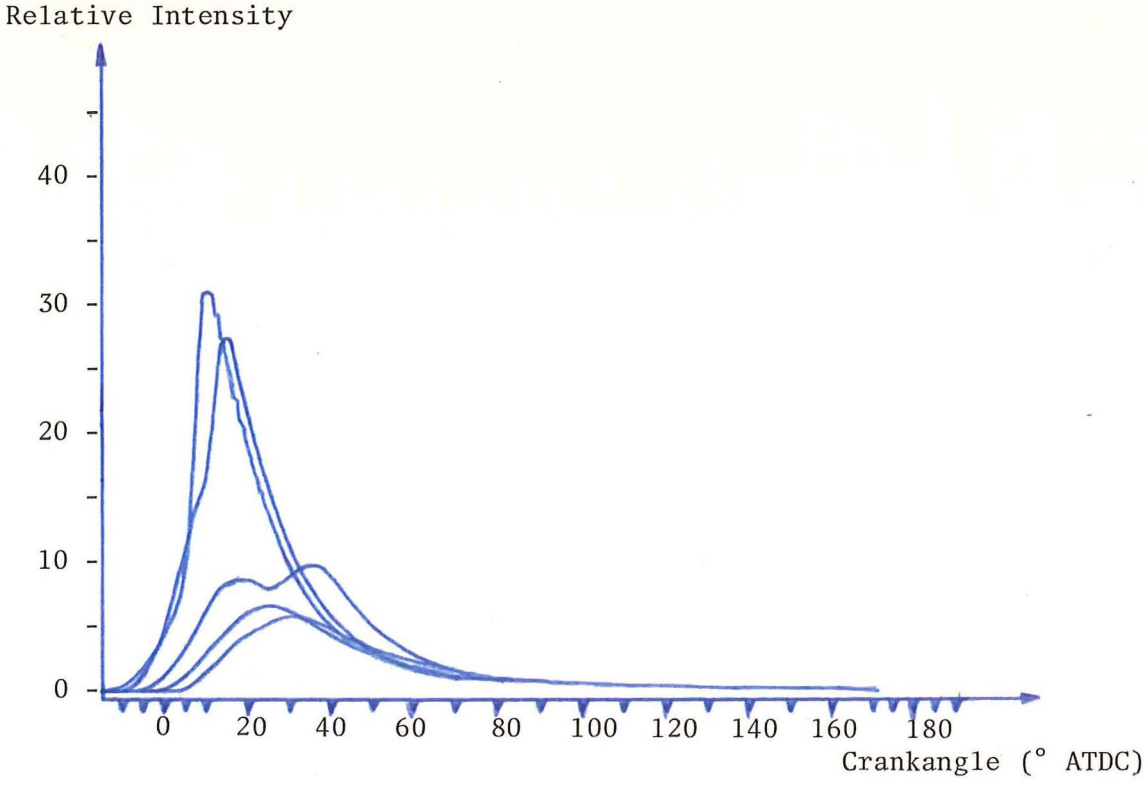

Figure 6.40 Combustion flame light intensity as a function of crankshaft angle (ignition advance settings from lowest to highest curve in order: 25°, 30°, 35°, 40°, 45° BTDC).

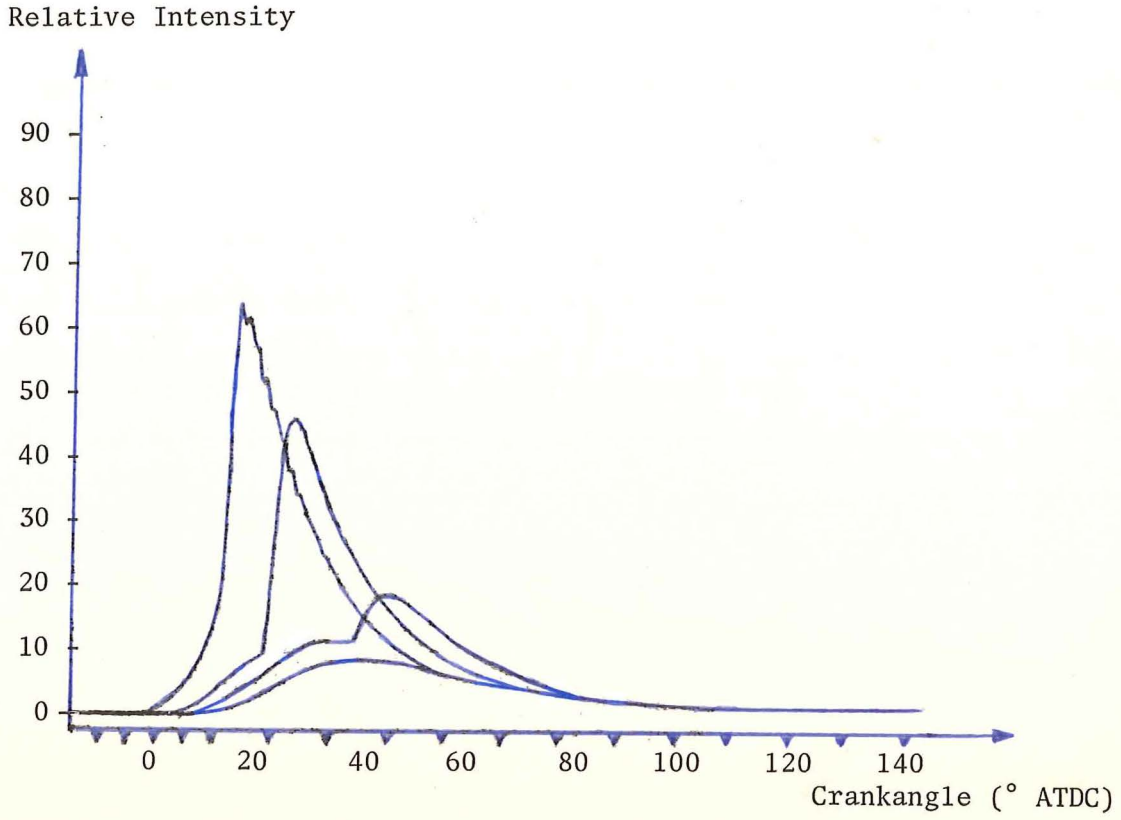

Figure 6.41 Combustion flame light intensity as a function of crankshaft angle (ignition advance settings from lowest to highest curve in order: 18°, 22°, 26°, 28° BTDC).

Knocking Combustion

Engine Speed: 15 r.p.s.

Engine Torque: Medium

Throttle Position: 2.1/20

Ignition Advance: 28° BTDC

Results: Figure 6.42.

Calculations

The frequency of the light intensity oscillations can be calculated by referring to Figure 6.42, which depicts 10 oscillations over approximately 8 crankshaft degrees. The 10 oscillations occur in a time interval of:

$$\frac{8°}{360°} \times \frac{1}{15\ (rps)} = 1.48 \times 10^{-3} \text{ secs} = 1.48 \text{ mS.}$$

So the average period of each oscillation is:

$$\frac{1.48 \times 10^{-3}}{10} = 148\ \mu S.$$

And the average oscillation frequency is: $\frac{1}{148 \times 10^{-6}} = 6.6$ KHz.

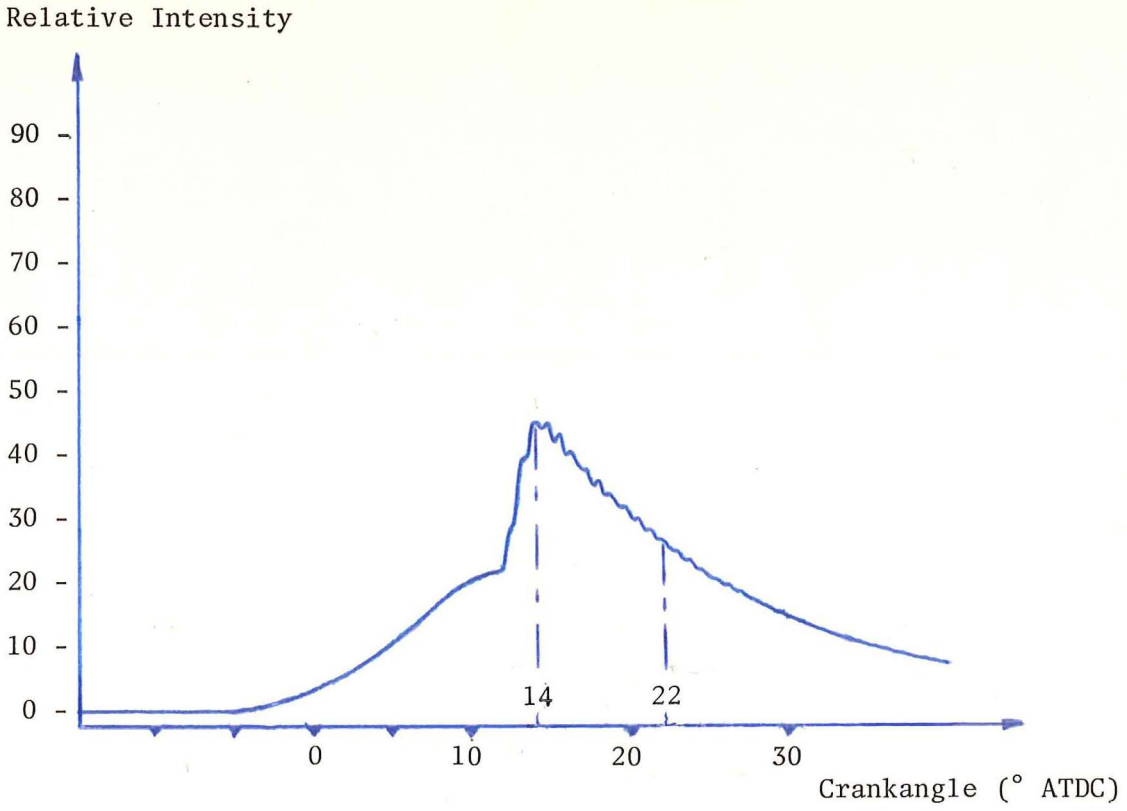

Figure 6.42 Combustion flame light intensity as a function of crankshaft angle during knocking combustion.

Cyclic Variation

Engine Speed: 30 r.p.s.

Results

Engine Torque	Throttle Position	Ignition Advance (°BTDC)	Figure
Low	1.7/20	34	6.43
Medium	3.1/20	32	6.44
High	20/20	14	6.45

Observations

It is to be noted that the curves on any single figure are due to cyclic variation alone. At low engine loads the curves remain bell-shaped unless the timing is advanced beyond MBT. The variation of the curve initiation angle appears to be no more than two crankshaft degrees in this operating condition (Figure 6.43). At medium loads and with the ignition timing set to MBT, the curves as observed on the oscilloscope most frequently had two local maxima with the second slightly larger than the first (the middle two curves of Figure 6.44). The extreme curves in this figure occurred relatively infrequently as compared to these two curves. The maximum variation of the curve initiation angle is approximately ten crankangle degrees over all the curves on this figure, and two crankangle degrees between the two frequently occurring double maxima curves. At high loads when the ignition timing is set to the knock limit (i.e. light pinging occurring on occasional combustion cycles), the cyclic variation is shown in Figure 6.45. The two middle curves occur the most frequently and the two extreme curves occur relatively infrequently. The maximum variation of the curve initiation angle is approximately seven crankangle degrees over all the curves and four crankangle degrees between the two middle curves.

The cyclic variation curves also appear to be similar in shape to the series of ignition advance curves just described in this section, at the equivalent engine loads. Thus, especially at medium and high torques, the cyclic variation curves appear to fluctuate from the bell-shaped retarded ignition timing curve to the curve depicting engine knock at advanced ignition settings.

The cyclic variation of the peak light intensities is approximately 40% at the low engine torque operating condition (Figure 6.43) and up to

70% at the medium torque condition (Figure 6.44). This relatively large variation in the light intensity peak amplitude is similar to the 50% variation in OH radical emissions in an SI engine observed by Smith and Starkman[54].

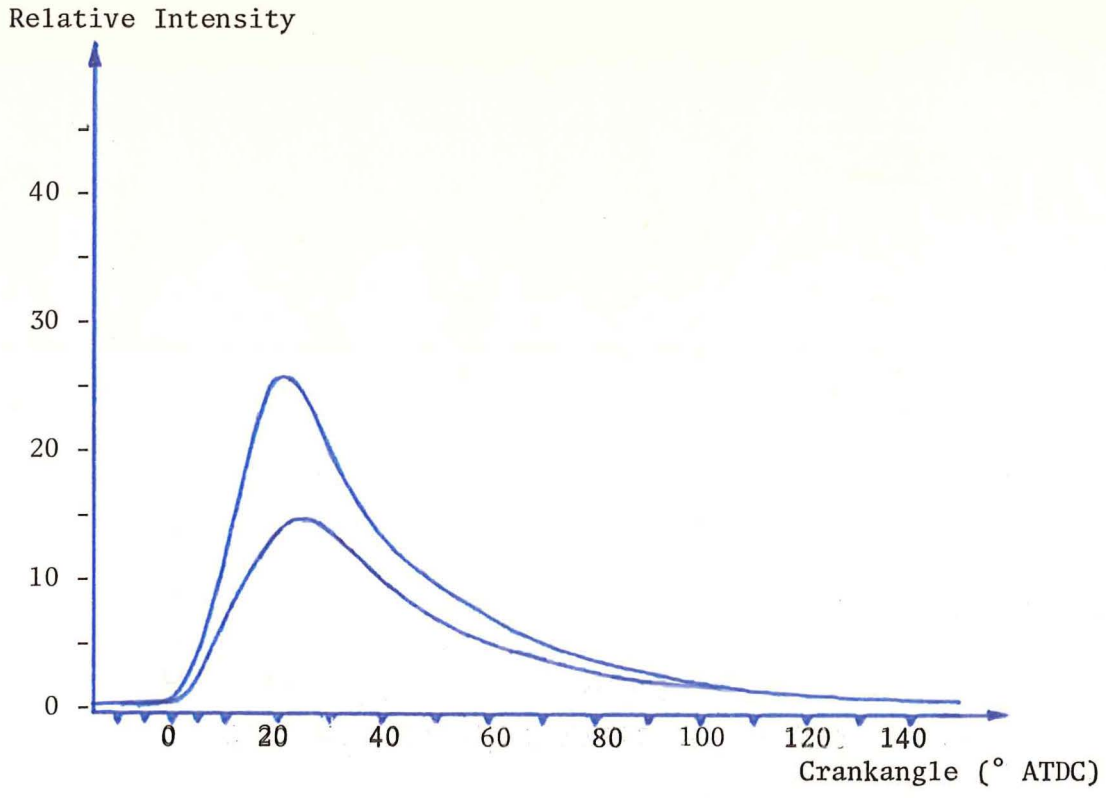

Figure 6.43 Combustion flame light intensity as a function of crankshaft angle showing cyclic variation (low torque).

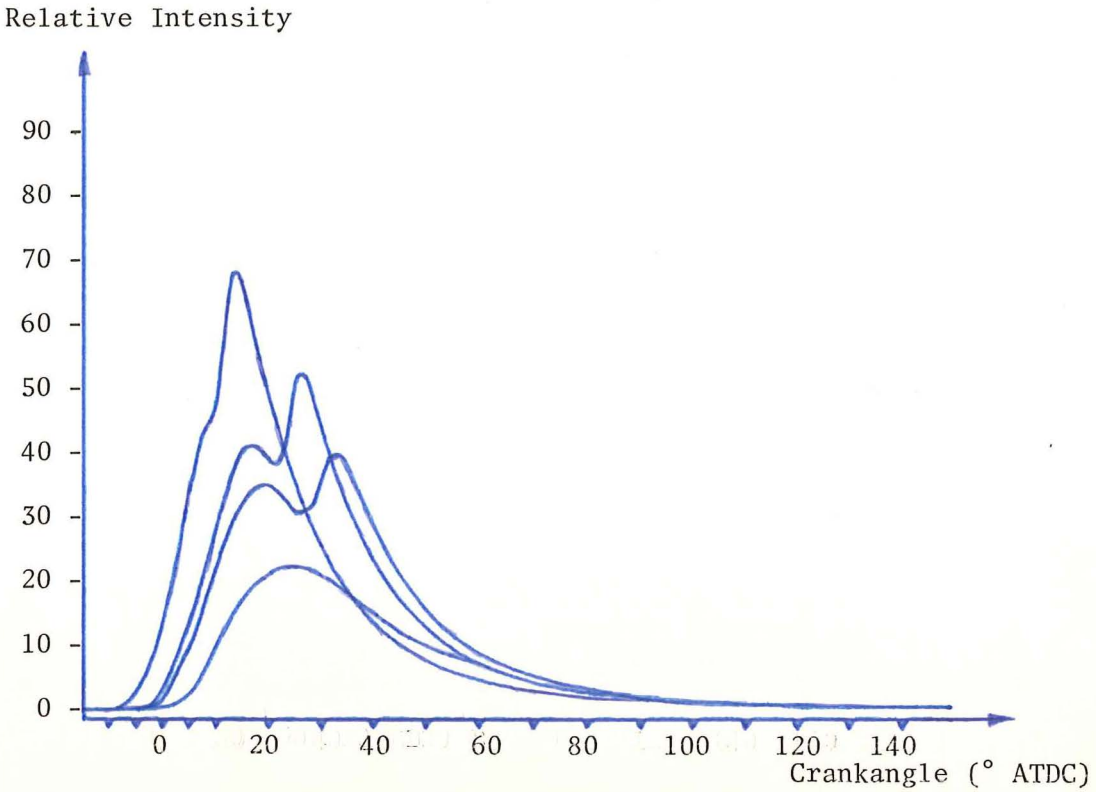

Figure 6.44 Combustion flame light intensity as a function of crankshaft angle showing cyclic variation (medium torque).

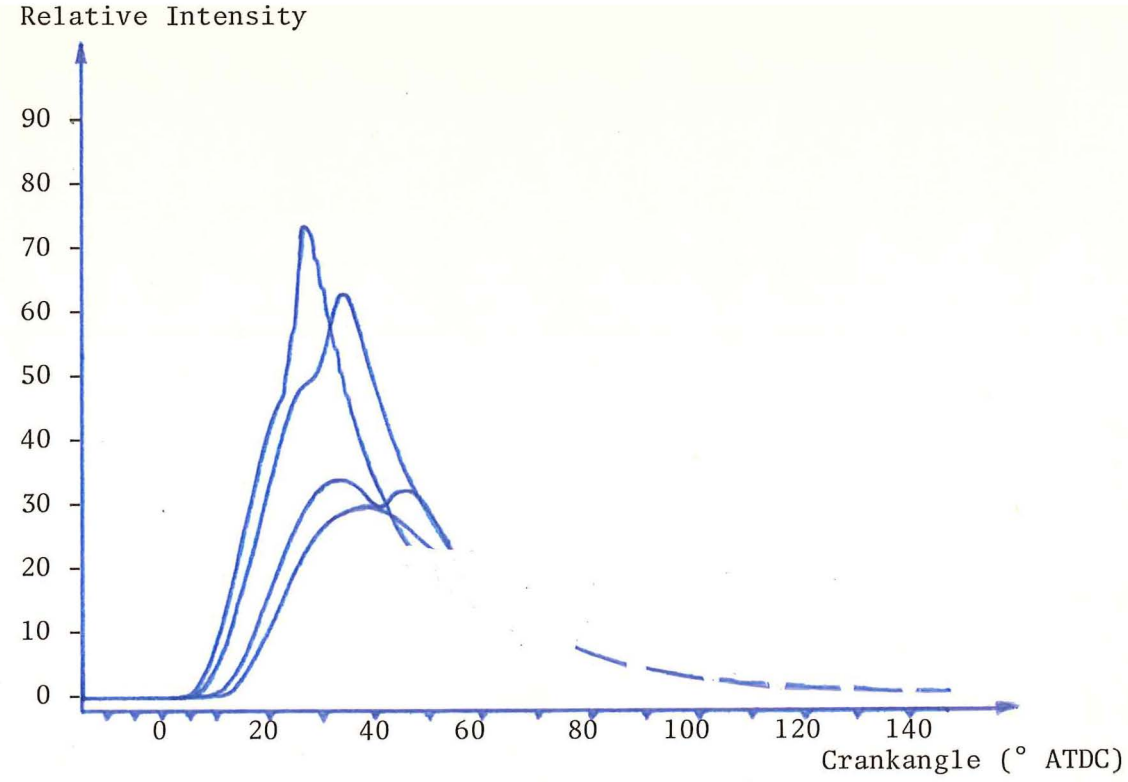

Figure 6.45 Combustion flame light intensity as a function of crankshaft angle showing cyclic variation (high torque).

6.2.2 The Response Curves from the Lead-Salt Detectors

6.2.2.1 The Response Curves from the Lead-Sulphide Detector

Engine Speed: 30 r.p.s.

Engine Torque: Low

Throttle Position: 1.7/20

Results

Ignition Advance (°BTDC)	Torque (Nm)	Figure
30	12.0	6.46
45	12.2	6.47
50	12.0	6.48

Observations

The graphs indicate that the lead-sulphide photodetector (upper trace) is more responsive to the cause of the second maxima than the silicon photodetector. The lead sulphide detector also appears to be more sensitive to the radiation emitted during the later stages of combustion than the silicon device. The silicon detector, however, gives a peak light intensity which increases significantly with an increase in the ignition advance whereas the lead sulphide detector output does not increase so appreciably when the ignition timing is advanced.

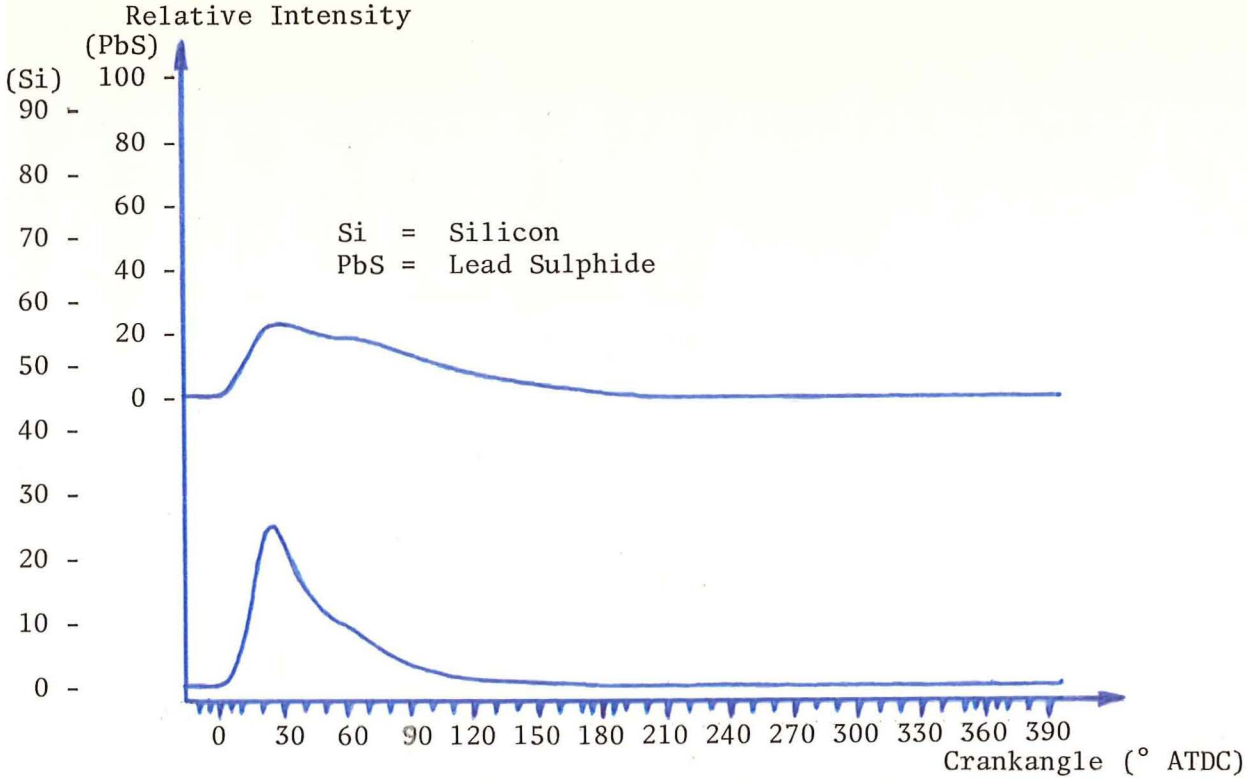

Figure 6.46 Combustion flame radiation intensity (upper curve PbS detector, lower curve Silicon detector) as a function of crankshaft angle (ign.adv.30° BTDC).

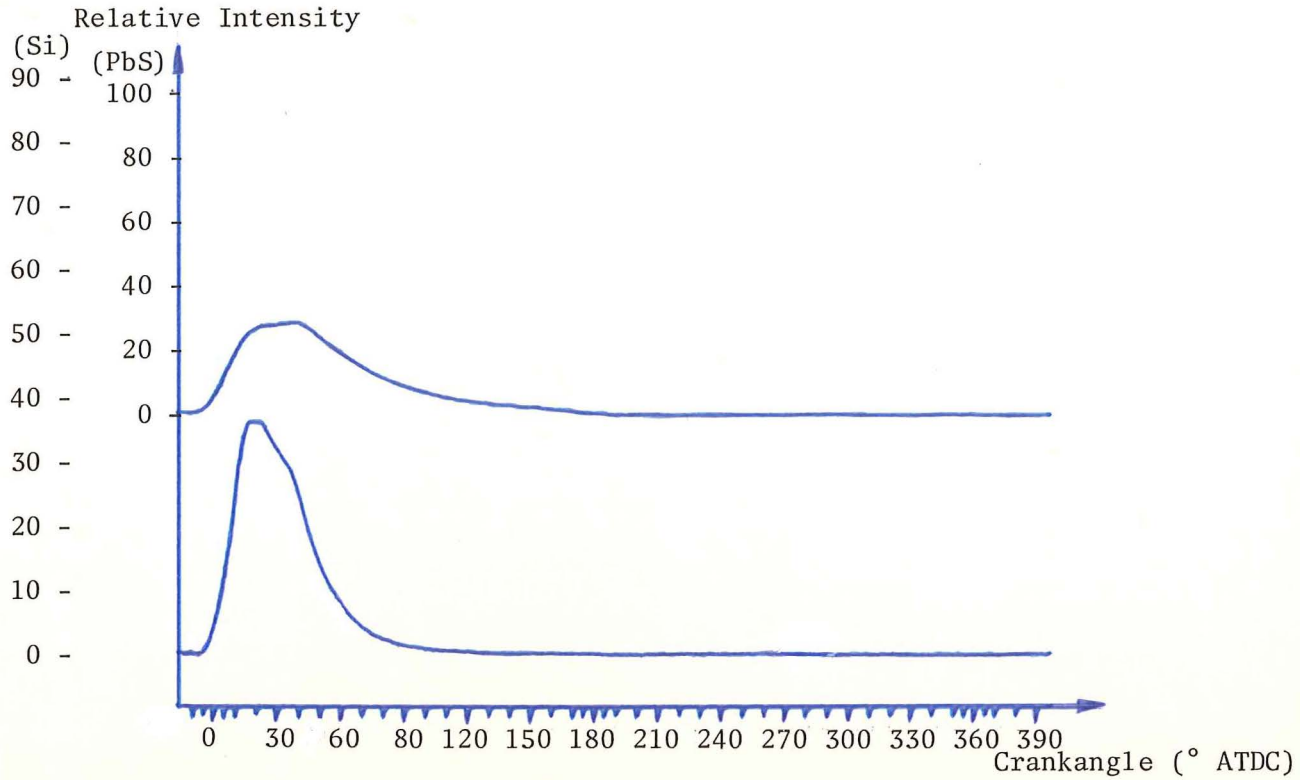

Figure 6.47 Combustion flame radiation intensity (upper curve PbS detector, lower curve Silicon detector) as a function of crankshaft angle (ign.adv.45° BTDC).

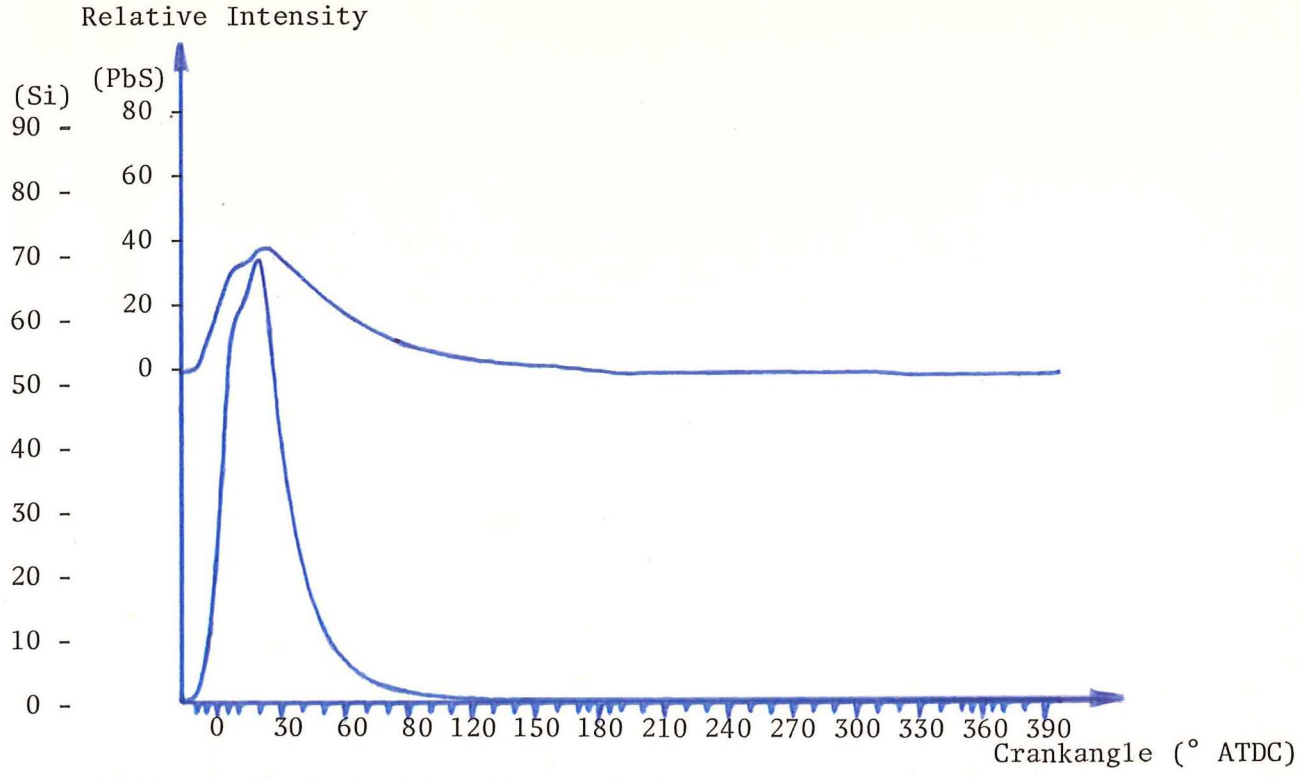

Figure 6.48 Combustion flame radiation intensity (upper curve PbS detector, lower curve Silicon detector) as a function of crankshaft angle (ign.adv.50° BTDC).

Engine Torque: High

Throttle Position: 20/20

Results

Ignition Advance (° BTDC)	Torque (Nm)	Figure
17	34.5	6.49
20	35.6	6.50
23	35.8	6.51

Observations

The lead-sulphide detector again shows improved response to the radiation emissions during the latter stages of combustion. It responds less to the combustion reactions which occur as the exhaust valve opens than the silicon photodetector response. The second maximum does not appear to dominate the curve quite so much in the case of the lead sulphide detector output.

At the most advanced ignition timing setting, knocking combustion is clearly shown on the silicon photodetector trace but can only just be discerned on the trailing edge of the lead-sulphide curve (Figure 6.51).

Calculations

The time constant for the lead-sulphide detector is typically 200 μS. Therefore the upper half-power frequency limit of the detector is:

$\frac{1}{200 \times 10^{-6}} = 5$ KHz. Thus the light intensity oscillations of approximately

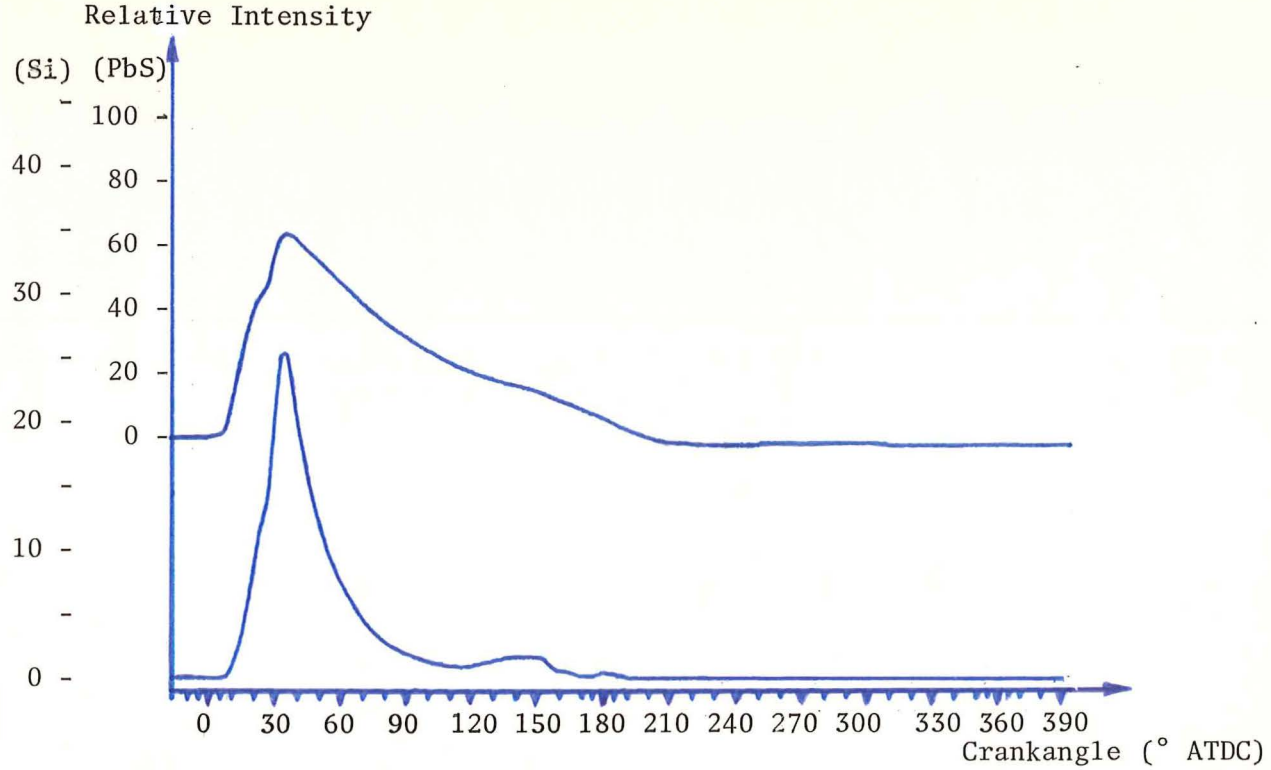

Figure 6.49 Combustion flame radiation intensity (upper curve PbS detector, lower curve Silicon detector) as a function of crankshaft angle (ign.adv.17° BTDC).

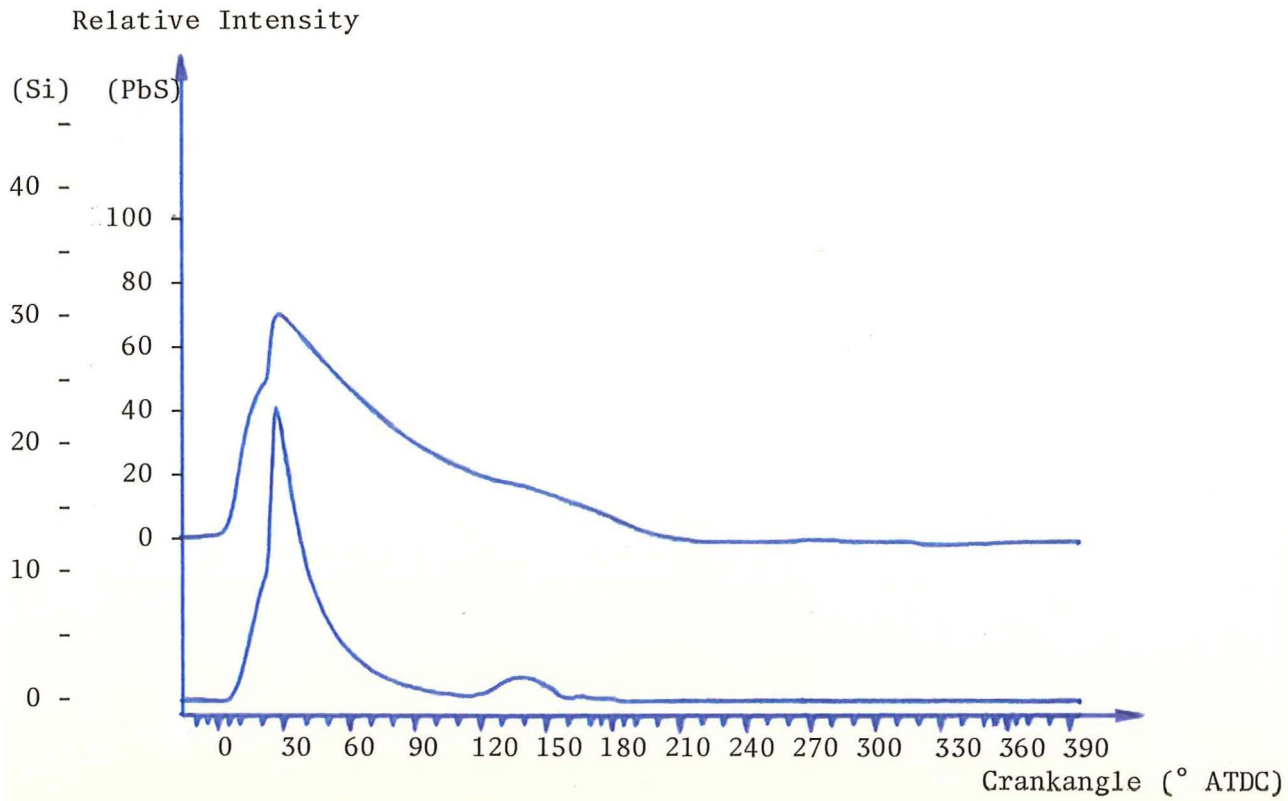

Figure 6.50 Combustion flame radiation intensity (upper curve PbS detector, lower curve Silicon detector) as a function of crankshaft angle (ign.adv.20° BTDC).

6.6 KHz caused by knocking combustion will be transmitted electrically from the lead-sulphide detector at less than half-power.

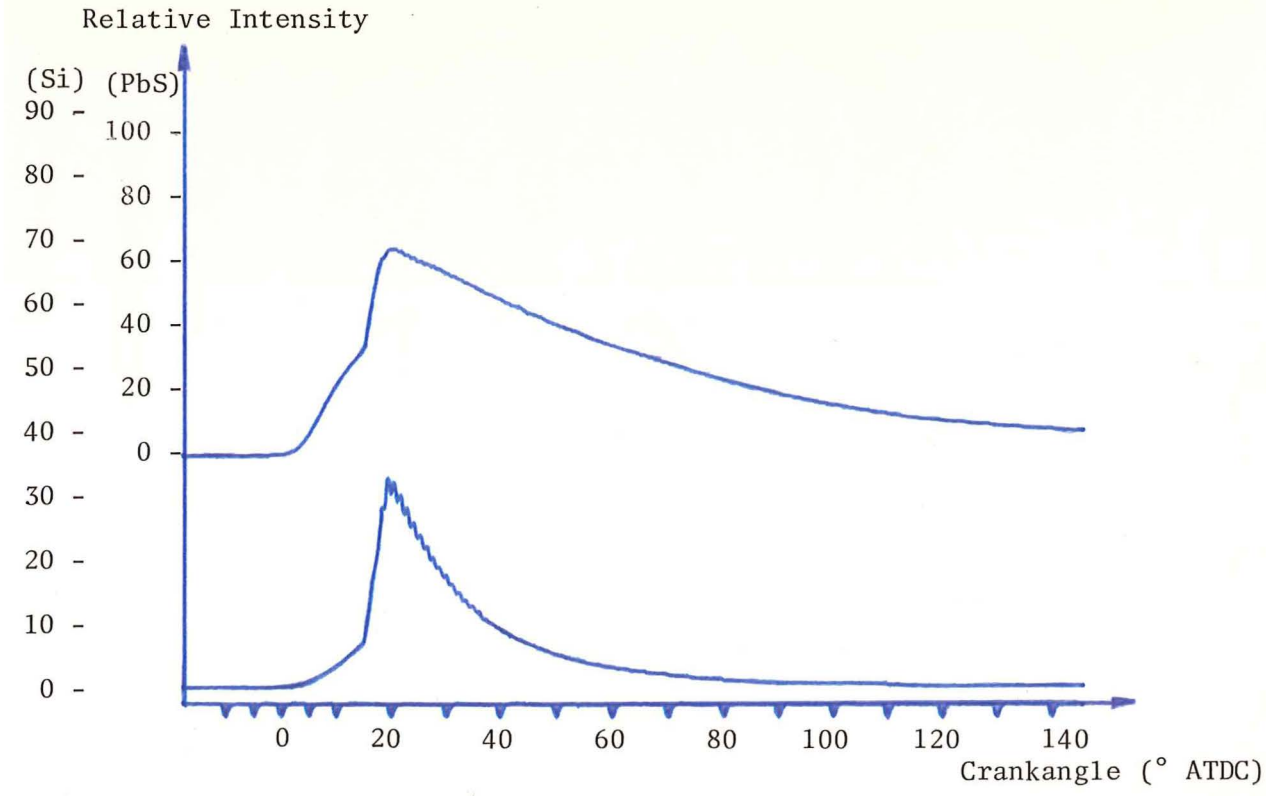

Figure 6.51 Combustion flame radiation intensity (upper curve PbS detector, lower curve Silicon detector) as a function of crankshaft angle (ign.adv.23° BTDC).

6.2.2.2 The Response Curves from the Lead-Selenide Detector

Engine Speed: 30 r.p.s.

Engine Torque: Low

Throttle Position: 1.6/20.

Results

Ignition Advance (° BTDC)	Torque (Nm)	Figure
35	11.5	6.52
45	11.4	6.53
50	11.1	6.54

Observations

The curves show that the lead-selenide detector (upper traces), as with the lead-sulphide detector, is more sensitive to the later stages of combustion than is the silicon photodetector. When there are two peaks the lead-selenide detector accentuates the second more strongly.

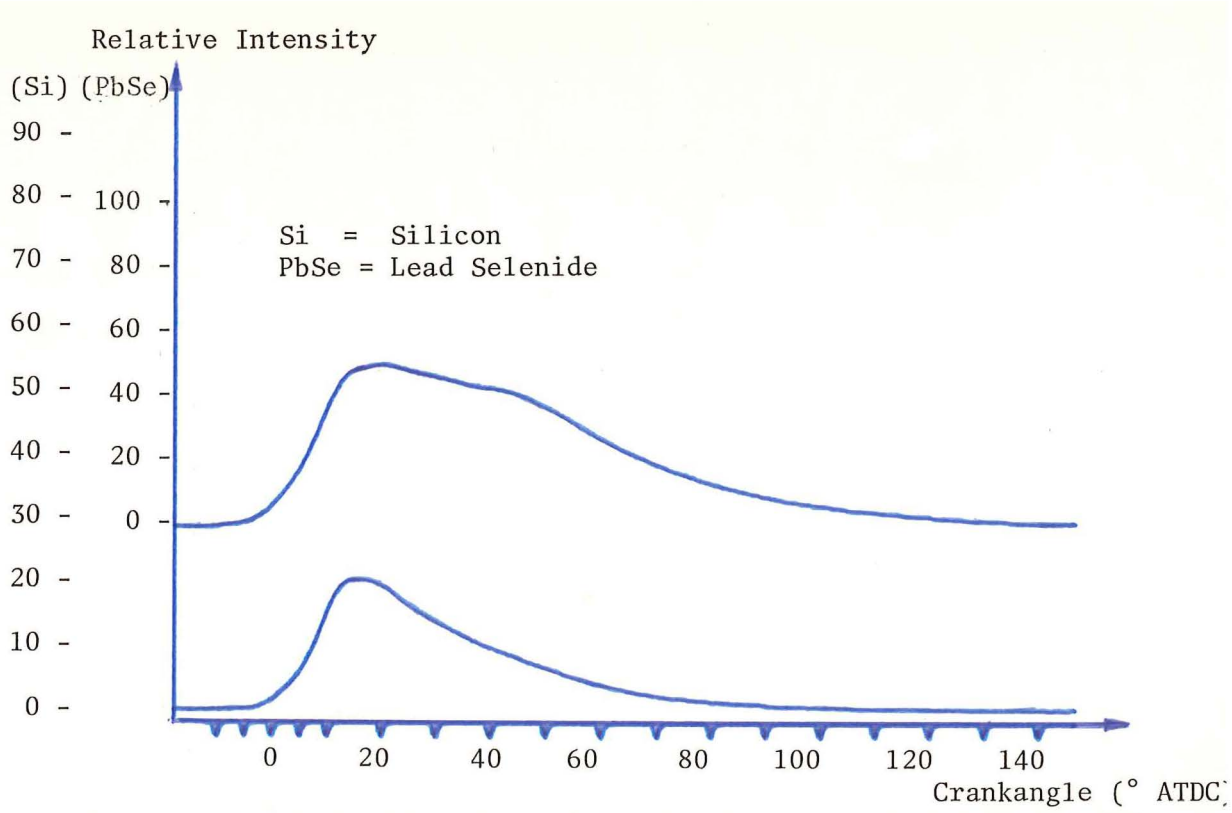

Figure 6.52 Combustion flame radiation intensity (upper curve PbSe detector, lower curve Silicon detector) as a function of crankshaft angle (ign. adv. 35° BTDC).

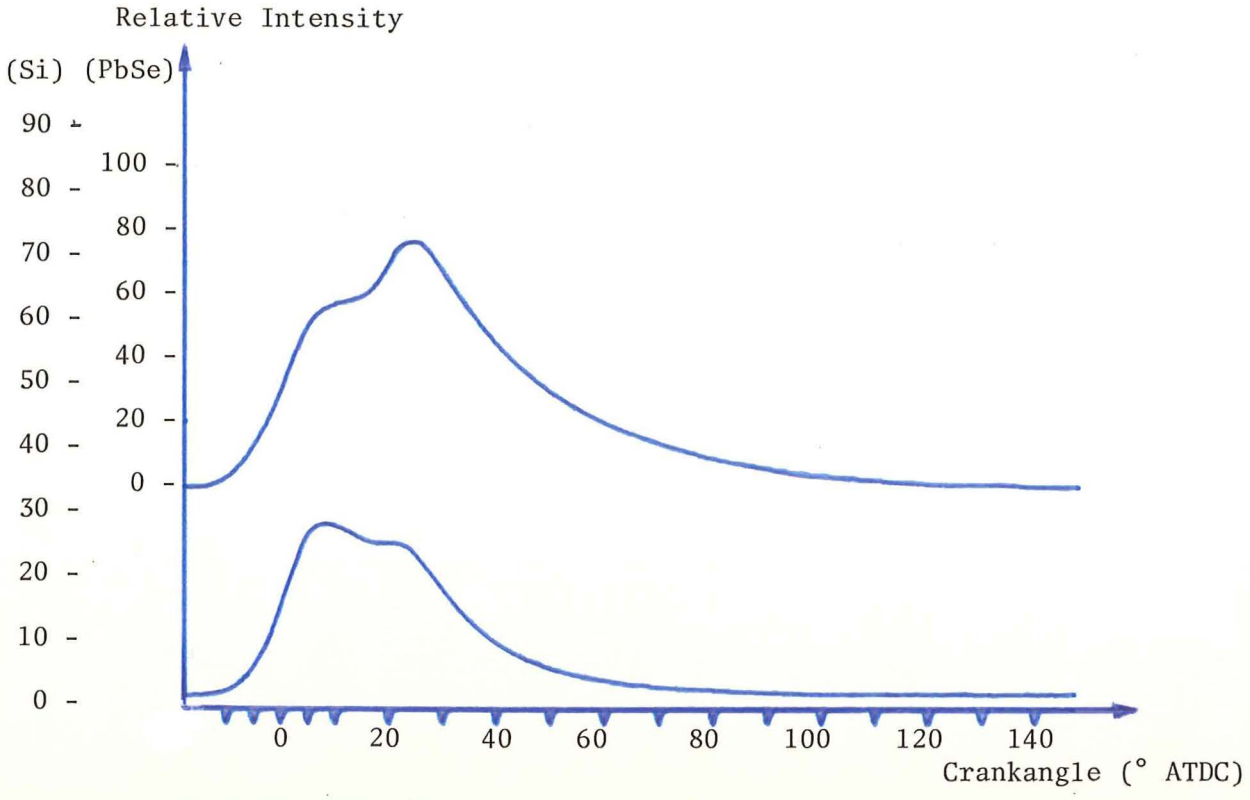

Figure 6.53 Combustion flame radiation intensity (upper curve PbSe detector, lower curve Silicon detector) as a function of crankshaft angle (ign. adv. 45° BTDC).

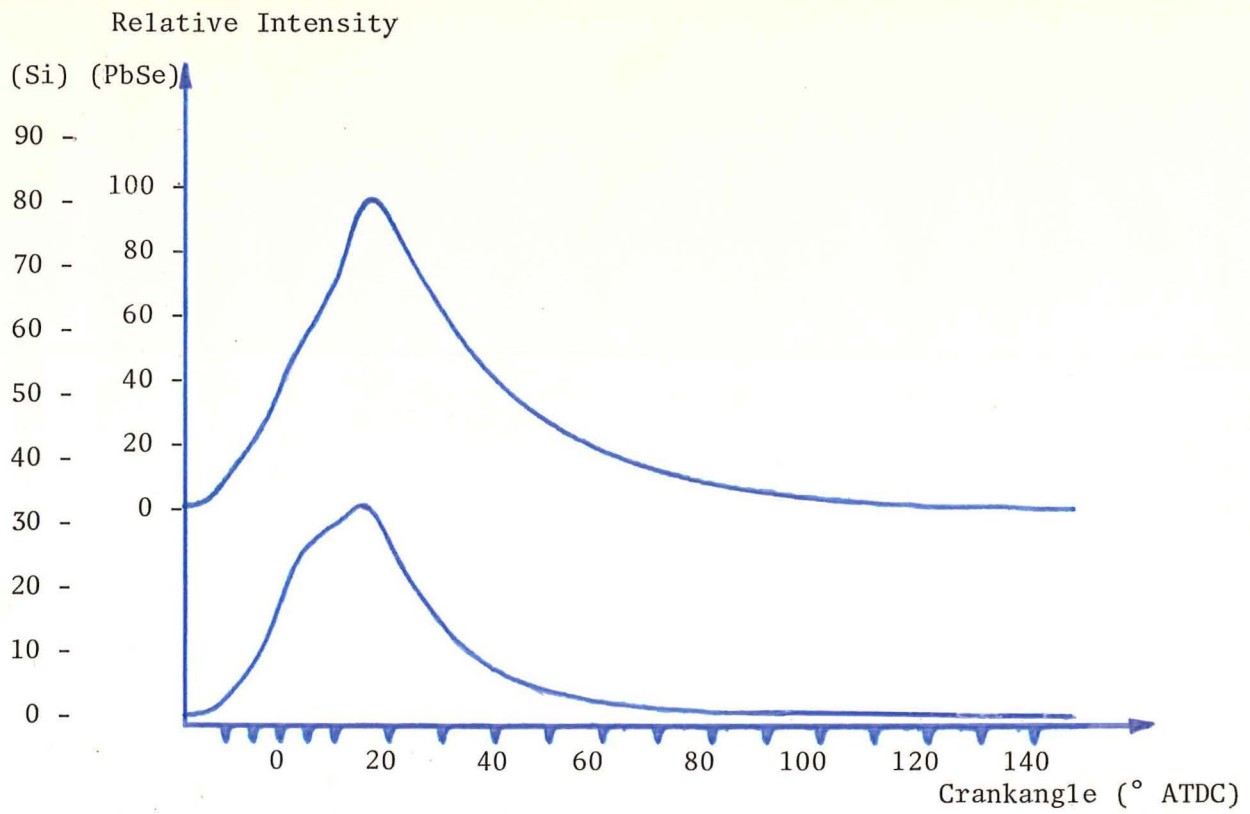

Figure 6.54 Combustion flame radiation intensity (upper curve PbSe detector, lower curve Silicon detector) as a function of crankshaft angle (ign. adv. 50° BTDC).

Engine Torque: High

Throttle Position: 20/20

Results

Ignition Advance (° BTDC)	Torque (Nm)	Figure
14	≈32.4	6.55
20	≈34.9	6.56
23	≈35.4	6.57

Observations

The lead-selenide detector curves have a peak amplitude which responds to changes in the ignition advance angle more positively than the lead-sulphide detector. That is, the lead selenide output amplitude increases quite significantly as the ignition timing is advanced and in this matter its response is quite similar to the silicon photodetector response. It also responds to knocking combustion with significant radiation intensity oscillations on the waveform trailing edge (Figure 6.57). They are the same frequency as those on the silicon detector trace which is to be expected.

The lead-selenide detector does not appear to respond to the disturbance as the exhaust valve opens (Figure 6.56).

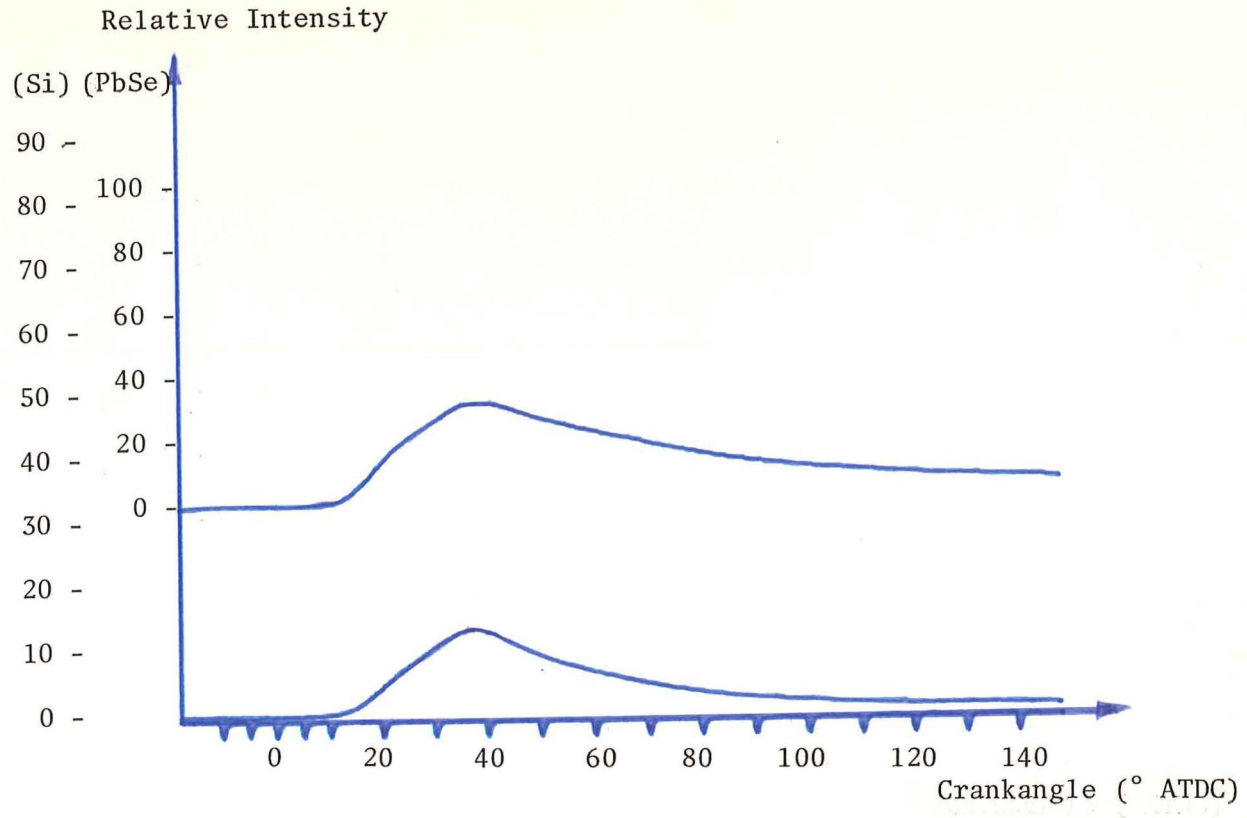

Figure 6.55 Combustion flame radiation intensity (upper curve PbSe detector, lower curve Silicon detector) as a function of crankshaft angle (ign. adv. 14° BTDC).

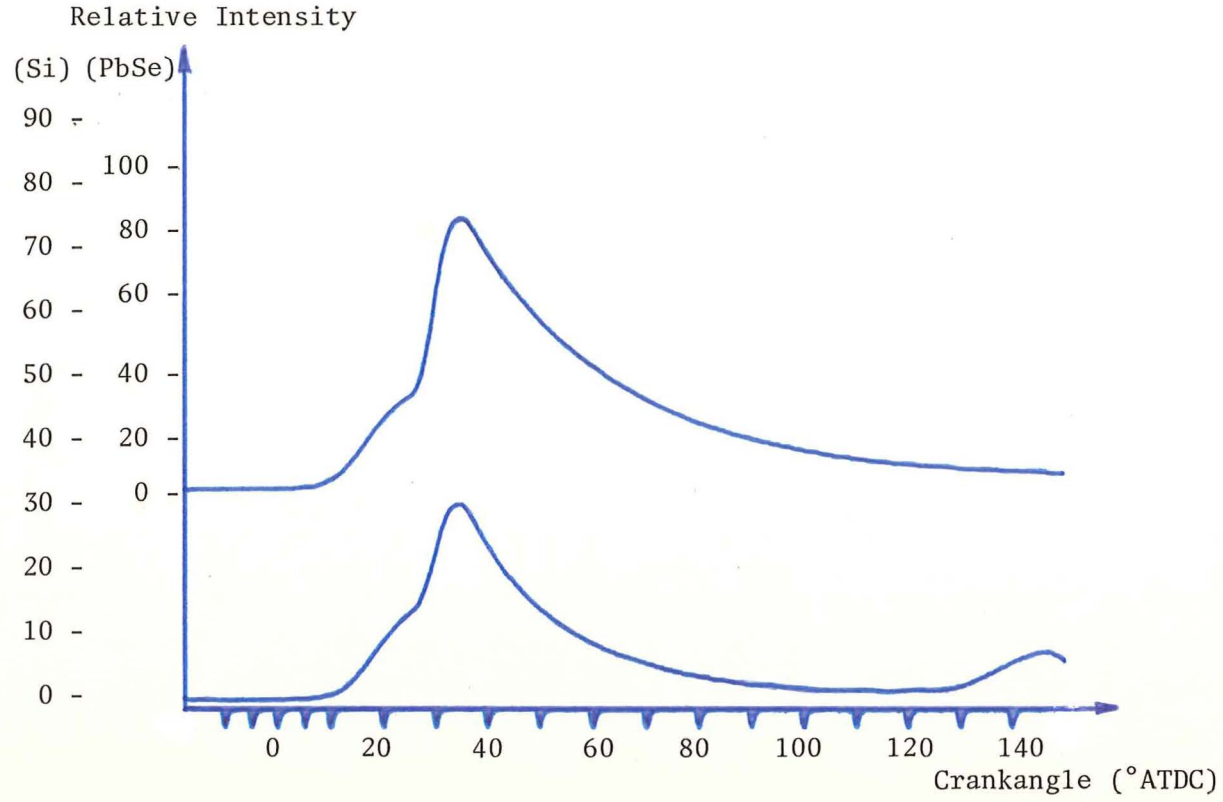

Figure 6.56 Combustion flame radiation intensity (upper curve PbSe detector, lower curve Silicon detector) as a function of crankshaft angle (ign. adv. 20° BTDC).

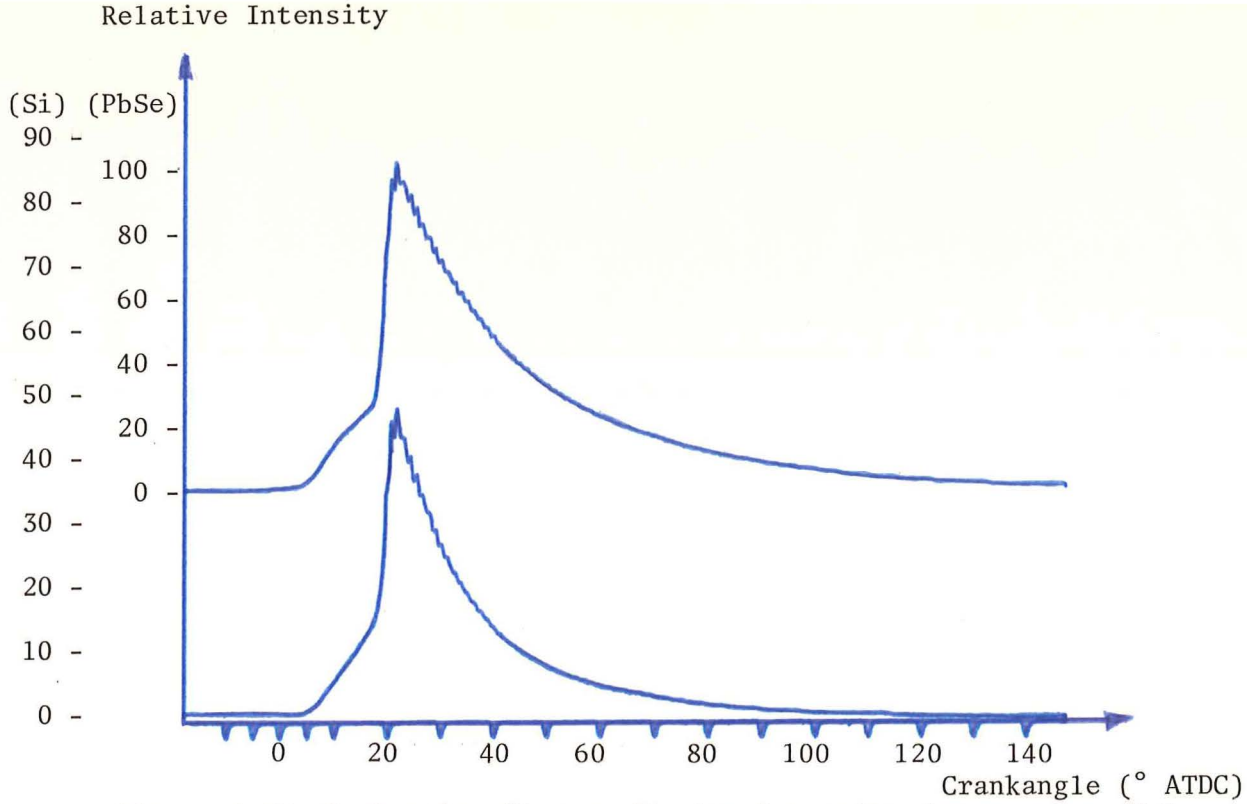

Figure 6.57 Combustion flame radiation intensity (upper curve PbSe detector, lower curve Silicon detector) as a function of crankshaft angle (ign. adv. 23° BTDC).

6.3 Light Intensity Measurements through the Optic Plug

6.3.1 Knocking Combustion in the Ricardo E6 Engine

Engine Speed: ≈30 r.p.s.

Engine Torque: Approximately 85% of maximum torque at 30 r.p.s. (29 Nm).

Throttle Position: 5.1

Ignition Advance: 35° BTDC.

Optic Plug Position: Mounted in the auxiliary port in the cylinder head.

Photodetector: Silicon.

Results

1. High tension lead connected to the optic plug; Figure 6.58.
2. High tension lead connected to the normal spark plug located at the opposite corner of the combustion chamber; Figure 6.59.

Observations

When the optic plug was used for sparking purposes to initiate the high temperature combustion reactions then the light intensity trace was of a different form to previously recorded curves, (Figure 6.58). It should be noted that although the engine was knocking heavily and continually, the light oscillations shown at the top of this curve were generally very low in amplitude, i.e. the easily recognisable light oscillations in this figure were not normally observed.

However, when the plug was used merely as a fibre optic window, located in the cylinder endgas region, the light oscillations were generally present on the trailing edge of the curve to the extent shown in Figure 6.59. When the plug was used in this manner, at the opposite end of the chamber to the spark plug, the light intensity curves are similar in shape to those previously recorded with a simple window mounted in the same position.

A comparison of the two curves shows that the light fluctuations occur in a different position in the top trace. The light intensity from the sparking optic plug has remained almost constant for the duration of the oscillations. The longer duration of this high amplitude light intensity is probably due to the combustion temperature gradient which yields higher temperatures and therefore more black body luminescence in the region surrounding the spark plug (refer to Section 4.4.1).

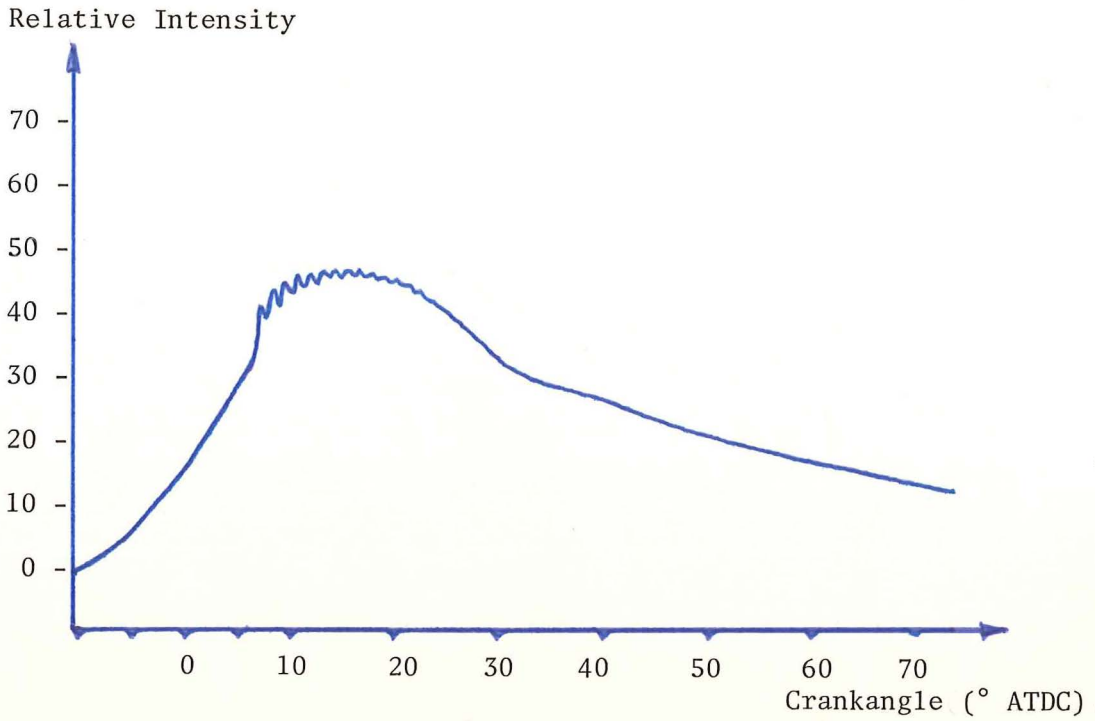

Figure 6.58 Combustion flame light intensity as a function of time, through the optic plug (sparking)

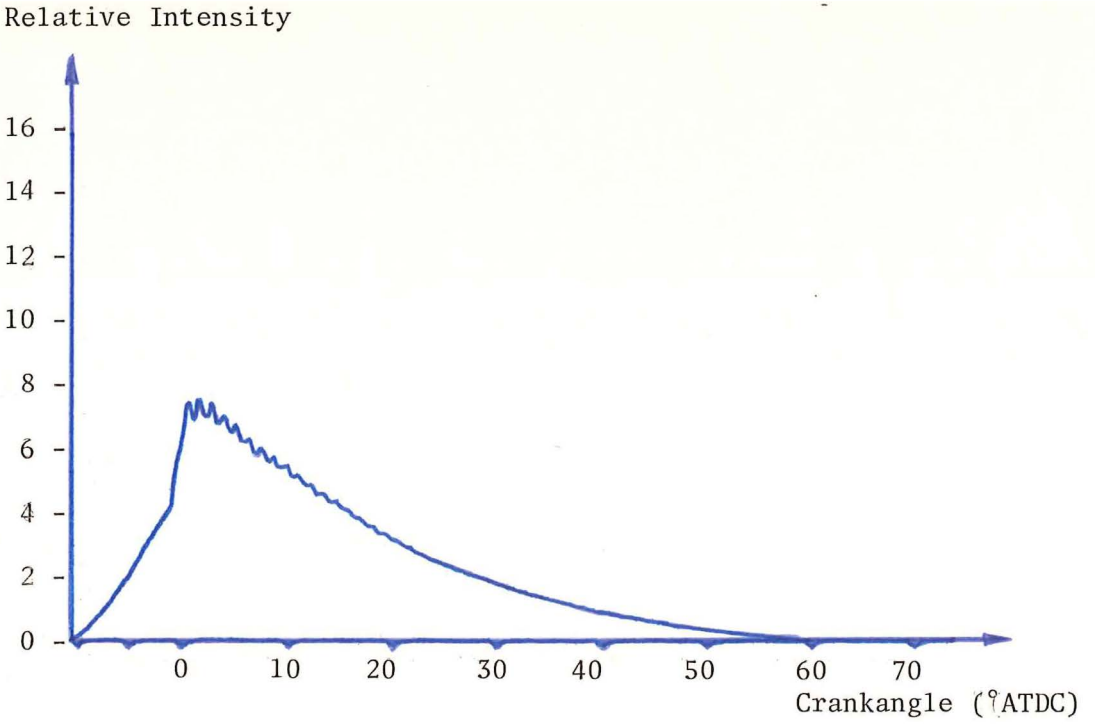

Figure 6.59 Combustion flame light intensity as a function of time, through the optic plug (used as a window in the cylinder endgas region)

6.3.2 Standard Combustion in the Cortina Engine

Engine Speed: 1700 r.p.m.

Engine Torque: 23.8 Nm

Ignition Advance: Set to manufacturer's specifications.

Optic Plug: Mounted in Number 1 cylinder.

Photodetector: Silicon

Observations

The double maxima trace in Figure 6.60 occurred less than 5% of the time, the dotted curve being most common. The x-axis time scale was calibrated from the oscilloscope time scale. The curve has similar characteristics to those produced from the Ricardo engine during low torque operating conditions.

6.3.3 Knocking Combustion in the Cortina Engine

Engine Speed: 1400 r.p.m.

Optic Plug: Mounted in Number 1 cylinder.

Photodetector: Silicon.

Results

Igniton Advance (° BTDC)	Audible Knock	Engine Torque (Nm)	Approx.% of each curve (refer to (Figure 6.60)	
			Dotted	Double Maxima
18 Standard	None	93.2	50	50
23	None	95.6	40	60
26	None	96.2	40	60
28	None	95.6	40	60
33	Light	94.4	40	60
38	Medium/ Heavy	91	40	60

Observations

The light intensity curves were similar to Figure 6.60 and this is used as a reference for a comparison of the percentage of double maxima traces to single maximum traces at each ignition advance setting. It is to be noted that generally the double maxima traces could barely be perceived as such.

When the igntion timing was advanced from the standard setting, there was a slight increase in the proportion of double maxima traces up until 23° advance, but upon further advancing the ignition time no noticeable changes occurred in the traces. Although the ignition timing was advanced until the engine was knocking relatively heavily, there was no sign of light intensity oscillations on any of the light intensity curves. The light intensity peak progressively increased in amplitude

as the ignition timing was advanced.

The optic plug gave similar results during knocking combustion no matter which cylinder the optic plug was installed in.

6.3.4 Knocking Combustion in the Lancer Engine

Observations

When the optic plug was installed in the Mitsubishi Lancer engine the light intensity curves were again similar to those in Figure 6.60. When the ignition timing was advanced at high engine torque in order to induce audible knocking combustion there was no apparent change in the shape of the light intensity curves and no appearance of light intensity oscillations of the trailing edge of any of the curves.

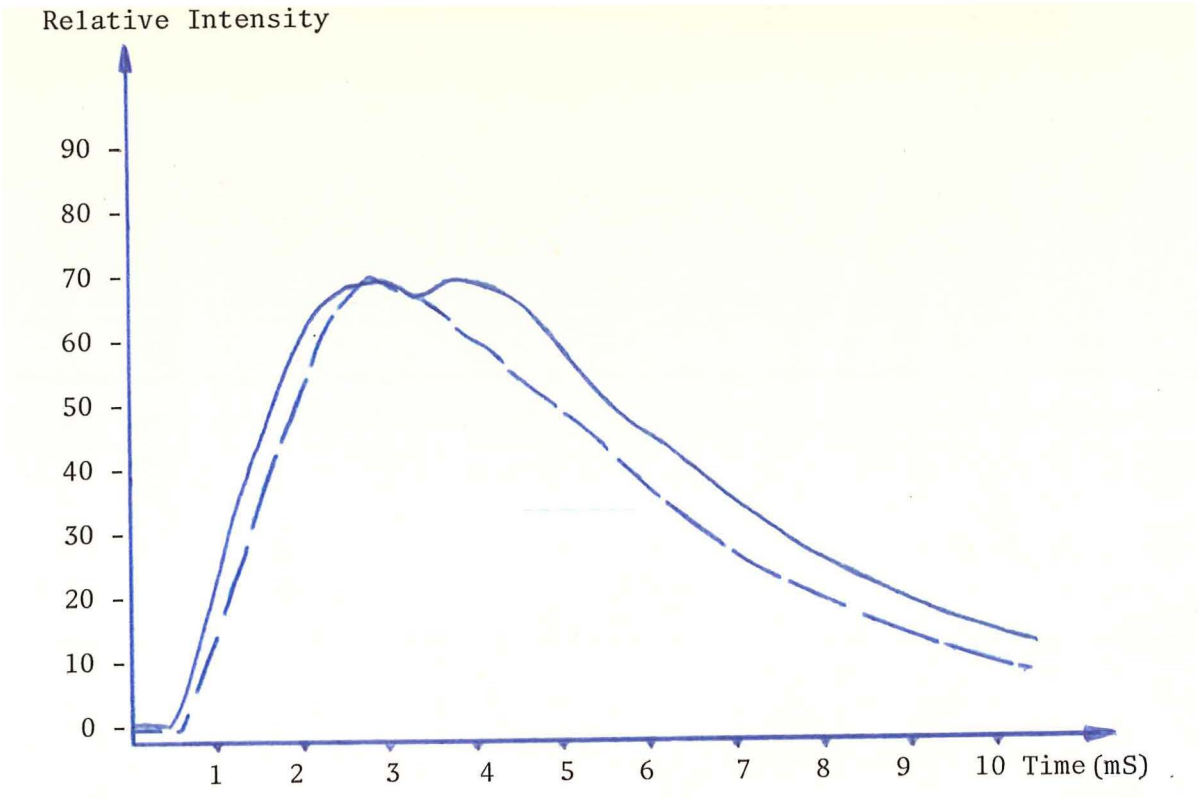

Figure 6.60 Combustion flame light intensity as a function of time from Ford Cortina engine.

6.3.5 The Effect of Combustion Product Fouling on the Light Intensity Measured through the Optic Plug

Amplification Circuitry: Figure 5.3 with R_f = 10 MΩ

Engine Timing: Standard

Operation Time:

The optic plug was operated in No.1 cylinder for a total time of approximately 41 hours commencing with the inner end of the fibre optic cable being clean and highly polished. For engine operation conditions during this time refer to Section 5.3.3.

After the completion of 41 hours, the plug was then briefly tested at three different loads and the light intensity recorded.

Results

Engine Speed (r.p.m.)	Engine Torque (Nm)	Figure
400	4.8	6.61
1500	13.4	6.62
3000	30.2	6.63

Observations

All three figures show good signal to noise ratio levels, the only exception being in Figure 6.61 when at idle, the high frequency interference becomes significant. This interference at the beginning of the curve could be significantly reduced through the use of a longer length of fibre optic cable to enable the amplification circuitry to be situated further from the engine. The interference could also be actively filtered out.

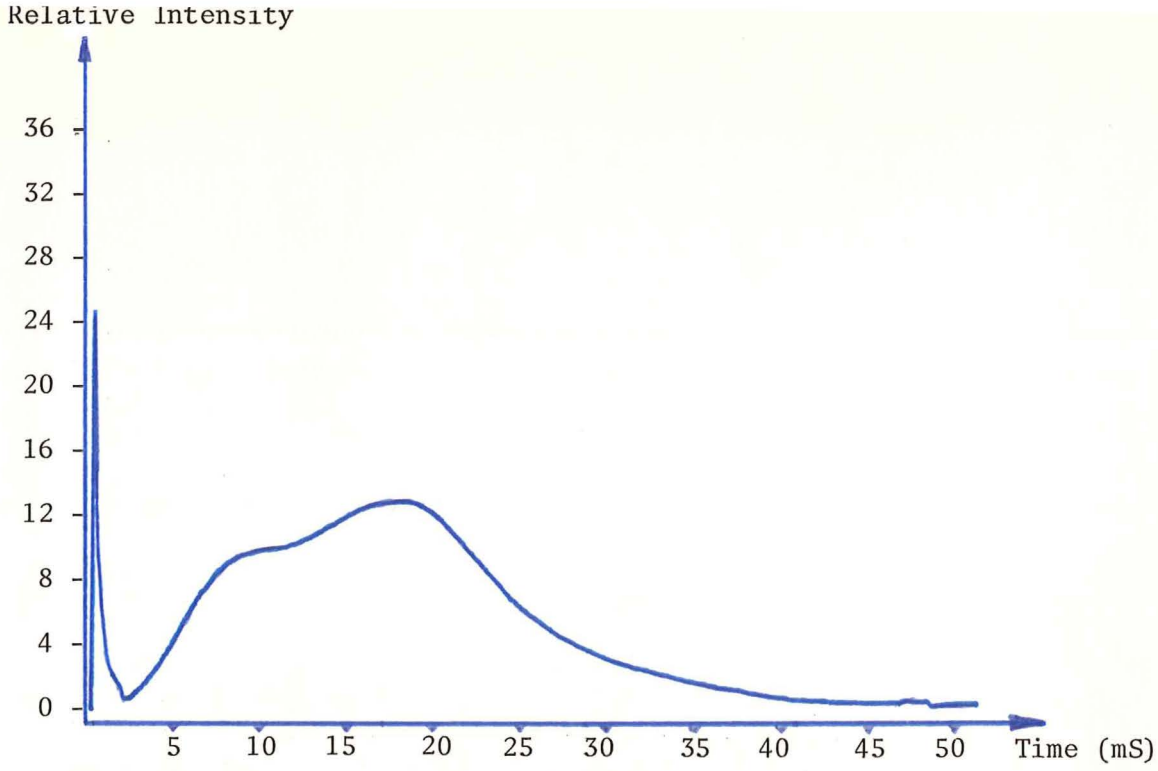

Figure 6.61 Combustion flame light intensity as a function of time from the Mitsubishi Lancer engine after 41 hours operating time (idle)

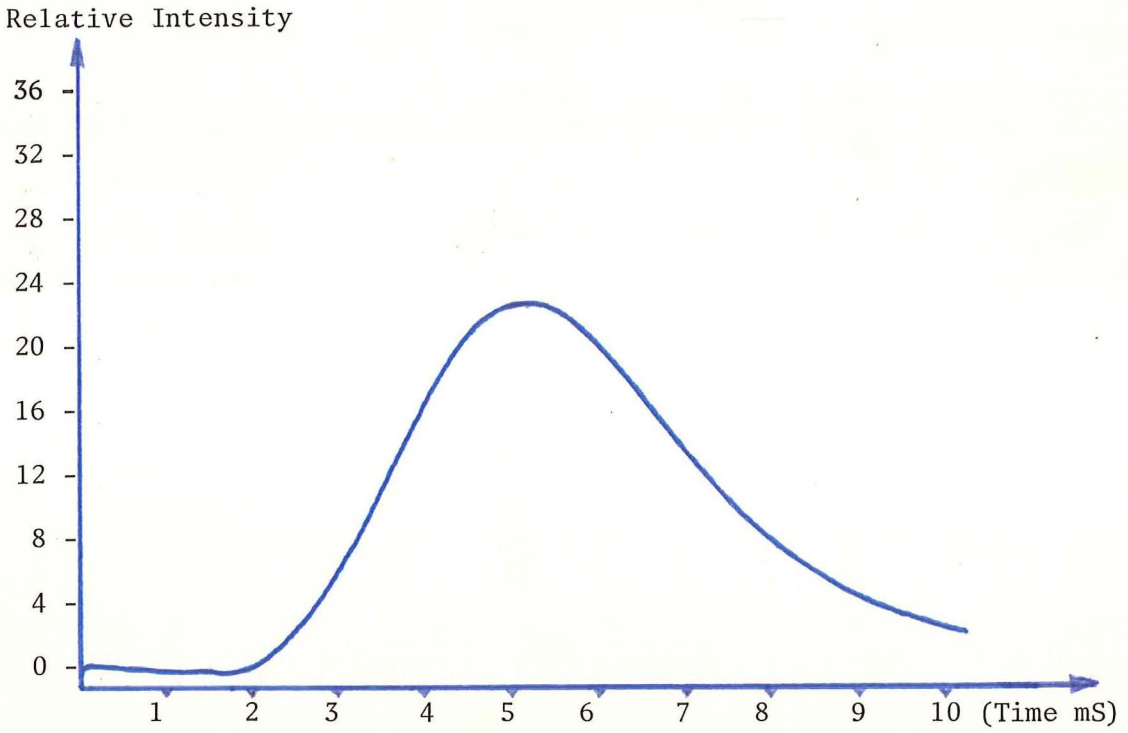

Figure 6.62 Combustion flame light intensity as a function of time from the Mitsubishi Lancer engine after 41 hours operating time (1500 r.p.m.)

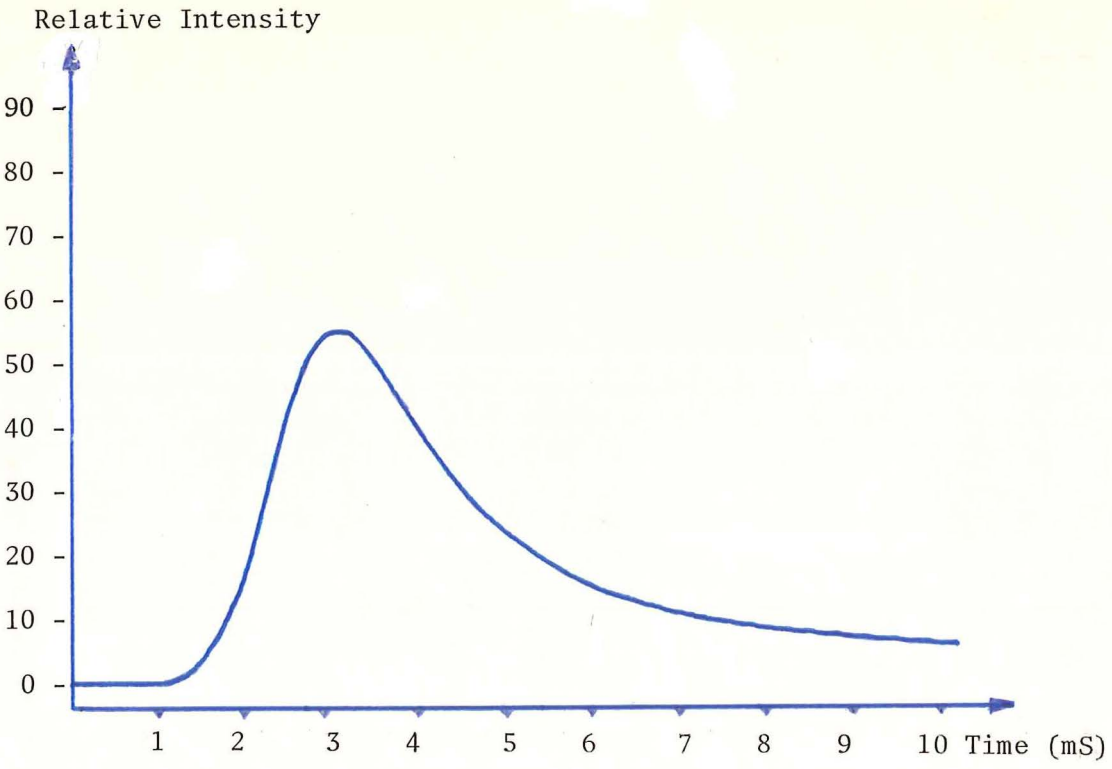

Figure 6.63 Combustion flame light intensity as a function of time from the Mitsubishi Lancer engine after 41 hours operating time (3000 r.p.m.)

Extended Operation Time:

The engine with optic plug installed, was operated for another 59 hours under the conditions cited in Section 5.3.3. The plug was then briefly tested at three different loads and the light intensity recorded in two cases.

Results

Engine Speed (r p.m.)	Engine Torque (Nm)	Figure
400	≈4.8	-
1500	13.4	6.64
3000	30.2	6.65

Other operating conditions: As described in the previous test.

Observations

No trace was taken at idle conditions since there was no recognisable signal to record. The low amplitude signal of Figure 6.64 was recorded at medium load and at the highest load (approximately 10 kW power output) the graph of Figure 6.65 reveals a good signal to noise ratio especially if the ignition system interference were to be removed as described previously.

The inner end of the optic plug is shown in Plate 6.5. This photograph was taken almost immediately after the above curves had been recorded. The combustion product build-up has completely obscured the inner end of the fibre optic cable situated in the middle of the centre electrode.

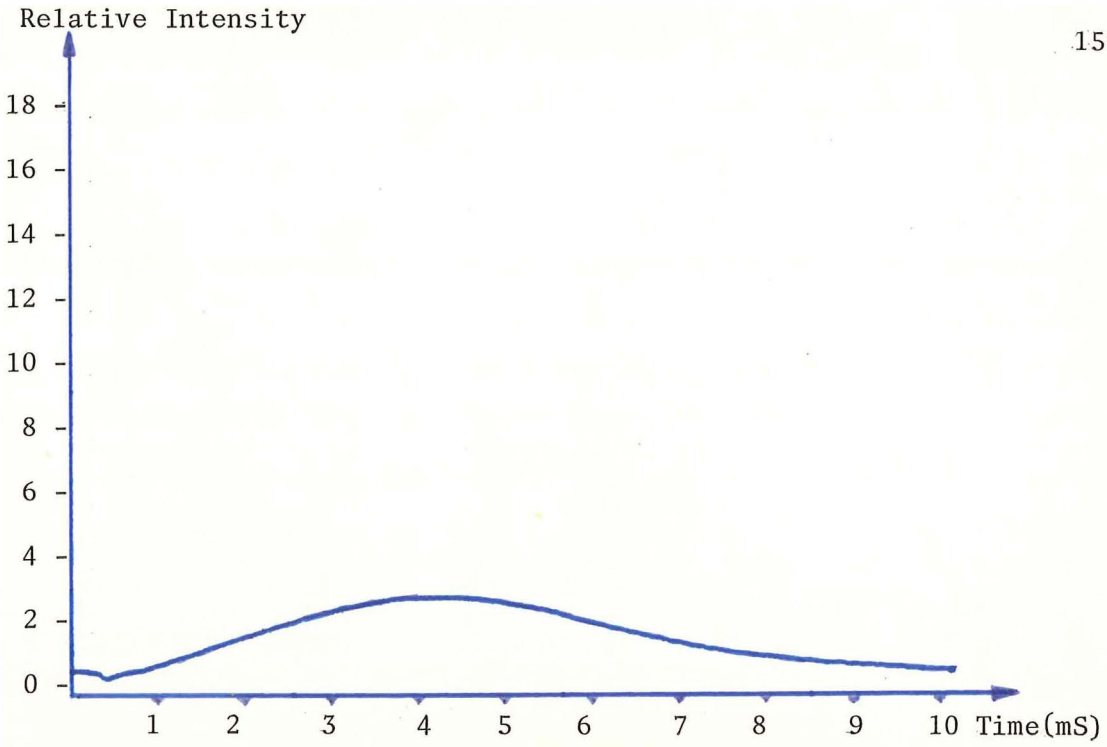

Figure 6.64 Combustion flame light intensity as a function of time from the Mitsubishi Lancer engine after 100 hours operating time (1500 r.p.m.)

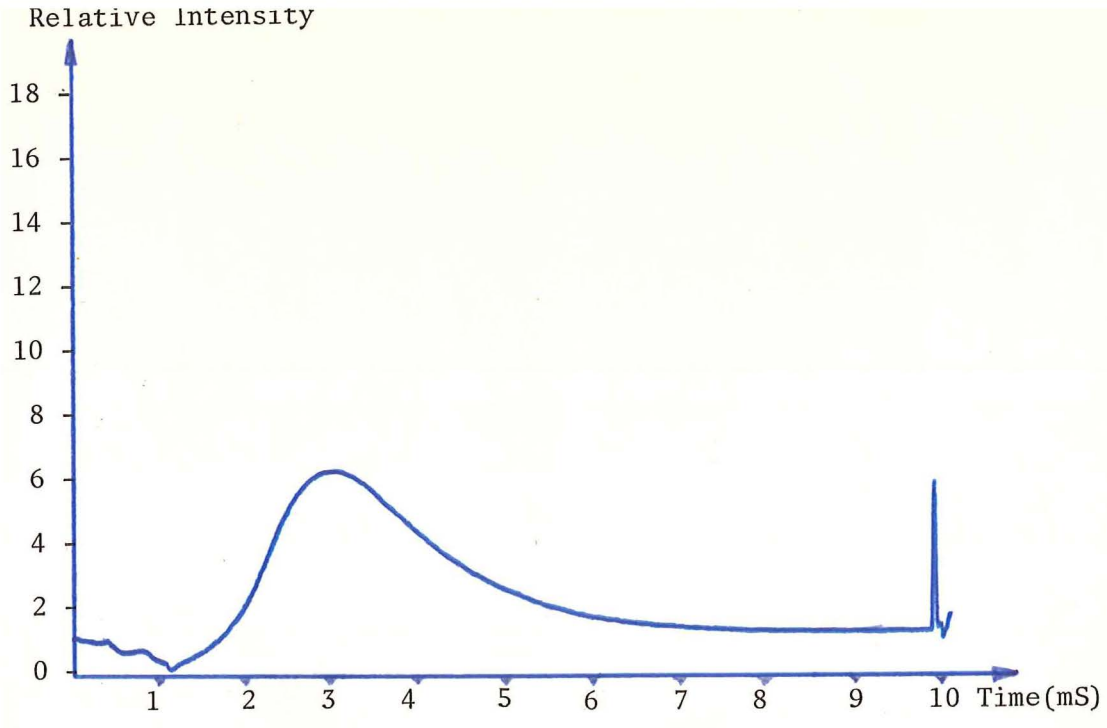

Figure 6.65 Combustion flame light intensity as a function of time from the Mitsubishi Lancer engine after 100 hours operating time (3000 r.p.m.)

Plate 6.5 Inner end of optic plug showing combustion product buildup (fibre optic strand is located in the middle of the centre electrode).

CHAPTER 7

DISCUSSION AND CONCLUSIONS

CONTENTS

CONTENTS (Continued)

INTRODUCTION

The object of the examination of the combustion flame light emissions in the Spark Ignition engine is to determine whether they provide suitable information on which to develop an adaptive transducer for an adaptive spark advance control system.

The results are discussed in this chapter with emphasis being given to any aspects of them which could be used to determine MBT, knocking combustion, and to a lesser extent, the stoichiometric air-fuel ratio. Some alternative adaptive control strategies are examined, which could be implemented on the basis of these results. Certain conclusions are presented at the end of the chapter, with recommendations for future research.

7.1 Discussion of Certain Aspects of the Combustion Flame Spectrum

7.1.1 Determination of Knocking Combustion from the Combustion Flame Spectrum

In this section the results and observations of the combustion flame spectra are discussed with regard to any characteristics suitable for knock detection and detection of the stoichiometric air-fuel mixture ratio.

From a comparison of the spectrum produced during knocking combustion (Fig. 6.4) with that of normal combustion (Fig. 6.3), the most easily discernible difference is in the relative intensities of the 580 nm band (refer to Section 6.1). During knocking combustion the light intensity at approximately 580 nm (yellow) increases relative to the background continuum as compared with its intensity during non-knocking combustion.

A suitable strategy for detecting knock could be to define it to be occurring whenever the light intensity in this 580 nm region exceeded that of the local minima either side of it by more than some pre-defined value. If it did exceed this value, then the ignition timing would be retarded until the relative intensity of the yellow spectral component decreased below the pre-defined limit.

The main disadvantage with this method of detecting knock is the lack of luminence or radiation power produced by such a narrow band of the electro-magnetic spectrum. For example, the separate spectral components of the combustion flame were recorded photographically with sufficient intensity only after approximately 67 combustion cycles were integrated onto one frame. If a photodetector was optically filtered to respond only to yellow wavelength radiation it would need to be extremely sensitive. It is not considered that a silicon photodiode detector would be sufficiently sensitive to monitor the yellow component of the spectrum, without integrating it over a number of combustion cycles, especially after the glass inner surface became contaminated due to solid combustion product buildup.

Further testing would also need to be undertaken to determine whether there was a significant increase in the yellow component of the hydrocarbon flame spectrum when the engine was lightly knocking since Fig. 6.4 depicts the spectrum resulting from heavy knock.

7.1.2 Determination of the Air-Fuel Ratio from the Combustion Flame Spectrum

The air-fuel mixture ratio is also an important engine operating variable which should be accurately controlled for effective engine performance and fuel economy. For this reason some testing was undertaken to determine whether the combustion flame light emissions could be used as an input to an air-fuel ratio controller.

The differences shown in the results of the flame spectrum at air-fuel ratios far from stoichiometric (11:1 and 17:1) could be detected by photodetectors with appropriate optical filters; however, for good overall performance the air-fuel ratio should be controlled close to stoichiometric. For example, the air-fuel ratio control systems currently used in automotive applications (Appendix 3.1) are able to detect differences in the air-fuel ratio of less than 1% (i.e., the difference between an air-fuel ratio of 14.7:1 and 14.8:1).

The flame spectra at these small deviations from stoichiometric were not recorded; however, the following conclusions are drawn from directly observing the flame. When the combustion flame is observed directly by looking through the glass window into the Ricardo engine combustion chamber, the effect in altering the air-fuel mixture ratio from 11:1 to 17:1 is immediately apparent as the flame colour changes from orange to blue. If the air-fuel ratio is increased from 14.7:1 to 14.8:1 no perceivable change in the flame colour takes place, and if the corresponding spectra were to be recorded, any changes in the spectrum would be considered to be too small to be detected without elaborate spectrum analysis equipment. Added to this, if changes in the spectrum were to be detected by optically

filtered photodetectors, the problem of detecting low light intensities would again become evident as small regions of the spectrum would be required to be separately monitored. The light from several combustion cycles could be integrated; however, this technique is undesirable since the engine may increase in speed by 25% in .05 seconds (≈1 combustion cycle; refer to Section 3.4.3) requiring a rapid increase in the fuel metering rate.

The combustion flame spectrum would also change whenever the fuel type is changed; for example, in changing from a hydrocarbon to an alcohol type fuel. The spark advance control system would be required to discern these changes in the fuel when it was installed in a dual fuel source vehicle so that it could continue to effectively control the air-fuel ratio close to stoichiometric.

For these reasons the visible flame spectrum was not analysed further as a means of providing for air-fuel ratio control.

7.2 The Photodetector Response to Changes in the Air-Fuel Ratio

The examinations of the effect of varying the air-fuel mixture ratio on the silicon photodetector output are given in Section 6.2.1.1. The changes in the curves recorded in this section do not follow any definite trends as the air-fuel ratio is altered, and are well within the bounds of the changes in the curves due to cyclic variation (refer to Section 6.2.1.3). From these results it is concluded that the silicon photodetector response to changes in the air-fuel ratio is of no value in maintaining it close to a stoichiometric value.

Tests were not performed to determine whether the lead-salt detector outputs varied significantly over small changes in the air-fuel ratio. From the results of the silicon photodetector tests it is to be expected that a 1%-2% change in the mixture strength from the stoichiometric setting would not change the response of the lead-salt detectors appreciably.

This lack of response from the photodetectors to small changes in the air-fuel ratio can, however, be used to advantage when the detectors are used as inputs to an ignition advance controller. The ignition advance control system would be unaffected by small fluctuations in the mixture strength since the photodetectors themselves would be unresponsive to these fluctuations.

7.3 Interpretation of the Photodetector Response Curves

The photodetector response curves are observed to be a strong function of the ignition advance angle (refer to Section 6.2.1.2) and the curves indicate that the photodetectors could provide the basis for a successful adaptive spark advance transducer. Therefore, the various characteristics of the photodetector response curves will be examined in detail in this section and several alternative methods of using these characteristics to define MBT and knocking combustion will be discussed in the succeeding sections.

7.3.1 Characteristics of the Silicon Photodetector Response Curves

7.3.1.1 The flame development period

The first general characteristic of the silicon photodetector response curves is that they do not begin to rise until a significant period of time after combustion is initiated by the spark. In terms of crankangle the photodetector response may be delayed by 30° after the spark has fired either at low or high engine torque outputs (Figs 6.26 and 6.32 respectively). This corresponds to approximately 25% of the total combustion crankangle period (from the spark firing crankangle to the return of the light intensity curves to zero light intensity approximately 100° ATDC), and this flame development period is similar to that reported by Agnew[16] (refer to Section 2.2.1).

7.3.1.2 The photodetector response curve initiation crankangle

The effect of advancing the ignition timing on the initiation points of the silicon photodetector response curves is to advance them correspondingly (refer to Section 6.2.1.3). The curves in Fig. 6.39 show that when the ignition was advanced by 25° then the curve initiation points advanced by approximately 23°. It is not expected that these advance angles should correspond exactly since the flame kernel will take more time to develop at more advanced ignition settings. This is because when the ignition timing is advanced the flame kernel is initiated in a less favourable environment composed of lower compression pressures, compression temperatures and differing turbulence levels. The growth of the flame kernel is inhibited, the light emissions are also inhibited and the initiation point on the photodetector curves is retarded slightly at the more advanced ignition setting.

7.3.1.3 The positive slope section

The increase in the positive slope of the light emissions curves at more advanced ignition settings is expected to be a result of two phenomena (refer to Section 4.3.5.3). Firstly, the faster combustion rate which

results from the higher compression pressures achieved at TDC means that the reactions including the light emitting chemiluminescent reactions are proceeding more rapidly. This would appear as an increased light intensity during the earlier stages of combustion. However, this increase in light intensity should not be regarded as being directly proportional to the increased combustion rate. The light transmitted through the window assembly represents the difference between the light emitted from the radicals participating in the chemiluminescent reactions and the light absorbed by these radicals through self-absorption[51]. When the combustion rate increases more radiation will be emitted, but self-absorption of the radiation will mean that it is not proportional to the increased combustion rate.

The second cause of the increased positive slope of the light emission curves when the ignition timing is advanced is by way of the hotter combustion temperatures created by the higher compression pressures at the more advanced setting. The higher temperatures would cause black body radiation of solid particles present to increase so that they would emit more visible and infra red radiation.

7.3.1.4 The peak amplitude

The increased peak amplitude of the light emissions as the ignition timing is advanced can be understood from the increased black body radiation at the elevated temperatures as described above. The greater intensity may also result from a greater overall number of chemiluminescent reactions occurring at the higher combustion temperatures. The higher combustion temperatures would cause a greater proportion of the intermediate reaction products to be formed in an excited chemiluminescent state.

7.3.1.5 The inflexions and double maxima

The inflexions and double maxima commented on in the results (Sections 6.2.1.2 and 6.2.1.3) are expected to be a consequence of the afterburning phenomena described in Section 4.3.3. The light emissions response curves (for example, Figs 6.39 to 6.42) show that as the ignition timing is advanced from a retarded position, a second maximum begins to form on the latter section of the curve (Fig.6.41) that is, towards the end of the combustion process. The development of this second maximum is expected to result from luminescence similar to that observed during normal combustion by Withrow and Rassweiler and depicted from the 19th combustion picture in Plate 4.6. They concluded that the glow was coming from excited carbon dioxide as it

participated in the reactions:

$$H_2 + CO_2 \rightleftharpoons CO + H_2O \qquad (a)$$

$$2CO_2 \rightleftharpoons 2CO + O_2 \qquad (b)$$

They suggested that these reactions were influenced by the temperature and pressure changes which occurred during the burning of the last section of the charge.

The burning carbon monoxide reaction is generally cited in literature as occurring during the later stages of combustion since it is a slow reaction and cannot proceed until the hydrocarbons have undergone high temperature oxidation[48, 51]. Therefore the chemiluminescent CO_2 formed from the second reaction above is most likely responsible for the light emissions in the second maximum. It is observed from the curves of Figs. 6.40 and 6.41 that as the ignition timing is advanced the second maximum increases in intensity and becomes more advanced along the crankangle axis. The increased intensity could be attributed to the higher combustion temperatures attained at more advanced ignition settings causing a greater proportion of chemiluminescent CO_2 to form from reaction (b) and possibly the reversal of reaction (a).

At still more advanced ignition settings the light intensity of the second maximum becomes dominant over the first and occurs relatively soon after the onset of combustion. The former effect can again be explained by the elevated combustion temperatures creating a greater proportion of excited CO_2. The latter effect could be a result of the increased rate of combustion at the higher compression pressures created by advancing the ignition timing. This would result in the flame propagating through the charge more rapidly and the burning carbon monoxide reactions beginning at a more advanced crankangle setting.

The re-illumination which causes the formation of the second local maximum on the light intensity curves could also be possibly explained from the increased thermal radiation of solid particles present in the gaseous combustion products. These particles (for example, carbon particles) would glow with greater intensity at higher temperatures such as those which are created around the spark plug region (refer to Section 2.1.3). An explanation similar to this has been suggested by Lewis[55]; "the re-illumination of the burned gas in normal combustion can be understood from the increase

in temperature on compression due to the burning of the rest of the charge without resorting to the afterburning explanation"(p.205). Solid particle black body radiation would be the cause of such illumination.

7.3.1.6 The light intensity oscillations

The light intensity oscillations (Fig. 6.42) which are shown on the negative sloped section of the curves during knocking combustion are the equivalent of those recorded by Withrow and Rossweiller in Plate 4.9. The frequency of the oscillations is approximately 6.6 kHz (refer to Section 6.2.1.3 - Knocking Combustion) and this is within the knock frequency range described by the Saab-Scania Company when using an accelerometer mounted to the engine block[11].

The light intensity oscillations are caused by the pressure curves which are induced during knocking combustion (refer to Section 2.1.2.3) and reflected from the combustion chamber surfaces. The light intensity oscillation peaks are caused from the corresponding pressure wave peaks as these cause a localised temperature increase. The light intensity oscillation minima are caused from the corresponding pressure wave minima from the reversal of the process just described.

The secondary light intensity disturbance observed on the curves taken at full engine load (Figs 6.37 and 6.38) are produced when the exhaust valve first opens towards the end of the combustion stroke. This second period of combustion is apparently being initiated by the opening of the exhaust valve under full load conditions when it is relatively hot. It is concluded that the hot exhaust valve is causing the combustion of unburned hydrocarbons as they travel past it and into the exhaust manifold. At lower engine loads when the exhaust valve is cooler, these intermediate combustion products from the flame quench zones of the combustion chamber (refer to Section 4.1.2.3) escape unburned and there is no evidence of this secondary combustion on the corresponding light intensity curves.

7.3.2 Characteristics of the Lead-Sulphide Photodetector Response Curves

The radiation intensity as detected by the lead-sulphide photodetector produces curves similar in shape to the silicon photodetector curves (Fig. 6.47). The curve initiation points in the figure are identical. Also, if the curves in this fugure had been amplified to the same height, then the positive slope sections at the beginning of each curve would have approximately the same slopes.

The lead-sulphide detector responds to infra-red radiation so that it is more sensitive to the rotation-vibration bands of H_2O and CO_2 and therefore to the reactions occurring during the later stages of combustion. It should also be more sensitive to the after-burning phenomenon if this is caused by the burning carbon monoxide reaction. A comparison of the curves in Fig. 6.47 reveals that the lead-sulphide detector does respond more to the emissions produced during the later stages of combustion than the silicon photodetector. However, this does not provide conclusive evidence that the second maximum is produced from CO luminescence alone since an increase in black body radiation from solid particle emissions would also cause an increase in the infra-red emissions (Fig. 4.4).

The lead-sulphide detector output curves do not decrease during the last stages of combustion, as rapidly as the silicon detector curves and this is due to the fact that the lead-sulphide detector responds to a greater extent to the thermal component of the gases. It is sensitive to the latent heat of the product gases even if they are not giving off radiation in the visible region.

The calculations in Section 6.2.2.1 show why the lead-sulphide detector does not respond significantly to the light intensity oscillations induced during knocking combustion. In effect, the detector is attenuating these oscillations by over 50% because of its slow response time (Fig.6.51).

7.3.3 Characteristics of the Lead-Selenide Photodetector Response Curves

The major difference between the lead-selenide detector response and the silicon detector response is in the increased sensitivity of the former to the emissions during the latter stages of combustion.

The most significant difference between the lead-selenide output to that of the lead-sulphide detector is the improved response time of the former device, which enables it to follow the light intensity oscillations produced during knock. Apart from this difference, the response curves of these two detectors are almost identical.

The secondary combustion at the opening of the exhaust valve does not cause any recognisable response from the lead-selenide detector (Fig. 6.56) so it appears that this combustion is not producing infra-red radiation in the combustion chamber. This is probably a result of the reactions only being initiated as the gases pass out of the exhaust port.

Then the visible light emitting reactions occurring at the beginning of this secondary combustion process would be detected by the silicon photo-detector but the infra-red emissions would not be detected because they would occur after the gas had passed into the exhaust manifold.

It should be noted that when a long length of fibre optic cable was used to conduct the light emissions to a location remote from the engine, it tended to attenuate the electromagnetic radiation of wavelengths greater than 2.5 μm (Fig. 5.1). As the lead-selenide detector was most sensitive to radiation from 2.5 μm to 4.5 μm, it could not be used in conjunction with the long length of fibre optic cable. (The lead-selenide detector response curves were recorded in the results section with the detector mounted over a 3 mm thick disc of glass.)

7.4 Interpretation of the Light Emissions Transmitted through the Optic Plug

7.4.1 The Optic Plug in the Ricardo Engine

The results and observations gained from the testing of the optic plug system in the Ricardo engine are given in Section 6.3.1. Two curves are shown, one from when the optic plug was used as the spark source located in the cylinder head auxiliary port (Fig. 6.58). The other curve was recorded with the optic plug installed in the same position but with the standard spark plug on the opposite side of the combustion chamber providing the source of ignition (Fig. 6.59). During this latter test the optic plug was used only as a window in the endgas region of the cylinder.

The fact that there are differences between these two curves suggests that the light emissions transmitted through the window were the emissions occurring in the localised region of the combustion chamber close to it. The observations given with the results note that the light intensity oscillations shown at the peak of Fig. 6.58 were uncommon and usually an order of amplitude smaller, whereas the oscillations shown in Fig. 6.59 were commonly observed on the oscilloscope during these engine operating conditions.

The reduced level of light intensity oscillations when the optic plug was used as a spark plug appears to be caused by the increased background illumination which occurs for sustained periods of time in the spark plug region of the chamber. The peak light intensity in Fig. 6.59 is approximately 15% of the peak in Fig. 6.58. This brighter and more sustained light intensity in the region of the spark plug is also observed from the

series of pictures of knocking combustion recorded by Withrow and Rassweiler (Plate 4.8). The pictures of interest in Plate 4.8 are Nos 14 to 21, since these cover the period of time when the light intensity is expected to be fluctuating. Picture 16 is observed to have the highest light intensity and would correspond to the light intensity peaks in Figs 6.58 and 6.59.

The sustained high intensity illumination shown in the left-hand half of the combustion chamber of pictures 14 to 21 would reduce the observed intensity of the low amplitude light intensity oscillations in this region of the chamber. However, the light intensity in the endgas region of the combustion chamber in pictures 14 to 21 is generally comparatively low so that in this region of the chamber the low amplitude light intensity oscillations due to knocking combustion, would contrast more clearly with the reduced background illumination. This explains why the comparatively strong light intensity oscillations shown in Figure 6.59 were commonly observed during knocking combustion.

It is concluded that if the light intensity oscillations are to be monitored with the minimum of background illumination interference, then the window system should be installed in the endgas region of the combustion chamber.

7.4.2 The Optic Plug in Automotive Engines

The response of the silicon photodetector to the combustion flame light emissions transmitted by the optic plug system is given in Section 6.3.3. The shape of the response curves did not alter at ignition advances close to the knock limit; however, it was observed that the light intensity peak steadily increased in amplitude as the ignition timing was advanced.

The double maxima in one of the curves in this figure is expected to be caused by the afterburning phenomenon described in Section 7.3.1.5.

There was no evidence of any light intensity oscillations on the curves during periods of heavy audible knocking combustion and the reasons for this are considered to be twofold. Firstly, the positioning of the fibre optic cable at the source of ignition of the mixture reduces the light intensity oscillations from knock for the reasons given in Section 7.4.1. Secondly, it is considered that the level of knocking combustion in the production engine was comparatively low compared to that induced in the Ricardo engine, even though the knocking combustion produced approximately

equivalent audible intensities in both cases. This would result from the less rigid construction of the automotive engine, making it more effective in propagating sound waves characteristic of knocking combustion into the environment surrounding the engine. Therefore, in order to detect the combustion flame light intensity fluctuations during knocking combination in an automotive engine, the window assembly should be located in the endgas region of the cylinder to maximise sensitivity to such fluctuations. Some methods of achieving this increased sensitivity are described in Section 7.6.4.

Certain characteristics of the photodetector response curves can be used to determine whether an engine is running at MBT or whether it is running at the knock limit. These characteristics will now be discussed along with appropriate methods through which they may be incorporated into a spark advance control system.

7.5 Determination of the Minimum Spark Advance for Best Torque and Knocking Combustion from the Light Emissions Curves

7.5.1 Determination of the Minimum Spark Advance for Best Torque

As the ignition timing is advanced the overall light emissions curves are advanced with respect to crankangle (refer to Section 6.2.1.3). This result indicates that it would be possible to establish MBT by locating the light emissions curve at some predetermined crankangle in a similar manner to the method of establishing MBT using combustion pressure. In the case of the latter method, MBT is achieved through advancing (or retarding) the ignition timing until the peak cylinder pressure occurs somewhere between 5° and 20° after TDC, dependent upon the particular engine and operating conditions.

In order to locate MBT from the light emissions curve some particular point on the curve must be selected on which to reference a crankangle position for best torque. The reference point should be relatively free from jitter due to cyclic variation and from an evaluation of the curves in Figures 6.43 to 6.45, the curve initiation point would appear to be least affected by cyclic variation. The initiation point jitter due to cycle variation ranges from 2 crankangle degrees at low load (Fig. 6.43) to 10 crankangle degrees at medium and high loads (Figs 6.44 and 6.45). On the basis of these results the light emissions initiation point jitters no more due to cyclic variations than to the pressure peaks observed by Boht and Quayle which varied by up to ±5 crankangle degrees (refer to

Section 3.4.3).

The light emissions curve initiation point must then be referenced to a crankangle setting which will ensure maximum torque is developed by the engine. Table 7.1 summarises the light emissions initiation crankangle (henceforth referred to as the initiation crankangle) which yields highest engine torque for various engine speeds and loads. The initiation crankangle for best torque ranges from 4° to 1° before TDC except at high engine loads when the knock limit causes it to be retarded to values somewhat after top dead centre.

A suitable strategy for obtaining best engine torque would therefore be to advance (or retard) the ignition timing until the light emissions initiation crankangle falls within the region of 4° to 1° before TDC whenever this did not produce knocking combustion.

The success of this strategy would depend upon the development of some form of cycle to cycle averaging algorithm which ensures that the spark timing is sufficiently buffered from the cyclic variation of the light emission curve initiation points so that it remains stable during steady state engine operation. The type of algorithm proposed by Boht and Quayle in order to overcome the equivalent cyclic variation of the peak pressure crankangle when this is used to determine MBT, could be adapted for use with the light emissions control system.

Figure	Engine Speed (rps)	Engine Torque	Initiation Angle	Initiation Angle Variations (Crankangle Degrees)
6.17	15	Low	3° BTDC	Low engine torque
6.20	15	Medium	1° BTDC	±1° (Figure 6.43)
6.23	15	High	8° ATDC*	
6.26	30	Low	3° BTDC	Medium engine torque
6.29	30	Medium	2° BTDC	±5° (Figure 6.45)
6.32	30	High	9° ATDC*	
6.35	45	Medium	4° BTDC	High engine torque
6.37	45	High	5° ATDC*	±5° (Figure 6.46)

*Initiation angles at the knock limit rather than for best torque.

Table 7.1 Light emissions initiation crankangle and initiation crankangle variation at various engine speeds and loads.

In addition, a method for detecting knocking combustion using suitable information from the light emissions curves must be developed. This would complement the previously described MBT determining strategy by adding an ignition retard sequence whenever a high incidence of knock was detected until the level of knocking combustion was reduced to an acceptable level (refer to Section 2.2.1). Two methods for using the light emissions curves to determine whether the engine combustion process is undergoing knock will be described in the next section, one of which was developed and tested under restricted engine operating conditions. Another possible method for detecting knock by using the 580 nm spectral band intensity has previously been described in Section 7.1.1.

7.5.2 Determination of Knock

The most direct method for distinguishing when knocking combustion is occurring is to analyse the light intensity curves for the light intensity oscillations superimposed on the latter section of the curve during knocking combustion (refer to Section 6.2.1.3; Knocking Combustion). These oscillations could be pre-amplified by differentiating the photodetector output (refer to Section 2.1.2.3) and monitored by electronic means (most likely through the use of microprocessor software). Then whenever knocking combustion occurred the corresponding light intensity fluctuations detected by the adaptive controller would result in it retarding the ignition timing until the knock intensity was reduced to an acceptable level.

This method of knock detection would be effective in situations where the window assembly is situated in the endgas region of the combustion chamber so that the light intensity oscillations are easily discernible. The method would be suitable for use with the window assembly installed in the auxiliary port of the Ricardo engine and it is expected that it could similarly be utilised when a window assembly is installed in the endgas region of one of the cylinders of a standard automotive engine. Knock detection by this method could not be used with the optic plug installed in an automotive engine since no light intensity oscillations are evident during knocking combustion (refer to Section 6.3.3).

An alternative method of deriving the knock limit is to monitor the peak light intensity amplitude since this increases as the ignition timing is advanced and knocking combustion is induced, Table 7.2 . The peak light intensity values in the table increase across a row as the ignition timing is advanced. The intensities of different sets of results in different

rows cannot be compared for the reasons given at the beginning of Section 6.2; however, it was observed during testing that the light intensity peak amplitude at the knock limit was relatively independent of engine speed. Therefore a method for eliminating knocking combustion is to ensure that the light intensity peak is limited to a pre-defined value through appropriate control of the ignition timing

Figure	Engine Speed (rps)	Engine Torque	Peak Light Intensity (Relative Units) with Ignition Timing Set:		
			Retarded	Best Torque	Advanced
6.16-6.18	15	Low	15	35	50
6.19-6.21	15	Medium	28	77	$\approx$100
6.22-6.24	15	High	15	57*	87(Knocking)
6.25-6.27	30	Low	22	57	57
6.31-6.33	30	High	32	35*	67(Knocking)
6.34-6.36	45	Medium	17	78	88
6.37-6.38	45	High	-	28*	52(Knocking)

*Peak light intensity at the knock limit rather than at best torque.

Table 7.2 The increase in peak light intensity as the ignition timing is advanced.

A knock detection system such as this was developed and tested at various engine speeds and loads (refer to Appendix 7.1). The system output consisted of 3 light emitting diodes (LED's); one to define retarded ignition timing, one to advise that the spark advance was set to the knock limit, and one to warn that knocking combustion was taking place through over-advance of the ignition timing. In this prototype system a human operator closed the control loop by observing the LED display and manually advancing or retarding the ignition timing until the LED designating that the spark advance was set to the knock limit was activated . An error in the ignition timing of 2 or 3 degrees advance would cause the LED display to change state and inform the operator of the maladjustment.

Although this method of knock detection is satisfactory during short term engine operation, a problem is encountered if the system is to be used for extended periods of time without being re-adjusted. The combustion product buildup on the inner surface of the window causes the peak light

intensity to decrease with continued engine operation and so the preset value to which the peak light intensity is compared must also be reduced. The reduction in the preset value should be directly linked to the degree of combustion product buildup on the window inner surface.

One method for automatic compensation of the preset value as a function of the combustion product buildup could be to utilise the characteristics of the lead-sulphide detector. An examination of the curves produced from the silicon and lead-sulphide two colour detector (Figs 6.46 to 6.51) reveals that the peak amplitudes of the lead-sulphide curves are not related so directly to the ignition advance as the silicon detector curves (Table 7.3). In the table the peak light intensities for both detectors are given as a function of ignition advance. At the low engine load the lead-sulphide detector output peak increases by 58% as the ignition timing is advanced from the retarded setting to the advanced setting. In comparison the silicon detector output increases by 172% over the same advance. At the high torque setting the lead-sulphide output peak increases by 15% whereas the silicon detector output increases by 48% as the ignition timing is advanced.

Figure	Engine Torque	Ignition Advance Setting	Peak Light Intensity (Relative Units)	
			Lead Sulphide Detector Output	Silicon Detector Output
6.46	Low	Retarded	24	25
6.47		Best Torque	30 ↓ 58% Increase	37 ↓ 172% Increase
6.48		Advanced	38	68
6.49	High	Retarded	64	25
6.50		Best Torque	72 ↓ 13% Increase	23 ↓ 48% Increase
6.51		Advanced	66	37

Table 7.3 Peak light intensities for the silicon and lead-sulphide detectors as a function of ignition advance (engine speed 30 rps)

It is expected that the peak amplitude of the lead-sulphide detector is strongly related to the combustion product fouling on the glass inner surface. This would need to be verified through long term testing but if it were found to be the case then the originally described preset reference value could possibly be replaced with a reference value determined from the lead-sulphide detector output.

7.6 Methods of Incorporating Light Intensity Detection Systems into Automotive Engines

7.6.1 The standard automotive engine

The combustion flame light intensity can be monitored in an unmodified automotive engine either by using an optic plug or by incorporating fibre optic cable into the cylinder head gasket (Fig. 7.1).

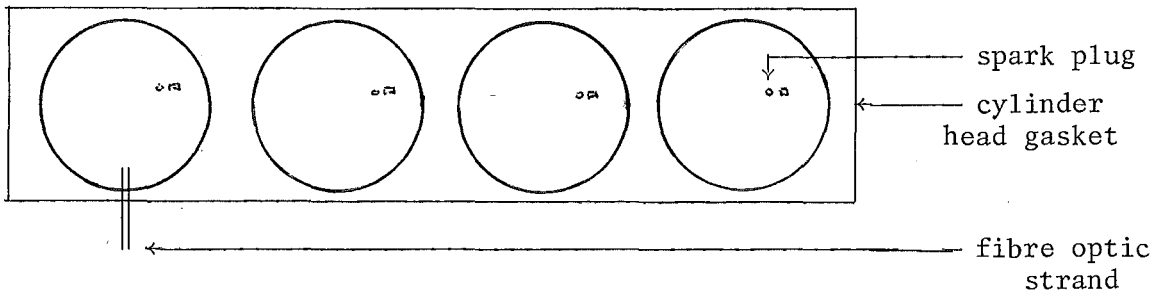

Figure 7.1 Cylinder head gasket modified to include a fibre optic strand into one cylinder.

Tests using the optic plug arrangement (Section 6.3.3) indicate that it does not respond to knocking combustion with light intensity oscillations on the waveform trailing edge (Fig. 6.60). The peak amplitude of the light intensity curve does, however, respond to an advance in the ignition timing by increasing in amplitude and it continues to increase as further advancement of the ignition timing induces knocking combustion. Therefore, the peak amplitude method of knock detection described in Section 7.5.2 would need to be implemented if the optic plug was to be used as the input to an adaptive spark advance control system in the automotive engine.

Incorporating a fibre optic strand into the cylinder head gasket could also be used to detect the light emissions produced by the combustion flame and the advantage of this method is that the fibre could be inserted into the endgas region of the cylinder where it is more likely to transmit the fluctuating light intensities associated with knocking combustion. This would enable the adaptive control strategy based on the light intensity oscillations (described in Section 7.5.2) to be implemented to ensure knocking combustion is very clearly distinguished from normal combustion.

The main difficulty anticipated with this method of flame light detection is in the way the fibre optic cable would be incorporated into the head gasket so that it continued to seal reliably and so it was no thicker than the original head gasket. Periodic replacement of the head gasket would also need to be considered as the combustion products would continue to contaminate the inner end of the fibre. Such replacement would be

expensive both in the cost of the head gasket and the labour involved in replacing it.

7.6.2 The Modified Automotive Engine

Modification of the engine cylinder head to enable the installation of a small window assembly in the endgas region of the chamber would have certain advantages. The light intensity oscillations, due to knocking combustion, could be directly monitored for precise ignition advance control at the knock limit and the window could also easily be replaced when necessary.

The window assembly could be a smaller version of the one installed in the Ricardo engine (Plate 5.4) with an 8 mm diameter external threaded section. The corresponding 8 mm diameter port could be cast into new automotive engine cylinder heads or in retro-fit applications the cylinder head would be drilled oversize, sleeved in order to seal the water jacket, and tapped with an 8 mm diameter threaded section.

By detecting knocking combustion from the light intensity oscillations rather than the peak light intensity, the problems associated with the combustion product contamination of the inner glass surface would be significantly reduced. The amplitude of the light transmitted through the glass would not affect the criteria by which the system identifies knocking combustion so that the only limiting factor to satisfactory system performances that the light intensity is strong enough to be detectable by the photodetectors.

7.6.3 Considerations for Use with Alternative Fuels

The use of alternative fuels in automobiles used in New Zealand is becoming more widespread. In this country the fuel most commonly used in the passenger vehicle has traditionally been petrol; however, the discovery and development of indigenous gas fields has led to the introduction of CNG and LPG as alternative fuel systems and in the future, Methanol-Petrol fuel blends may be introduced.

Each type of fuel requires a different ignition advance surface over the engine operation range in order to maintain efficient combustion. When a vehicle is equipped to use more than one type of fuel, the ignition system should therefore automatically adjust the ignition advance settings to suit the type of fuel used. This compensation could be achieved through the development of an ignition advance controller with two programmed sets of ignition advance surfaces, one for each type of fuel, or through

the use of a fully adaptive spark advance system which was not affected by the type of fuel used. Some of the response characteristics of the photodetectors will now be examined to determine whether they could provide the necessary information to an adaptive spark advance controller while remaining uninfluenced by the type of fuel used for combustion.

The combustion flame light emissions peak intensity is expected to vary depending upon the combustion fuel (for example, LPG is known to burn with low intensity light emissions in the visible region of the spectrum which would cause a corresponding decrease in the response of the silicon photodetector). The emissions in the infra-red region of the spectrum are also expected to alter in intensity through the use of different fuels since the flame temperature, which can be sustained prior to knocking combustion being induced, will depend on the fuel used. Such a change in flame temperature will also bring about a change in the infra-red emissions (Fig. 4.4). This suggests that the peak intensity response from the lead-salt detectors would be influenced by the type of fuel used for combustion.

The method described in Section 7.5.1 for determining MBT from the light emissions curves should be satisfactory for use with any type of fuel; however, the light intensity initiation crankangle setting for best torque may vary depending on the fuel used. In this case the spark advance controller would have to reset the initiation crankangle value for best torque whenever the fuel was changed.

If the spark advance controller used the peak amplitude light intensity method described in Section 7.5.2 in order to determine whether the engine was knocking, it would need to alter the preset value to which the light intensity peak was compared whenever the fuel was changed. However, if the light intensity fluctuations were monitored in order to detect knocking combustion, then no controller parameters would need to be altered when the fuel was changed since these fluctuations are expected to occur during knocking combustion independent of the fuel used in the engine.

It is therefore expected that an adaptive spark advance controller based on appropriate information from the light emissions could be successfully developed for use on multi-fuel vehicles. Further research is required in this area.

7.6.4 Long Term Operation

The results of the long term testing of one of the optic plugs (refer

to Section 6.3.5) revealed that combustion product fouling of the glass does not become a problem until at least 40 hours of engine operation. At an average vehicle speed of 50 km/hr, this would correspond to a distance travelled of 2000 km. However, when the operation time of the optic plug was extended to 100 hours, the glass became sufficiently contaminated to yield unsatisfactory light transmittance to the photodetector especially at idle. The combustion product buildup on the inner end of the optic plug after this latter operation period is shown in Plate 6.5. It is not expected that the combustion product contamination would be any more severe than this if the plug had been used for at least 10,000 km in a road vehicle. If this does represent the level of combustion fouling after 10,000 km, then the optic system could be expected to provide a sufficiently strong signal to the adaptive controller input for medium term engine operation.

The expected life of an automotive spark plug is approximately 16,000 km[13]. Thus in order for an optic plug to operate satisfactorily over the entire life of the spark plug, the photodetector amplifier output should be improved especially at idling and low load operating conditions. The amplifier output could be multiplied by a factor of 10 through the use of a 100 MΩ feedback resistor (R_f) instead of the 10 MΩ resistor which was used during the long term testing.

The photodetector output could also be increased by improving the fibre optic cable to photodetector interface. The interface configuration used duing the experimental testing is shown in Fig. 7.2(a).

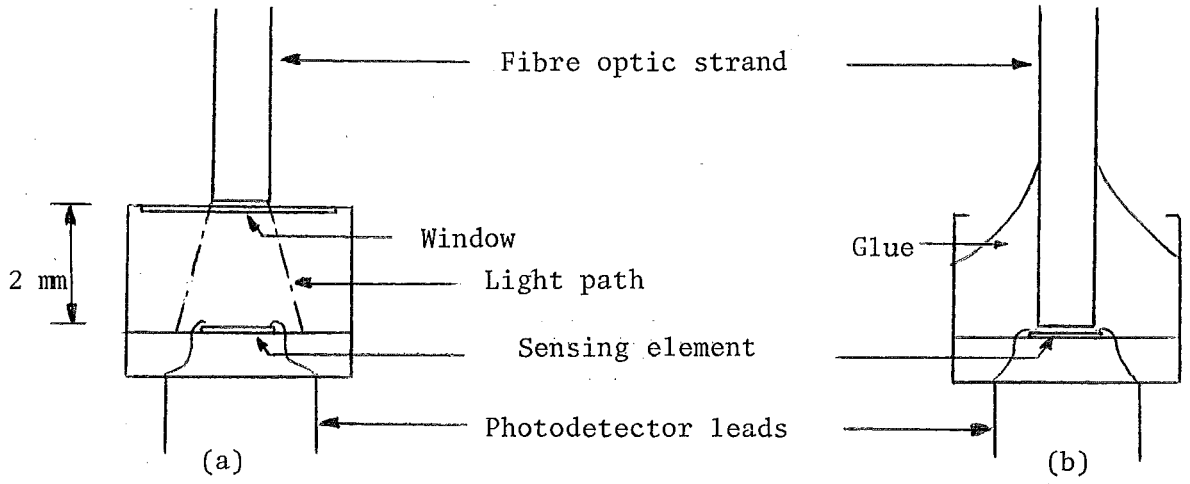

Figure 7.2 (a) The relationship of the outer end of the fibre optic cable to the photodetector sensing element, as used in the experimental tests.

(b) An improved interface between the fibre optic cable and the sensing element.

The end of the fibre optic cable was approximately 2 mm away from the sensing element so that some of the light radiated out from the optic strand was not incident upon the sensing element. The optic strand could be brought into closer proximity to the sensing element by altering the interface configuration as detailed in Fig. 7.2(b). By ensuring that all the radiation emitted from the end of the fibre optic cable is received by the photodetector sensing element, the photodetector output would be expected to increase by 50% to 100%.

7.7 Conclusions and Recommendations for Future Work

An examination of some of the properties of the Spark Ignition engine combustion flame light emissions has been undertaken in this report. The principal object of the examination was to determine whether the light emissions could provide suitable input information to an adaptive spark advance controller to enable it to control the ignition timing for effective combustion; that is, to produce best engine torque, or if this would induce knocking combustion, to operate the engine at the knock limit.

A method of determining the minimum ignition advance for best torque (MBT) using the light emissions versus crankangle curves has been proposed. The method is based on the premise that at MBT the point of initiation of the light emissions curves will correspond to a fixed crankangle setting and the ignition advance can be adjusted to obtain the correct correspondence. A similar method has been proposed for defining MBT based on properties of the combustion pressure versus crankangle curves, and this would tend to verify the validity of the suggested method of using the light intensity curves for determining MBT.

Several methods for defining knocking combustion have been described based on either the peak amplitude of the light intensity curves or on the light intensity fluctuations which occur on the decreasing section of the curves when the engine is knocking. Both methods were examined and the latter method cannot be used in combination with the optic plug assembly installed in an automotive engine. The former method of defining knocking combustion was developed and tested under limited engine operating conditions for a relatively short period of time and was found to work successfully. However, over long periods of engine operation, this system would have to be refined by introducing compensation for the combustion product contamination of the the glass surface in the combustion chamber.

A compensation technique using the response curves from the lead-sulphide detector was discussed in connection with this problem and it requires further analysis and testing.

The long term reliability of the light emissions based adaptive spark advance controller has been considered from the perspective of the limiting factor, the combustion product buildup on the glass surface. This would eventually render all of the above modes of operation ineffective if the contamination completely blocked the flame light emissions from being transmitted through the glass and to the detector. The effect of relatively long term engine operation on the light transmitted through the optic plug has shown that the system could be expected to operate satisfactorily for at least 2000 kilometres in an automotive application and the suggested modifications could enable the system to be used for up to 20,000 kilimetres before the glass was cleaned or replaced.

The possible effects of using alternative fuels on the flame light emissions have been discussed as these considerations are of particular importance in vehicles destined for the New Zealand market. Tests should be carried out in order to thoroughly examine the similarities and differences in the light emissions from different fuels as detected by the photodetectors so that provisions could be made for the adaptive controller to make appropriate adjustments to the control algorithms as necessary.

The benefits of installing a glass window assembly in the cylinder endgas region of an automotive engine in order to provide the most accurate knock detection system have already been described. The window assembly should be fitted to an appropriately modified automotive engine cylinder head so that further investigations can be made on the light intensity fluctuations during knocking combustion in an automotive engine.

Finally, a better understanding of the feasibility of such a light emissions based adaptive spark advance controller could be gained through development and testing of a complete prototype system initially on the Ricardo engine and then on automotive engines.

APPENDIX 3.1

MICROPROCESSOR CONTROL OF AIR-FUEL RATIO, EGR AND THERMOACTOR AIR

The general functions of an automative microprocessor control system are to regulate the air-fuel mixture ratio, the ignition advance, the exhaust gas recirculation (EGR) rate, and the thermactor air supply.

The air-fuel mixture ratio is normally monitored by an oxygen sensor mounted in the exhaust manifold. A low concentration of exhaust oxygen indicates a rich intake air-fuel mixture, and a high exhaust oxygen concentration implies that the intake mixture is lean (Fig. 3.8). The exhaust manifold oxygen sensor is made from zirconium oxide based ceramic which is extremely sensitive to oxygen concentration, and in combination with an appropriate controller, can control the air-fuel ratio within the range of 14.7:1 to 14.9:1 under steady state operating conditions (Fig. 3.9)[43,44].

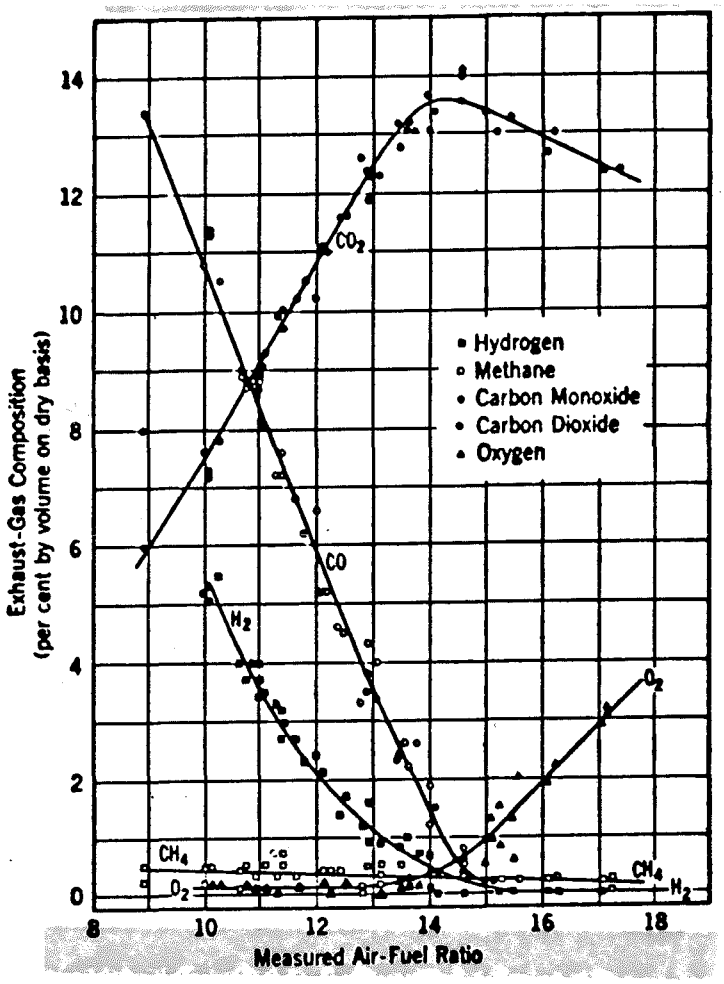

Figure 3.8 Exhaust gas composition versus air-fuel mixture ratio[45].

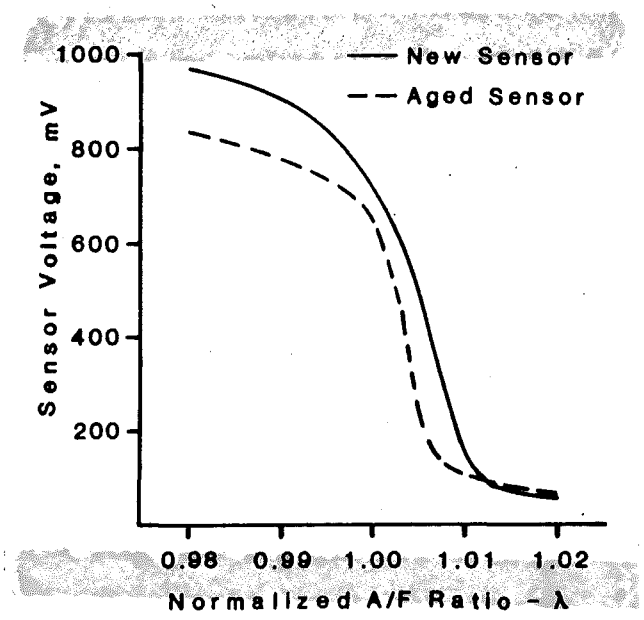

Figure 3.9 Voltage characteristics of exhaust gas oxygen sensor as a function of the air-fuel equivalence ratio λ[43].

The microprocessor based controller controls either fuel injectors or a carburettor to vary the air-fuel mixture ratio. When fuel injectors are used the length of the injector pulse is controlled, and when a carburettor is used, it is calibrated lean and is fitted with one supplementary fuel enrichment solenoid. This solenoid is controlled by a square wave power supply from the microprocessor, the duty-cycle of which determines the amount of extra enrichment the carburettor receives via the supplementary solenoid injector.

Exhaust gas recirculation is used to control NO exhaust emissions. These emissions are reduced when combustion chamber temperatures are reduced because then the nitrogen present in the intake mixture is less likely to oxidise to NO. Recirculating exhaust gases into the intake mixture helps to reduce the cylinder gas temperatures and pressures and therefore this control technique lowers the NO emissions level.

The EGR rate can be governed by passing the recirculating exhaust gases through a vacuum controlled valve. The vacuum control is from the intake manifold vacuum, so that heavy EGR flow occurs during open throttle conditions and EGR is restricted as the throttle is closed. The microprocessor adds further sophistication to this control system through the addition of a solenoid over-ride on the vacuum control line[30,42].

Thermactor air is supplied to the exhaust manifold and catalytic

converters in order to allow them to more effectively control the NOx and CO emissions. A high level of oxygen in the exhaust will help oxidise CO to CO_2 but will also increase the concentration of NO_2 from the reaction

$$NO + \tfrac{1}{2}O_2 \rightarrow NO_2.$$

Alternatively, a lower concentration in the exhaust gases is less likely to oxidise CO and NO[45]. Therefore by controlling an air supply to various regions of the 3-way catalytic converters they are able to balance the emitted levels of NOx and CO in order to meet the emissions regulations[32]. The microprocessor determines when and where the air is directed to within the exhaust system depending upon the engine operating conditions.

APPENDIX 4.1

HYDROCARBON BOND ENERGIES AND

THEIR RELATIONSHIP TO

1. CRACKING ENERGIES
2. KNOCK RATINGS

CRACKING ENERGIES

When considering the initial breakdown of a hydrocarbon molecule, the C-C bond energy is observed to be less than the C-H bond energy; however at low temperatures the H atom is most susceptible to oxidation by O_2:

$$RH + O_2 \rightarrow R + HO_2.$$

At high temperatures the initiation reverts to the fragmentation of the C-C bond. In contrast, the C=C bond is exceptionally strong but it is susceptible to attack from electron seeking radicals

$$CH_2 = CHCH_3 + OH \rightarrow \underset{\underset{OH}{|}}{CH_2} - CHCH_3 \xrightarrow[\text{decompose}]{\text{rearrange}} CH_2O + C_2H_5$$

The H bond in the following unsaturated hydrocarbon is weakened due to the C=C bond so that an alkyl radical is readily formed:

$$CH_2 = CH\text{-}\overset{\circ}{C}H_2 \rightarrow \bar{C}H_2\text{-}\bar{C}H\text{-}\bar{C}H_2$$

with the radical stabilised by the electron distributing itself across the whole molecule.

HYDROCARBON KNOCK RATINGS

The chemical structure of hydrocarbons also determines to some degree their knock resistance allowing the following broad classifications to be made:

[aromatics, alkenes highly branched alkanes] > [low branched alkanes cyclic alkanes] > [straight chain alkanes]

(a) Highly branched alkanes have much better knock resistance than straight chain alkanes.

(b) Alkenes have a higher knock resistance than alkanes of the same chain length[49].

APPENDIX 4.2

THE FORMATION OF CARBON PARTICLES

Solid carbon may be formed during the combustion process whether the mixture is fuel lean or fuel rich. In fuel rich systems it can be observed usually as black sooty smoke or as a deposit on the combustion vessel surfaces. Soot is a chemical combination of hydrogen and carbon atoms, the ratio of which depends on when in the reaction process it is being detected. The hydrogen-carbon ratio appears to be relatively independent of the type of fuel burned and there is normally at least 10% hydrogen present corresponding to the empirical formula C_8H. The total soot particle size will vary from 40-2000Å.

The particles will be formed from the process termed nucleation whereby a 'sticky' nucleus will cause colliding atoms to adhere to it. The exact nature of this process is uncertain but it could be initiated by positive ions forming the centre of the nucleus.

APPENDIX 4.3

PRE-IGNITION GLOWS AND COOL FLAME LIGHT EMISSIONS

Cool flames emit a faint blue colour characteristic of excited formaldehyde and yield Emeléus's formaldehyde (CH_2O) bands between 370 and 480 nm. A similar system appears as a pre-ignition glow just prior to ignition in engines and in the unburnt mixture ahead of the flame front during auto-ignition. Gaydon & Moore[51] have examined these glows just prior to ignition of propane/air mixtures, considered also to be typical of higher hydrocarbons, and conclude they differ somewhat from that of the cool flame. In weak mixtures the glow is similar to that of the hot flame showing CH, HCO, OH bands and a continuum most likely from CO. For rich mixtures the spectrum is between that of the cool flame and hot flame (Plate 4.3) with strong HCO emission, some CH and formaldehyde observable, but weak OH and no C_2. The normal hot flame shows the C_2, CH, HOC and OH bands as it burns through the mixture.

The majority of the electromagnetic radiation from cool flames is emitted in the infra-red region with prominent bands at 2.8 and 4.4 μm. This radiation is, however, less intense than that emitted by the hot flame.

APPENDIX 5.1

GENERAL SPECIFICATIONS OF THE RICARDO E6

NO. 27/49 AND No. 138/82

The general specifications of the Ricardo 138/82 engine[64] follow and when the specifications of the Ricardo 27/49 engine differ they are included in brackets.

THE RICARDO E6 VARIABLE COMPRESSION ENGINE

General Specification

Serial Number	:	138/82 (27/49)
Number of Cylinders	:	1
Bore	:	76.2 mm
Stroke	:	110 mm
Capacity	:	507 cc
Compression Ratio	:	4.5-20 (5-20)
Valves	:	Overhead; operated by overhead cams and finger followers.
Valve Timing	:	Inlet opens : 8° BTDC (9° BTDC) Inlet closes : 36° ABDC Exhaust opens : 42° BBDC (43° BBDC) Exhaust closes: 8° ATDC
Tappet Clearances (cold):		Inlet : 0.15 mm Exhaust : 0.25 mm (0.20 mm)

The 138/82 Ricardo was fitted with electronic ignition and petrol injection whereas the 27/49 Ricardo was fitted with a magneto ignition system and a carburetted fuel system.

Manufactured by Ricardo Consulting Engineers Ltd, Sussex, England.

FIG No: 1.

Drg No: L.F 2054

DATE: 1-8-80

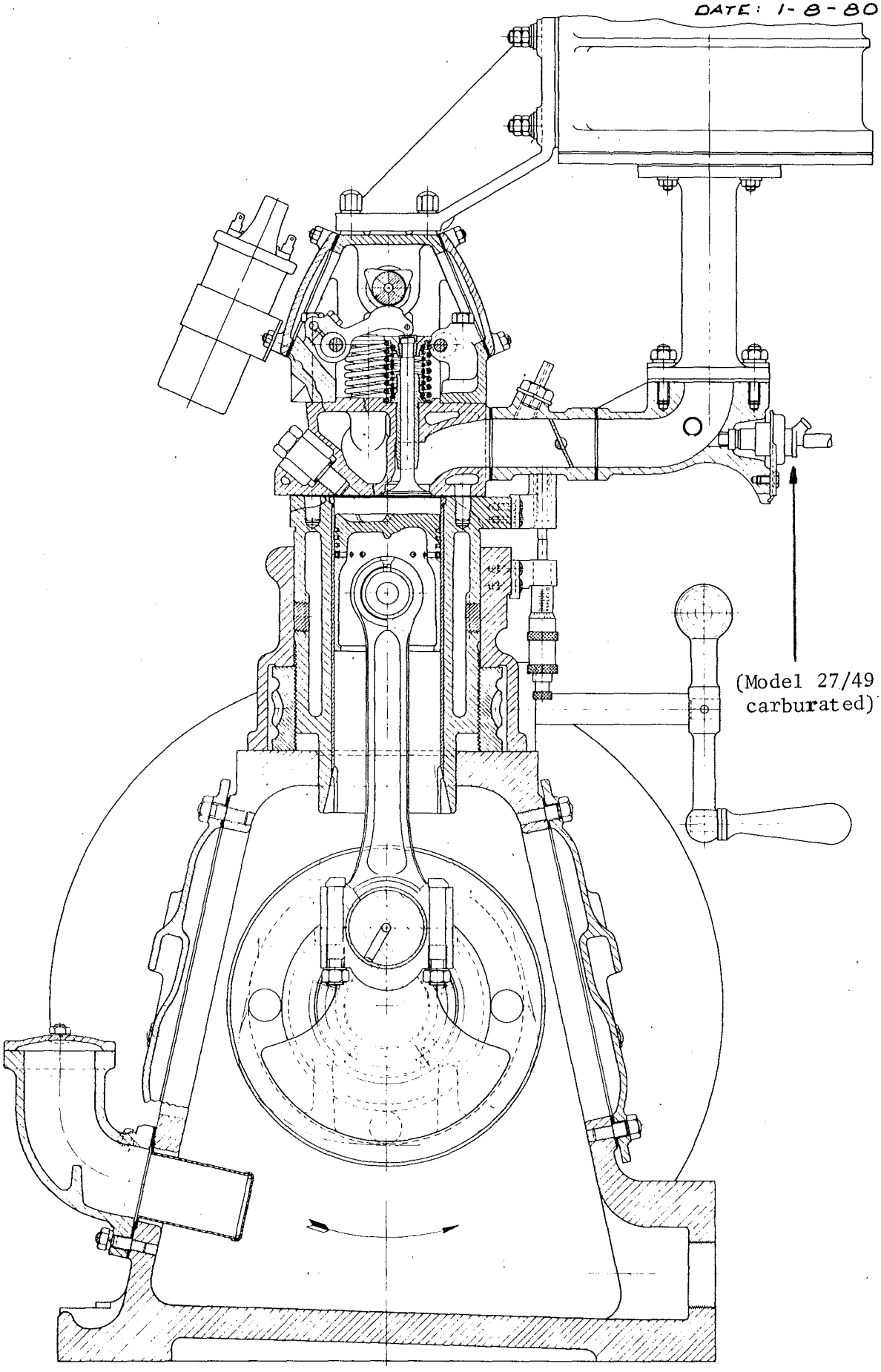

CROSS SECTIONAL ARRANGEMENT OF VARIABLE COMPRESSION RESEARCH ENGINE

3" BORE X 4 3/8" STROKE - PETROL VERSION

APPENDIX 5.2

SPECIFICATIONS OF THE SILICON PHOTODETECTOR

UDT SILICON DETECTOR/AMPLIFIER PRELIMINARY SPECIFICATIONS (25° C ambient)

MODEL : UDT 455

Characteristics	Conditions	Min.	Typ.	Max.	Units
Active Area			5.1		mm^2
Spectral Range		350		1100	nanometers
Responsivity	λ = 850	.35			amps/watt
Capacitance	(1) V_D = 0 Volts		50	75	picofarads
	(2) V_D = 10 Volts		15	20	picofarads
	(3) V_D = 50 Volts		7	10	picofarads
Supply Voltage		±5	±15	±18	volts, dc
Input Offset Voltage	R_S = 50 Ω		0.5	3	millivolts
Input Offset Temperature Coefficient			4	15	microvolts/°C
Input Bias Current			15	200	pico amps
Gain Bandwidth Product			5.4		megahertz
Slew Rate		5-	15		volts/microsecond
Open Loop Gain	DC	50	200		volts/millivolt
Bandwidth - 3dB	(Rf = 10ΩM)				
	(1) V_D= 0 Volts		70		kilohertz
	(2) V_D = 15 Volts		78		kilohertz
Input Noise Voltage	100 Hz		20		nanovolts/$\sqrt{Hz}$
	1 KHz				nanovolts/$\sqrt{Hz}$
Input Noise Current	100 Hz, 1 KHz		.01		picoamps/$\sqrt{Hz}$
Detector Saturation Current			1		milliamp (peak)
N.E.P.	AC, 1 KHz, 850 nm		$5x10^{-13}$		watt/$\sqrt{Hz}$
Dark Current	V_D = -10 Volts		20	50	nanoamps
Breakdown Voltage	I_D = 10 μAmp	50			volts
Temperature	Operating	0		+70	°C
	Storage	-65		+150	°C
Field of View			70		degrees
Package Style			10-5		

Manufactured by United Detector Technology Incorporated, California, U.S.A.

APPENDIX 5.3

SPECIFICATIONS OF THE SILICON AND LEAD-SULPHIDE TWO-COLOUR DETECTOR

Typical Spectral Response of
Silicon Photocells

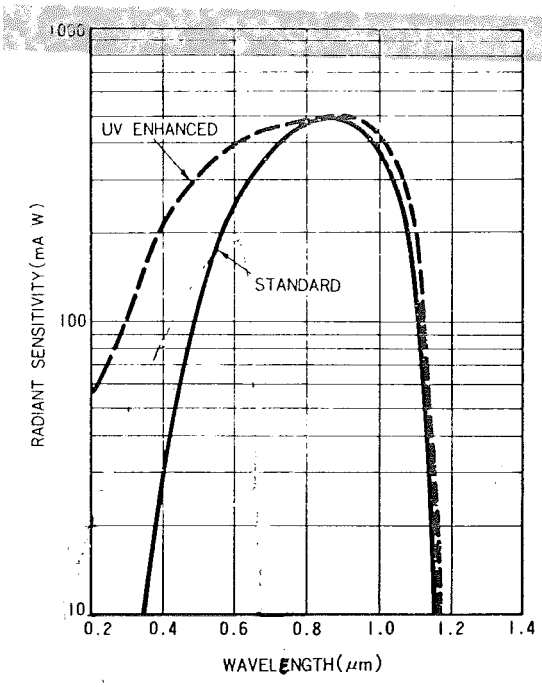

Typical Spectral Response of
Lead Sulphide Detectors

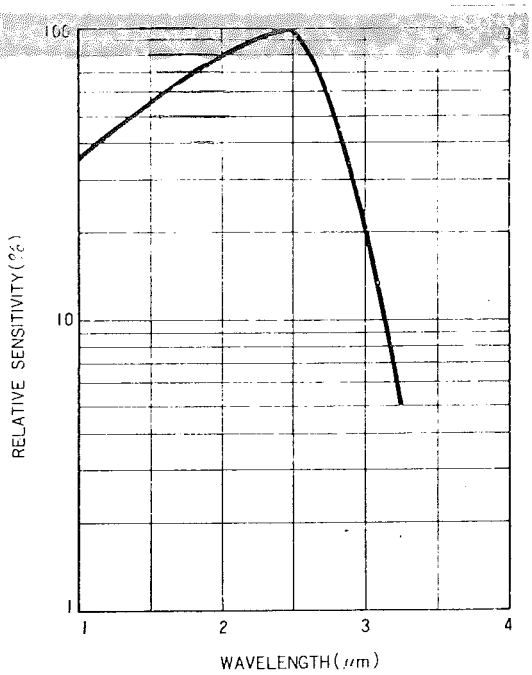

Dimensional Outline (mm)

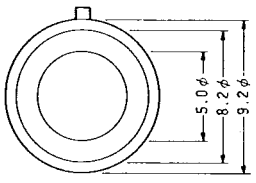

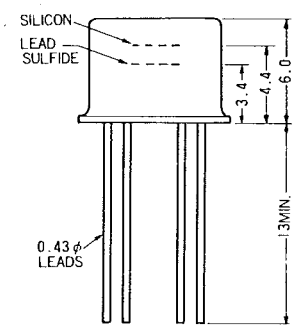

Silicon photocell has a spectral response range from 0.3 to 1.15 μm and transmits radiations beyond the upper limit. Lead sulfide photoconductive cell has a spectral response from the silicon's upper limit to 3.1 μm. Making use of these facts, a silicon and lead sulfide two color detector has been devised. This detector consists of a silicon photocell front element and a lead sulfide photoconductive cell back element in a TO-5 case. A fused silica window is used to maximize the transmission of both UV and infrared radiations.

Applications of this detector may include spectrophotometers, flame monitors and temperature measurement equipments which require a widely extended spectral response.

Two types of color detectors have been devised using a standard silicon photocell and an UV enhanced silicon photocell. Other detector combinations such as silicon and lead selenide can be supplied in a variety of package configurations.

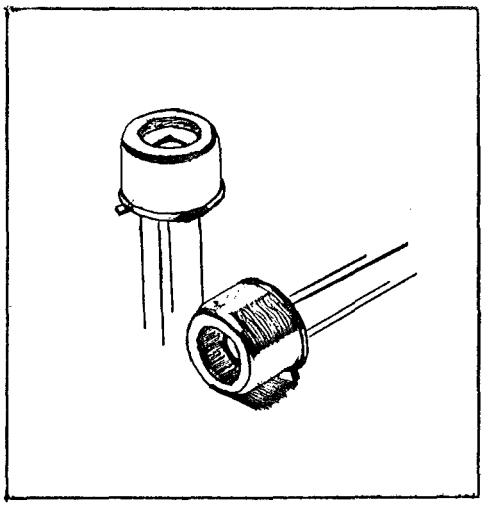

SPECIFICATIONS (Tentative)

	(K1713) Standard	(K1713-01) UV Enhanced	Units
Silicon			
Spectral Response	0.43 to 1.14	0.2 to 1.15	μm
Peak Response Wavelength	0.9	0.95	μm
Photosensitive Area	2.5 x 2.4	2.5 x 2.4	mm
Radiant Sensitivity at 254 nm	-	80	mA/W
at 633 nm	300	380	mA/W
at 930 nm	500	500	mA/W
NEP (Noise Equivalent Power)	6×10^{-15}	6×10^{-15}	$W/Hz^{1/2}$
D*	2×10^{14}	2×10^{14}	$cm \cdot Hz^{1/2}/W$
Short Circuit Current	5	5	μA
Dark Current (V_R=10mV)	5	5	pA
Shunt Resistance	2	2	GΩ
Rise Time (10% to 90%, R_L=1kΩ, V_R=0V)	0.3	0.2	μs
Junction Capacitance	80	65	pF
Maximum Reverse Voltage	5	5	V

Lead Sulfide	
Spectral Response	1.1 to 3.1 μm
Peak Response Wavelength	2.5 μm
Dark Resistance	0.5 to 2.0 MΩ
D* (λp, 900, 1)	1×10^{11} $cm \cdot Hz^{1/2}/W$
Rise Time (0 to 63%)	100 to 400 μs

Hamamatsu Corporation, Middlesex, U.S.A.

APPENDIX 5.4

SPECIFICATIONS OF THE SILICON AND LEAD-SELENIDE TWO-COLOUR DETECTOR

SILICON & LEAD SELENIDE TWO COLOR DETECTOR

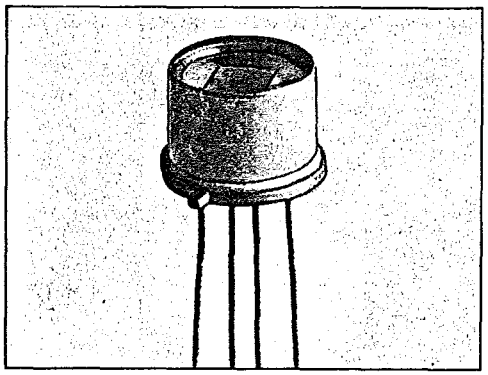

9002 TYPE

FEATURES

- TWO COLOR "IN-LINE" DETECTOR
- EXTENDED SPECTRAL RESPONSE 0.35μm to 4.7μm
- ROOM TEMPERATURE OPERATION
- HIGH DETECTIVITY
- LONG TERM STABILITY
- RUGGED
- COMPACT

DESCRIPTION

Silicon detects radiant energy over the spectral range of 0.35 to 1.13 micrometers and transmits it beyond the upper limit. Lead selenide detectors begin to respond significantly in this region and extend out to 4.7 micrometers. Taking advantage of these facts, a detector has been devised to give an in-line "two color" sensor which combines the features of both devices to yield an extended range, high detectivity detector. This device consists of a low noise silicon photovoltaic detector front element and a lead selenide photoconductor back element, precision stacked together, and suitable for room temperature operation. The TO-5 style package is backed filled with dry nitrogen prior to sealing. Its rugged construction enables this device to be used in a wide range of hostile environments that demand a high degree of electrical, optical, and mechanical reliability.

The 9002 "two color" detector has been used in many types of military systems such as gun flash and rocket ignition applications. By observations of the two color regions, spectral signatures are identified to obtain target-to-background discrimination. The scientific and commercial communities are rapidly finding this type of detector to be a problem solver for applications requiring an extended spectral detection range.

An anti-reflection coating is applied to the front surface of the silicon detector to maximize the transmission of infrared radiation in the lead selenide range. A suitable filter may also be placed immediately behind the silicon wafer to limit the lead selenide's response to specific wavelengths of interest.

Other detector combinations such as Silicon and Lead Sulfide are available. On special order, other configurations and customized packaging will be provided.

MECHANICAL

TO-5 STYLE

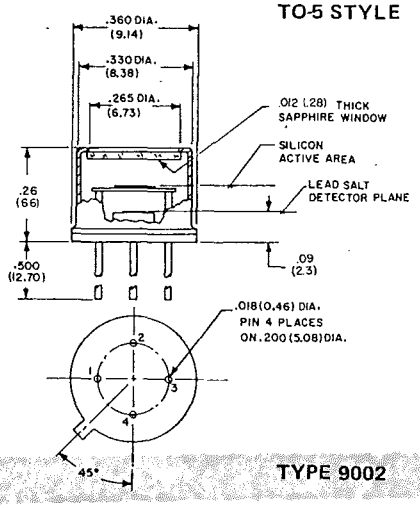

TYPE 9002

PIN CONNECTIONS

1 and 3 Silicon (P.V.)
2 and 4 Lead Selenide (PbSe)

DIMENSIONS IN INCHES (mm)

Manufactured by Infrared Industries Inc., Orlando, U.S.A.

PARAMETER	OPERATING CONDITIONS	SILICON			UNITS
		min	typical	max	
Temperature			+25		°C
Active area			5.1		mm^2
Operating Voltage			0	10.0	Volts
Capacitance	0 volts		150.0	250.0	Picofarads
Shunt Reistance	0 volts	100.0	300.0		Megohms
D*	0 volts (0.9, 100, 1)		1.0		$X10^{13}$ CM $Hz^{½}W^{-1}$
Spectral Sensitivity	0 volts, 0.9μm	0.47	0.50		Amps/Watt
Spectral range	0 volts	0.35		1.13	μm
Cathode common with case			No		

PARAMETER	OPERATING CONDITIONS	LEAD SELENIDE			UNITS
		min	typical	max	
Active area			5.1		mm^2
Operating Bias Voltage			100		Volts with R_L=1 megohms
D*	(pk, 100, 1)		4		$X10^{8}$ CM $Hz^{½}W^{-1}$
Resistance		0.05	0.5	2.0	Megohms/□
Time Constant			5	20	μsec
Temperature			+25		°C
Spectral Range		1.1		4.7	μm

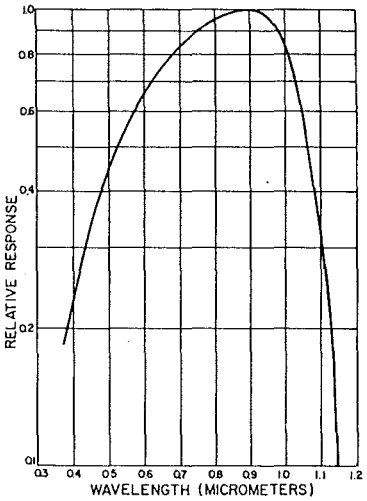

SILICON PHOTOVOLTAIC DETECTOR

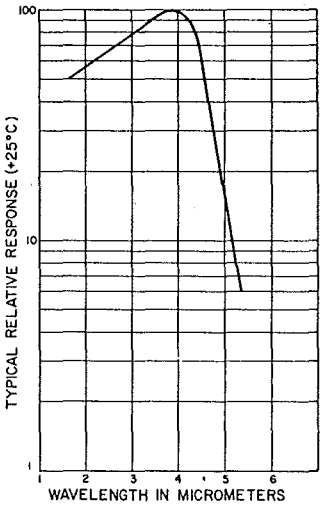

LEAD SELENIDE DETECTOR

OPERATING CIRCUITS

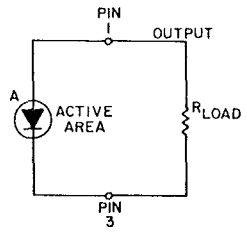

SILICON PHOTOVOLTAIC DETECTOR

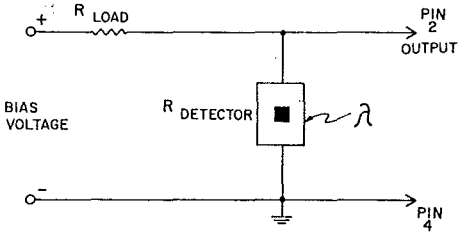

LEAD SELENIDE DETECTOR

APPENDIX 5.5

FIRST PROTOTYPE OPTIC PLUGS

The first prototype optic plugs were developed by constructing a pyrex glass insulator around the centre electrode, as shown in Plate 5.16. The glass insulator simulated the shape of the ceramic insulator of an aero-engine spark plug which can be disassembled, as shown in the Plate. The aero-engine plug housing was then assembled around the glass insulator and centre electrode.

After some initial testing, this type of optic plug was abandoned since it was found difficult to obtain the correct centre electrode temperature. It was also considered to be too great a task, both in time and cost, to develop a series of these plugs with heat ranges emulating the range of spark plugs currently available.

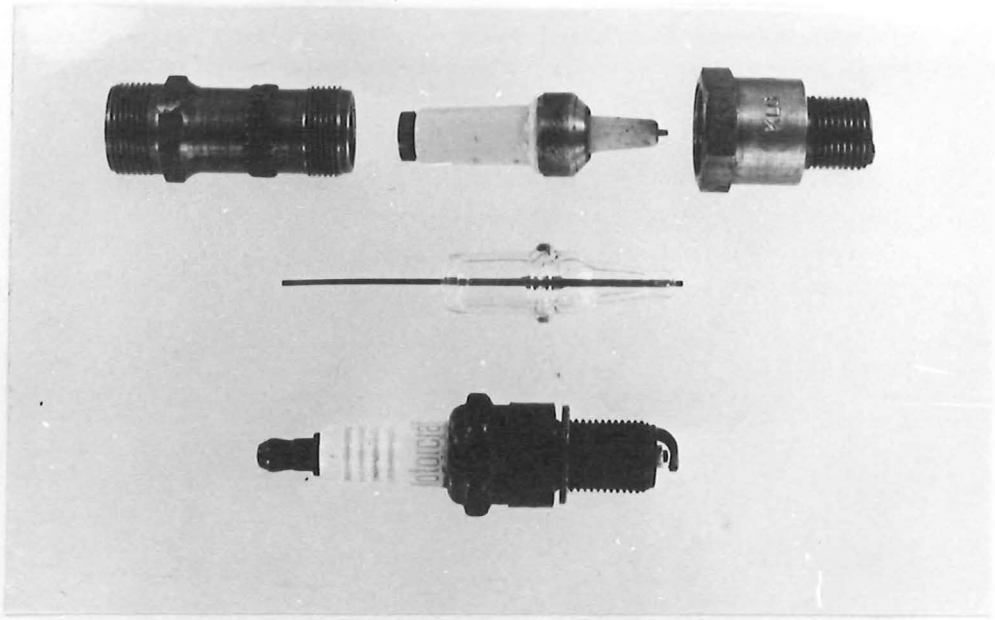

Plate 5.16 The prototype optic plug used pyrex glass insulator (middle) instead of the porcelain insulator (top). This was inserted into the aero-engine spark plug casing (top). A standard spark plug is shown at the bottom of the plate for comparison.

APPENDIX 5.6

LIGHT TRANSMISSION THROUGH FIBRE OPTIC CABLE

A fibre optic cable consists of a number of fine strands of glass which are surrounded and protected by a sheath and are capable of transmitting light from one end of the cable to the other[63, 65]. The strands function independently of one another and transmit the light by refracting it internally whenever it impinges upon the strand | cladding, (Fig. 5.8). In order for the light to be refracted sufficiently at this refractive surface, the strand core and cladding must have significantly different refractive indexes.

This concept of light transmission can be illustrated by considering the example of a water-air interface (Fig. 5.9). When light is directed from within the water towards the water-air interface along line 1, it will be refracted away from the vertical axis at the water-air interface to follow the path 1'. If the light ray is now brought closer to the direction of line 2, a situation will eventually be reached when the light is refracted back into the water to follow the path 2'. The angle θ is the angle at which the light is refracted just enough to remain within the water.

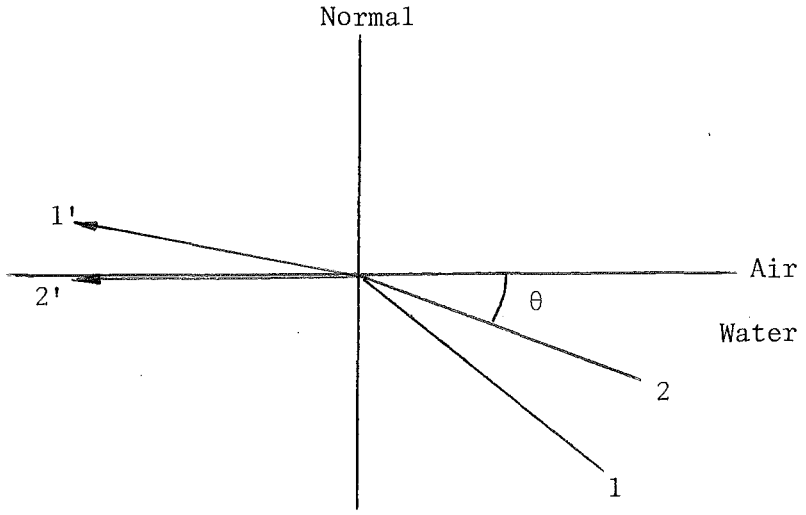

Figure 5.10 Refraction of light at a water-air interface.

Referring to the fibre otpic strand in Fig. 5.8, the core and cladding have comparative refractive indexes similar to the water-air interface. Therefore, so long as the light incident upon the end of the fibre optic strand falls with the angle θ (Fig. 5.8), it will be

totally internally refracted as it passes down the strand. The total acceptance angle of the optic strand is defined as 2 x θ. The core is generally made of high purity glass for good light transmission. The cladding is generally made of glass of a different refractive index or a silicon polymer. A fibre optic cable will consist of a bundle of these strands or a single large diameter strand, in both cases sheathed with a protective outer plastic jacket.

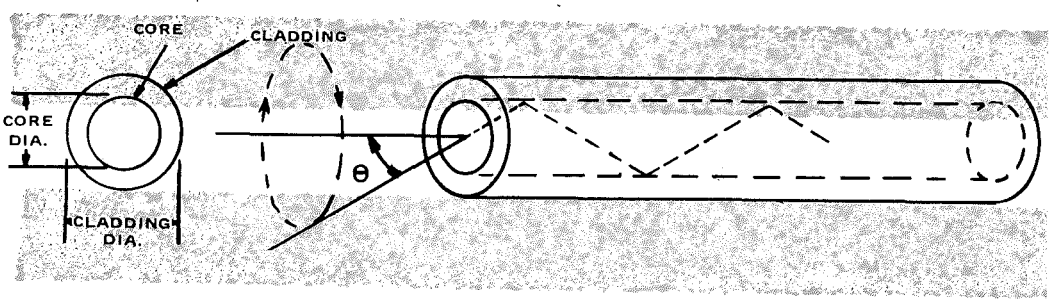

Figure 5.8 Fibre optic strand showing core, cladding and acceptance angle θ[63].

APPENDIX 7.1

A KNOCK DETECTION SYSTEM BASED ON THE PEAK AMPLITUDE OF THE LIGHT INTENSITY

The occasional light knock is manifest in any S.I. engine running close to optimum efficiency and is to be considered quite acceptable. It is therefore necessary to design circuitry which does not respond to individual pulses but samples a sequence before the output registers knocking combustion. Consequently, some form of averaging must be incorporated into the first stage of the circuit.

ANALOGUE SYSTEM

A simple averaging device is an integrator and one might expect that a long succession of auto-ignition pulses would cause the integrator output to increase. An integrator with appropriate time constant was applied to the phototransistor output. Results were not encouraging as the integrator output did not rise significantly during periods of knocking combustion. An inspection of Figs 7.3 and 7.4 reveals that the knocking combustion light emission pulses are very similar in area to the non-knocking pulses, in fact it is the amplitude difference that is immediately apparent from the Figures. The averaging circuitry should therefore be amplitude selective and so a comparitor was linked to the phototransistor.

DIGITAL SYSTEM

The comparitor was referenced at the voltage level corresponding to the line drawn across Figs 7.3 and 7.4 The comparitor output is either high or low depending on whether or not a knocking combustion pulse is received. To this device digital averaging circuitry was developed which is described in general by the block diagram of Fig 7.5 and the following explanation:

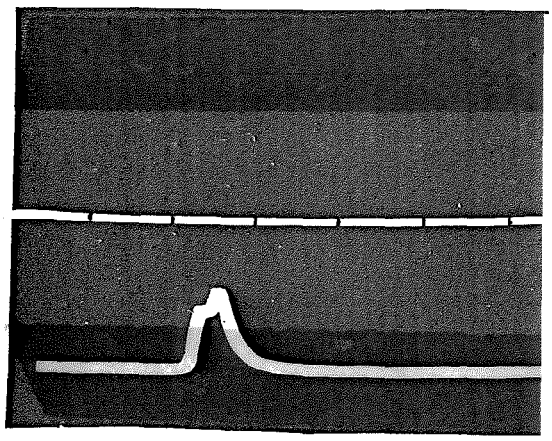

Figure 7.3 Phototransistor output under normal engine operation.

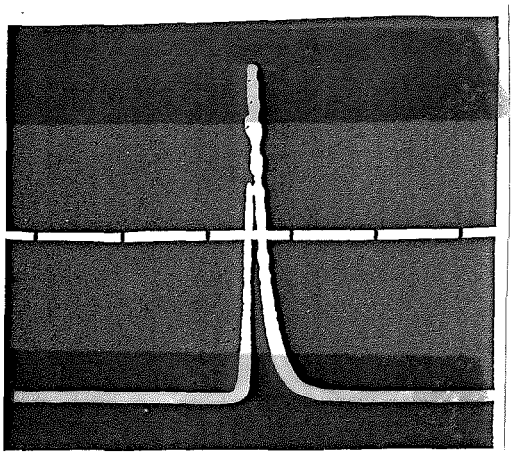

Figure 7.4 Phototransistor output with the engine knocking.

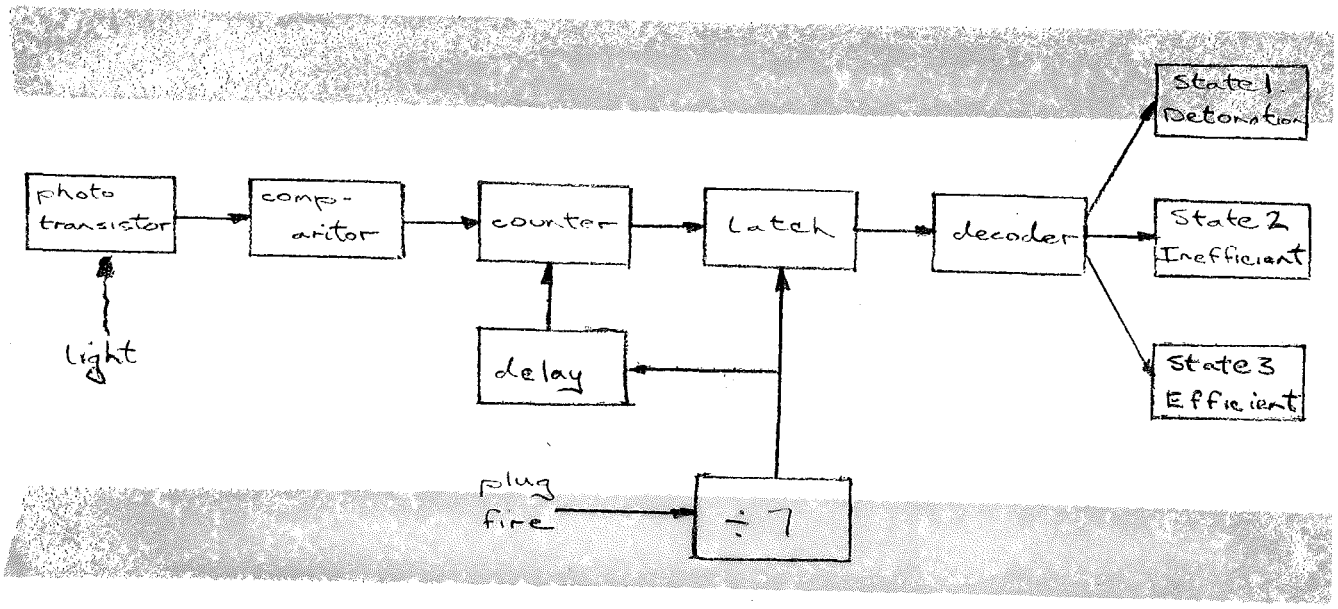

Figure 7.5 Block diagram of knock detection circuitry.

The comparitor output is connected to the counter. The counter is reset every 7th spark-fire, but immediately prior to being reset, the count number is latched. This latched count number is then decoded into 1 of 3 states by appropriate logic circuitry which is relayed to one of three LED's:

State 1 — If nearly every combustion event in the batch of 7 auto-ignited, the counter would count up 6 or 7 and the 'knock' LED would light up.

State 2 — If less than 2 combustion strokes in the batch auto-ignited the counter would count 0 or 1 and the 'Inefficient Operation' LED would conduct.

State 3 — If the count ranges from 2 to 5, the engine is lightly knocking in a non-destructive manner and therefore operating at optimum efficiency. The third LED conveys this information.

The circuitry represented by the block diagram of Figure 7.5 is schematically presented in Fig. 7.6 with each IC numbered. A detailed description of the function of each of the circuit components will now proceed from the phototransistor to the IC's in chronological order.

The supply is +10V and is fed to all chips and transistors in the diagram. The phototransistor is configured as an emitter follower and its output (Figs 7.3 and 7.4) is linked to a variable reference level comparitor (1).

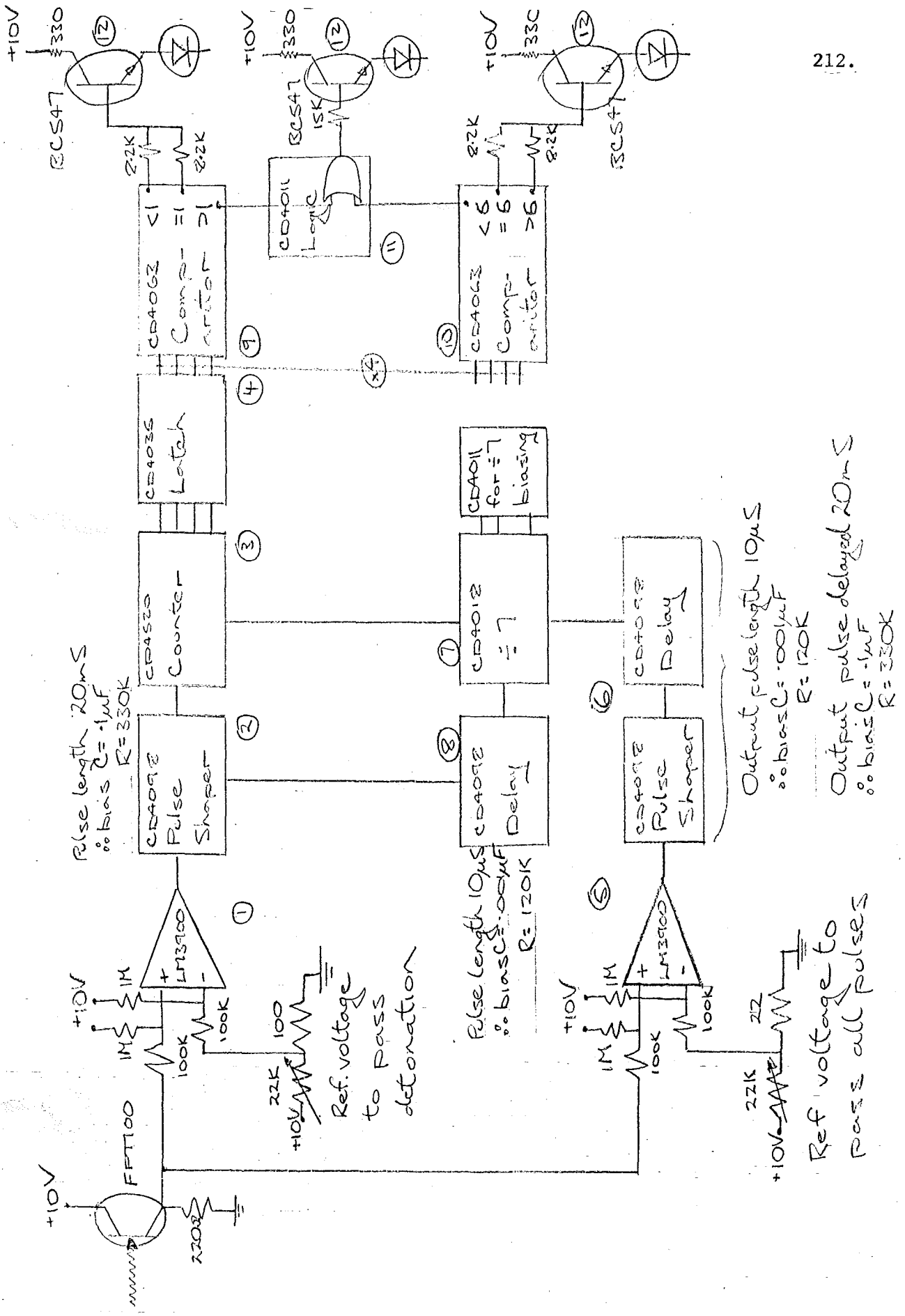

Figure 7.6 Circuit diagram of knock detector.

(1) The comparitor (1) reference level is adjusted so that only the auto-igniting pulses cause the output to go high. The comparitor output over one pulse is sketched in Fig. 7.7.

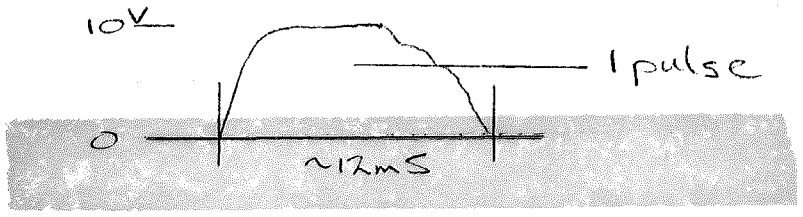

Fig 7.7 Comparitor output when the engine is knocking.

(2) The monostable multivibrator (2) shapes the comparitor output pulse:
- (a) to create an adequately short rise time for the counter, and
- (b) to lengthen the pulse to 20 mS ensuring the trailing edge drops rapidly and that the counter is not activated twice by one pulse.

(3) The binary counter (3) counts up from zero to a maximum of seven before it is reset.

(4) The counter is reset immediately after the latch (4) has recorded the count number.

(5) The timing of the counter reset and latch enable pulse is derived from the phototransistor output. Comparitor (5) has a very low reference level so that all pulses force the output high and enter the dual monostable multivibrator (6).

(6) The dual multivibrator (6) serves two main purposes:
- (a) it shapes the pulse in the same manner as the multivibrator (3), and
- (b) it delays the pulse. Then this pulse can first be recorded on the latch if it was auto-ignition. The delay time is 10 μS.

(7) The output from the multivibrator (6) enters a frequency divider (7) which divides by 7. This output serves to 'enable' the latch and then reset the counter every 7th spark-fire.

(8) To ensure the count number is latched before the counter is reset, delay is introduced with multivibrator (8). This triggers from the trailing edge of the latch pulse and goes low 10 μS afterwards.

(9), (10), (11) The latch output is decoded by circuitry (9), (10) and (11). The operation of this circuitry is depicted best in the diagram; suffice to say that the comparitor reference levels are preset by tying the appropriate reference pins to the supply.

(12) The three outputs drive three LED's (12) with the aid of the driver transistors.

RESULTS

The system was tested by installing it on the Ricardo E6 engine and by using a human operator to alter the ignition timing in response to the LED display. Engine optimisation was easily achieved over a series of different loadings and speeds. However, further testing is necessary to determine that the sub-system operates satisfactorily as engine coolant temperature is varied.

REFERENCES

1. Romans Chapter 15, verse 5, New American Standard Bible, Foundation Publications, U.S.A., 1975.

2. Vichnievsky, R., Combustion in petrol engines. In Joint Conference on Combustion; The Institution of Mechanical Engineers, The American Society of Mechanical Engineers, Boston, Mass. and London; 1955.

7. Benson, R.S. and Whitehouse, N.D. Internal Combustion Engines, 1st ed. Manchester, University of. Pergamon Press, Oxford; 1979.

8. Obert, E.F. Internal Combustion Engines, 3rd ed. Wisconsin, University of. International Textbook Company, Pennsylvania; 1970.

9. Sokolik, A.S., Self-ignition, flame and detonation in gases". In Automotive Engineering, vol.88 No.7, Society of Automotive Engineers, Dallas, U.S.A., July 1980.

10. Ball, G.A., Photographic studies of cool flames and knock in an engine. In Fifth Symposium (Int.) on Combustion. The Combustion Institute, U.S.A.; 1954.

11. Turbo boost controlled by knock detection. In Automotive Engineering, vol.88 No.6, Society of Automotive Engineers, Dallas; U.S.A., June 1980.

12. Measuring high-speed knock. In Automotive Engineering, vol.85 No.5, Society of Automotive Engineers, Dallas, U.S.A.; May 1977.

13. Champion Booklet. Spark plug and ignition systems; Champion Spark Plug, New Zealand Limited, Auckland, New Zealand; ≈1974.

14. Boht, S.R. and Quayle, R.S. The control of ignition timing to achieve maximum fuel economy. In Third International Conference on Automotive Electronics. Mechanical Engineering Publications Ltd, London; 1981.

15. Hansel, J.G. A turbulent combustion model of cycle to cycle combustion variations in Spark Ignition engines. New Jersey, Esso Research & Engineering Co. In Combustion Science and Technology, vol.2; 1970.

16. Agnew, W.G. Fifty years of combustion research at General Motors. Michigan Research Laboratories, General Motors Corporation, vol.4, Progress in Energy and Combustion Science, Pergamon Press; 1978.

17. Clark, C.L. et al. Economic, environmental and energy implications of engine ping: A preliminary analysis. Washington, Dept of Technology and Human Affairs, University of. In International Journal of Environmental Studies, vol.16; 1981.

18. Spreadbury, F.G. Electrical ignition equipment, 1st ed. London, Paddington Technical College of, Constable and Company, London; 1954.

19. Progress toward Federal emissions research goals: A status report. In Automotive Engineering, vol.88 No.7, Society of Automotive Engineers, Dallas, U.S.A; July 1980.

20. Fuel economy regulation costs studied. In Automotive Engineering, vol.88 No.1, Society of Automotive Engineers, Dallas, U.S.A.: Jan 1980.

21. Hagen, D.F. An interactive approach to electronic engine controls at Ford Motor Company. In Second International Conference on Automotive Electronics. The Institution of Electrical Engineers, London; 1979.

22. Simariaitis, D.J. MISAR an electronic advance. In Automotive Engineering, vol.85, No.1, Society of Automotive Engineers, U.S.A.; Jan. 1977.

23. Schwarz, H. Features and facilities of a digital electronic spark advance system and its advantage compared with mechanical systems. In The Second International Conference on Automotive Electronics. The Institution of Electrical Engineers, London; 1979.

24. Optimiser invokes adaptive strategy for best spark advance. In Automotive Engineering, Vol.86, No.7, Society of Automotive Engineers, Dallas, U.S.A.: July 1978.

25. Boht, S.R. and Quayle, R.S. The control of ignition timing to achieve maximum fuel economy. In Third International Conference on Automotive Electronics. Mechanical Engineering Publications Ltd, London; 1981.

26. Engine control sensors for the '80s: A preview. In Automotive Engineering, vol.88, No.4, Society of Automotive Engineers, Dallas, U.S.A.: April 1980.

27. Emissions during warmup period studied. In Automotive Engineering, Vol.88, No.5, Society of Automotive Engineers, Dallas, U.S.A.; April 1980.

28. Lean combustion : A review. In Automotive Engineering, Vol.93, No.3, Society of Automotive Engineers, Dallas, U.S.A.; March 1984.

29. Microprocessor control improves economy, reduces emissions. In Automotive Engineering, Vol.88 No.2, Society of Automotive Engineers, Dallas, U.S.A.; Feb. 1980.

30. Toyoda, T. et al. Some of the new control strategies for electronic engine control system. Japan, Toyota Motor Company Ltd of. In Third International Conference on Automotive Electronics. Mechanical Engineering Publications Ltd, London; 1981.

31. Engineering highlights of the 1980 Automobiles. In Automotive Engineering, Vo.87, No.10, Society of Automotive Engineers, Dallas, U.S.A.; Oxt. 1979.

32. G.M. Expands C-4 system use. In Automotive Engineering, Vol.88 No.8, Society of Automotive Engineers, Dallas, U.S.A.; Aug. 1980.

33. d'Orsay et al. New components and recent developments in ignition systems. In Second International Conference on Automotive Electronics. Institution of Electrical Engineers, London; 1979.

34. G.M.Expands C-4 system. In Automotive Engineering, Vol.88, No.8, Society of Automotive Engineers, Dallas, U.S.A.; Aug. 1980.

35. Landman, L.C. Knock sensor vehicle test program. U.S. Environmental Protection Agency, Control Technology Assessment and Characterisation Branch, Plymouth Rd, Michigan, U.S.A.: 1981. (Supplied by BUSAR Research and Development Reports, Queensland, Australia.)

36. Piezoelectric sensor determines cylinder pressures. In Automotive Engineering, Vol.87, No.5, Society of Automotive Engineers, Dallas, U.S.A., May 1979.

37. Boht, S.R. and Quayle, R.S. The control of ignition timing to achieve maximum fuel economy. In Third International Conference on Automotive Electronics. Mechanical Engineering Publications Ltd, London; 1981.

38. Robbi, A.D. and Fenrara, C.J. Rhombic - A digital ignition controller. New Jersey, R.C.A. Laboratories. In Third International Conference on Automotive Electronics. Mechanical Engineering Publication Ltd, London; 1981.

39. EFI Tailored to smaller engines. In Automotive Engineering, Vol.88 No. 8. Society of Automotive Engineers, Dallas, U.S.A.; Aug. 1980.

40. Fuel system adapts to varying alcohol content. In Automotive Engineering Vol.88 No.2, Society of Automotive Engineers, Dallas, U.S.A.; Feb. 1980.

41. Heywood, H.B. Pollutant formation and control in Spark Ignition engines. In 15 Symposium (International) on Combustion. The Combustion Institute, U.S.A.; 1975.

42. Feedback control permits heavy EGR rates. In Automotive Engineering, Vol.88, No.6, Society of Automotive Engineers, Dallas, U.S.A.; June 1980.

43. Oxygen sensors revisited. In Automotive Engineering, Vol.88 No.4, Society of Automotive Engineers, Dallas, U.S.A.; April 1980.

44. Engineering highlights of the 1981 automobiles. In Automotive Engineering, Vol.88, No.10, Society of Automotive Engineers, Dallas, U.S.A.; Oct. 1980.

45. Patterson, D.J. and Henein, N.A. Emissions from combustion engines and their control Michigan, University of, Ann Arbor Science, Michigan; 1972.

46. Gaydon, A.G. and Wolfhard, H.G. Flames. Their structure, radiation and temperature. 3rd ed. Rev., London, Imperial College of. Chapman and Hall; 1970.

47. Glassman, I. Combustion. New Jersey, Princeton University. Academic Press, London; 1977.

48. Bradley, J.N. Flame and combustion phenomena, 1st ed. Essex, University of. Methven & Co., London; 1969.

49. University of Leeds. Dept of Fuel and Combustion Science. Houldsworth School of Applied Science. Series of lectures on Fundamentals of Engine Exhaust Pollution; 1974.

50. Woodleif, T. Jr., S.P.S.E. Handbook of Photographic Science & Engineering. Society of Photographic Scientists and Engineers. J. Wiley & Sons, Inc., U.S.A.: 1973.

51. Gaydon, A.G. The spectroscopy of flames. 2nd ed. London, Imperial College of. Chapman & Hall; 1948.

52. Gaydon, A.G. Spectroscopy and combustion theory. 2nd ed. Rev. London, Imperial College of. Chapman & Hall. 1948.

53. Levedahl, W.J. Multistage autoignition of engine fuels. In Fifth Symposium (Int.) on Combustion. The Combustion Institute, U.S.A.; 1954.

54. Smith D.S. and Starkman, E.S. A spectroscopic study of the hydroxyl radical in an internal-combustion engine. In Thirteenth Symposium (International) on Combustion. Combustion Institute; 1970.

55. Lewis, B. The experimental side of combustion research in engines. In Frontiers in Chemistry, Vol.II; The Chemical Background for Engine Research. Interscience Publishers, New York; 1943.

56. Champion Spark Plugs (N.Z.) Ltd Booklet; 1981 Spark Plug Recommendations. Champion Spark Plug Company, N.Z.: 1981.

57. Heraeus. In Quartz Glass for Optics, Heraeus Silica and Metals Ltd.

58. Infrared Industries Inc. The Spectrum of Electro-optical Components, Waltham, Ma 02154, U.S.A.: 1980.

59. Smith, R.J. Circuits devices and systems. Stanford University, Professor of Electrical Engineering of., 3rd ed. Wiley, U.S.A.: 1976.

60.

61. Topics in applied physics. Vol.19,Optical and Infrared Detectors. 2nd ed. Springer-Venlag, Berlin, Heidelberg New York; 1980.

62. Stimson, A. Photometry and radiometry for engineers. Eastman Kodak Company. Wiley, U.S.A.: 1974.

63. Math Associates Inc., Fiber Optics, Components, Systems and Accessories, New York 11050. 5 Manhasset Avenue; 1981.

64. Gould, C.S.W. The Ricardo Eg/MK6 variable compression engine, serial No. 138/82. Sussex Ricardo Consulting Engineers Ltd; 1982.

65. The Optical Industry and Systems Purchasing Directory, 27th ed. Pub. by Optical Spectra Magazine, U.S.A.; 1981.